Alma Mater Studiorum – Università di Bologna

DOTTORATO DI RICERCA IN

CHIMICA

Ciclo XXX°

Settore Concorsuale: 03/C2

Settore Scientifico Disciplinare: CHIM/04

STUDY OF VANADIUM CONTAINING CATALYSTS FOR THE UPGRADING OF BIO-BASED BUILDING BLOCKS

Presentata da: Francesco Puzzo

Coordinatore Dottorato
Prof. Aldo Roda

Supervisore
Prof. Fabrizio Cavani

Co-Supervisore
Dott. Carlo Lucarelli

Esame Finale Anno: 2018

SYNTHESIS OF PYRUVIC ACID FROM ACETOL

Abstract

Negli ultimi anni, a causa della continua diminuzione delle fonti fossili e dell'incremento della emissione di gas serra, la ricerca ha focalizzato l'attenzione sullo sviluppo di nuovi processi che permettano la trasformazione di materie prime derivanti da fonti rinnovabili in energia, combustibili e chemicals. Nello specifico, questa tesi focalizza l'attenzione su due processi, il primo riguarda la trasformazione del 1-butanol in buteni e anidride maleica mendiate un processo di disidratazione e ossidazione in fase gas utilizzando catalizzatori a base di ossidi misti di vanadio e fosforo; il secondo riguarda la trasformazione dell'idrossiacetone in acido piruvico mediante un processo di doppia ossidazione selettiva, anch'essa in fase e utilizzando differenti catalizzatori a contenenti Vanadio.

I risultati hanno mostrato come le condizioni operative, le proprietà della superficie catalitica e la sua interazione con le molecole di substrato influenzano notevolmente il percorso di reazione.

In the last years, due to the continuous decreasing of the starting material deriving from the fossil sources and the increasing of the greenhouses emissions, the research has focused their effort on the developing of new industrial processes based on the transformation of starting materials deriving from the renewable sources into energy, fuels and chemicals. In particular, the aim of this thesis involves the investigation of two different processes: the first concerns the transformation of 1-butanol into butenes

and maleic anhydride by oxidehydration process carried out in gas phase using vanadium/phosphorous mixed oxides. The second process regards the transformation of acetol to pyruvic acid by gas-phase selective oxidation reaction, using different vanadium-containing systems as catalysts.

The results have shown the operative condition, the textural properties of the catalysts and the interaction between the substrate and the catalytic surface influence notably the reaction pathway.

INTRODUCTION

1 Aim of the thesis

During my PhD, which was carried out in the Laboratory for the Development of Industrial Processes in the Department of Industrial Chemistry "Toso Montanari" of the Alma Mater Studiorum, University of Bologna, I focused on developing and improving processes related to the production of *monomers* and *specialty chemicals* by gas phase transformation of different *bio-based building blocks* using vanadium-containing catalysts as heterogeneous catalytic systems. In particular, I investigated two different processes – the first is related to the improvement of the productivity of C_4 unsaturated monomers, such as butenes and maleic anhydride, by means a gas phase oxydehydration reaction of 1-butanol, which was carried out in a *one-pot* approach, while the second concerns the production of pyruvic acid by the selective oxidation in gas phase of acetol.

The choice to investigate the production of C_4 unsaturated molecules from 1-butanol is motivated by the continuous growth of the polymer market for these molecules and the higher atomic efficiency of this process compared to the other processes based on renewable sources. Furthermore, it is essential to concentrate on the production of 1-butanol from renewable sources, because it is necessary to decrease the cost of the starting materials in order to improve the economic sustainability of the entire process. Regarding the production of pyruvic acid from acetol, this study is part of an ampler field, which focuses on upgrading glycerol into specialty chemicals and monomers.

In order to improve the economical sustainability of the production process, it is necessary to enhance the value of not only the main product, but also all the co-products obtained; this aspect is fundamental for the production of biodiesel from renewable sources. To reduce the price of biodiesel, it is necessary to valorise glycerol and use it as a starting material for the production of molecules with high value as monomers and specialty chemicals. In this context, pyruvic acid was chosen as one of the target molecules because it finds application in food, pharmaceutical, and agrochemical industries; it follows that the development of a process in which pyruvic acid can be produced from glycerol could help in its valorisation. The choice to investigate the transformation of acetol into pyruvic acid is linked to the already well-known capability of glycerol to be converted into acetol by dehydration.

An in-depth analysis conducted on both of the above-mentioned processes will be described in detail in the following sections. For the transformation of 1-butanol into butenes and maleic anhydride, an acid catalytic system with redox properties is necessary as both dehydration and oxidation reactions occur; in the case of the oxidation of acetol into pyruvaldehyde and pyruvic acid, the process involves an oxidative dehydrogenation (ODH) reaction in order to produce pyruvaldehyde, the selective oxidation of which yields the corresponding carboxylic acid.

Because both processes require catalysts with acid/base and redox sites, vanadium-containing catalysts were considered as they exhibit the textural properties necessary for both processes to occur. Different vanadium-containing catalysts with different textural properties were tested for both processes in order to investigate their catalytic behaviour and correlate it to their textural properties and structures.

For a better comprehension of the entire work, in Figure 1-1 is reported the work breakdown structure for both processes investigated.

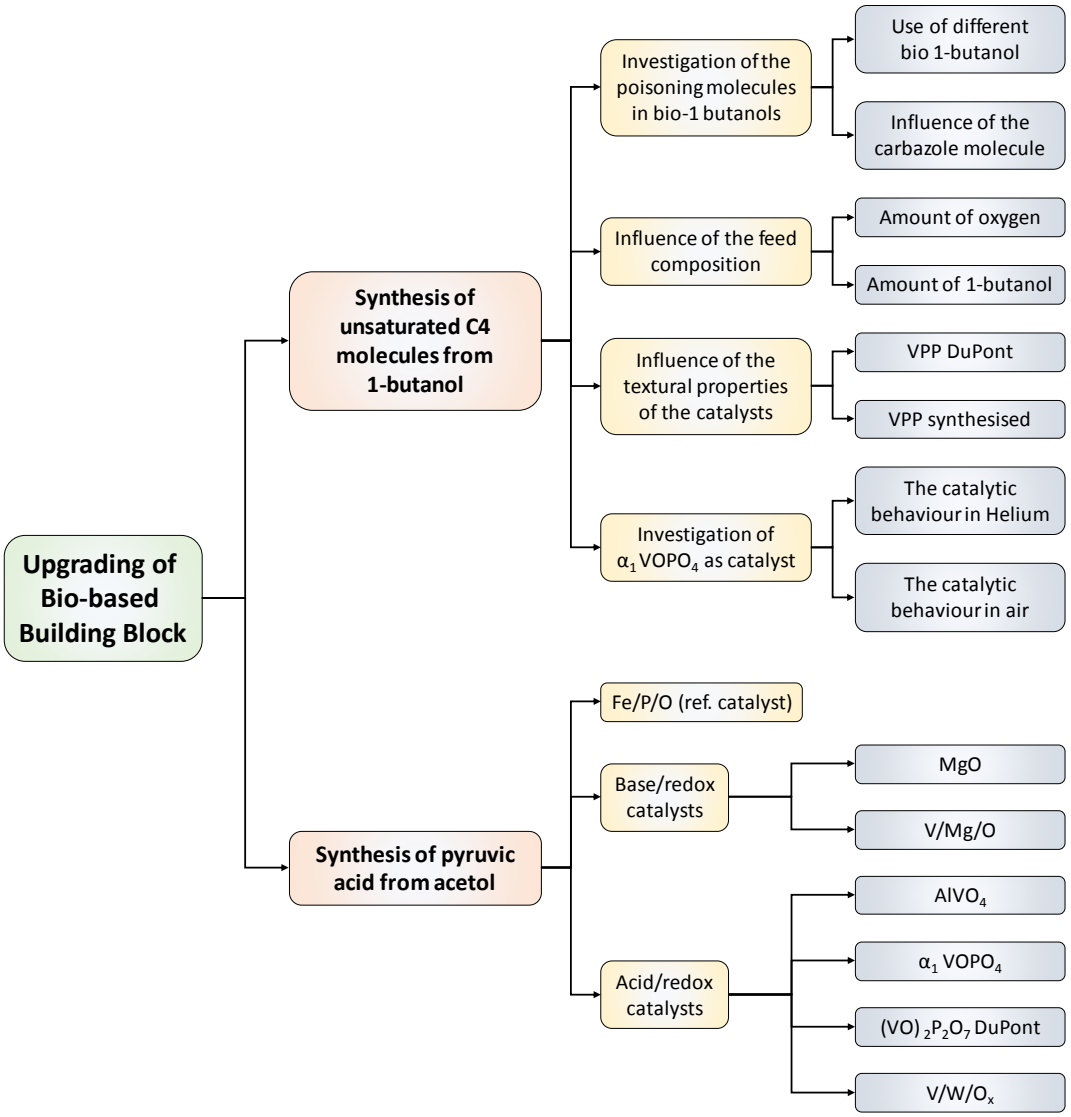

Figure 1-1 Work breakdown Structure of the two processes investigated in this thesis.

2 Biomasses and biorefinery

In the past few decades, the need to reduce dependence on fossil sources in order to decrease greenhouse emissions led the entire scientific community to focus on the development of new processes to produce chemicals, fuels, and energy from renewable sources. The principles of green chemistry [1] and green engineering [2] form the basis of the entire research activity in this field, and the search for a route to transition from the old processes to new processes.

Biomass plays an essential role in this context; in less than 15 years, the transformation of feedstock, such as maize or edible oil seeds, which were in competition against the edible uses (1st generation), to raw materials not in competition with edible materials (2nd generation) has been accomplished [3]. Some examples of such biomasses are plants with high contents of lignocellulosic components; these are grown in fields that are not suitable for food cultivation. Further, they can be obtained from waste from the agricultural and food industries and algae [4].

Along with the evolution of biomasses, the methods to process them have also undergone a shift, from processes to produce syngas, ethanol, and energy to processes to produce molecules of high value, both as intermediates and specialties [5].

Biorefinery is a facility that transforms biomasses (crops, oils, and agricultural waste) into chemicals, fuels, and energy [6]. During the past few years, industries and universities collaborated on several projects in order to harness their combined knowledge. Examples of these collaborations include MATRÌCA (Versalis and Novamont) [7], BETA RENABLES (Chembiotex and TPG) [8], CHEMLOT InSciTe (partnership between DMS and different universities) [9], and

EUROBIOREF (consortium of 29 partners from 15 different countries of the EU). The last, thanks to the involvement of different partners, led to the development of an entire production chain for different chemicals, materials, and energy from biomasses; it was implemented concretely by installing a pilot plant in Norway for the transformation of lignocellulosic raw materials [10].

In general, a biorefinery disassembles biomasses into their basic building blocks and uses them as starting materials to obtain products with high added value and tries to reduce wastage. Due to the huge multiplicity, variety, seasonality, and composition of biomasses, each one needs a different treatment procedure.

Biomasses are generally composed of three parts –oleaginous components, lignocellulose, and protein. Thanks to the development of technology, it is possible to select and grow biomasses characterised by a high content of one of these three parts [11,12].

The first step in the transformation of biomasses is a physical pre-treatment step; it typically consists of crushing, chopping, dry and wet milling, centrifugation, and squeezing to separate the liquid part from the solid, favouring also the successive treatments for this latter [3]. Particular emphasis is paid to the transformation of lignocellulose because it is the major component in biomasses and can be disassembled into simple sugars and phenolic molecules that can be transformed by chemical and fermentative processes. Lignocellulose is a complex matrix composed of three components: cellulose, hemicellulose, and lignin; cellulose is a linear polymer of glucose, in which β-1,4 links are present between sugar molecules. Hemicellulose is a branched polymer composed of C5 and C6 sugars as xylose and fructose linked by

1,2 and 1,4 bonds and lignin is a polymer composed of phenolic monomers, such as guaiacol, *p*-cumaryl, and syringyl alcohols. Pre-treatment of lignocellulose is necessary to destroy the complex structure of the matrix and separate each component in order to facilitate the subsequent processes [13].

After the separation of the constituent parts of the biomass, each component is subjected to a depolymerisation process in order to obtain monosaccharides from cellulose and hemicellulose and phenolic compounds from lignin [14–16]. These molecules are used as the *platforms* to produce several kinds of intermediates, called *building blocks*, by means of chemical or fermentative treatments [17]. Examples of *building blocks* include ethanol, succinic acid, lactic acid, furfural, 5-hydroxyl methyl furfural (HMF), and catechol.

The transformation of the oleaginous and proteinous parts leads to the production of other building blocks from oil seeds, glycerol, and fatty acid methyl esters (FAME) [18]; while from the proteinous part are obtained amino acids[19]. Figure 2-1 depicts the general scheme for the production of chemicals, materials, and fuels from biomasses.

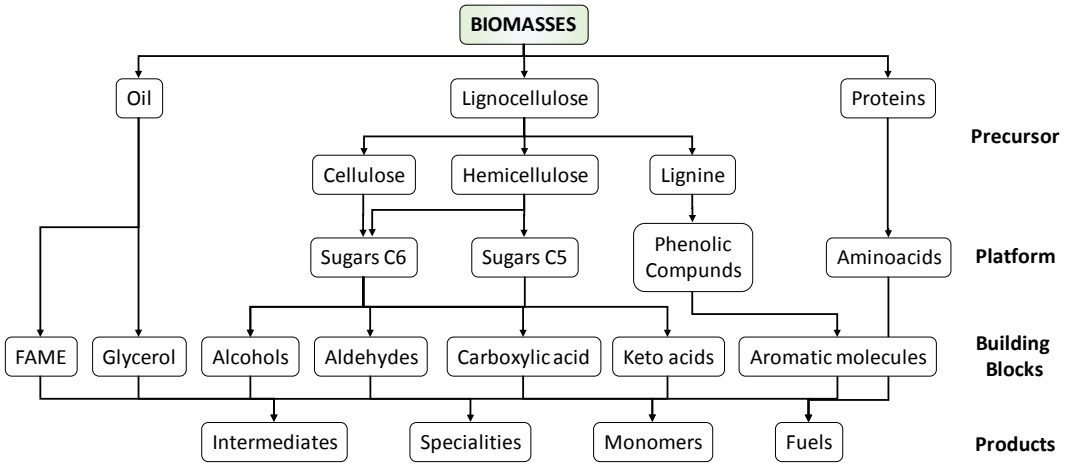

Figure 2-1 General tree scheme of the transformation of biomasses into chemicals, materials, and fuels

The *building blocks* are then transformed into final products via several chemical and biotechnological processes [20]. The transformation of these molecules in a biorefinery leads to the final products, monomers, and specialties, but fuels and intermediates are also produced.

The last two centuries are often considered as the age of polymers, thanks to the discovery and development of thermoset resins, such as Bakelite, thermoplastics, such as polyolefins (polyethylene and polypropylene), polyesters, and polyamides, and rubbers, such as polyisoprene and polybutadiene. Research on these materials is abundant and has been primarily focused on their production processes with an emphasis on high performance and high yield in order to substitute traditional materials, such as metals and ceramics. An extraordinary example of a product in which high-performance polymers have substituted traditional materials is the aircraft Boeing 787; 50% of this new aircraft is composed of polymeric composites, leading to a 20% decrease in weight, which has a positive impact on fuel consumption and maintenance [21].

The continuous growth of the polymer market motivates researchers to investigate the possible uses of biomasses for polymer production via two different routes; the first route involves the development of monomers to substitute the traditional ones derived from fossil sources and the second route is focused on the development of alternative production processes for the same monomers using biomass as the starting material. Examples of the first route include studies on the possible uses of 2,5-furandicarboxylic acid (FDCA) as an alternative to terephthalic acid to produce bottles and films [22] or pelargonic acid for the production of the 3rd generation of Mater-Bi [7]. Examples of the second route include the production of bio-PET, developed and supplied by PepsiCo and The Coca Cola Company; bio-PET is obtained by the transformation of sugars via chemical and fermentative processes into ethylene glycol and terephthalic acid [23,24]. Another example is the 100% bio-based Nylon 6,6 produced by Rennovia via the transformation of glucose into adipic acid and hexamethylenediamine [25]. Several reports are available on the production of light olefins, such as ethylene, propylene, and C_4, from renewable sources [26]. The importance of these molecules lies in their high volumes of production, correlated with the high volumes of production of their corresponding polymers.

3 Vanadium containing catalysts

Vanadium-containing catalysts are one of the most studied catalytic systems, thanks to their peculiar properties deriving from the presence of vanadium ions.

Vanadium has a $4s^2\ 3d^3$ electronic configuration and can assume different oxidation states, but the most common ionic states range from +3 to +5. The different oxidation

states of this element affect all of its properties, such as its Lewis acidity and the coordination geometry it can assume in complexes and solids.

The reduction potential of the couples V^{+5}/V^{+4}, V^{+4}/V^{+3}, and V^{+3}/V^{+2} are +1,00 V, +0,34 V, and –0,36 V, respectively. V^{+2} and V^{+3} ions are present only at very low pH values in the form of $[V^{(II)}(H_2O)_6]^{+2}$ and $[V^{(III)}(H_2O)_6]^{+3}$, while V^{+4} and V^{+5} are present as oxo- and polyoxo-species, respectively, due to the high density of charges on the V ions and their Lewis acid properties [27].

Vanadium can also form different kinds of polyoxo ions, as shown in Figure 3-1, in which it can transform from VO_2^+ into$V_{10}O_{27}(OH)^{5-}$; in other words, from cationic species to anionic species with the possibility of forming different kinds of complexes and salts [28].

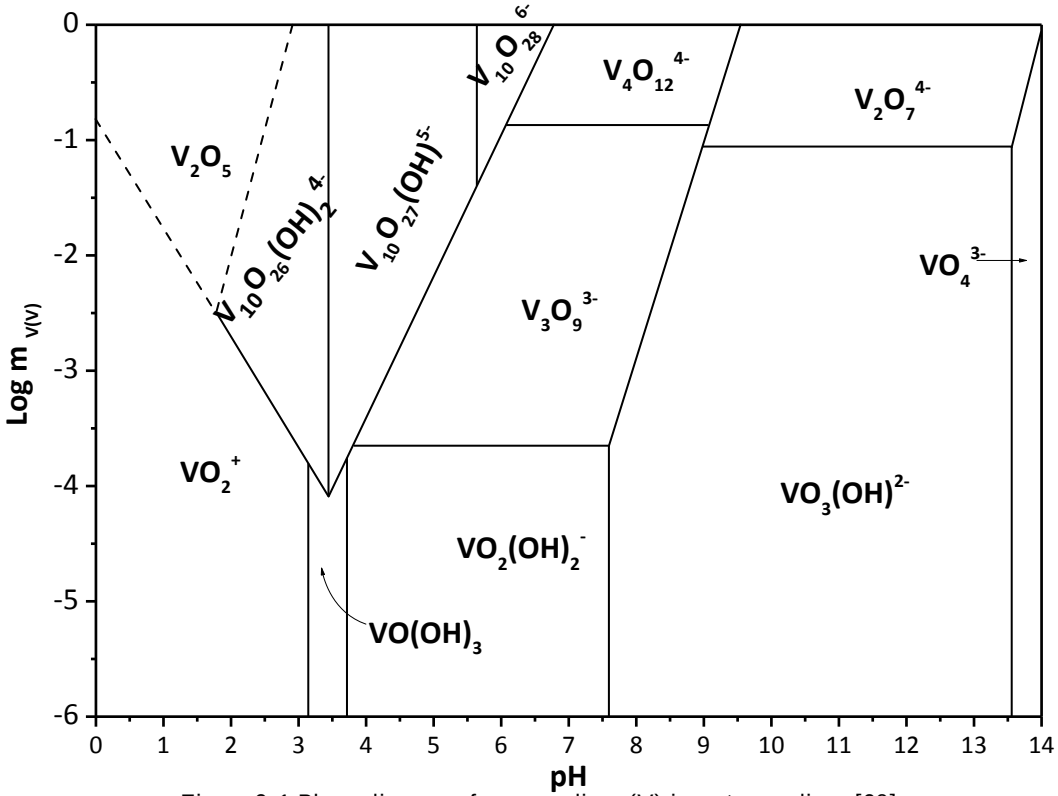

Figure 3-1 Phase diagram of oxovanadium (V) in water medium [28]

Regarding the coordination number (CN) and geometry of the complex, in general, vanadium species can assume variables from 3 to 8 and exhibit a geometry ranging from planar to dodecahedral, even if the most common geometries are tetrahedral and octahedral, as illustrated in Figure 3-2.

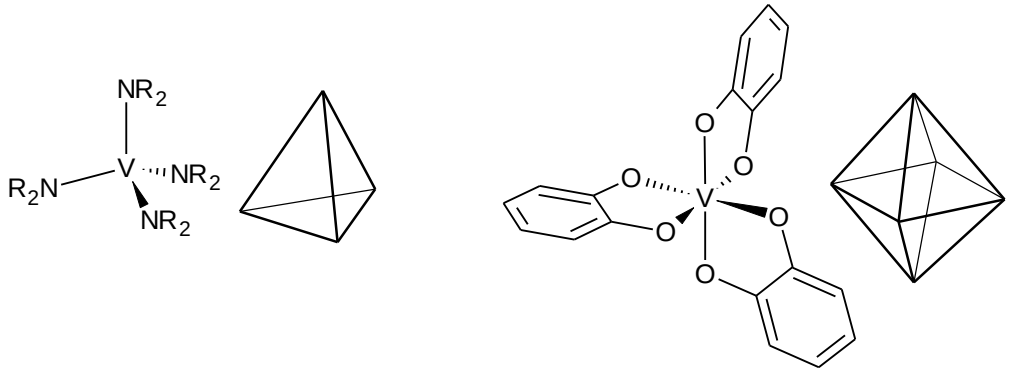

Figure 3-2 Structures of some vanadium complexes with tetrahedral and octahedral structures

As a catalyst, vanadium is one of the most important elements for selective oxidation; examples of industrial processes that use vanadium-containing catalysts are included in Table 3-1.

In the examples cited above, vanadium is present in different oxidation and coordination states together with other elements, both metallic and non-metallic.

The huge variety of vanadium-containing catalysts is correlated to its peculiar properties discussed above, in particular, the CN and geometry of the complexes. The development of these catalysts leads to the investigation of different aspects of the catalytic systems, including the interaction between the active phase and the support and the structure and the oxidation state.

Catalyst	Reaction	Ref.
VO_x/SiO_2	Oxidation of SO_2 to SO_3	[29]
Mo/W/V/O (Mo_5O_{14} type)	Oxidation of acrolein to acrylic acid	[30]
Mo/V/Te/(Sb)/Nb/O (M1 phase)	Ammoxidation of propene to acrylonitrile	[31]
V/P/O	Oxidation of *n*-butane to maleic anhydride	[32]
Mo/V/P/O (Keggin type)	Oxidation of methacrolein to methacrylic acid	[33]

Table 3-1 Vanadium-containing catalysts used in industrial selective oxidation processes

The influence of the interactions between vanadium species and supports has been analysed based on a monolayer of V_2O_5 supported on different oxides, such as Al_2O_3, TiO_2, ZrO_2, and SiO_2. VO_x species could be deposited on the supports creating isolated, polymeric, and monolayers of $[VO_4]$ or V_2O_5 nanoparticles, as shown in Figure 3-3; different species have different catalytic behaviours (in general, nanoparticles are less active) and their formation is correlated with the amount of vanadium ions deposited as well as the interaction between vanadium and the surface of the support.

On comparing different oxides, such as MgO, CeO_2, ZrO_2, TiO_2, Al_2O_3, and SiO_2 as supports, it was found that SiO_2 exhibited the lowest number of V for generating a monolayer, 2 vanadium atoms/nm^2 correspond to the isolated species of VO_4, while the other supports could contain higher amounts of vanadium atoms on the monolayer with a range of 6–8 vanadium atoms/nm^2.

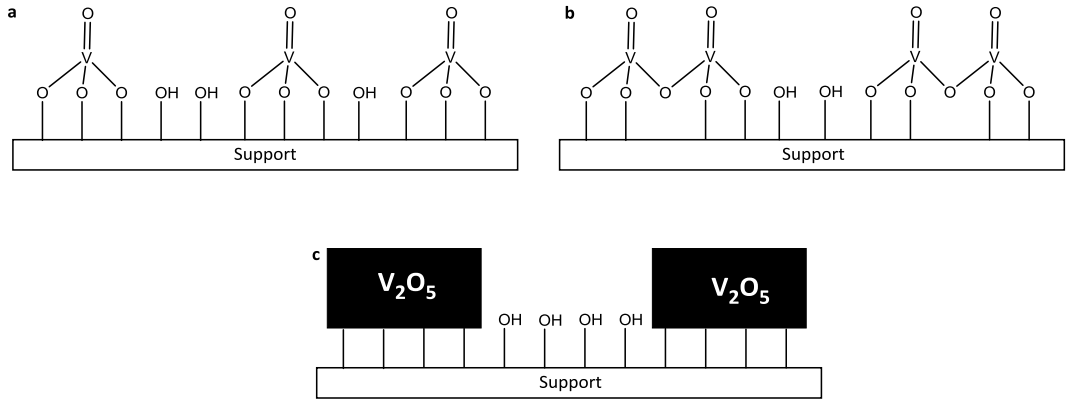

Figure 3-3 Different vanadium oxide species on supports.
a: Isolated vanadate; **b:** polyvanadate; and **c:** nanoparticles of V_2O_5

The difference between the amounts of V species that can be supported on SiO_2 and other supports can be correlated to the low reactivity of the hydroxylic groups present on the SiO_2 surface; this also accelerates the mobility of VO_x towards the surface, leading to aggregated nanoparticles of vanadia. Interaction with the support modifies the reactivity of the vanadium species; an example of this influence can be observed by comparing the reducibility of V^{+5} to V^{+4} using H_2 as the reductant, because the strength of V-O-M and V-O-V modifies the electron density of the VO_x species [34].

The structure of bulk vanadium mixed oxide influences the reactivity of vanadium. An example of this effect can be found in the Mo/W/V/O systems used for the selective oxidation of acrolein to acrylic acid. The capability to form different crystalline structures of molybdenum oxides led to an investigation on which phase is the most active and selective for the oxidation of acrolein into acrylic acid. Typical Mo/O phases can assume monoclinic $Mo(IV)O_2$, orthorhombic $Mo(VI)O_3$, and tetragonal Mo_5O_{14} structures, but only the tetragonal phase is the most active and selective for this reaction [35]. The formation of a M_5O_{14} crystalline structure is strictly correlated with the synthesis and treatment of the precursor that can evolve into an orthorhombic

phase, which is thermodynamically active. Regarding the elements present in the Mo/V/W/O catalyst, the presence of vanadium ions generates redox couples responsible for the selective oxidation reaction, while tungsten ions help to create and maintain a M_5O_{14} type structure [36].

To understand the influence of the oxidation state of V, vanadium/phosphorous oxides can be considered. $(VO)_2P_2O_7$ is the active and selective phase for the gas phase oxidation of *n*-butane into maleic anhydride, but the real catalytic system is much more complex than this; over the years, many efforts have been undertaken to understand the active phase, but this aspect is not yet fully understood. The actual catalyst is composed of different phases of V/P/O, in which vanadium ions assume different oxidation states; $(V^{+4}O)_2P_2O_7$ is the main phase. Other phases, including $(V^{+5}O)PO_4$, are also present along with a little amount of V^{+3} species. The presence and amount of each phase significantly affects the conversion of *n*-butane and selectivity towards maleic anhydride [37].

PART ONE

SYNTHESIS OF UNSATURATED C_4 MOLECULES FROM 1-BUTANOL

1 Introduction

1.1 Market and uses of unsaturated C_4 molecules

Unsaturated C_4 molecules, some of which are illustrated in Figure 1-1, find applications in many fields; they are used as intermediates for other molecules, as monomers (THF), specialties (phthalates), and fuel additives (XTBE) or directly as monomers to prepare polymers.

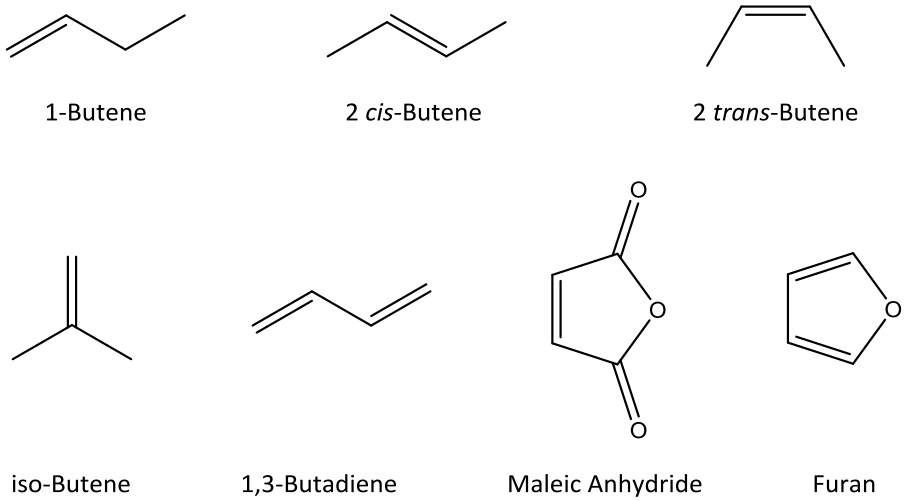

Figure 1-1 Examples of unsaturated C_4 molecules

C_4 olefins are used mainly to produce alkylated gasolines and additives for gasoline, such as MTBE and ETBE; 1-butene is also used in combination with ethylene for the synthesis of propylene by metathesis reaction or as a monomer for the production of polyethylenes [38].

More than of 94% of 1,3-butadiene (1,3-BDE) consumption can be attributed to polymer production, in particular elastomers, such as polybutylene, styrene-butadiene rubber (SBR), and nitrile rubber (NBR), but it can also be used to produce acrylonitrile-butadiene-styrene (ABS) and styrene-butadiene-styrene (SBS) plastics [39].

Another molecule widely used in the polymer industry is maleic anhydride (MA); 70% if its consumption can be attributed to the production of unsaturated polyester resins (UPR) and alkydic resins; the remaining 30% is used as a starting material for producing other molecules. Thanks to the presence of two carboxylic groups and one unsaturated site, MA can undergo different reactions, some of which are listed below and reported in Figure 1-2.

- Hydrolysis leading to the formation of maleic (Z-isomer) and fumaric (E-isomer) acids.
- Cycloaddition reactions, such as the Diels-Alder reaction, using 1,3-butadiene as the diene molecule; the reaction yields aromatic and aliphatic anhydrides, such as phthalic and tetrahydrophthalic anhydrides [40].
- Reduction reactions yielding succinic anhydride, 1,4-butanediole, and tetrahydrofuran.

Furan, and its derivatives, are used as starting materials to produce specialty chemicals used in different fields, including pharmaceuticals, textiles, and dyes [41].

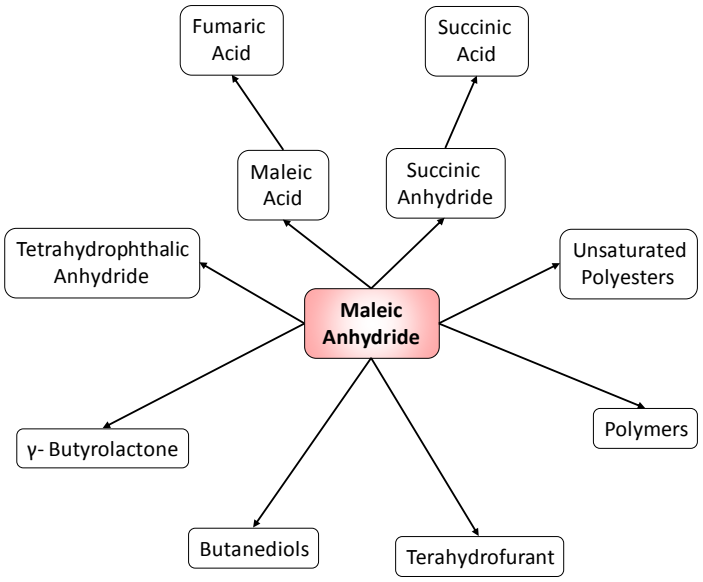

Figure 1-2 Scheme of the main products obtained from maleic anhydride

1.2 Production of C_4 olefins: From old to new processes

The production of olefins is usually carried out inside oil refineries, because more than 80% is used, as mentioned earlier, to produce fuels and additives.

Almost 70% of butane production is based on the fluid catalytic cracking (FCC) process of gas-oil fractions; the outlet steam obtained, denoted as *raffinate 1*, is composed of 1-, 2-, and *iso*-butenes, in which a 1 to 2 butene ratio is close to the thermodynamic value. Further, 26% of butene production is based on the steam cracking process (SCP) of naphtha; here, 50% of the outlet steam consists of 1,3-butadiene. Therefore, it is necessary separate it from the other C_4 molecules by distillation to obtain pure 1,3-BDE and *raffinate 1* steam of the same quality as that obtained from the FCC process. *Raffinate 1* is subjected to a separation step in order to extract *iso*-butene from the mixture because it is used, as mentioned previously, to produce XTBE molecules. The stream containing a mix of linear butenes is denoted as *raffinate 2*; this mix, rich in 1-butene, is subjected to distillation and adsorption in order to separate the two structural monomers. Figure 1-4 illustrates a simplified scheme for the production of C_4 molecules from the main processes.

Only 4%–5% of butane production is based on the dehydrogenation of *n*-butane (BDH); in this case, the outlet stream has the same composition as *raffinate 2*.

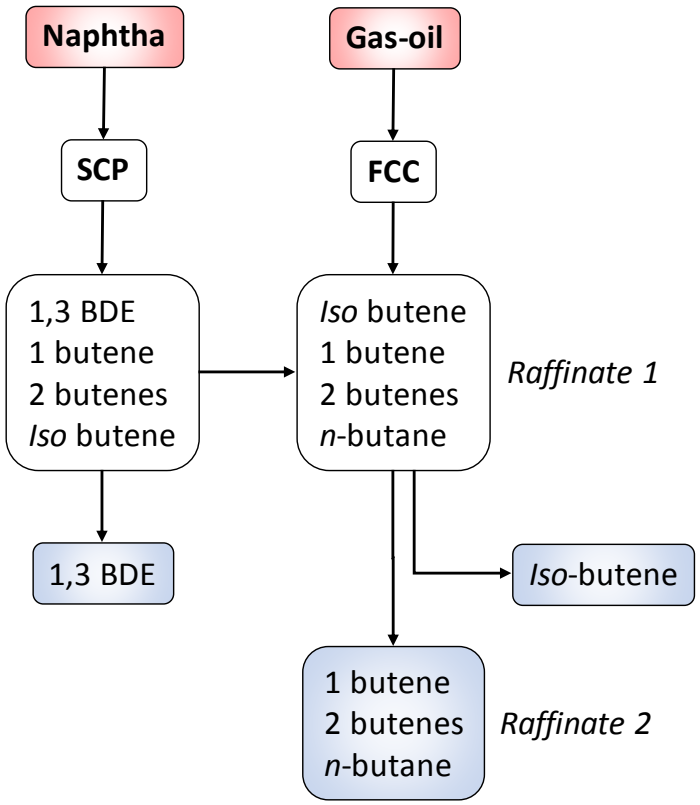

Figure 1-4 General scheme of the production of saturated and unsaturated C_4 molecules

Several processes are currently being studied for the production of olefins and 1,3-BDE from renewable sources and these processes can be divided into two different approaches as shown in Figure 1-3. The first approach is based on the direct transformation of the *building blocks* (see section 0) into the compounds of interest, while the second approach is based on the direct transformation of a *precursor* (see section 0) into a *bio*-naphtha fraction, which could be used along with the traditional naphtha-oil fraction [26]. Figure 1-5

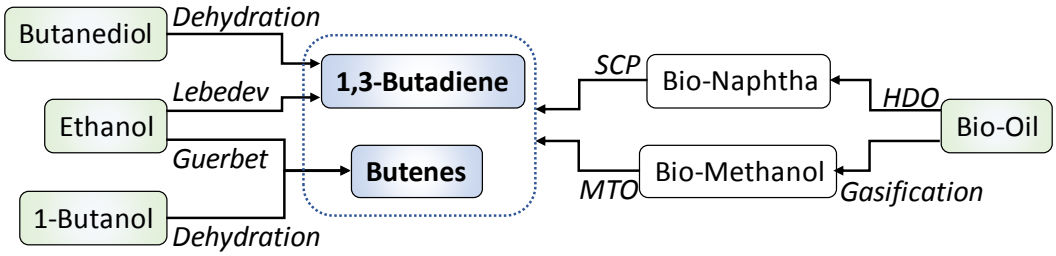

Figure 1-3 General scheme for the production of olefins from renewable sources

Regarding the production of 1,3 BDE from building blocks, the diene could be obtained or from ethanol by two processes, the Lebedev and Ostromislensky reactions, or by double dehydration of different butanediols. The Lebedev and c processes are based on the gas phase condensation of two molecules of ethanol or one of ethanol and one of acetaldehyde, respectively. These processes, which occur in different conditions, need catalytic systems with acidic and basic properties, respectively; the most investigated catalytic systems for these processes are magnesium- and silica-mixed oxides, and they are found to exhibit the best performance in terms of the 1,-BDE yield [42,43].

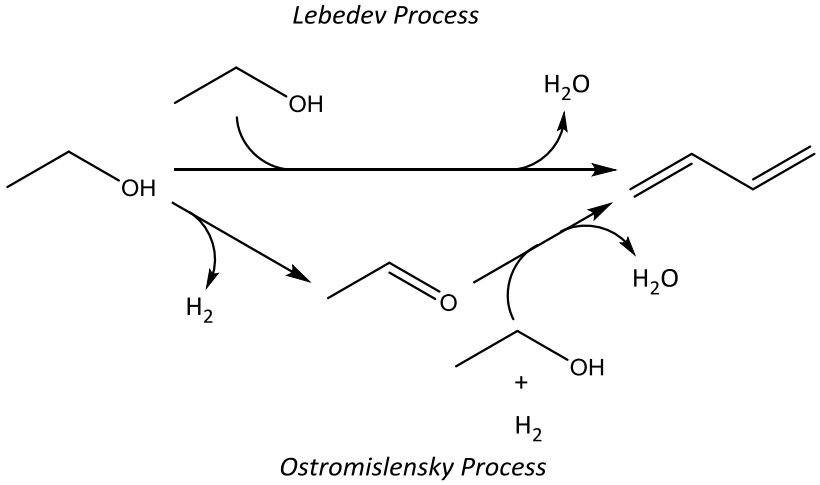

Figure 1-5 Lebedev and Ostromislensky processes for the production of 1,3-BDE

The other process widely used to produce 1,3 BDE is the dehydration of C_4 diols obtained by fermentative processes; however, several problems arise during this process, in terms of selective transformation into 1,3 BDE due to the formation of alkenolic species as intermediates, which can undergo other reactions [44].

Butenes can be obtained by the gas phase dehydration of 1-butanol (see section 1.5 for more details) using acid catalysts with low to medium acidity, such as aluminium oxides and zeolites; the latter are also used for the skeletal isomerisation of linear butenes into

iso-butene [45–47].

Bio-oil, obtained from renewable sources, can be treated to produce bio-naphtha or bio-methanol, which can in turn be transformed into butenes and butadiene. In the case of bio-naphtha, it can be obtained by the hydrodeoxygenation (HDO) of bio-oil; hydrogenation, hydrocracking, deoxygenation, and decarbonylation reactions occur in the presence of H_2 [48]. Bio-naphtha, obtained by the HDO process, can be used in SCP as the naphtha obtained from refineries [49].

Another possible route to transform bio-oil into butenes and butadiene is the gasification of the produced bio-methanol and its successive transformation by methanol to olefins [48,50,51].

1.3 Production of Maleic Anhydride: from old to new processes

National Aniline and Chemicals was the first industry to start the commercial production of MA in 1930 using the Weiss and Downs process with benzene as the

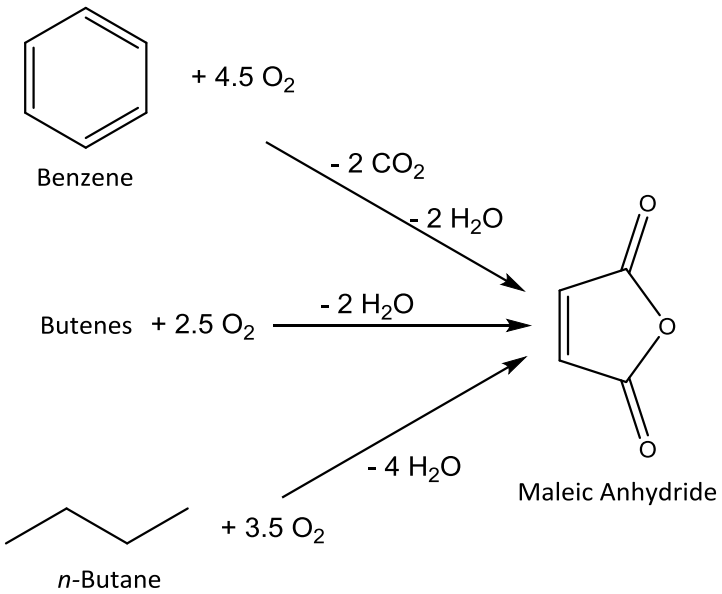

Figure 1-6 General reaction schemes for the industrial production of maleic anhydride by selective oxidation processes

starting material.

Until 1960, the production of MA was based on the selective oxidation of benzene or butenes; however, nowadays, selective oxidation of *n*-butane is considered the main MA production process. Gas phase oxidation of benzene is carried out in a gas phase reactor with a fixed catalytic bed composed of V/Mo species supported on an inert material with high thermal conductivity. The high exothermicity of the reaction necessitates the removal of high amounts of heat in order to avoid the formation of "hot spots" on the surface of the support and prevent secondary reactions that can lead to total combustion [52]. The drawbacks of this process include its low atomic efficiency – 1/3rd of the carbon atoms are converted into CO_2 – and the very high toxicity of benzene; thus, benzene should be completely removed from the outlet gas stream of the reactor in order to adhere to the stringent norms on the emission of carcinogenic compounds into the atmosphere [53]. All of these factors and the increasing price of benzene lead to studies on new processes based on cheaper starting materials, such as C_4 compounds (for e.g., butenes and *n*-butane). The first industrial plants based on these processes were established in the U.S.A. and Europe in 1960, but the olefin process was rapidly abandoned due to its higher price compared to *n*-butane. On the other hand, the selective oxidation of *n*-butane continued to grow until it became the main process for the production of MA globally (at present, there are only a few plants in some developing countries, such as China and India).

The growth of this process is also correlated with the development of catalysts, such as vanadyl pyrophosphate $(VO)_2P_2O_7$ (VPP), which can activate paraffins for selective oxidation. Over several years, different processes have been developed to improve the yield of MA. A general scheme for the production of MA is represented in Figure 1-7

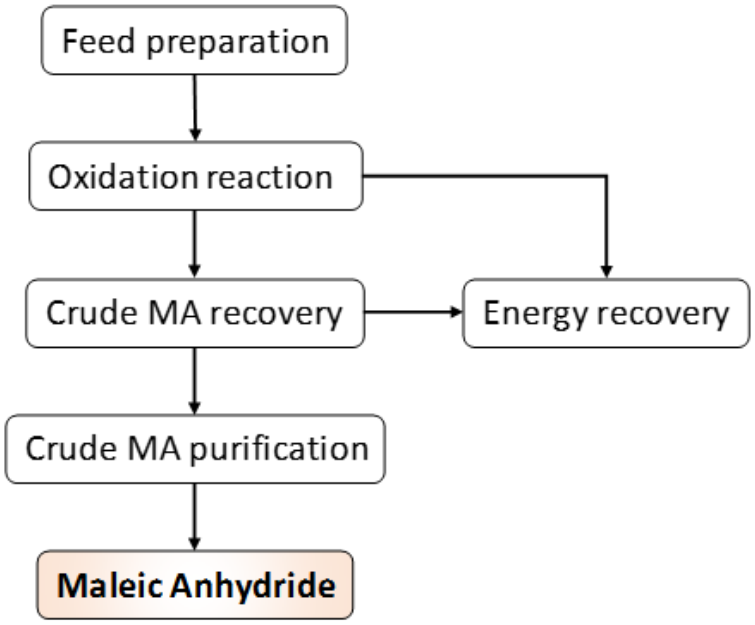

Figure 1-7 General scheme for the production of MA by the selective oxidation of *n*-butane

The feed preparation consists of a mix of reagents with additives used as catalyst promoters. For the oxidation process, different reactor configurations have been developed; fixed, fluidized, and transported reactors were used in the past, but fixed and fluidized reactors are the only industrially used designs now [54]. In a fixed bed reactor, low concentrations of *n*-butane are used in the feed (1,7% in air) at temperatures around 400 °C; under these conditions, the MA yield is around 60%. This configuration also allows the retrofitting of benzene plants. A fluidized bed configuration can work at higher concentrations of *n*-butane in the feed (~4% in air); this leads to a high transformation into MA even if the yield is only around 50%. This process also allows more efficient heat removal and recovery as well as easier catalyst

replacement. A transported bed was used by Dupont in a *circulated fluidized bed reactor* for the production of THF from *n*-butane [55]. This technology is based on the oxidation of *n*-butane by the oxygen lattice of the VPP and re-oxidation of the spent catalyst in another reactor; this approach allows a very high concentration of the alkane in the feed mixture (around 20%), leading to a MA yield of 36%.

The outlet gas from the reactors is sent to the recovery zone; here, MA is separated from the stream by solubilisation in water (aqueous recovery) or in an organic solvent [56]; in the first process, a cheap solvent is used but it might lead to the hydrolysis of the anhydride into dicarboxylic acids; on the other hand, the organic solvent prevents hydrolysis of the anhydride, but it should exhibit low toxicity, a low boiling point, and be capable of dissolving MA. Pure MA is then obtained over two distillation steps in order to remove the solvent and the undesired products synthesised during the reaction.

The outlet gas of the separation process, which contains non-converted hydrocarbons, is sent to an energy recovery unit, where it is incinerated to produce energy for internal uses.

Over the past few years, several studies have been conducted on the production of MA from renewable sources; furanic compounds, such as furfural and 5-hydroxymethyl furfural (HMF), are some of the widely studied chemicals [57] and these mechanisms are illustrated in Figure 1-8.

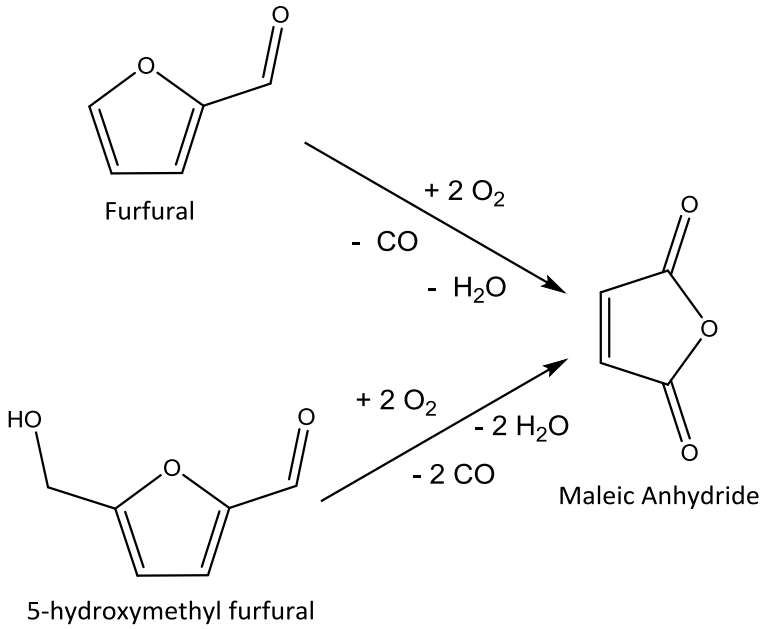

Figure 1-8 General reaction schemes for the production of MA from furanic compounds

Selective oxidation of furfural in the liquid phase was investigated using both homogeneous and heterogeneous catalysts and different oxidants. Phosphomolybdic acid was used as a homogeneous catalyst in a biphasic process in order to minimise undesired reactions, such as polymerisation, using pure oxygen as the oxidant [58]. The biphasic process was carried out using tetrachloroethane and water; oxidation took place in the aqueous phase, in which the catalyst was present along with a low concentration of furfural and oxygen. Under these conditions, furfural was converted into maleic acid favouring then the continuous dissolution in the aqueous phase of the aldehyde. The maximum yield of maleic acid obtained was around 40% with a conversion of 50%. Heterogeneous catalysts were also investigated; different Mo/V mixed oxides were tested and they showed good activity and selectivity towards MA, achieving a complete conversion of furfural and 63% MA yield [59]. The conversion of furfural into MA by gas phase selective oxidation was studied using VO_x/Al_2O_3 as a heterogeneous catalyst because it is known to catalyse the selective oxidation of *n*-

butane into MA [60]. The amount of VO_x species on the surface, furfural/O_2 ratio, and temperature significantly influenced MA yield, which exhibited a maximum value of 70% at 320 °C.

Regarding the oxidation of HMF, there are several reports focused on its liquid phase selective oxidation using molecular oxygen with different homogeneous catalysts. $VO(acac)_2$ exhibited the best catalytic performance, with complete conversion and 50% MA yield [61].

However, all the above described processes face several problems, such as the formation of undesired products, polymerisation reactions, and low atomic efficiency due to decarbonylation and decarboxylation. An alternative to these processes could be based on the transformation of a C_4 molecule obtained from renewable sources. A simple molecule with 4 carbon atoms obtainable from biomasses is 1-butanol (see section 1.5). The selective oxidation of 1-butanol into MA is illustrated in Figure 1-9; it has been investigated previously using a gas phase reaction.

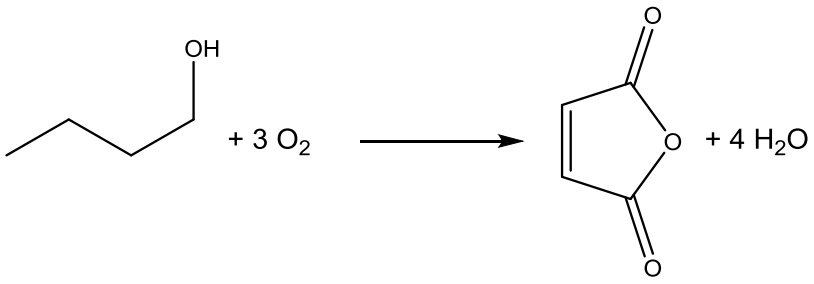

Figure 1-9 Reaction of selective oxidation of 1-butanol into MA

The investigation was carried out in gas phase using air as the oxidant and VPP, supplied by DuPont, as a multifunctional catalyst. The study paid attention to several aspects of the process including those listed below [62].

- Optimization of the operation parameters, such as temperature, partial pressure of the reagent in the feed, and contact time, which led to a MA yield of 38%.
- *In*-situ DRIFT experiments and catalytic tests where possible intermediates were fed led to the hypothesis of a possible reaction pathway, in which the key intermediate is crotonaldehyde, as shown in Figure 1-10.
- It is possible to use bio 1-butanol in the feed mixture and obtain the same results as those obtained with 1-butanol derived from a chemical source, but only if it does not contain any poisoning molecules.

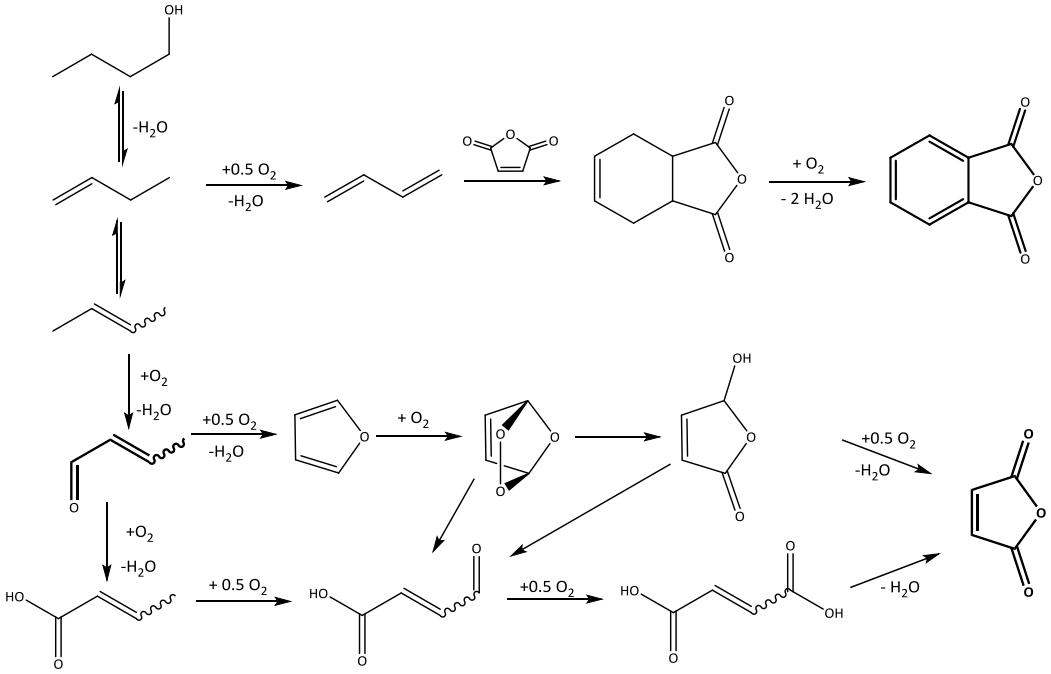

Figure 1-10 Scheme of reaction pathway of oxidehydration reaction of 1-butanol into MA

1.4 Aim of the work

As described in section 1, during the course of my PhD, I investigated the transformation of 1-butanol into butenes and MA by gas phase (oxy)dehydration using different vanadium-containing catalysts in order to improve the productivity of the processes.

The transformation process can be described in terms of the reaction pathway reported in Figure 1-10; it includes two steps – the dehydration of alcohols into respective olefins and the oxidation of olefins into MA. In this context, it is possible to hypothesize three different plant designs, that are reported in Figure 1-11. The first design, named the *two-step approach*, concerns the use of two different catalysts in two distinct reactors; each catalytic system is optimized for each specific reaction operating at the optimum operation conditions. The second and the third approaches use a single reactor but two different catalytic designs. In the *two-pot approach*, two catalysts are used for catalysing both reactions under the same operation conditions.

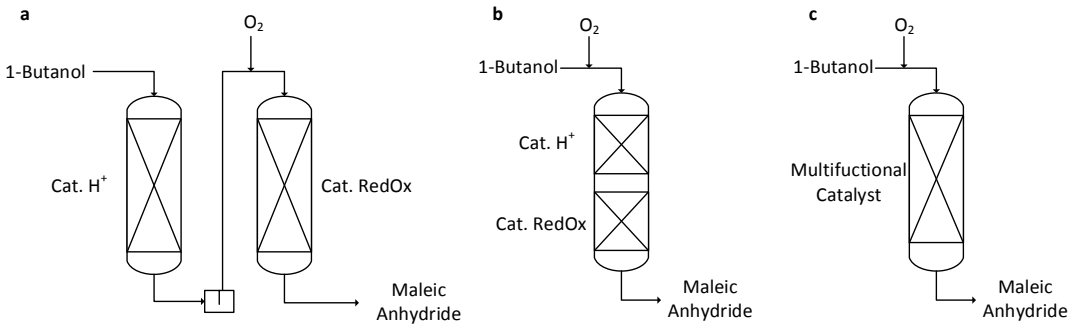

Figure 1-11 Possible plant design for a multi-step process.
a: *Two-step* approach. **b:** *Two-pot* approach. **c:** *one-pot* approach

Meanwhile, the *one-pot approach* allows the use of a multifunctional catalytic system, which possesses all the active sites necessary for catalysing both reactions under the same operation conditions. The *one-pot* approach is used for investigating the transformation of 1-butanol into butenes and MA using a gas phase reaction due to its advantages compared to the other approaches, in particular the lower investment costs and simpler plant management.

Catalytic systems based on $VOPO_4$ and $(VO)_2P_2O_7$ were investigated for the transformation of 1-butanol into butenes and maleic anhydride by gas phase processes,

because these systems present the acidic sites necessary for the dehydration reaction, which leads to the production of butenes; further, redox sites are necessary for the selective oxidation of olefins into MA [63–66].

In the next section, I will describe some aspects of the production of 1-butanol and the properties of the V/P/O systems, in order to explain the reasons behind choosing these species as the reactant and catalysts.

1.5 A C4 biobased building block: 1-butanol

1-butanol is a colourless liquid at room temperature; its properties are listed in Table 1-1

Formula	C_4H_9OH
Molecular weight (g/mol)	74.12
Melting point (°C)	-89.3
Boling point (°C)	118
Viscosity at 20 °C (mPa s)	3.0
Heat of vaporization (J/g)	591.64
Heat of combustion (kJ/g)	36.111
Flammable limits (%vol)	Lower: 1.4; Upper: 11.3
Solubility in water (wt% at 30 °C)	7.85
Solubility of water (wt% 30 °C)	20.62

Table 1-1 Physical properties of 1-butanol

1-butanol finds application as a solvent in paints and surface coatings and it is also used in the production of butyl esters, which are used in several fields, including in polymers (acrylate and methacrylate), plasticisers (phthalate), and solvents (acetate) [67].

The industrial production of 1-butanol relies on two processes based on *oxo-synthesis* and the *Reppe process* using propylene as the starting material; therefore, the price of this alcohol is linked to the price of oil [68] (Figure 1-12).

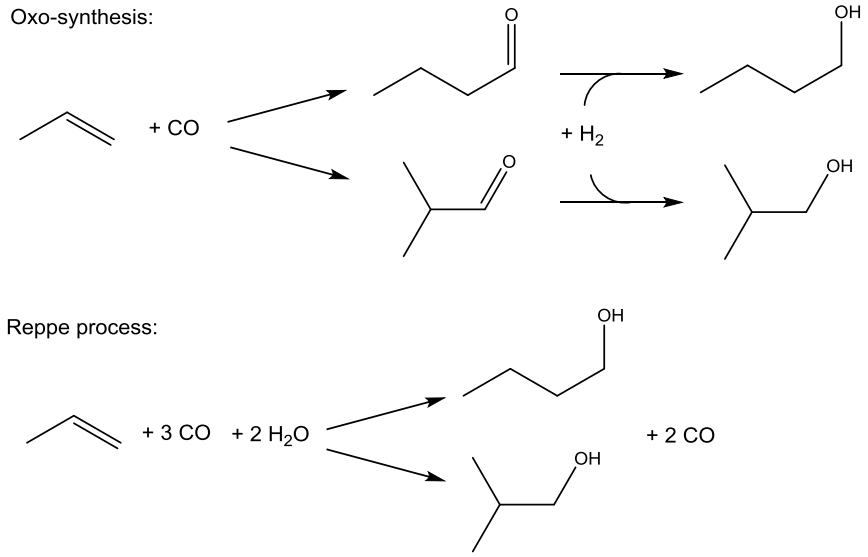

Figure 1-12 Scheme process for the industrial production of 1-butanol

Another process, is the *Guerbet* process, which is based on the condensation of two molecules of ethanol.

Many efforts were undertaken to improve the yield of 1-butanol; mainly, the catalytic behaviour of both homogenous and heterogeneous catalytic systems was investigated using gas and liquid phase reactions.

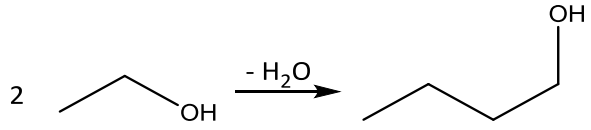

Figure 1-13 Guerbet reaction of ethanol for the production of 1-butanol

Regarding the gas phase reaction, most studies focused on understanding the reaction pathway and studying the catalytic properties necessary for the process, investigating several kinds of heterogeneous catalysts, such as metal oxides, mixed transition metal oxides, and hydroxyapatites [69].

In the case of reaction pathways, they are still being debated. However, literature reports two different pathways. The first includes all condensation, while the second involves a carbanion species [70], as shown in Figure 1-14 and Figure 1-15.

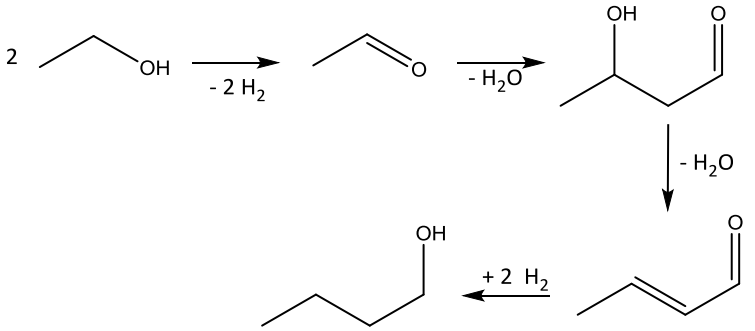

Figure 1-14 Reaction mechanism based on the formation of acetaldol

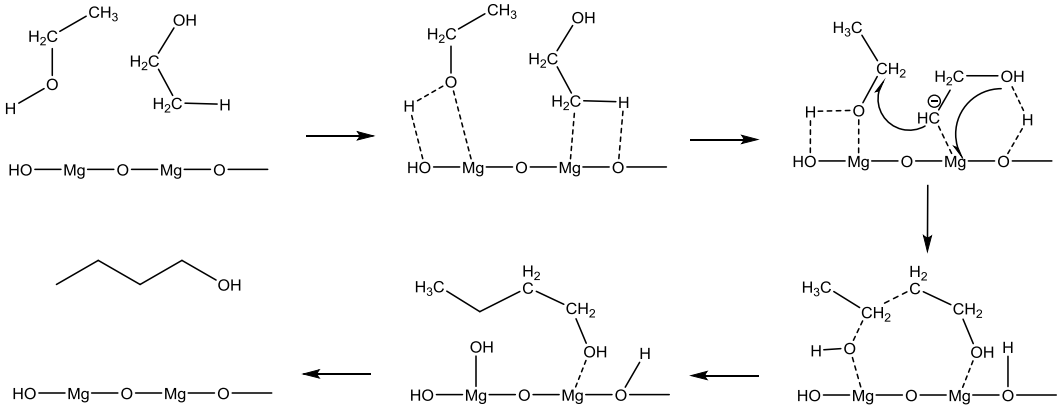

Figure 1-15 Reaction mechanism based on the formation of carbanion species

Furthermore, in the liquid phase, heterogeneous catalysts based on transition metals, such as Ni, Co, and Cu or noble metals, such as Ru, Rh, Pd, Pt, and Au, supported on acidic and basic supports, such as Al_2O_3, CeO_2, and La_2O_3, have been investigated[71]. The results on heterogeneous catalysts indicate low 1-butanol yields; further, they also experienced problems in terms of the stability of the catalyst. One of the problems is

correlated with the complex reaction mechanism and therefore, it is necessary to use catalysts of appropriate acid/base properties.

In the case of homogenous catalysts, N-Ru and N-Rh complexes exhibited the best performance, with selectivity values greater than 80% for 1-butanol but low conversion [72,73]. In this case, the problem lies in the separation and recycling of the catalyst and additives.

Another green route for the production of 1-butanol from biomass is the ABE process, a fermentative process of sugar and biomass using different kinds of *Clostridium* bacteria, such as the *C.acetobutylicum* ATCC 824 and *C.beijerinckii* NCIMB 805212 strains, which leads to the production of acetone, ethanol, and butanol [74,75]. The process was developed during World War I in the United Kingdom. However, it too faces several problems, including a low selectivity towards 1-butanol and the low tolerance of the bacteria used for fermentation towards the butanol produced. A reduction in oil prices led to the abandonment of the ABE process; however, it experienced a revival under the aegis of green chemistry and genetic science. The improvement of bacterial tolerance towards butanol, ability to use renewable sources of low cost, and government funding are leading to the (re)opening of such plants [76].

1.6 V/P/O system: Properties and applications

As described in section 3, vanadium-containing catalysts are used for the selective oxidation of several starting materials; in this context, vanadium/phosphorous oxides have received much attention.

Due to the capability of vanadium and phosphorous to assume different oxidation

states and exist as different species, it is possible obtain different V/P mixed oxides, with different structures and catalytic behaviours.

$(VO)_2P_2O_7$ (VPP) is the V/P/O system that exhibits the best performance, in terms of selectivity, conversion, and productivity for the selective oxidation of *n*-butane into MA. The investigation and development of the catalysts includes different aspects [77], such as those listed below.

- Method of synthesis
- Ratio of the elements in the structure and their oxidation states
- Presence of dopants
- Role of the active sites in the reaction pathway for selective oxidation

Regarding the method of synthesis, the general scheme reported in Figure 1-16 includes three different steps. The first involves the preparation of vanadyl hydrogen phosphate hemihydrate, $(VO)HPO_4{\cdot}0{,}5H_2O$ (VHP), which acts as the precursor for VPP. Thus, the precursor should be thermally treated to obtain the VPP phase, and at the end the activation step, where VPP undergoes superficial transformation for obtain the catalyst with the best performances.

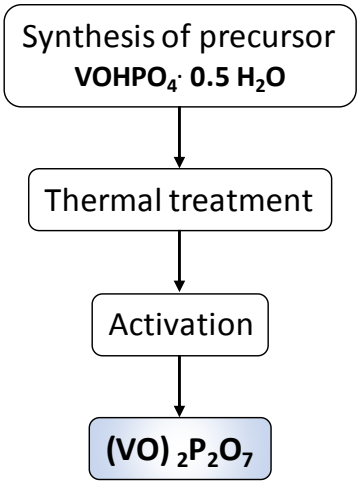

Figure 1-16 Scheme for the synthesis of the $(VO)_2P_2O_7$

The synthesis of VHP can be carried out according to three different synthetic routes, but in general, the process involves the reduction of V_2O_5 into V_2O_4 and its reaction with H_3PO_4. The difference between the three routes lies in the process employed for the reduction of V_2O_5; the oldest is named VPA and is based on the reduction of vanadium oxide with HCl or hydrazine in an aqueous medium [78].

$$V_2O_5 + 2\ HCl \longrightarrow V_2O_4 + Cl_2 + H_2O$$

$$0.5\ V_2O_4 + H_3PO_4 \longrightarrow VOHPO_4 \cdot 0.5\ H_2O + 0.5\ H_2O$$

This method leads to the formation of a precursor with a very low surface area (3–5 m^2/g) and also to the presence of a $VO(H_2PO_4)_2$ phase.

The second route is named VPO and includes reduction of vanadium oxide by alcohols and glycols, such as *iso*-butanol and 1,4-butandiol, in an organic medium [79].

$$V_2O_5 + i\text{-}C_4H_9OH \longrightarrow V_2O_4 + i\text{-}C_4H_8O + H_2O$$

$$0.5\ V_2O_4 + H_3PO_4 \longrightarrow VOHPO_4 \cdot 0.5\ H_2O + 0.5\ H_2O$$

The organic species used to reduce vanadium are trapped inside the crystal structure, thus increasing the surface area of the catalyst as well as its defects; further, it increases the proportion of the (001) plane, which corresponds to the (100) plane of VPP that exhibits the highest density of active sites [80].

The last route is named VPD and is divided into two steps; the first is the formation of $VOPO_4{\cdot}2H_2O$ and it is later followed by reduction by alcohols [81].

$$V_2O_5 + 2\ H_3PO_4 \longrightarrow 2\ VOPO_4 \cdot 2H_2O + H_2O$$

$$2\ VOPO_4 \cdot 2H_2O + i\text{-}C_4H_9OH \longrightarrow VOHPO_4 \cdot 0.5\ H_2O + i\text{-}C_4H_8O + 3\ H_2O$$

This method allows control over the morphology and defects of the precursor; further, it also leads to a high surface area (30 m^2/g). However, the disadvantage lies in the

increased proportion of the non-selective (220) plane.

The precursor is then subjected to a thermal treatment step in order to remove two molecules of water from the lattice, which leads to the formation of the VPP phase. The structure of VHP, reported in Figure 1-17 is composed of pairs of [VO_6] octahedra sharing a face linked by hydrogen phosphate tetrahedral groups. One

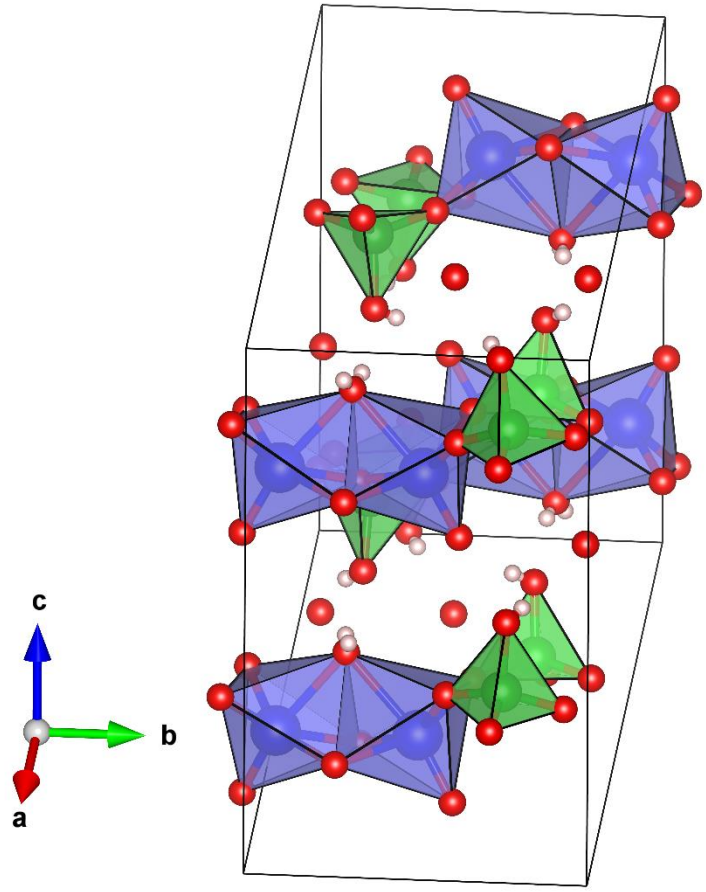

Figure 1-17 Crystalline structure of $(VO)HPO_4{\cdot}0{,}5\ H_2O$.
Blue octahedrals represent the [VO_6]; green tetrahedrals represent the [PO_4]

molecule of water is shared between two adjacent vanadium atoms oriented in the *trans* position with respect to the V=O bonds; it leads to the formation of a layered structure. The layers are held close to each other by hydrogen bonds between the P-OH groups [82].

Synthesis by the VPO method leads to the insertion of organic species between the layers, which decreases the distance between the planes and favours the formation of crystals with higher exposure of the (100) plane, which is responsible for the selectivity towards MA [80].

VPP phase is built of pairs of [VO_6] octahedra linked through a common hedge, forming double chains of octahedral connected by the hedge-oxygen in the *c* direction and by pyrophosphate groups, with a phosphorous-bridge bond. Along the chains, single bond V-O and double bond V=O are alternate, respectively 1.60 Å and 2.30 Å long as reported in Figure 1-18.

The transformation of VHP into VPP involves a *topotactic* rearrangement of the structure. It involves the loss of two molecules of water, one of which is shared between two vanadium atoms, while the second molecule of water is formed due to the condensation of two hydrogen phosphate groups to form a pyrophosphate group.

$$2\ VOHPO_4 \cdot 0.5\ H_2O \longrightarrow 2\ VOHPO_4 + H_2O$$

$$2\ VOHPO_4 \longrightarrow (VO)_2P_2O_7 + H_2O$$

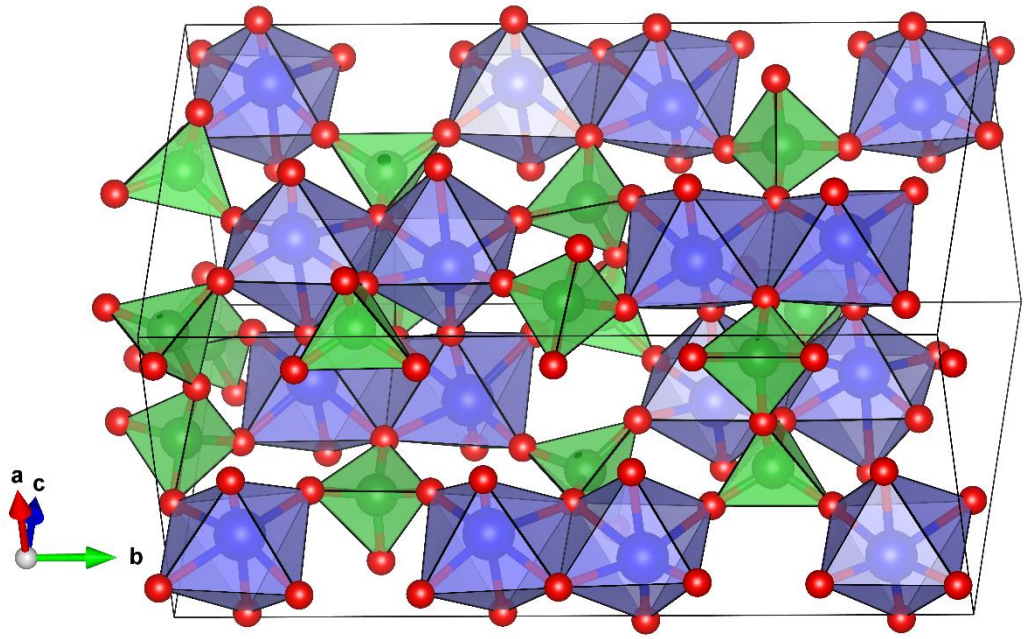

Figure 1-18 Crystalline structure of $(VO)_2P_2O_7$.
Blue octahedrals represent the $[VO_6]$; green tetrahedrals represent the $[PO_4]$

Different thermal treatments have been developed to remove both water molecules and organic (VPO/VPD) or inorganic (VPA) residues in order to enhance the formation of the VPP phase. Generally, the process is divided into two steps. The first is carried out at a low temperature (under 350 °C) in the presence of oxygen to remove the residues and avoid the oxidation of V^{+4} ions and the second step is carried out at higher temperature in an inert atmosphere to remove water molecules, thus leading to the topotactic transformation of VHP into VPP.

The VPP obtained after thermal treatment does not exhibit the best catalytic performance. For this reason, it is necessary to include an *activation* or *equilibration* process during the feeding of the *n*-butane/air reaction mixture. This step favours several superficial transformations leading to the formation of different oxidation states of vanadium and phosphorous oxides, creating a complex and stable mosaic of V/P/O systems [83]. In general, the P/V ratio is in the range 1.05–1.1, with the

average oxidation state of vanadium in the range of 4.00–4.05.

The P/V and V^{+4}/V^{+5} ratios are the main parameters affecting the catalytic behaviour of the VPP catalysts. The P/V ratio influences the formation of some $VOPO_4$ phases over others; a ratio greater than 1 (near 1.02) helps the formation of a δ phase, which is the most selective towards MA but less active, but a higher ratio leads to the formation of an inactive α $VO(PO_3)_2$ phase. A ratio equal to or lower than 1 helps the formation of an α phase, which is more active but less selective for the oxidation of *n*-butane [84].

The V^{+4} and V^{+5} species are involved in the selective oxidation of *n*-butane into MA according to the Mars van Krevelen mechanism [85]; the amount and kind of each vanadium ion species significantly affect the process and are also strictly correlated to the operation conditions of the process. This increases the difficulty in finding the exact ratio between all the phases present on the surface [86].

Regarding the role of the dopant species, the effects of various elements on the acidity responsible for the activation of C-H for the selective oxidation of *n*-butane, prevention of over-oxidation of the products, reducing the activation time of the catalyst, and controlling the redox properties by modifying the V^{+4}/V^{+5} ratio, are studied.

Many elements have been investigated as dopant elements [86,92,93] and some of them that increase the performance of the reaction for the selective oxidation of *n*-butane into MA are reported in Table 1-2.

Dopant	Effect of the dopant	Ref.
Co	Control of the optimal V^{+4}/V^{+5} surface ratio and the Lewis acidity	[87]
Ce+Fe	Improvement of redox properties	[88]
Fe	Fe replaces V^{+4} in VPP phase increasing the re-oxidation rate	[89]
Ga	Increase of surface area and the intrinsic activity	[90]
Nb	Increase the acidity, defects and the oxidation state of the surface	[91]

Table 1-2 Main dopant elements in the VPP catalyst for the selective oxidation of *n*-butane into MA

Vanadyl pyrophosphate is a complex system with a large number of phases and a variety of species, which are involved in catalytic processes; VPP finds application not only in the selective oxidation of *n*-butane, but also in other reactions, some of which are reported in Table 1-3 [94].

Type of reaction	Reagent	Product
Oxidative dehydrogenation	Isobutyric acid	Methacrilic acid
	Alkanes	olefins
Allylic oxidation	Olefins	Diolefins
	2,5-dihydrofuran	furan
Electrophilic O-insertion	Methacrolein	Methacrilic acid
	Furan	Maleic anhydride

Table 1-3 Some reactions catalysed by VPP

The ability of VPP to catalyse a wide variety of reactions can be attributed to its different active sites, such as those listed in Table 1-4.

Active sites	Main function
Lewis acidic sites (Vanadium)	Alkane activation
Bröensted acidic sites (P—OH)	H-abstraction and product desorption
Redox couple: V^{+4}/V^{+5}, V^{+3}/V^{+4}	Alkane activation
Redox couple: V^{+3}/V^{+5}	Several hypothesis
Bridged oxygen: V-O-V and V-O-P	ODH and oxygen insertion
Terminal oxygen: $(V=O)^{3+}$, $(V=O)^{2+}$	Oxygen insertion
Adsorbed molecular oxygen: species η^1-peroxo and η^2-superperoxo	Total combustion to CO_x

Table 1-4 Active sites present on the VPP catalytic surface

The Lewis and Bronsted sites, deriving from vanadium ions and P-OH groups, respectively, are correlated with C-H bond activation and H-extraction from the substrate [95]. In the case of vanadium ions, $(V=O)^{+3}$ species are active in oxygen insertion, while $(V=O)^{+2}$ ions are involved in H-extraction and allylic oxidation [96]. However, the role of V^{3+} is not completely clear; it is theorised that small amounts of V^{3+} and its associated anionic vacancies could positively affect catalytic activity. Bridge oxygens of the V-O-P species are involved in the oxidative dehydrogenation (ODH) of paraffins to olefins and the adsorbed molecular oxygens in the η^1-superoxo and η^2-peroxo species are responsible for the over-oxidation reaction owing to their strong and non-selective nucleophilicity.

2 Experimental Part

2.1 Catalysts preparation

Vanadyl pyrophosphate Dupont (VPP)

The VPP catalyst was vanadyl pyrophosphate delivered by DuPont, which used in process for the oxidation of *n*-butane into MA in a circulating-fluid-bed reactor. Details concerning the characteristics of the catalysts are reported in the literature [97]

Vanadyl pyrophosphate by organic medium synthesis (VPO)

The VPO catalyst was prepared by the organic route: $(VO)HPO_4 \cdot 0.5H_2O$ (VHP), precursor of vanadyl pyrophosphate, was synthesized by suspending the desired amounts of V_2O_5 (99% Sigma Aldrich) and H_3PO_4 (98% Sigma Aldrich) in isobutanol (99% Sigma Aldrich) in order to have a P/V ratio equal to 1.1. Figure 2-1 shows the equipment (a three-necks flask) used for the VPO precursor synthesis.

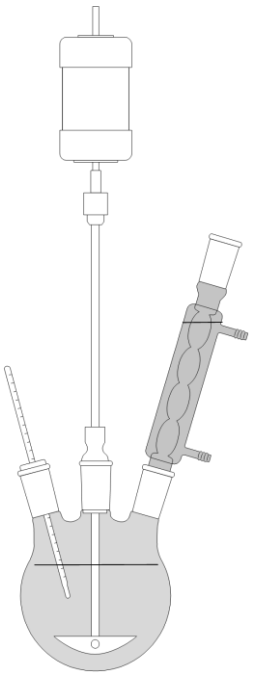

Figure 2-1 Apparatus for lab-scale catalyst synthesis

The precipitation of hemihydrate acid vanadyl orthophosphate occurred through the reactions reported in paragraph 1.6. The mixture was heated at reflux temperature (120°C) for 6 h. The colour varied from dark orange of V_2O_5, to an intense light blue, which is characteristic of $(VO)HPO_4 \cdot 0.5H_2O$. After filtration, the obtained precipitate was thermally treated according to the following procedure:

- drying at 120°C for 12 h in static air to obtain **VHP**;
- pre-calcination in flowing air (130 ml/min), with temperature gradient (1°C/min) from room temperature up to 300°C, followed by an isothermal step at 300°C in air for 6 h;
- thermal treatment in flowing N2 (17 ml/min), with temperature gradient (1°C/min) from room temperature up to 550°C, and final isothermal step at the latter temperature for 6 h for obtaining the **VPO** catalyst.

Vanadyl phosphate dihydrate (VPD)

$VOPO_4 \cdot 2H_2O$ (VPD) was synthesised by suspending the desired amounts of V_2O_5 (99% Sigma Aldrich) and H_3PO_4 (85% Sigma Aldrich) in water. Phosphoric acid was added in excess (P/V= 4), since in a stoichiometric amount, it does not permit the complete dissolution of V_2O_5 and leads to incomplete conversion of vanadium pentoxide. The equipment used for VPD synthesis is the same as that shown in Figure 2-1. The mixture was heated at reflux temperature (100°C) for 17 h, under vigorous stirring: the colour changed from dark orange of V_2O_5 to bright yellow, indicating the formation of $VOPO_4 \cdot 2H_2O$. The mixture was left for one day at ambient temperature, and the solid obtained was recovered by filtration and dried for few hours at 100°C.

Calcination was performed over the catalyst directly inside the laboratory-scale reactor from room temperature up to 440°C, followed by an isothermal step at 440°C for 24 hours.

2.2 Laboratory-scale plant tests

Catalytic tests were carried out in a continuous-flow, fixed bed, quartz reactor. The system permits variation of different reaction parameters: feed composition, contact time, and temperature. The laboratory plant is schematized in Figure 2-2. The apparatus could be divided into three main parts:

- Feed part
- Reaction part
- Downstream part

Feed part:

Gases (He, air) were fed to the reactor, in separated streams or simultaneously, by two mass-flow meters, and their flow was measured using a bubble flow meter; 1-butanol was fed by a syringe pump, which was properly calibrated for the desired quantity of liquid flow. 1-butanol was vaporized in the reactor inlet line, which was heated to 160°C, where the gases mixed. The entire inlet flow could be sent to the reactor and or to the gas chromatograph, in order to check the real entrance flow.

Reaction part:

The fixed bed reactor is a quartz tube, operating at atmospheric pressure. The thermocouple is positioned in the inner part of reactor inside a thin quartz tube at the level of the catalytic bed. The reactor is inserted inside a Lenton oven LFT 12/25/250

with inner diameter of 2.5 cm and external diameter of 25 cm. The exit of the reactor emerging outside the oven is wrapped with a heater string kept at 220°C, in order to prevent crystallization and condensation of the products.

Downstream part:

Upon exit from the reactor, the flow of gas products is split: one part is sent for on-line GC-FID analysis by opening the on/off valve; the other part is passed through a crystallizer, then to a glass bubbler filled with acetone, in order to condense the remaining organic products in the crystallizer, and then sent for on-line GC-TCD analysis.

Product Analysis:

The reactants and products were analysed using a Varian CP-3380 gas chromatograph, equipped with the following columns and detectors:

- Semicapillar CPSil-5CB column (30 m length; i.d. 0.53 mm; stationary phase of 100% dimethylpolysiloxane with a thickness of 3.00 μm). This column separates the maleic anhydride, by-products (acetic acid, acrylic acid, and other light compounds, e.g., butenes), and 1-butanol (in and out). The correspondent detector is a FID.
- Packed Carbosieve SII column (2 m length, stationary phase of active carbons having dimensions of 80–100 mesh). In this column, CO, CO2, H2O, O2, and N2 are separated and detected by a TCD.

The carrier gas used is He, and the temperature ramp program of the oven is as follows: 7 min at 40°C, after which the temperature is increased up to 220°C at 30°C/min, and this is followed by a final isothermal step at 220°C for 10 min.

It is worth noting that both the semicapillary column and the packed column are connected for on-line analysis using a six-way valve for each analysis: the sampling loop valve for the FID analysis is about 350 μL and is maintained at 200°C, while the sampling loop valve for the TCD analysis is about 500 μL and is maintained at 40°C.

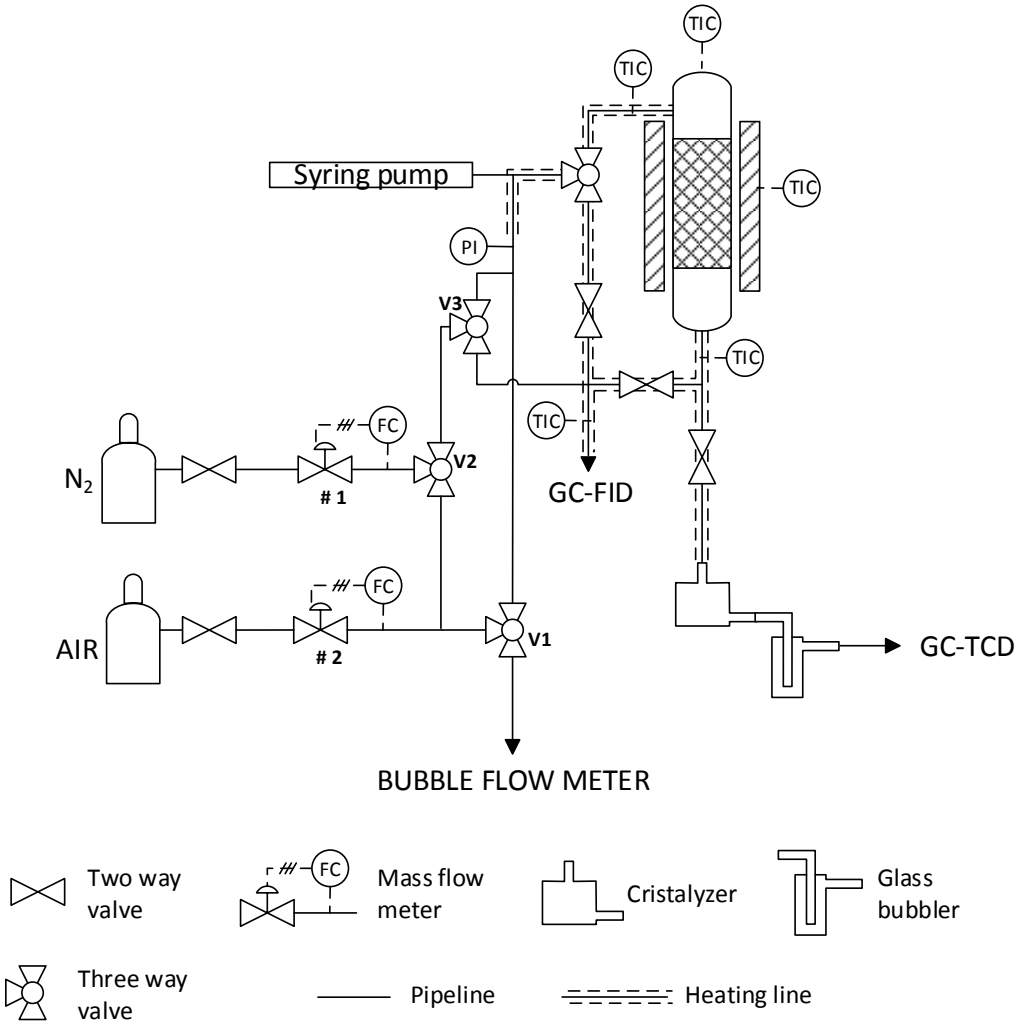

Figure 2-2 Scheme of laboratory-scale plant tests

2.3 Data elaboration: conversion, yield, and selectivity

Through gas chromatograph analyses, the percentage values of conversion, yield, and selectivity were determined, by using the following equations:

$$Conversion = \frac{mol\ of\ converted\ reactant}{mol\ \ of\ fed\ reactant} \times 100$$

$$Yield_x = \frac{mol\ of\ product_x/stoichiometric\ coeff.}{mol\ \ of\ fed\ reactant/stoichiometric\ coeff.} \times 100$$

$$Selectivity_x\ = \frac{Yield_x}{conversion} \times 100$$

$$Carbon\ balance = \frac{\sum Yield}{conversion} \times 100$$

2.4 Catalyst characterization

Raman spectroscopy

Raman analyses were carried out using a Renishaw Raman System RM1000 instrument, equipped with a Leica DLML confocal microscope, with 5x, 20x, and 50x objectives, video camera, CCD detector, and laser source Argon ion (514 nm) with power 25 mW. The maximum spatial resolution is 0.5 μm, and the spectral resolution is 1 cm^{-1}. For each sample, a wide number of spectra were collected by changing the surface position. The parameters of spectrum acquisition are generally selected as follows: 5 accumulations, 10 s, 25% of laser power to prevent sample damage, and 50x objective.

In-situ Raman experiment

In-situ Raman experiment analyses were performed using a commercial Raman cell (Linkam Instruments TS1500). Approximately 5-10 mg of the sample was used for the analysis. The gas flow, fed from the start of the experiment, was about 10 ml/min of air. Spectra were recorded at room temperature (rt), while the temperature (heating rate of 100°C/min) was increased up to the desired temperature during the isotherm period. The laser power used was 25%, which permits good spectrum acquisition without damaging the sample; the other acquisition parameters were as follows: 10 accumulations, 10 s each; 20x objective.

X-ray powder diffraction

The X-ray powder diffraction (XRD) measurements were carried out using a Philips PW 1710 apparatus, with Cu Kα (λ = 1.5406 Å) radiation in the range of 5°<2θ <60°, with steps of 0.05 grade, and signal acquisition for 3 s in each step. Reflects attribution was done by the Bragg law, by using the d value: 2d sen θ = nλ and by comparing the results obtained with those reported in literature.

Specific surface area (BET single point)

The specific surface area was determined by N_2 adsorption at -196 °C (the boiling T of nitrogen), with a Sorpty 1750 Instrument (Carlo Erba). The sample was heated at 150°C under vacuum, to eliminate water and other molecules eventually adsorbed on the surface. After this pre-treatment, the sample temperature was maintained at -196 °C in a liquid nitrogen bath, while the instrument slowly sent gaseous N_2, which was adsorbed on the surface. Using the BET equation, the volume of monolayer and

finally the sample surface area could be calculated.

Thermogravimetric analysis:

The thermogravimetric analysis was performed using a DST Q 600 of TA instrument, under air flow (30 ml/min), from room temperature up to 450°C, with two heating rates: first, 5°C/min until 200°C and relative isotherm for 10 min; second, 10°C/min until 450°C and an isotherm for 20 min.

Energy Dispersive X ray spectroscopy:

Energy dispersive X-ray spectroscopy (EDX) analysis was performed using a LINK ISIS Oxford instrument, with the SEMQUANT program that introduces ZAF correction. The acquisition time for all elements was 100 s.

Temperature programmed surface reaction experiment:

Temperature programmed surface reaction (TPSR) experiments were carried out with methanol as the probe molecule, using the Autochem II of Micromeritcs associated to a mass spectrum detector MKS Cirrus. The sample was subjected to an initial pre-treatment, by heating at 300°C under He, in order to clean the surface from the adsorbed molecules. The adsorption was carried out at 100°C by pulsing methanol vapours (0.0414 mol%) in the helium flow, which was repeated 50 times, for saturating the surface with the probe molecule.

Desorption was realized by feeding helium and heating the sample at 5°C/min from 100°C until 550°C and the isotherm at that temperature for 30 min. A part of the outlet gases was sent to the mass spectrum detector.

3 Results and discussion

3.1 Characterization of vanadyl pyrophosphate

The catalysts tested for the (oxi)dehydration reaction of 1-butanol into olefins and MA were characterized by Raman spectroscopy, XRD, EDX, TGA, and BET surface area analysis.

3.1.1 Vanadyl pyrophosphate Dupont (VPP)

Vanadyl pyrophosphate catalyst delivered by DuPont was in the form of spherical powder composed by a core of vanadyl pyrophosphate and shell of porous silica.

Raman spectroscopy

To verify the phases present on VPP DuPont catalysts, a series of spectra was collected by changing the focused position over the sample. The spectra of the fresh catalyst are reported in Figure 3-1 and present characteristic bands at 1177, 1124, 1013, and 915 cm^{-1} of the VPP phase.

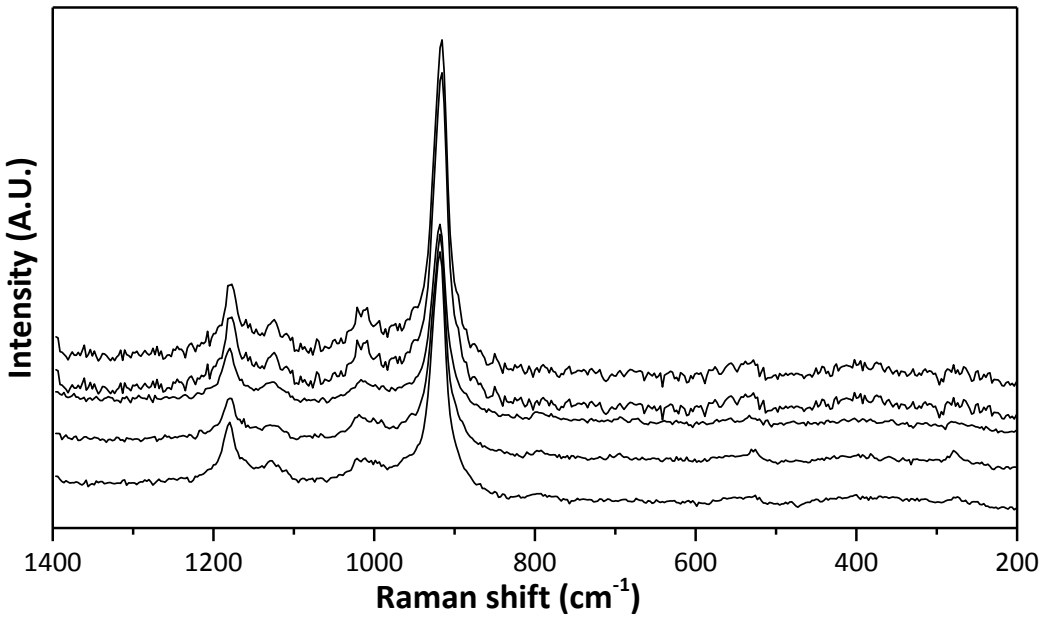

Figure 3-1 Raman spectra of VPP Dupont acquired on different spots of the catalyst

X-ray diffraction analysis

XRD analysis on the fresh VPP DuPont catalyst reported in Figure 3-2 confirms the presence of the VPP phase.

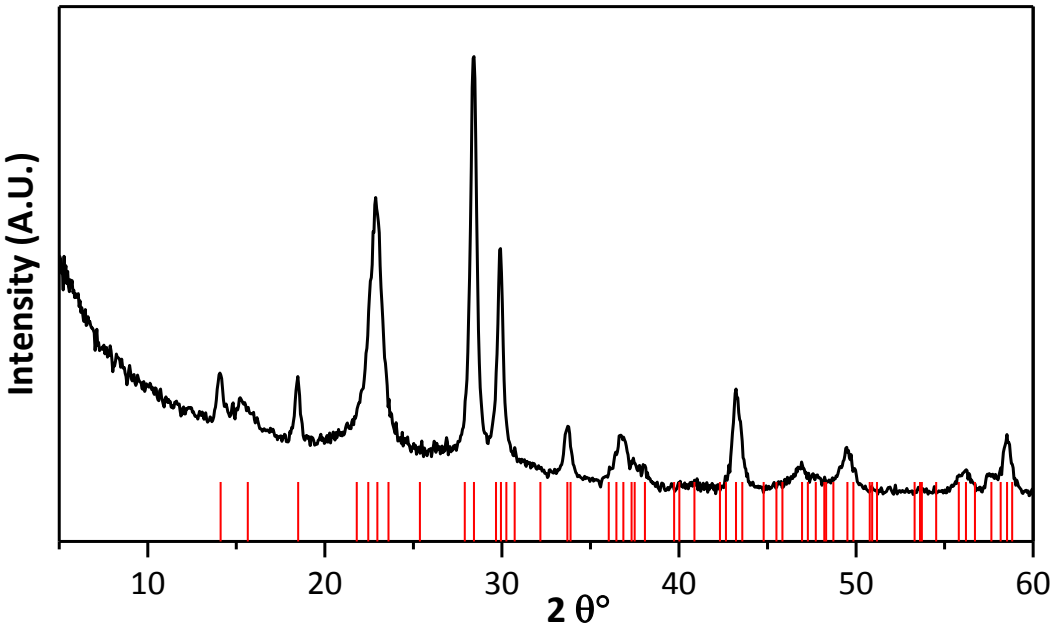

Figure 3-2 XRD analysis of VPP DuPont. Red lines represent the pattern of $(VO)_2P_2O_7$

Elementary analysis by EDX spectroscopy

The elementary analysis by EDX spectroscopy confirmed the presence of 12 wt% SiO_2 and showed a P/V ratio equal of 1.02.

BET analysis

The surface area of the sample was measured by the BET method. For the fresh catalyst, this value is 40 m^2/g.

3.1.2 Synthetized vanadyl pyrophosphate (VPO)

Raman spectroscopy of precursor (VHP)

The Raman spectra acquired on different spots of the precursor show the band 980 cm^{-1} attributable to the vanadyl hydrogen phosphate hemihydrate phase. The absence of other bands confirms the absence of other phases and the complete transformation of V_2O_5 into $(VO)HPO_4 \cdot 0{,}5\ H_2O$.

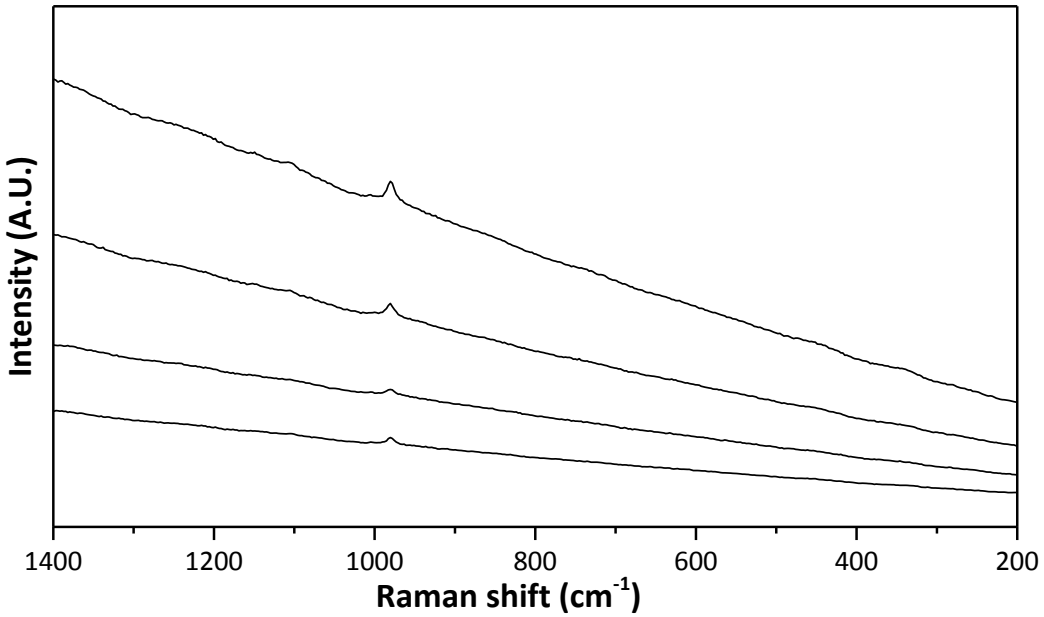

Figure 3-4 Raman spectra of VHP precursor of VPO.

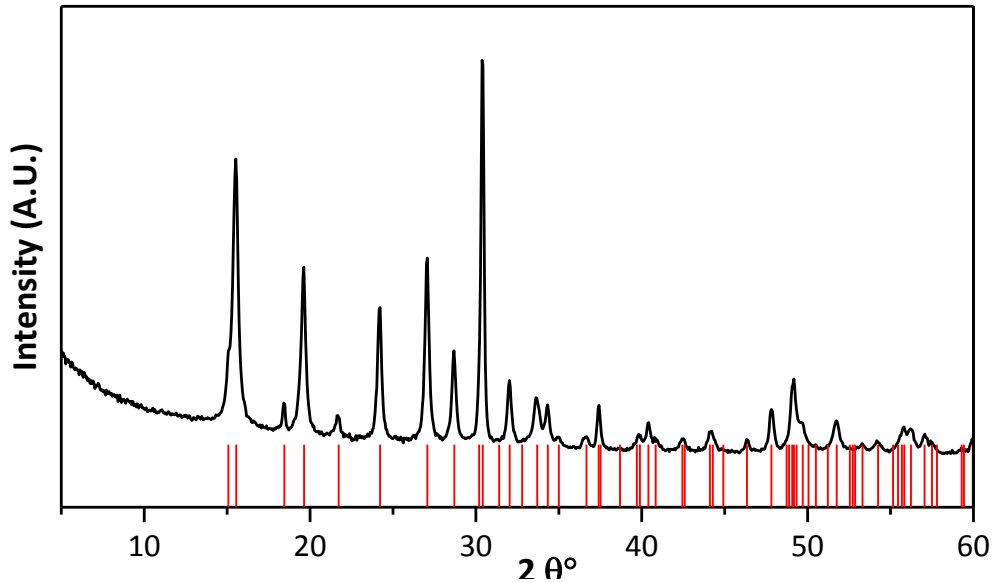

Figure 3-3 XRD analysis of VHP precursor. Red lines represent the pattern of $(VO)HPO_4 \cdot 0{,}5\ H_2O$

XRD analysis of precursor (VHP)

XRD analysis of the precursor confirms the formation of the $(VO)HPO_4 \cdot 0,5\ H_2O$ and the absence of the signals derived from the starting materials.

Raman spectroscopy of final catalyst (VPO)

The Raman spectra of the fresh catalyst obtained after the thermal treatment, and reported in Figure 3-5, show the presence of both the VPP phase, due to the bands at 1180, 1124, 915 and 267 cm^{-1}, and the α_1 $VOPO_4$ phase, due to the bands at 1015 and 526 cm^{-1}.

XRD analysis

XRD analysis on the fresh catalyst in Figure 3-6 confirms the presence of the VPP phase and, unlike the Raman analysis results, signals derived from the $VOPO_4$ phase are observed, suggesting the oxidized phase is present only in very low amount.

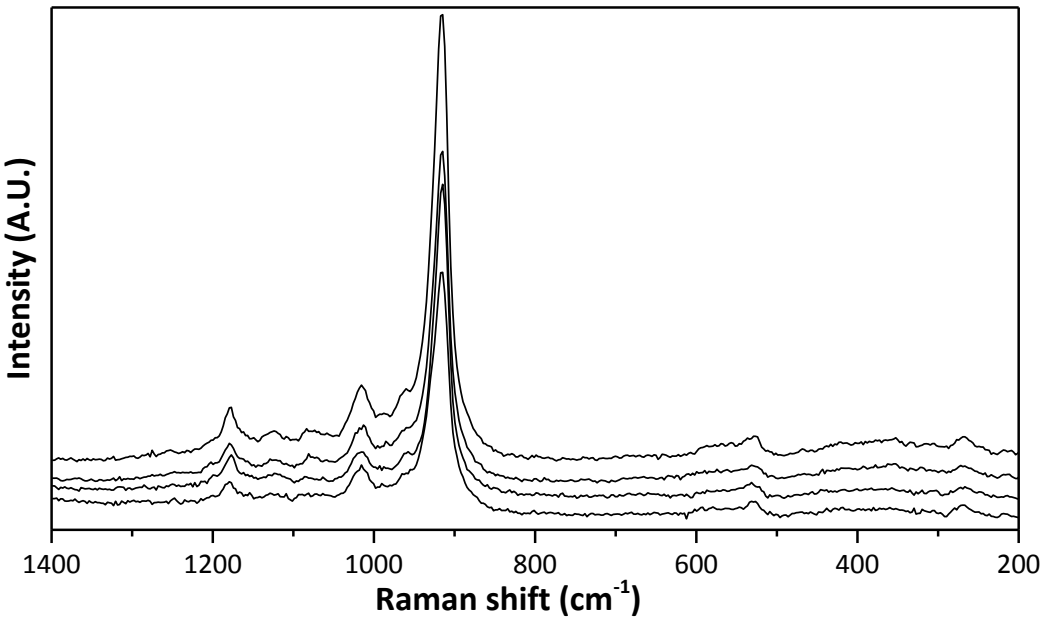

Figure 3-5 Raman spectra of VPO catalyst after thermal treatment

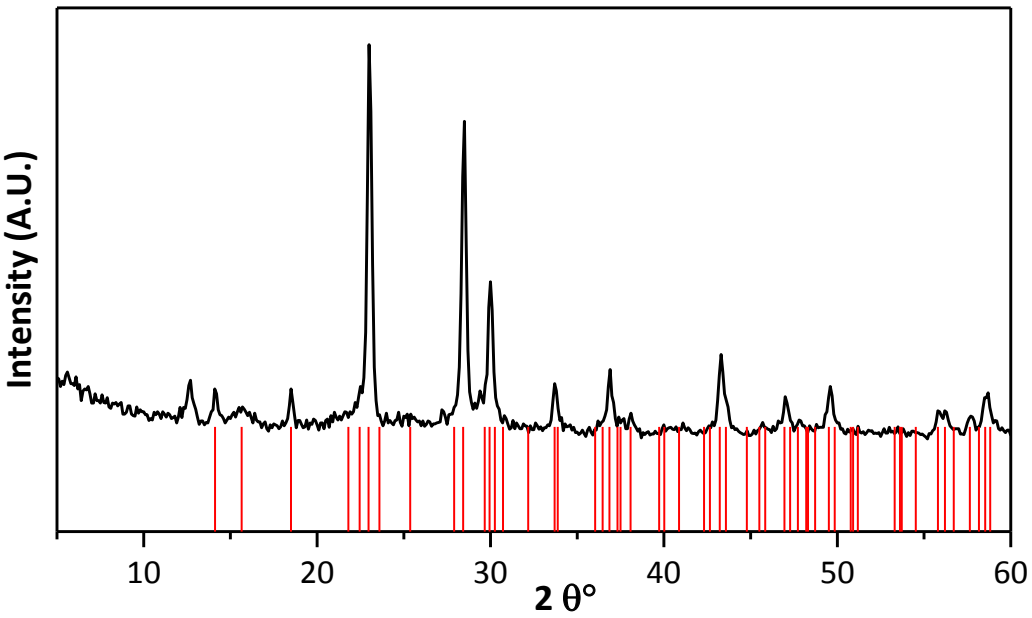

Figure 3-6 XRD analysis of VPO fresh catalyst. Red lines represent the pattern of $(VO)_2P_2O_7$

Elementary analysis by EDX spectroscopy

The elementary analysis by EDX spectroscopy shows a P/V ratio equal to 1.01, indicating the complete incorporation of all amount of P and V atoms, used for the synthesis, in the crystalline structure.

BET analysis

The BET specific surface area of the fresh catalyst is 20 m^2/g.

3.2 Characterization of vanadyl phosphate (VPD)

XRD analysis

The XRD analysis on the yellow/green solid shows the presence of vanadyl phosphate dihydrate phase and, in minor amount, the α_1 $VOPO_4$ phase as reported in Figure 3-7.

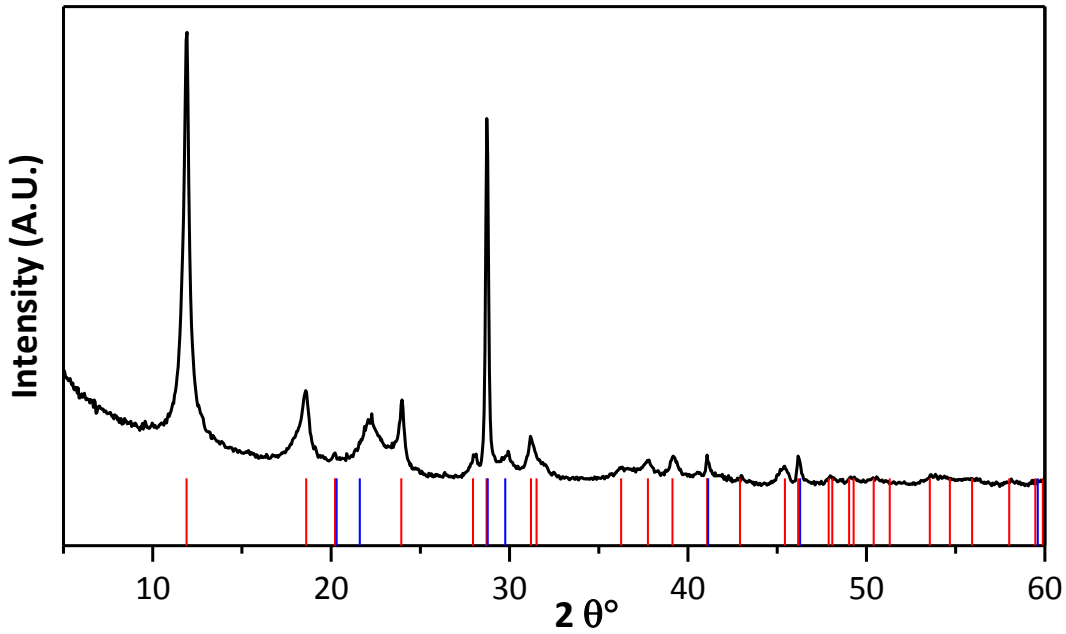

Figure 3-7 XRD analysis of VPD catalyst before calcination treatment. Red lines represent the pattern of $VOPO_4 \cdot 2H_2O$ phase; blue lines represent the pattern of α_1-$VOPO_4$ phase

Ex-situ Raman spectroscopy analysis

Raman spectra acquired at different spots of the sample, presented in Figure 3-8 show different bands, correlating to the presence of both VOPO4.2 H2O and α_1 $VOPO_4$. The bands correlated to the dehydrated system are at 1036, 984, 946, and 535 cm^{-1}, while the bands associated with the α_1 phase are at 1146, 1036, 924, 571, 452, and 424 cm^{-1}.

A comparison of the spectra shows a variation in the intensity of the peaks, indicating a non-homogeneous distribution of these phases in the catalyst.

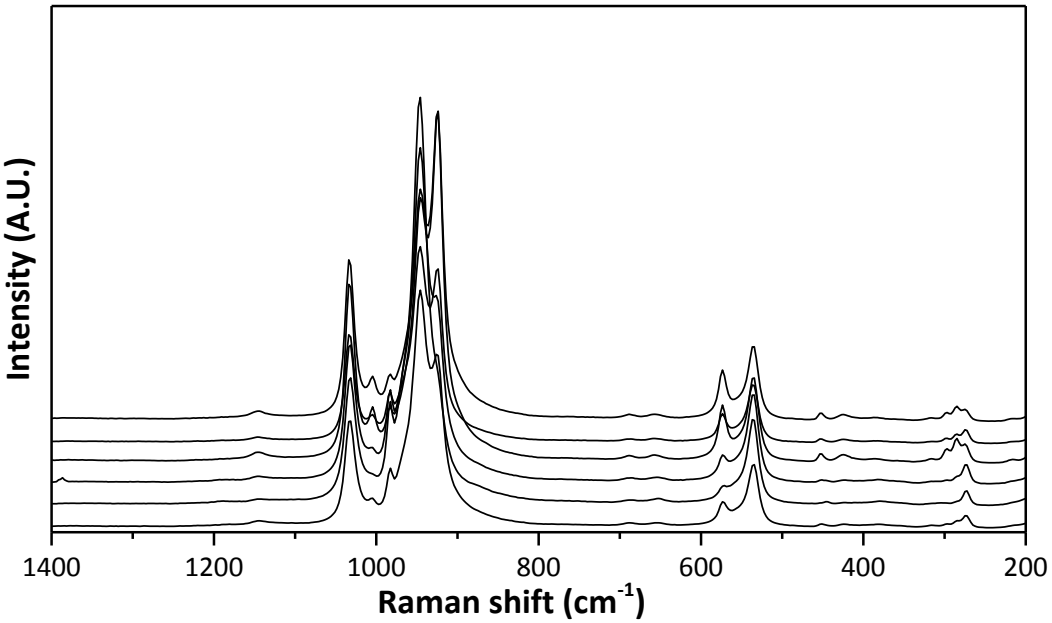

Figure 3-8 *Ex-situ* Raman spectra acquired on different spots of VPD

In-situ Raman spectroscopy and TGA

The calcination process of the catalyst was also investigated, by monitoring the transformations that occur during the thermal treatment by *in-situ* Raman spectroscopy, which results are reported in Figure 3-9.

The spectra acquired at room temperature (black line) show the presence of both the dihydrate and α_1 phases of $VOPO_4$, while the spectra acquired at 100°C (red line) show the presence of only the α_1 phase, because the band at 984–946 cm^{-1} disappeared and the intensities of the bands at 571 and 535 cm^{-1} changed to reach a unitary ratio.

A further increase of temperature does not affect the catalyst because the spectra remain the same, which indicates that the loss of the water molecules takes place at a very low temperature.

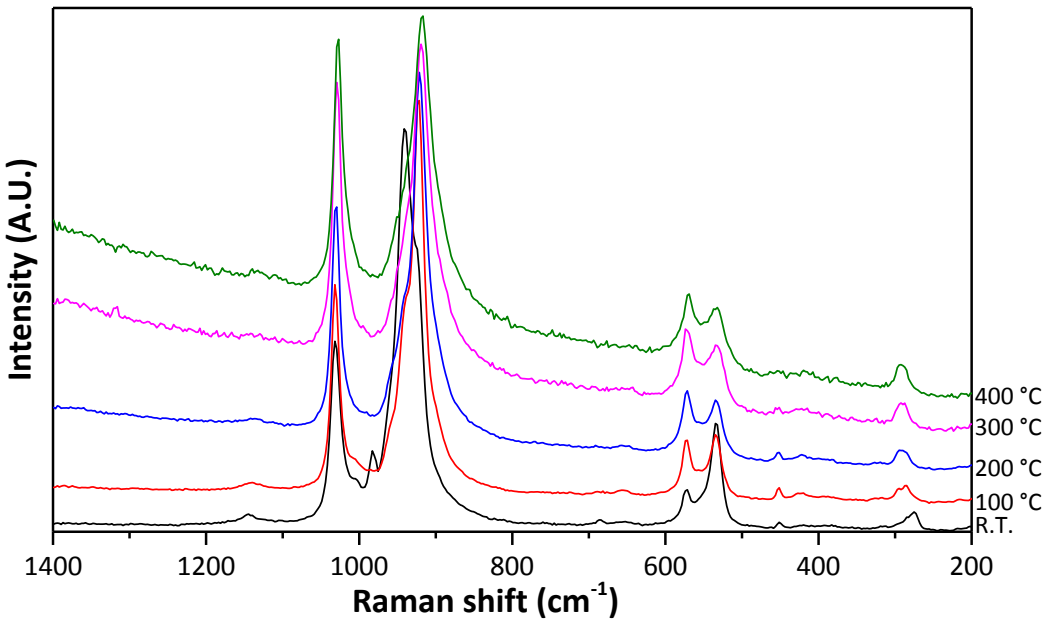

Figure 3-9 *In-situ* Raman spectra acquired on the same spot of VPD, at different temperatures and air feed rates

In order to better understand this effect, TGA was carried out on the fresh sample. The results in Figure 3-10 show two different weight losses; the first was at 73°C with –8% of weight loss and the second was at 101°C with a 5.6% weight loss, which equals a total loss of 13.6%. The theoretical loss of weight of $VOPO_4 \cdot 2\ H_2O$ to obtain the anhydrous phase is 17.4%. The difference between the real and theoretical weight loss confirms that the catalyst is composed of both the dihydrate and anhydrous phases of $VOPO_4$, and that the loss of two molecules takes place by two consecutive reactions that occur at different temperatures, confirming the results reported in the literature [98–101].

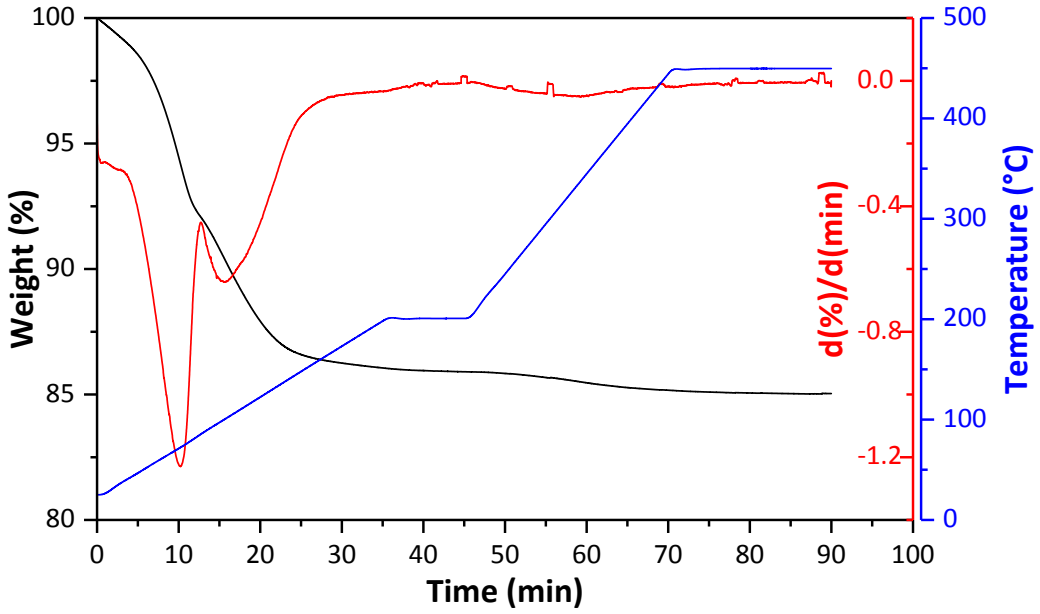

Figure 3-10 TGA of VPD catalyst using air as the carrier gas. Black line represents the percentage loss of weight; blue line represents the temperature ramp; red line represents the derivatives of the weight as a function of time

Elementary analysis by EDX spectroscopy

The elementary analysis by EDX spectroscopy shows a P/V ratio equal to 1.00, indicating the presence of vanadium phosphate in the catalyst.

BET analysis

The specific surface area measured for VPD was 5 m^2/g; the low value may be due to the fact that during the aging treatment of the solid in its mother liquor structural rearrangements cause an increase in the crystallinity of the solid, thus decreasing the surface area.

In Table 3-1 are resumed the results obtained from the characterisations techniques of the V/P/O catalysts investigated.

Sample Name	Phase (XRD, Raman)	S.S.A. (m^2/g)	P/V ratio (EDX)
VPP DuPont	$(VO)_2P_2O_7$	40	1.02
VPO	$(VO)_2P_2O_7$	20	1.01
VPD fresh	$\alpha_1 VOPO_4 + VOPO_4 \cdot 2H_2O$	/	/
VPD calcined	$\alpha_1 VOPO_4$	5	1.00

Table 3-1 Resuming table of the V/P/O catalysts with the main characterisations

3.3 Investigation of the poisoning effect on the oxidehydration reaction with bio-1-butanol

As mentioned before, the possibility of using bio 1-butanol (BBn), obtained by fermentative processes, as the starting material to produce MA by the gas phase oxidehydration reaction was investigated, using vanadyl pyrophosphate (VPP), supplied by Dupont, as the multifunctional catalyst.

Three different BBn, supplied by 3 different companies, were tested for investigating the catalytic behaviour with VPP as a function of the temperature, and the results are compared with the ones obtained with 1-butanol obtained from conventional chemical sources (CB), as shown in Figure 3-11.

In all cases complete 1-butanol conversion was achieved; moreover, in addition to the products reported in Figure 3-11, acetic and acrylic acid were also detected, with a sum of their yield being less than 20%. The maximum yield to MA observed for all butanols tested is in the temperature range from 340 to 360°C; at low temperatures, the main products observed are butenes, while at high temperatures, overoxidation with the formation of CO and CO_2 are favoured.

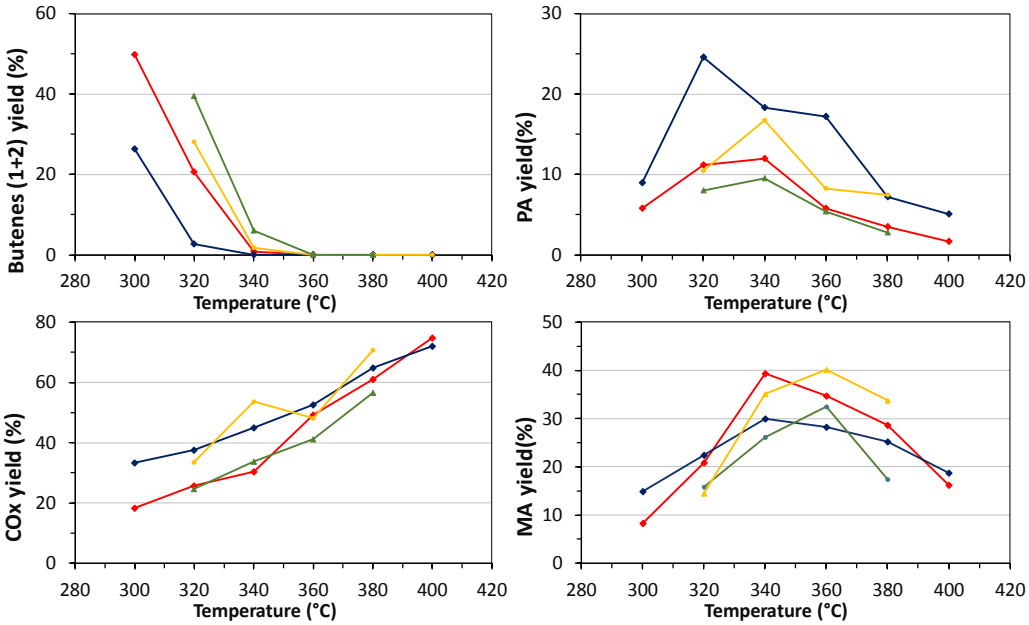

Figure 3-11 Comparison of catalytic behaviour of VPP Dupont catalyst for the oxidehydration reaction of 1-butanol in air in function of the temperature for different 1-butanol. Feed: 1% mol/ 1-butanol, 20% O_2, remain part N_2. W(weight of the catalyst)/F (flow of the inlet feed): 1,3 g_{cat}·s/mL.
Red lines represent the chemically 1-butanol; Blue lines represent BB-1;
Orange lines represent BB-2;Green lines represent BB-3;

Analysis of the difference between the butanols, BB1 (blue lines) showed the lowest yield into butenes and MA, with the highest yield into PA reaching 25% at 320°C, and the yield into CO_x was higher compared to CB. Similar to BB1, BB2 (green lines) also presented a low selectivity into MA, but BB3 (orange lines) showed the same behaviour as that of CB (red lines), thus achieving the same maximum yield into MA at 360°C. To understand the different behaviours of BBn, GC/MS analysis was conducted on the alcohols in order to detect the impurities present. All BBn presented purity higher than 99.5%, with water content less the 1%, and different impurities were detected, as reported in Table 3-2 . A comparison of the impurities present in BBn showed that only BB1 presented an amino compound, the 5H-Naphtho[2,3-C]carbazole-5-methyl (5HNC5M), an antibiotics released by the microorganism used for the fermentative process [102]. Purification treatments with active charcoal and

bleaching earth for different treatment times were conducted on BB1 to obtain BB-1 pure (obtained after 5 h of treatment) and BB-1 superpure (obtained after 24 h of treatment). Both alcohols were tested under the same conditions of the other BBn, and the best results in terms of MA and PA are reported in Figure 3-11.

Code	pH	Impurities
Chemical 1-butanol	5.8	1-propanol, ethanol, 2-butanol, n-butylether, acrolein, ethylbutanoate,propylpropionate
Bio 1-butanol BB1	5.3	**After Claisen**: 1-propanol, 1,1-dibutoxybutane, 2-methyl-1-butanol, butyraldehyde, furan, acrolein, benzaldehyde, 2-butanol, isobutanol, propionaldehyde, 3-methyl-1-butanol, butylacetate, butylformate, styrene, $C_{21}H_{15}N$ (tentative identification: 5H-Naphtho[2,3-C]carbazole-5-methyl) (5HNC5M)
BB1-pur	5.3	As BB1, but with lower concentrations
BB1-superpur	6.1	As BB1-pur, but with much lower concentrations: 1,1-dibutoxybutane, 1-propanol, 2-butanol, 1-butanol 3-methyl, 1-propanol 2-methyl, methanol. **After Claisen** : Acetone, 1-propanol, butanal, 2-butanol, 1-propanol 2-methyl, 1-butanol-2-methyl, butylacetate, acetone dibutylacetal, 1,1 dibutoxy butane.
BB-2	6.3	Ethylpropionate, butylpropionate, 2-methyl-1-butanol, butylacetate, ethanol, 1-propanol, butylacetate, 1,3 butanediol
BB-3	6.1	n-butylether, 1,3 diazine, 1-propanol, butyraldehyde, 2-butanol, 1-butanol 3-methyl, 1,1-dibutoxybutane, methanol, acetone, 2-propanol 2-methyl, 2-pentanol, 1,3 butanediol. **After Claisen:** 1-propanol, butyraldehyde, 2-butanol, 2-pentanol, isobutanol, 1-butanol-2-methyl, 1-butene-2-butoxy, 2-butene-1-butoxy, n-butylether, butylacetate, 1,1-dibutoxybutane, 1,3-diazine (CAS 000289-95-2)

Table 3-2 Impurities detected by GC and GC/MS analysis in all butanol tested

The results showed that the short purification treatment only led to a partial removal of the impurities; in fact, the yield into MA should be lightly increased, while the yield into PA remained the same. Instead, when a long purification treatment was completely successful, GC/MS analysis confirmed very low concentration of the impurities and the catalytic tests showed the yield into MA reached the value obtained with the chemical 1-butanol, similar to the yield into PA.

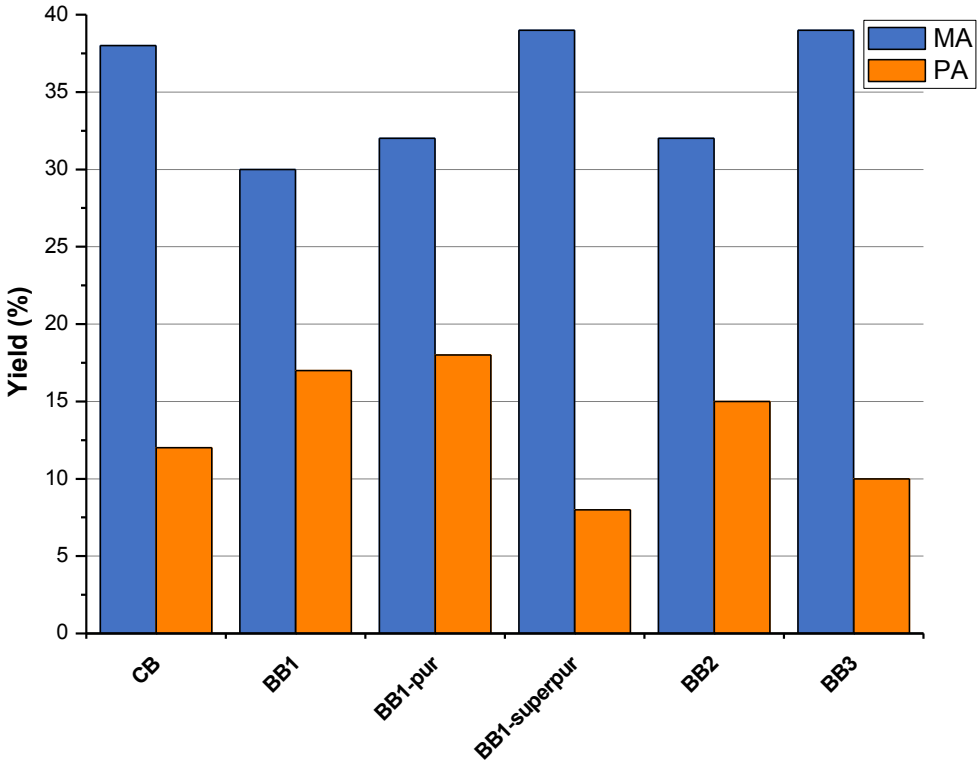

Figure 3-12 Best MA and PA yields obtained with VPP catalyst feeding either chemical 1-butanol (CB) or bio-1-butanol samples (BB). T: 340–360°C; feed: 1 mol% 1-butanol, 20% O2, remainder N_2; W/F: 1.33 g·s/mL

Having confirmed the disappearance of 5HNC5M by both GC/MS analysis and catalytic tests, it was therefore decided to investigate in detail the influence of this impurity and its poisoning effect on the catalyst. To understand the possible causes of the decrease in the yield into MA with BB, the catalytic behaviours of CB and BB-1 during at 340°C were monitored and compared. The results, shown in Figure 3-13 and

Figure 3-14, respectively, revealed the same catalytic behaviour for both alcohols at the beginning of the experiments. As the experiment progressed, for CB, there is only a slight decrease in the selectivity into MA during the first hour, whereas the catalytic behaviour of BB-1 is completely different.

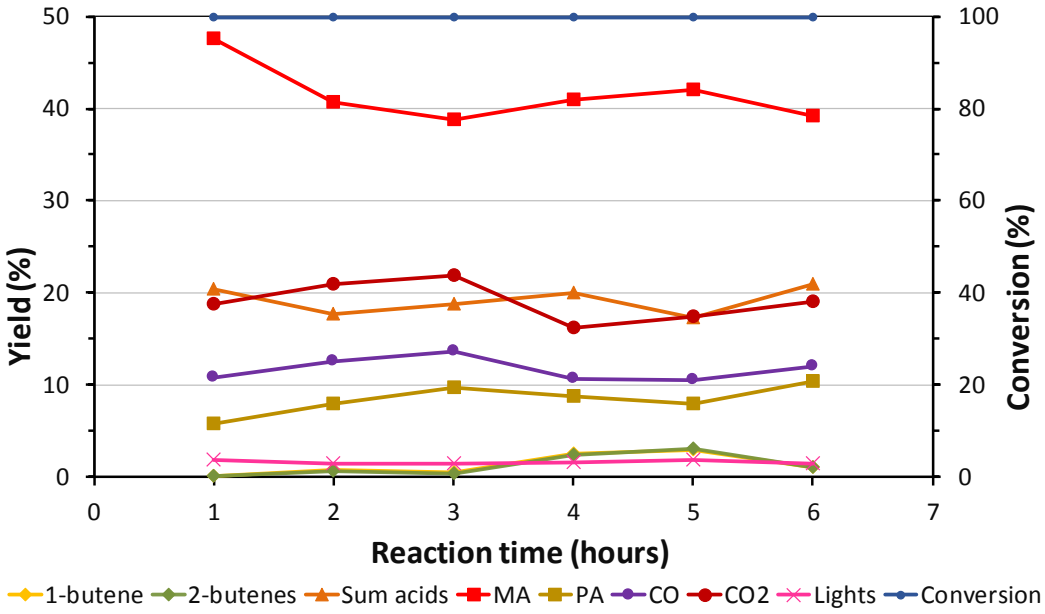

Figure 3-14 Catalytic behaviour of VPP Dupont in oxydehydration reaction with BB1 in air in function of the reaction time. Feed: 1% mol 1-Butanol, 20%mol O_2, remain N_2 T: 340°C; W/F:1,3 g_{cat}·sec/mL

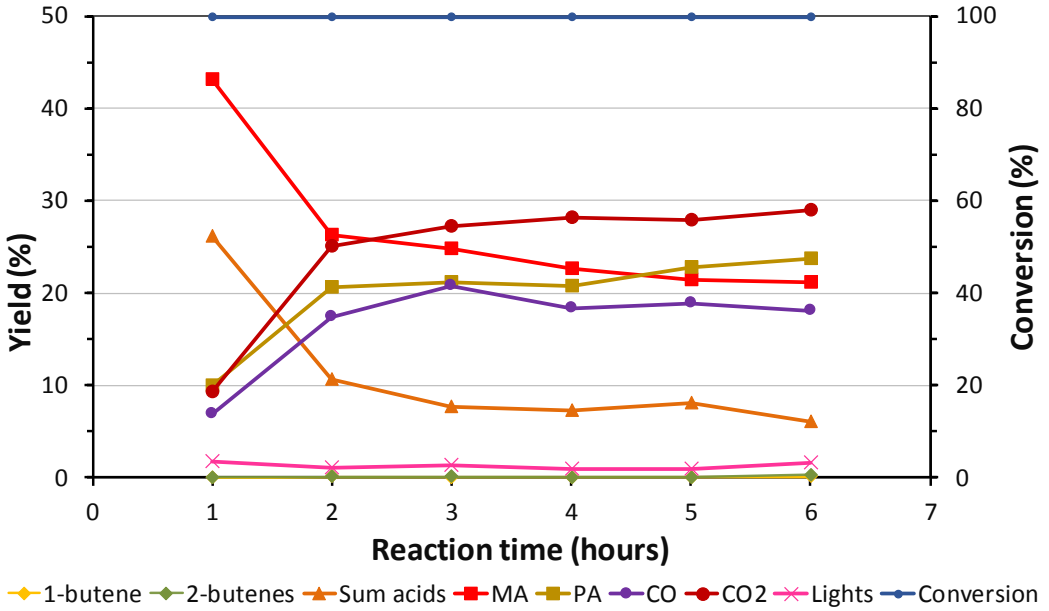

Figure 3-13 Catalytic behaviour of VPP Dupont in oxydehydration reaction with chemical 1-butanol in air as a function of the reaction time. Feed: 1% mol 1-Butanol, 20%mol O_2, remain N_2 T: 340°C; W/F:1,3 g_{cat}·sec/mL

A decrease in the selectivity into MA in favour of CO, CO_2, and phthalic anhydride appears after the first hour.

The trends of the yield for the BB-1 is derived from a transformation of the catalytic surface, correlated to a possible accumulation of 5HNC5M on the surface that modifies its characteristics, favouring the undesired reaction. This hypothesis is supported also considering that the impurities present in the BB-1 are the same as those present in the CB, or that they present characteristics not much different to the ones produced during the reaction.

To further confirm the poisoning effect of 5HNC5M, catalytic tests with chemical butanol intentionally poisoned with anthracene and the carbazole (the three molecules are shown in Figure 3-15) were carried out, in order to determine which part of the molecule negatively affects the reactivity of BB-1.

a

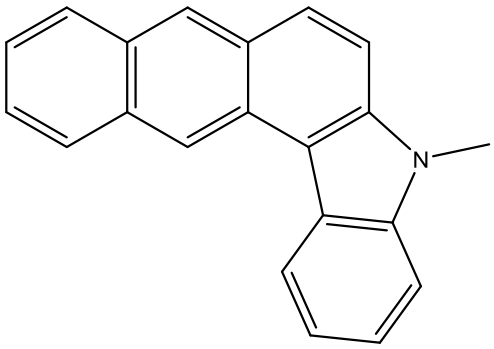

5-methyl-5*H*-naphtho[2,3-*c*]carbazole (**5HNC5M**)

b

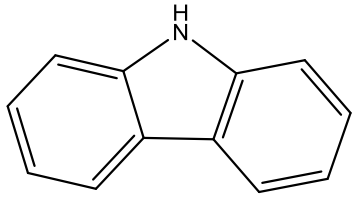

9*H*-carbazole

c

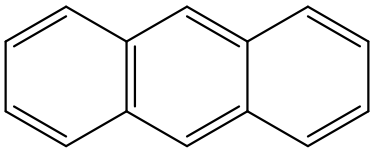

anthracene

Figure 3-15 **a**: Poisoning molecule presents in the BB-1; **b** and **c:** molecules intentionally added to the CB, for miming the groups present in **a**.

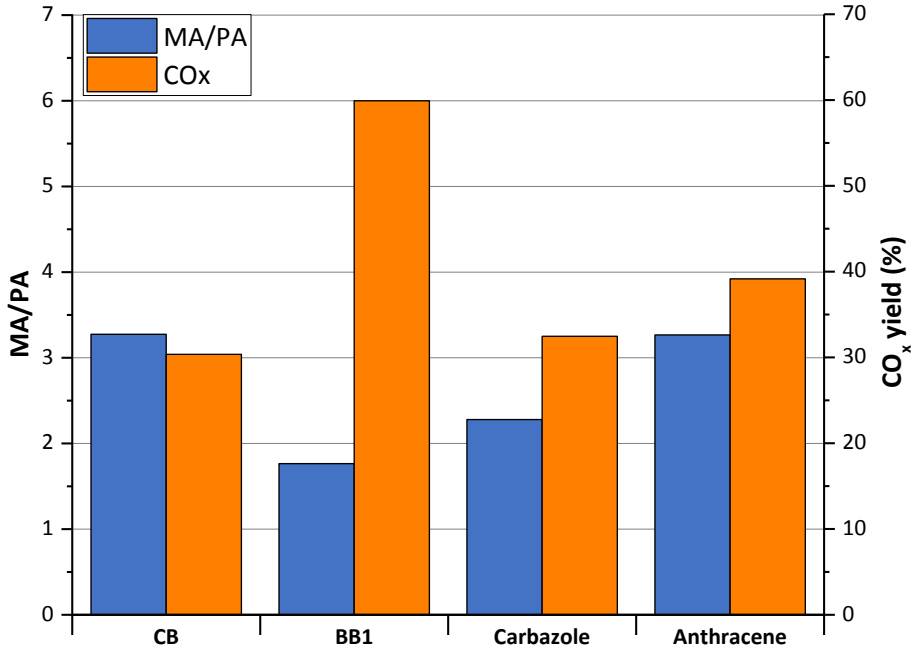

Figure 3-16 MA/PA ratio and yield into CO_x obtained during oxidehydration reaction of different 1-butanol with VPP. Temperature: 340 °C. Feed: 1% mol 1-Butanol, 20% mol O_2, remain N_2. W/F: 1,3 g_{cat}·s/mL

Chemical 1 butanol intentionally poisoned with or 0.01 *wt%* of carbazole or 0.01 *wt%* of anthracene was tested under the best operative conditions obtained from the previous tests. The results, shown in Figure 3-16 as the ratio of the yield into MA and PA and the sum of yields of CO and CO_2, revealed no particular influence of the anthracene in the MA/PA ratio, which remained the same as that for CB, while the presence of carbazole showed a decrease in the same ratio, from 3.2 to 2.2.

This variation, correlated to the increase in the formation of PA, could be attributed to the increase in the Diels Alder reaction between MA and 1.3 BDE that could occur in the homogeneous phase. Regarding the yield into CO_x, an increase in this value was observed for both poisoning molecules; this effect could be correlated to the preferential adsorption of the poisoning molecules on the active sites that catalyse the oxidation reactions, then favouring the overoxidation in homogeneous phase.

These results confirm the negative effect of the carbazole in the feed, and therefore, successive catalytic tests were carried out using only the carbazole as the poisoning molecule. The influence of the concentration of the carbazole in the CB was then investigated, and the results, shown in Figure 3-17, revealed multiple effects of the carbazole on the surface. A very low concentration of carbazole is required to decrease the MA/PA ratio, which remains the same also at high amounts of the poisoning molecule.

The variation in the concentration of carbazole has a stronger effect on the yield into CO_x, because an increase from 30% to 37% was correlated, as mentioned before, to the increase in the overoxidation of the homogeneous phase.

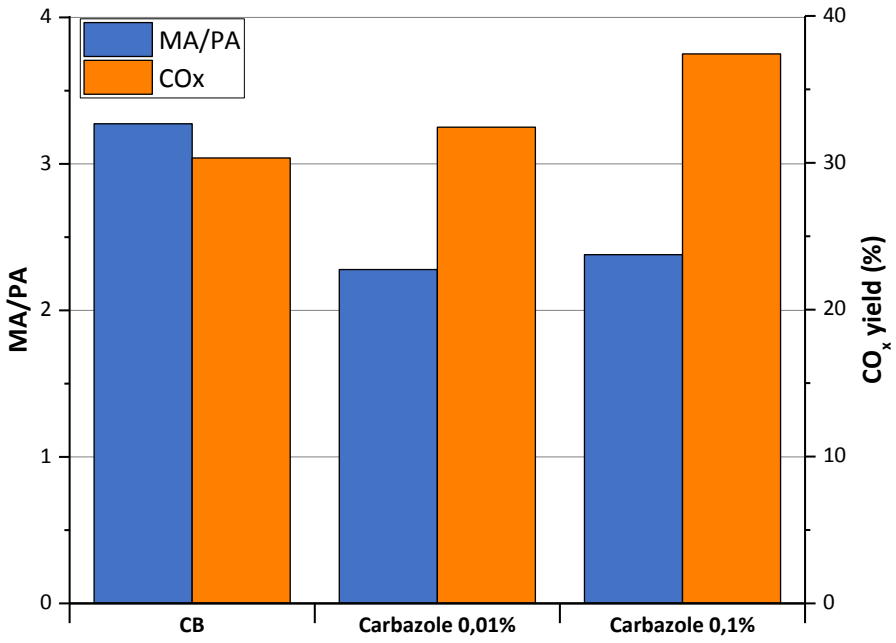

Figure 3-17 MA/PA ratio and yield into CO_x obtained during oxidehydration reaction of different 1-butanol containing a different amount of carbazole. Temperature: 340 °C. Feed: 1% mol 1-Butanol, 20% mol O_2, remain N_2. W/F: 1,3 g_{cat}·s/mL

These results show the strong effect of the poisoning molecule on the catalytic surface, and it is thus possible to hypothesize an acid/base interaction between the "base"

carbazole (due to the presence of the amino group) with the acid sites, favouring the desorption of the species from the surface and disfavouring their re-adsorption, increasing their concentration in the gas phase and thus favouring the reaction in the homogeneous phase.

To better understand the poisoning effect of the carbazole, a catalytic test at 320°C was carried out, in order to analyse the poisoning effect of the molecule in different conditions that lead to different intrinsic catalytic behaviours of VPP.

In Figure 3-18, the MA/PA ratios and the yields into CO_x obtained with CB and CB poisoned with 0.1%*w/w* of carbazole at 320 and 340°Care compared, and the same

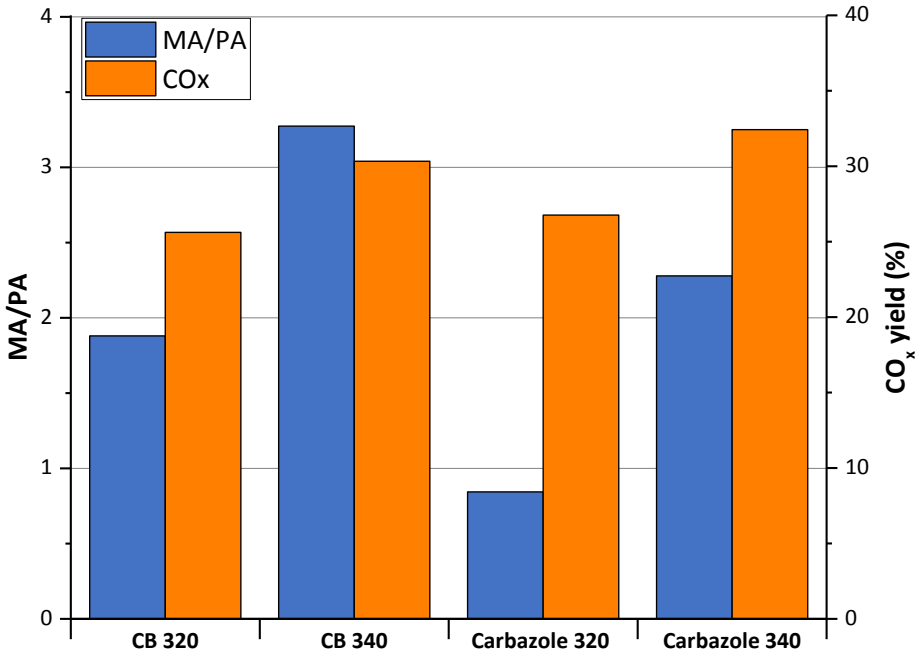

Figure 3-18 MA/PA ratio and yield into CO_x obtained during oxidehydration reaction of pure 1-butanol and 1-butanol containing 0.1% %wt of carbazole. Temperature: 320 and 340 °C. Feed: 1% mol% 1-Butanol, 20% mol% O_2, remain N_2. W/F: 1.3 g_{cat}·s/mL

effect of the carbazole at both temperatures can be observed. The decrease in the MA/PA ratio at 320°C and 340°C is the same as the increase in the yield into CO_x.

This effect further confirms the strong interaction between the catalytic surface and the carbazole, because at a lower temperature and different catalytic behaviour of VPP, is shown the same poisoning effect.

In conclusion, it is confirmed that the poisoning effect of carbazolic species for the oxidehydration reaction of 1-butanol on VPP could be attributed to the interaction between the base amino group and the acid surface of the catalyst. The strong interaction is confirmed by the poisoning effect observed with the carbazole, intentionally added to the CB, also at very low concentration and at low temperature. About the presence of the polycycles aromatic part, this participates also in the poisoning effect but in minor part, favouring the overoxidation of the species on the surface.

3.4 Influence of the composition feed on the yield and productivity of MA

In order to improve the yield into MA by the oxidehydration reaction of 1-butanol on vanadyl pyrophosphate DuPont (VPP), it was decided to investigate the influence of the feed composition. At first, the influence of the partial pressure of oxygen was investigated at 340 °C, the temperature at which the maximum yield into MA was obtained. The results, shown in Figure 3-19, revealed the fundamental role of this parameter. At very low partial pressure of oxygen, the presence of butenes suggests the low rate of their selective oxidation into MA; this behaviour could be correlated to the low amount of V^{+5} species present on the surface that, by the redox couple V^{+4}/V^{+5}, are

the sites responsible for the oxidation. The increase in the molar fraction from 0.02 to 0.05 led to an increase in the non-selective oxidation in the homogenous phase; this means that non-selective oxidation reactions are favoured with respect to the selective ones. This effect could be explained considering that these side-reactions occur in homogeneous phase between oxygen and 1-butanol or the intermediates not adsorbed on the surface, owing to the saturation of the VPP surface by these species; an increase in the oxygen favours the side-reaction more compared to the selective oxidation.

The further increase in the partial pressure of oxygen in the feed favours the selective oxidation of the adsorbed species on the surface to MA, indicating the formation of even higher amount of V^{+5} species on the surface. With the increase in oxygen, the sites can establish the redox cycle for the selective oxidation, leading to the maximum yield into both maleic (39%) and phthalic (12%) anhydrides; the best results are obtained by feeding 20% of oxygen.

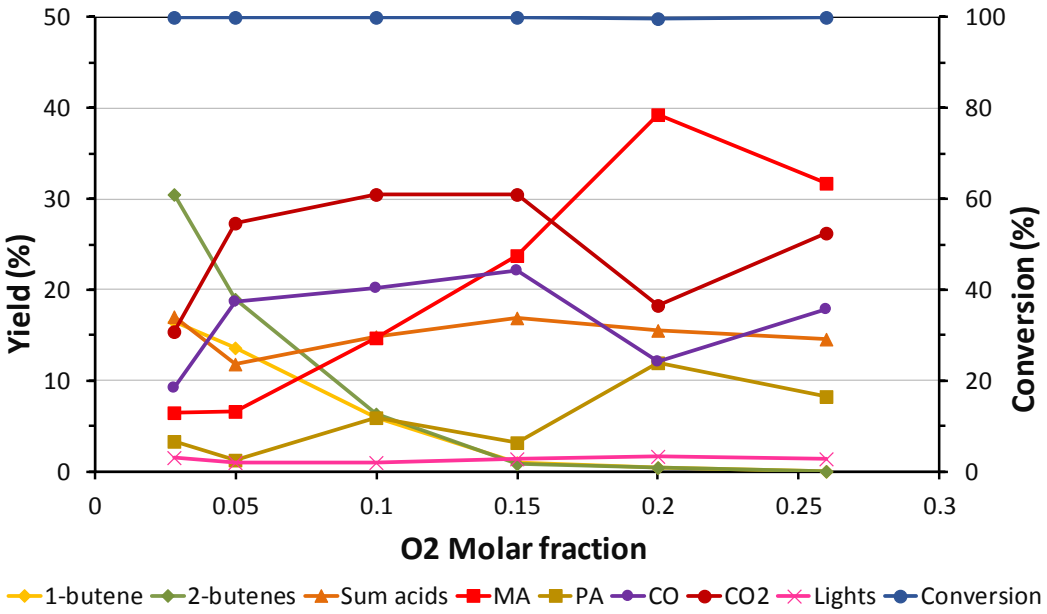

Figure 3-19 Catalytic behaviour of VPP Dupont in the oxydehydration reaction with 1-butanol as a function of the O_2 fraction molar. Feed: 1%mol 1-butanol, x% mol O_2, remain N_2 T: 340°C; W/F:1,3 g_{cat}·sec/mL

The increase in V^{+5}, in addition to the increase in the selectivity into MA, increases the oxidation rate of the adsorbed species on the catalytic surface of VPP, increasing the adsorption rate of the intermediates; this leads to a decrease in these species in the homogenous phase, thus disfavouring the side-reactions occurring in that phase.

At high partial pressure of oxygen, the high presence of V^{+5} species on the surface favours both the selective and non-selective oxidation reactions, as can be observed by the increase in the yield into CO_x and the decrease in all the species.

The relevant role of the oxygen on the production of MA and PA was observed to have an important impact on the amount of V^{+5}, and it was therefore decided that the influence of 1-butanol would be investigated in order to understand better the influence of the saturation of the catalytic surface. Catalytic test was carried out feeding 0.4% of 1-butanol in air at different temperatures, investigating then the catalytic behaviour of VPP in "lean" conditions. The results obtained from this test are shown in Figure 3-20.

At very low temperatures, the catalytic system showed high yields into butenes, 76% and 15% into 1- and 2-butenes, respectively; the molar ratio of 2-butenes to 1-butene is lower than the thermodynamic value (4.98 versus 6.08) [103], indicating the higher E1 elimination reaction rate, for the formation of 1-butene, compared to the isomerization rate. Regarding the dehydration reactions that occur at low temperatures, also *n*-butyl ether (NBE) was also observed, but in yield lower than 1%, underlining the low concentration of 1-butanol in the feed disfavours the condensation reaction.

The increase in temperature favours the oxidation reactions that take place on the olefins; the yield into 2-butenes showed a higher rate of depletion compared to the 1-butene, until 300°C, indicating that the oxidation reactions are quicker than the isomerization, and the oxidations of 2-butenes are quicker than that of 1-butene.

The oxygenated products are MA and PA, derived from the selective oxidations of the olefins, CO and CO_2, derived from the overoxidation of the intermediates, and light acids (acetic and acrylic acid), derived from the oxidative cleavage of the intermediates.

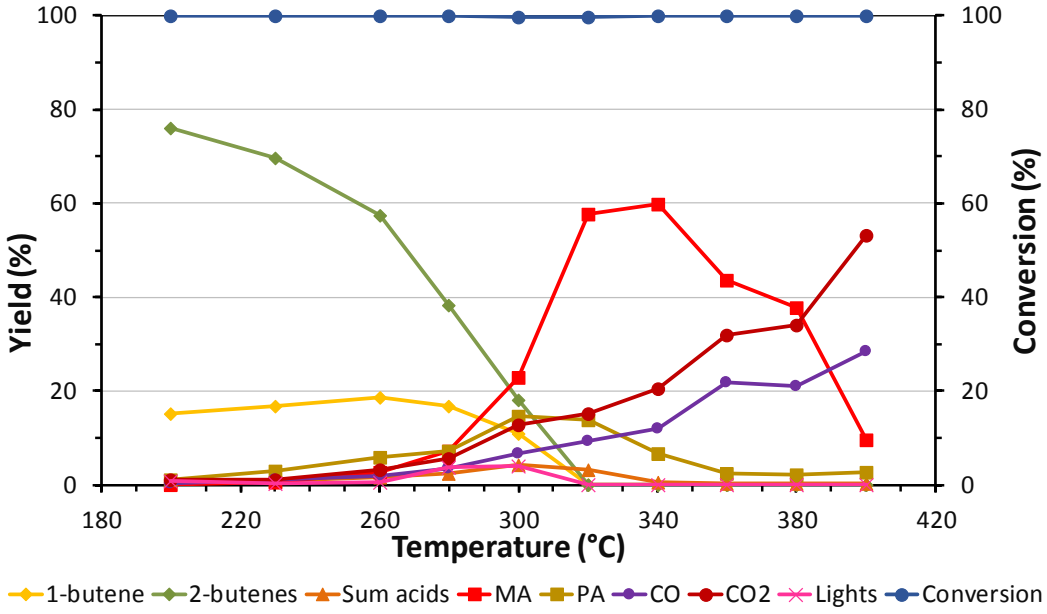

Figure 3-20 Catalytic behaviour of VPP Dupont in the oxydehydration reaction with 0.4% %mol 1-butanol in air function of the temperature. Feed composition: 0.4% %mol 1-butanol, 20% %mol O_2, remain N_2; W/F:1,3 g_{cat}·sec/mL

The formation of MA and PA already at 260°C confirmed the presence and the activity of V^{+5} species that could catalyse both the insertion of oxygen (for the production of MA) and the oxidative dehydrogenation that leads the formation of 1,3-BDE. The low concentration of 1-butanol helped prevent the saturation of the active sites, favouring the adsorption of oxygen, the dehydrogenation of the olefin, and then increasing the cycle V^{+4}/V^{+5}, that is responsible for catalysing these reactions.

The maximum yield achieved into PA is 15% at 300°C, while for MA is 60% at 340°C; the different temperatures for the maximum yield could be explained by taking into account the processes that occur; until 300°C, both the oxidative dehydrogenation to 1,3-BDE and the oxidation to MA occur favouring the Diels Alder reaction with the formation of PA. At higher temperatures, the high amount of oxygen and the low concentration of olefins on the surface (owing to the low concentration of 1-butanol in the gas phase), favour the selective oxidation with oxygen insertion rather than the oxidative dehydrogenation reaction, thus disfavouring the production of PA in favour of MA. At temperatures higher than 340°C, CO_x becomes the main products, indicating that overoxidation reactions, that take place either on the catalytic surface or in the homogeneous phase, are predominant.

A comparison of the catalytic behaviour of VPP DuPont for the oxidehydration reaction of 1-butanol at different temperatures with 0.4% (red lines), 1% (blue line), and 2% (orange lines) (these last two were already investigated before, and the results are already published in [62]) of alcohol, reported in Figure 3-21, helps understand in detail the role of 1-butanol in the reaction. In all of the catalytic tests, complete conversion was observed, indicating the high catalytic activity of the VPP. The strong interaction between 1-butanol and the catalytic surface is even more emphasised with the increase in the concentration of the alcohol in the feed. In the case of 2%, the high amount of alcohol causes a strong variation in function of the temperature. At low temperature, a decrease of the selective oxidation products is observed (the maximum yield into MA+PA is less than 30%) with an increase of the yield into olefins (60% at 300°C).

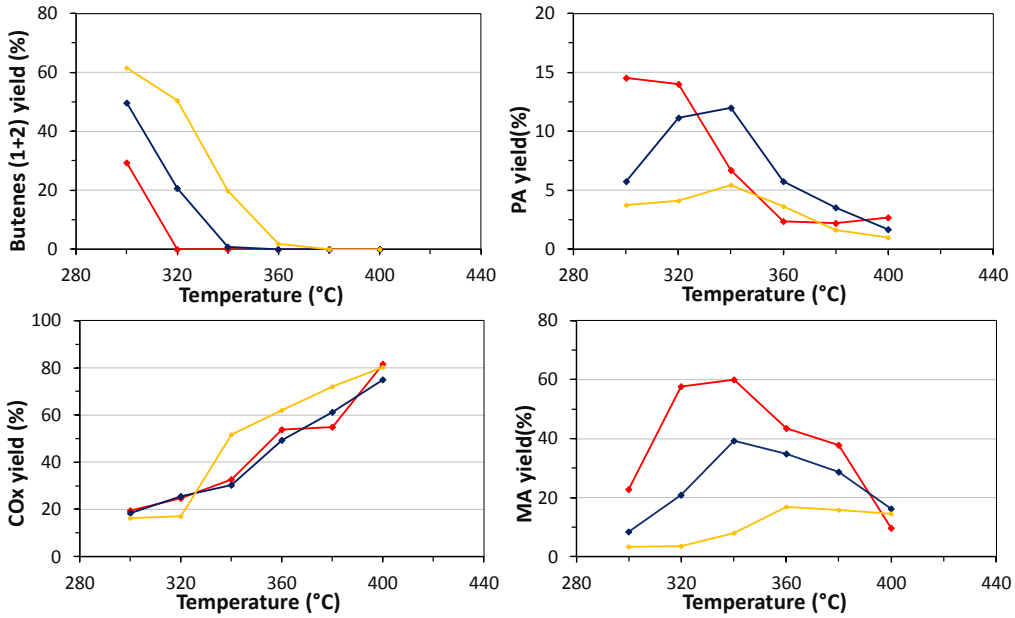

Figure 3-21 Comparison of catalytic behaviour of VPP in the oxidehydration reaction with 1-butanol in air in function of the temperature and the concentration of the alcohol. Feed composition: X% %mol 1-butanol, 20% %mol O_2, remain N_2; W/F: 1.3 $g_{cat}{}^{s}$/mL.

Red lines: 0.4% 1-butanol; Blue lines: 1% 1-butanol; Orange lines: 2% 1-butanol.

A different effect is observed operating at the "lean carbon" condition. The lower coverage of the surface enhances the redox cycle of vanadium ions, thus increasing the yields into MA and PA (60% and 15%, respectively). A decrease in the temperature for the maximum yield is observed, confirming the stronger oxidant power of the catalyst.

In conclusion, the ratio and the amount of 1-butanol and oxygen in the feed play a fundamental role in the oxidehydration reaction over VPP Du Pont; the main role of the oxygen is to sustain the V^{+4}/V^{+5} redox couples necessary for the oxidation reactions, which also notably influences the concentration of the species in the homogeneous phase. The strong interaction of 1-butanol with the surface strongly influences the entire process, and a higher amount of alcohol overcomes the selective oxidation reaction in favour of both the dehydration, at low temperature, and the overoxidation of MA on the catalytic surface.

3.5 Influence of the acid and redox properties of VPP catalysts on the oxidehydration reaction of 1-butanol

The presence of the amorphous porous silica on the VPP Du Pont could modify the catalytic behaviour of the active phase, for this reason a pure $(VO)_2P_2O_7$ was synthesised by the VPO method, and results obtained were compared with those achieved with VPP DuPont. In order to investigate the catalytic behaviour of VPO, catalytic tests varying the temperature were carried out.

The results, reported in Figure 3-22, showed complete conversion of the alcohol in the entire range of temperature studied the same trend was observed for the VPP in the previous sections 3.3 and 3.4. About the distribution of the products, VPO presented a high selectivity into butenes at 320 °C, that represent the main products with 77% selectivity while the oxygenated species such as CO, CO_2, light acids (acetic and acrylic acid) and "others" were the minor part. CO, CO_2 and light acids derived from the overoxidation and oxidative cleavage that occurred on both butenes and intermediates; while "other" represented the sum of the intermediates and side-products of selective oxidation of olefins into MA, as showed in the reaction mechanism reported in Figure 1-6. Increasing the temperature, a drastically drop of butenes formation was observed in favour of the oxygenated compounds; after 360 °C, the main product became MA, followed by CO_2. The selectivity to "others" increased also, confirming the increase of the capability of the VPO in the selective oxidation of butenes into MA.

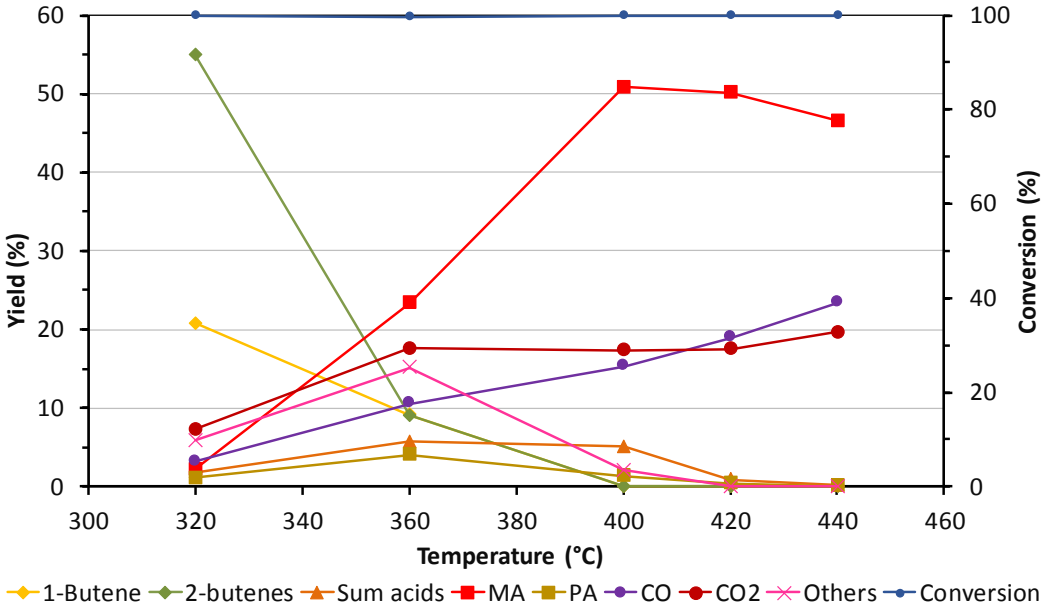

Figure 3-22 Catalytic behaviour of VPO in the dehydration reaction with 1-butanol in air in function of the temperature. Feeding: 1%mol 1-butanol, 20%mol O_2, remain N_2; W/F:1,3 g_{cat}·sec/mL

A not negligible amount of PA was also observed, indicating the lower reaction rate of the oxidative dehydrogenation of butenes that led to the formation of 1,3-BDE compared to their oxidation into crotonaldehyde. At 400 °C, the yield into MA was 50%, achieving its maximum value; about the other products, only CO and CO_2 continued to be the predominant side-products; butenes, PA and "others" dropped to zero.

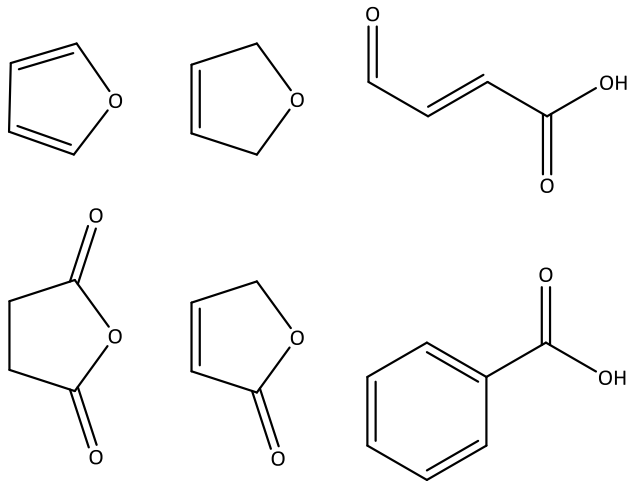

Figure 3-23 Main molecules detected and reported as "others"

A further increase of the temperature led to a slightly decrease of the yield into MA and an increase of yield into CO_x.

The results reported in Figure 3-22 have shown the best yield to MA is obtained at 400 °C, it was then decided to study the stability of the VPO catalyst at that temperature during the reaction stream. The results, reported in Figure 3-24, showed the complete conversion of 1-butanol yet after 1 hour of reaction and after that was kept constant. Analysing the distribution of the products, that are MA, CO_x and the other, it was not observed any significant variation of their selectivity. All of these results underline the high stability of both acid and redox sites of the VPO catalyst during the oxidehydration reaction.

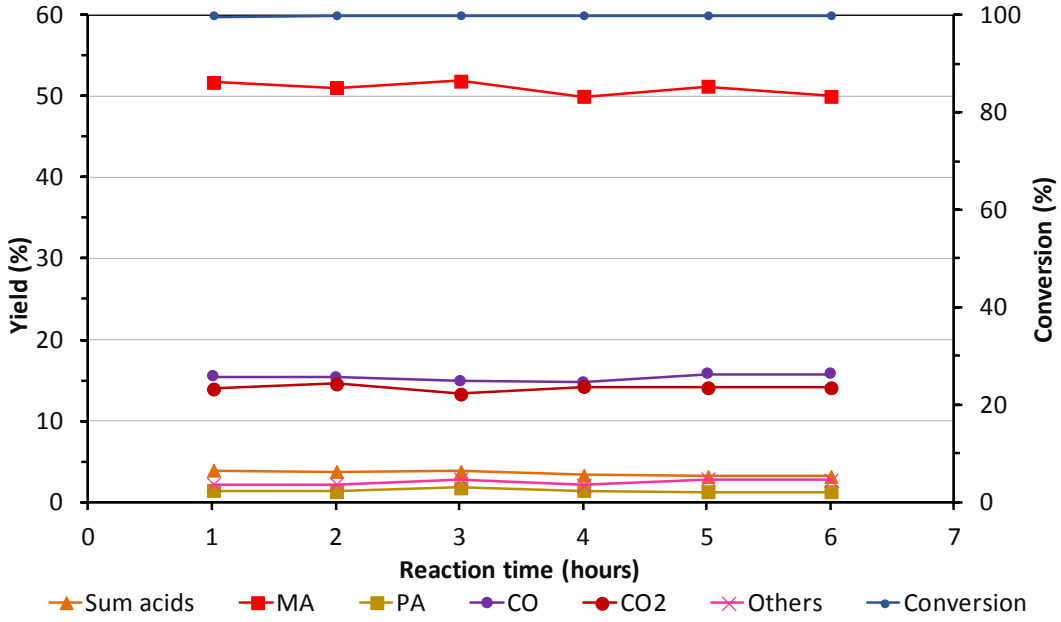

Figure 3-24 Catalytic behaviour of VPO in the dehydration reaction with 1-butanol in air at 400 °C during the reaction time. Feeding: 1%mol 1-butanol, 20%mol O_2, remain N_2; Temperature: 400 °C; W/F:1,3 g_{cat}·sec/mL

Comparing then the results obtained with VPO and VPP, many differences can be observed. In Figure 3-25 the trends of the main products for both catalysts are reported in function of the temperature.

Analysing the results at low temperature, VPO presents a lower yield in all oxidised products compared to VPP, indicating a lower oxidant power of the redox sites in these conditions. The increase of the temperature favours, for both catalytic systems, the oxidation reactions, but in a different way: the maximum yield into MA for the VPP is 40% at 340 °C, while for the VPO is 50% at 400 °C. The recorded difference could be explained considering a different interaction between the olefins and the surface of the catalysts.

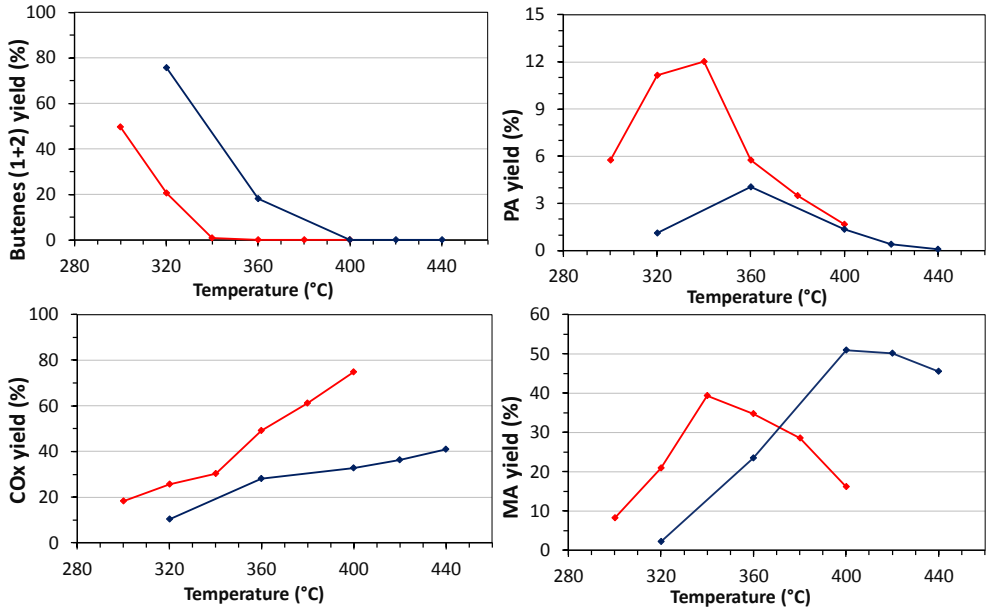

Figure 3-25 Comparison of catalytic behaviour of VPP and VPO for the oxidehydration reaction of 1-butanol in air at different temperature. Feed: 1% mol 1-butanol, 20% mol O_2, remain N_2; W/F 1,3 g_{cat}*s/mL. **Red lines:** represent the VPP catalyst; **Blue lines** represent the VPO catalyst

The different interaction of the olefins with the two catalysts can also explain the different trend of CO_x and PA observed: the higher amount of CO_x could derive from the stronger interaction of the intermediates and MA with the catalytic surface that leads the overoxidation of the species. About the formation of PA, the lower formation of this anhydride could be associated to the stronger interaction of 1,3-BDE and MA over the catalytic surface.

In order to investigate deeply the different catalytic behaviour of VPO with respect to VPP and its possible cause associated to the different interaction between the alcohol and the catalytic surface, it was then decided to study the catalytic behaviour of VPO at 400 °C varying the molar fraction of 1-butanol.

In Figure 3-26 is reported the catalytic behaviour of VPO in function of the concentration of 1-butanol in the feed at 400 °C, that is the optimal temperature where the maximum yield in MA was obtained. Under these conditions, complete conversion was always observed, independently from the amount of 1-butanol fed. At very low molar fraction of alcohol, VPO catalyst showed the highest selectivity into MA, achieving the 62% of yield. In these conditions, CO and CO_2 were also observed, deriving from the overoxidation that occur at high O_2/1-butanol ratio. The increase of the concentration led to a lightly decrease of the yield into MA in favour of the oxygenated products such as CO, CO_2, "others" and light acids.

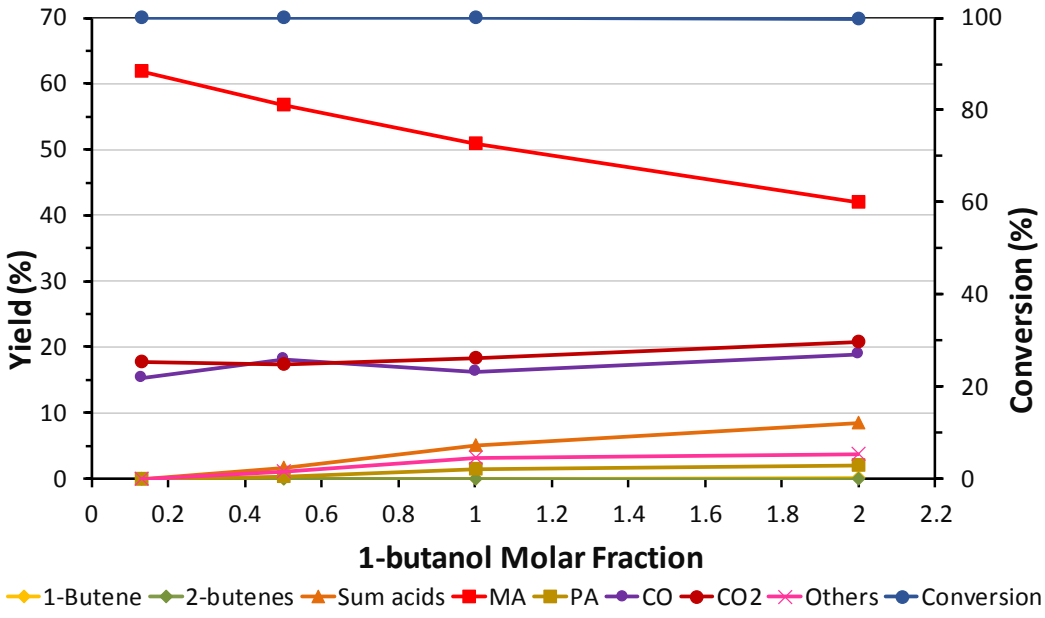

Figure 3-26 Catalytic behaviour of VPO in the dehydration reaction with 1-butanol in air in function of the molar fraction of 1-butanol. Feeding: x%mol 1-butanol, 20%mol O_2, remain N_2; Temperature: 400 °C; W/F:1,3 g_{cat}·sec/mL

The formation of these compounds indicates that a phenomenon of surface saturation is taking place. The increase of the molar fraction affected even more the catalytic activity of VPO disfavouring the selective oxidation reaction, the yield into MA achieved 40%, whereas the oxidative cleavage and the overoxidation reactions were more preferred. The decrease of the selectivity into MA could be correlated to the inaccessibility of the redox sites hindering the complex mechanism of oxidation of the olefins into the desired product. This hypothesis is also supported by the increase of the "other" with the increase of the concentration of the alcohol, indicating a not complete transformation of the intermediates in MA. About the increase of the yield into light acids, also this can be correlated to the saturation of the catalytic surface because it could lead to an increase of the non-selective oxidation that occurs in gas phase or on the catalytic surface.

Comparing the effect of the concentration of 1-butanol in the feed on the catalytic behaviour of VPP and VPO in their best conditions, it is possible to understand better the effect of the interaction of the alcohol with the catalytic surface.

In Figure 3-27 the catalytic behaviour of VPO at 400 °C and VPP at 340 °C in function of the molar fraction of 1-butanol is reported.

The concentration of 1-butanol influences in different manner the two catalysts, this also suggests the different interaction of the alcohol with the surface of VPP and VPO catalysts. Analysing the results, it is possible to observe the similar behaviour of VPP and VPO at low fraction molar; the low coverage of the butenes on the surface leads the catalysts to catalyse selectively the formation of MA, in fact the maximum yield into the anhydride is obtained.

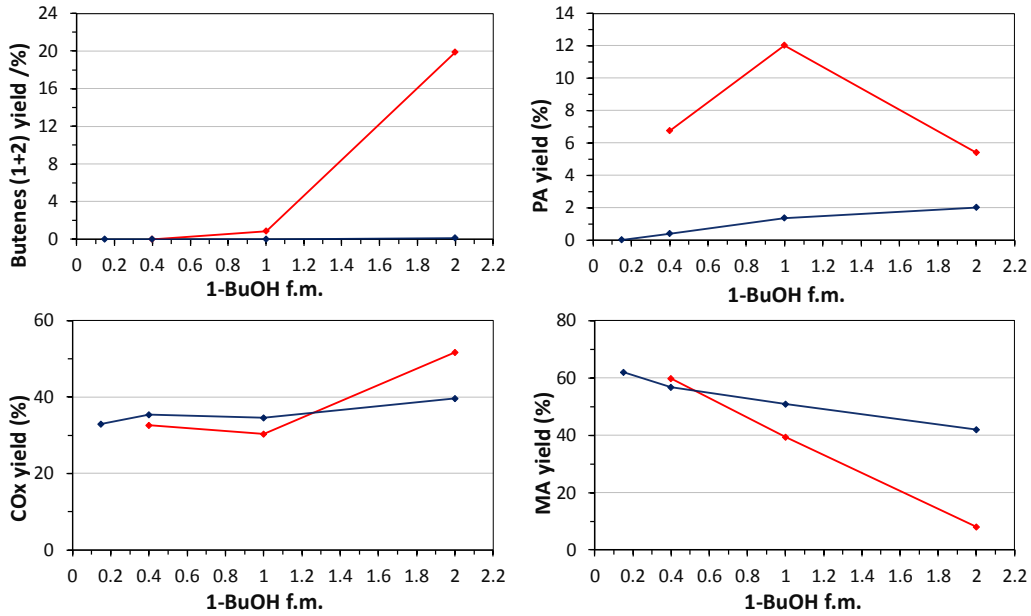

Figure 3-27 Comparison of catalytic behaviour of VPP and VPO for the oxidehydration reaction of 1-butanol in air at different molar fraction of alcohol. Feed: X% mol 1-butanol, 20% mol O_2, remain N_2; W/F 1,3 g_{cat}*s/mL. **Red lines** represent the results of VPP catalyst obtained at 340 °C; **Blue lines** represent the results of VPO catalyst obtained at 400 °C.

About the side-products at low concentration, PA was present at higher yield for VPP respect to VPO; this suggests a different interaction of the olefins with the surface. On the VPP surface, the olefins and MA interact more strongly respect to VPO, leading to the formation of PA.

The increase of the concentration of the alcohol has a detrimental effect for the process, the yield into MA decreases in favour of CO_x and other products such as butenes and PA. This is a further evidence of the even more strong interaction between the organic species with the catalytic surface.

Analysing in deep this detrimental effect, VPO suffered at a limited extent this effect with respect to VPP; this underlines the lower interaction between the catalytic surface of VPO and olefins compared to VPP. A weaker interaction, also at high concentration of alcohol, hinders the decrease of the selectivity into MA and the formation of PA; the depletion of MA for VPO is by 22%, while for the VPP is by 50%.

In order to confirm the different interaction of 1-butanol with both catalysts, TPSR (Temperature Programmed Surface Reaction) experiments were carried out using methanol as probe molecule.

This kind of experiment is widely used for investigating the active sites present on the surface and it is based on the adsorption of methanol on the surface at a fixed temperature, in order to saturate the catalytic surface; a flow of inert gas is then sent on the sample and the temperature is raised in order to desorb the species from the surface. The outlet stream is analysed by means of a mass spectrometer in order to detect the species desorbed.

Different reactions of methanol can take place on the catalytic surface, in function of the acid/base and redox sites present. In Figure 3-28 is reported the reactions scheme that occur with methanol on the surface over acid/base sites (blue arrows) or redox sites (red arrows) [104,105].

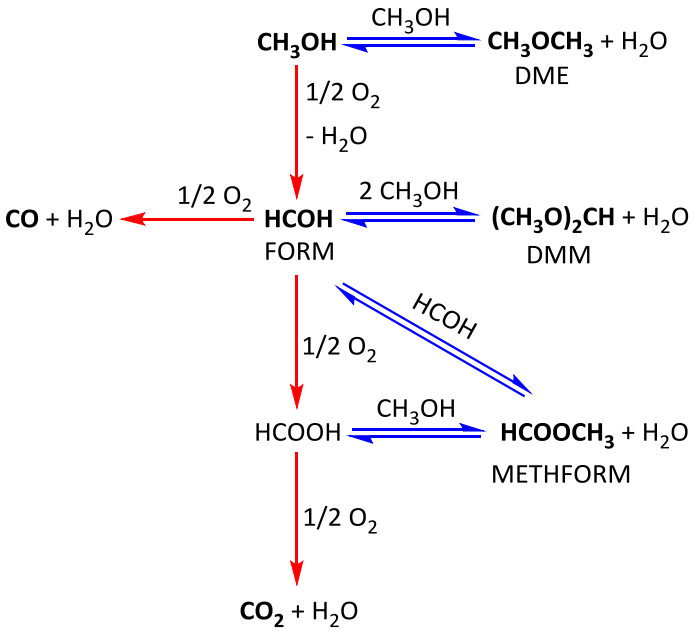

Figure 3-28 Reaction scheme of methanol over acid/base and redox sites. Blue arrows indicate the reaction takes place over acid/base sites. Red arrows indicate the reaction takes place over redox sites

Figure 3-29 shows the pulse shape (as determined by the mass specra detector) for the two catalysts investigated during the adsorption phase of methanol.

The different shape of pulses for the two catalysts provides indications concerning their surface chemical-physical features. In fact, in the case of VPO, very narrow pulses suggest negligible diffusional steps and limited chemical interaction between methanol and surface sites, whereas the opposite is true for VPP. It is worth noting that the overall area of pulses is similar in the two cases. To be more precise, the comparison between the overall amount of methanol pulsed on catalysts and the amount of methanol which has not been adsorbed indicates that with VPO only a very minor fraction of methanol remains adsorbed on catalyst, between 1 and 2%, whereas in the case of VPP the amount of methanol retained is close to 8-9%. This is a further indication that interaction phenomena, which evidently occur more extensively with VPP than with VPO, may be responsible for the different shape of pulses.

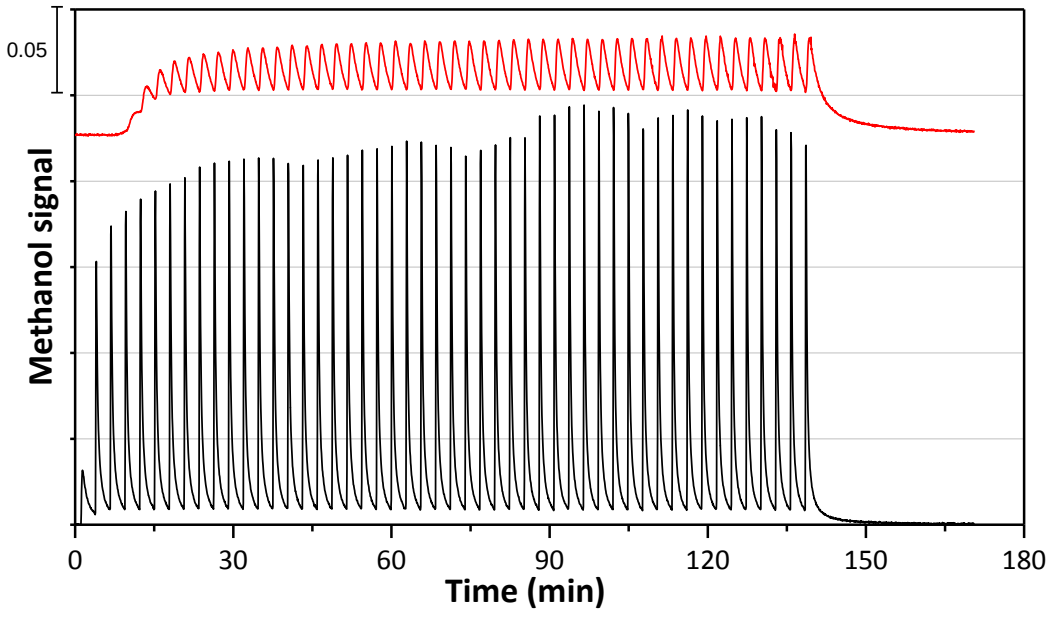

Figure 3-29 MS signal of methanol acquired during its adsorption over VPP and VPO.
Black line corresponds to VPO; **red line** corresponds to VPP.

Besides the fraction which is retained on catalyst surface, a certain amount of the methanol fed is transformed into formaldehyde, as shown in Figure 3-30.

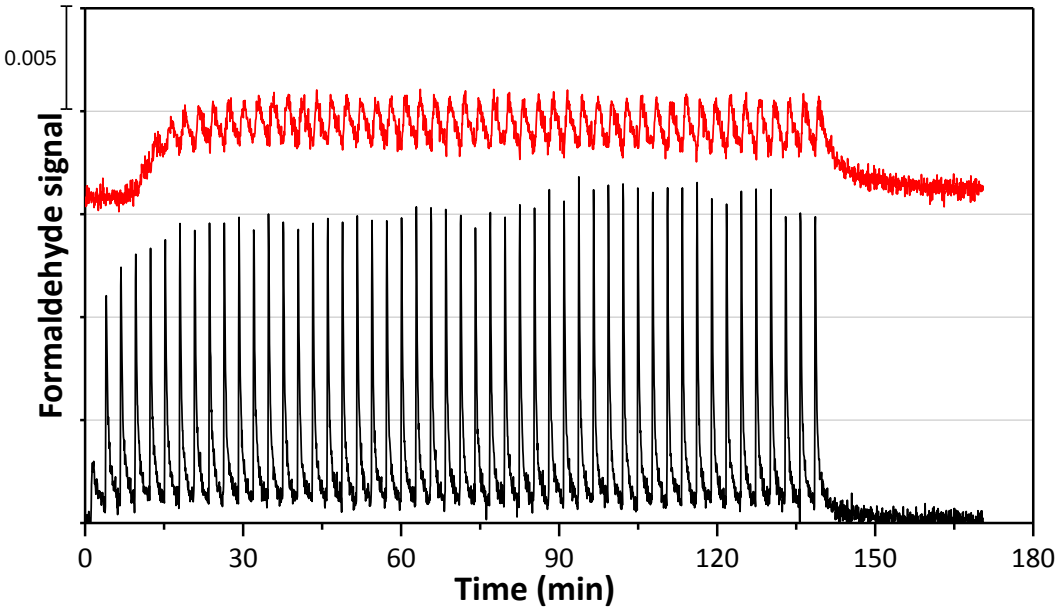

Figure 3-30 MS signal of formaldehyde acquired during the adsorption of methanol over VPP and VPO.

Black line corresponds to VPO; **red line** corresponds to VPP.

After adsorption of methanol, a TPD was carried out, while monitoring the nature and amount of products formed and desorbed. It is shown that in the case of VPO, which had adsorbed a very small amount of methanol, the signals associated to products are in general less intense than in the case of VPP. The desorption of methanol is reported in Figure 3-32 where it is possible to observe the desorption takes place between 100 and 200°C with both catalysts. About the produts, formaldehyde forms and desorbs in two different ranges of temperature, 120-200°C and 200-350°C as showed in Figure 3-31.

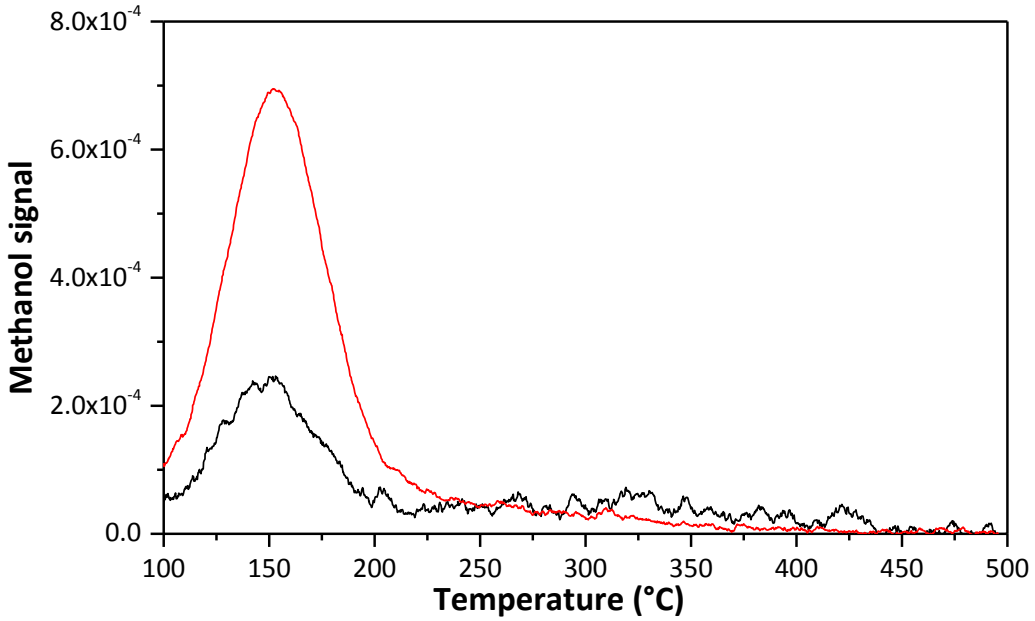

Figure 3-32 MS signal of methanol acquired during the TPD of methanol of VPP and VPO.
Black line corresponds to VPO; **red line** corresponds to VPP.

It may be hypothesized that at low temperature, formation occurs by oxidehydrogenation of methanol (previously adsorbed); this reaction may occur with co-generation of water, while V sites become progressively more and more reduced. In

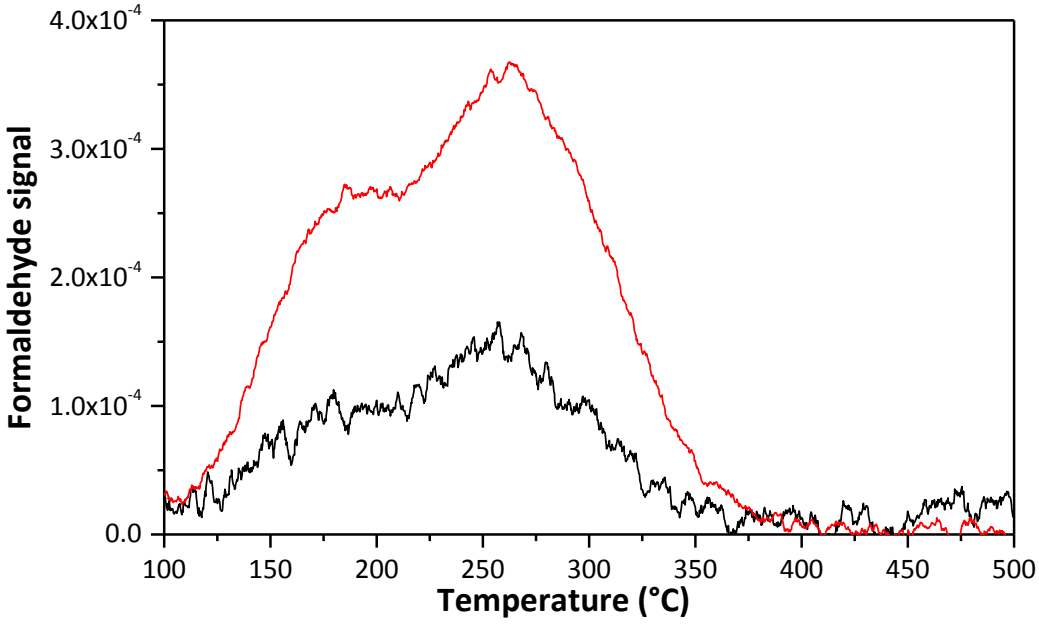

Figure 3-31 MS signal of formaldehyde acquired during the TPD of methanol on VPP and VPO.
Black line corresponds to VPO; **red line** corresponds to VPP.

the high-T range, instead, the reaction may occur by dehydrogenation, with co-production of H_2.

CO is formed in very small amount, in the temperature range of 250-to-350°C for the VPP catalyst, and probably at slightly higher temperature for VPO; in the latter case, however, the CO signal is hardly distinguishable (Figure 3-33). CO_2 is formed also in very small amount, at above 300°C with VPO; surprisingly, no CO_2 formation is detected for the VPP (Figure 3-35).

No methylformate, dimethylether and dimethoxymethane are formed; this suggests that no bimolecular reactions occurred, probably because of the very low concentration of methanol and formaldehyde adsorbed (Figure 3-34).

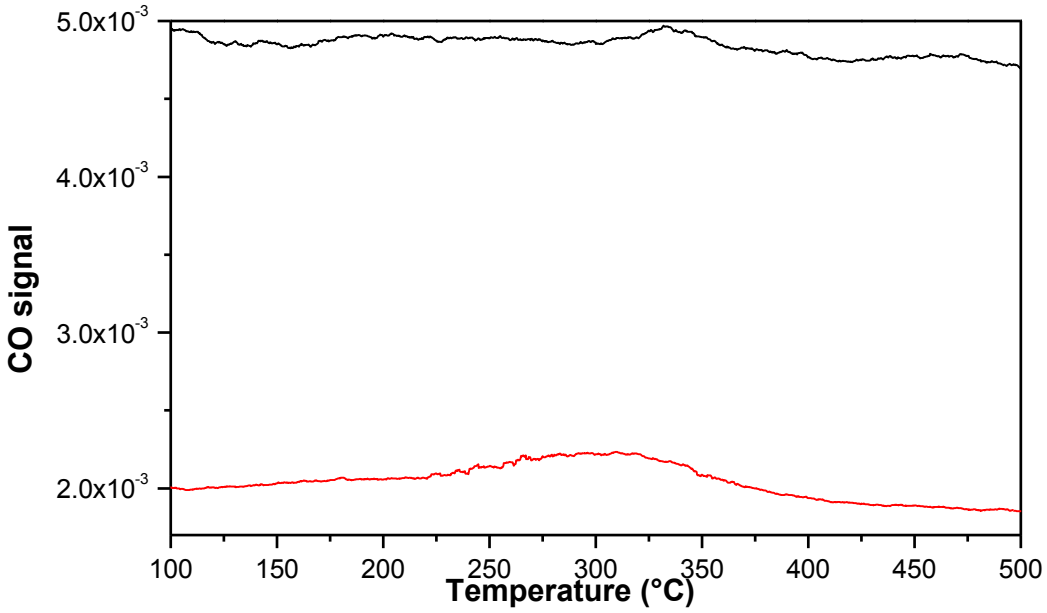

Figure 3-33 MS signal of CO acquired during the TPD of methanol on VPP and VPO.
Black line corresponds to VPO; **red line** corresponds to VPP.

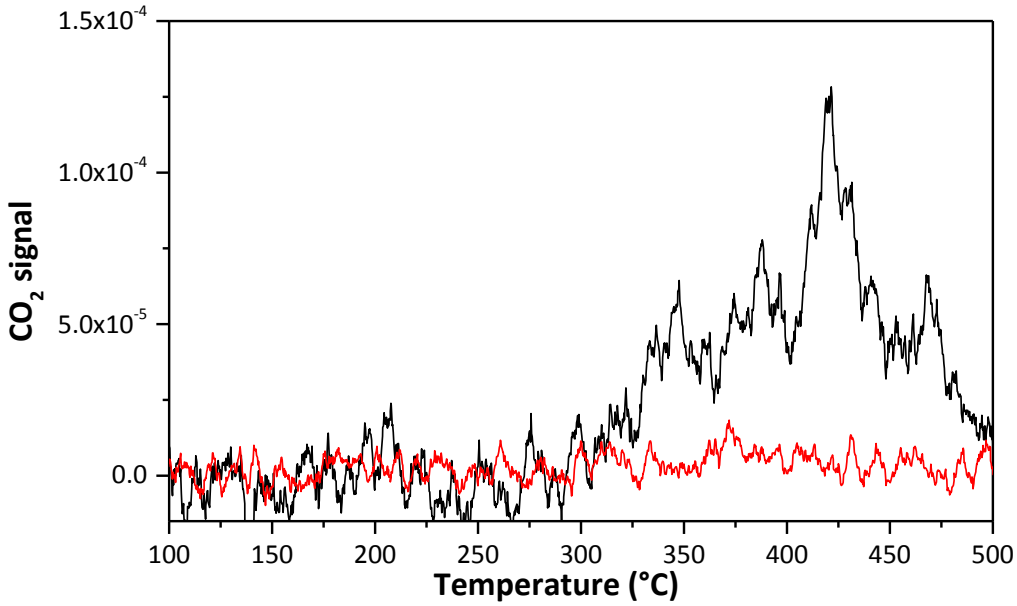

Figure 3-35 MS signal of CO_2 acquired during the TPD of methanol on VPP and VPO.

Black line corresponds to VPO; **red line** corresponds to VPP.

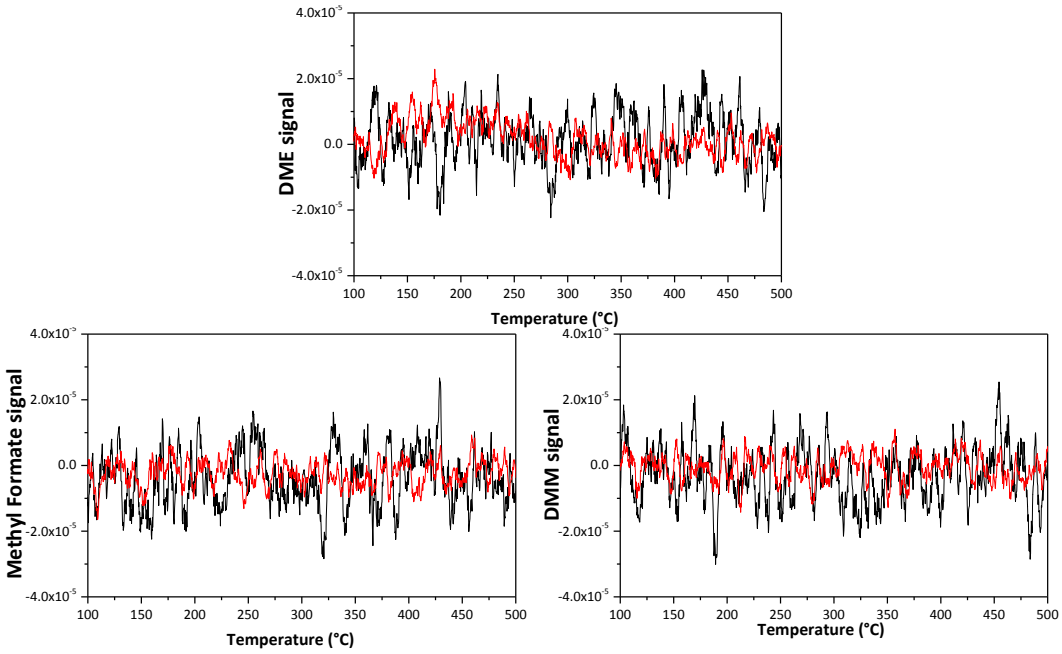

Figure 3-34 MS signal of DME, methylformate and DMM acquired during TPd of methanol on VPP and VPO.

Black line corresponds to VPO; **red line** corresponds to VPP.

These results can be useful for the interpretation of catalytic results during butanol oxidehydration. As shown in Figure 3-25, major differences between the two catalysts are the following:

- With the VPP, the higher yield to MA is shown 340°C; higher temperatures lead to a fall of MA yield, with formation of CO and CO_2. At 400°C, yield to MA is ca 16%. With the VPO catalyst, instead, best MA yield is shown at 400°C, and higher temperatures lead to only a slight decline of selectivity, with a corresponding increase of CO.
- The two catalysts differ a lot also in regard to phthalic anhydride yield. With VPP best PA yield is close to 12% at 340°C, which however declines rapidly when the T is increased, in the same way as for MA yield. With VPO, best PA yield is no higher than 5%, at 360°C, with a decline of it at T higher than 360°C.
- The formation of light acids (acetic acid, acrylic acid) is also quite remarkable with VPP (higher overall yield close to 19% at 320°C), whereas it is no higher than 5-6% (at 360-400°C) with VPO.

The results of catalytic experiments indicate that the VPP catalyst likely holds a stronger surface acidity than VPO, and that this acidity is responsible of the greater yield to both light acids (probably deriving from cracking reactions), and PA, the formation of which is known to occur via a Lewis-acid catalysed Diesl-Alder addition between the intermediately formed butadiene and MA. Acidity may also be responsible for the enhanced dehydration of butanol to butenes, which occurs at lower temperature for the VPP than for VPO (with the latter catalyst complete transformation of butanol to butenes occurs at ca 320°C, with the former one already at 270-280°C). This allows

to convert butenes into MA at much lower temperature with the VPP than with VPO. On the other hand, acidity may also be responsible for the rapid decline of MA selectivity observed with the VPP; MA, once formed, interacts more strongly with the catalyst surface and undergoes consecutive transformation into CO and CO_2. Conversely, with VPO desorption may occur more easily (also because of the higher temperature), so saving MA from consecutive combustion. These data also agree with the stronger interaction between methanol and catalyst as recorded by means of methanol pulse experiments.

Also catalytic tests carried out in function of 1-butanol molar fraction, reported in Figure 3-27, support these conclusions. Because of the weaker interaction between 1-butanol and catalyst surface shown by the VPO catalyst, surface saturation is much more difficult to achieve than with VPP; VPO can then operate at higher 1-butanol inlet partial pressure showing a less enhanced decline of MA yield. With VPP, the stronger interaction between the alcohol and catalyst surface may cause a lower availability of oxidising sites, those which are needed for the oxidation of intermediately formed butenes. In fact, with VPP at 2% butanol in inlet feed, some amount of butenes is formed, whereas with VPO no olefins are produced.

In conclusion, VPO showed a different catalytic behaviour for the oxidehydration reaction of 1-butanol, comparted to VPP. The difference of the two catalysts is correlated to the presence of a different amount of acid sites on the surface, that causes a different interaction between the species and the surface. A high amount of acid sites, in particular the Lewis ones, leads to an increase of the interaction of the adsorbed species with the surface, so favouring the consecutive reactions. This phenomenon is

observed comparing the contribution of oxidation reactions; in the case of VPP, where the interactions are stronger, these reactions take place at lower temperature compared to those that occur on the VPO; reactions catalysed by Lewis sites are also more favoured.

On the other hand, VPO, showing a lower interaction with 1-butanol, presents a higher selectivity into MA at higher temperature with a minor formation of side-products, in fact only MA, CO and CO_2 are formed.

3.6 Vanadyl phosphate as an alternative catalyst for the (oxi)dehydration of 1-butanol

A different V/P/O system was investigated for the (oxi)dehydration reaction of 1-butanol into butenes and MA. α_1 $VOPO_4$ (VPD) was tested as a multifunctional catalyst for this process because, as mentioned in section 1.6, it presents both acid and redox sites able to catalyse both the dehydration reaction to butenes, and the oxidation reaction, transforming the olefins into MA.

The first catalytic test was carried out by feeding 1 mol% of 1-butanol in helium, in order to investigate its dehydrative properties for producing olefins.

In Figure 3-36 are shown the yield, conversion, and carbon balance of the catalytic tests in function of temperature after one hour of reaction; the products detected were butenes, *n*-butyl ether, and butyraldehyde.

By analysing the catalytic behaviour of VPD at very low temperatures, the conversion of 1-butanol was around 66%, indicating the relatively low catalytic activity. In these conditions, butenes represent the main products with a yield into 2-butenes of 34%,

and for 1-butene, the yield was 12%; a little amount of *n*-butyl ether was also detected. A lack of carbon balance was observed and this could be attributable to the strong adsorption of 1-butanol on the surface.

By increasing the temperature up to 280°C, almost complete conversion is achieved. Regarding the products, 70% of 2-butenes and 20% 1-butene are the maximum yield into the olefins achieved; regarding the minor products, a drop of yield into *n*-butyl ether resulted in negligible amount of butyraldehyde.

The increase in the temperature not only disfavours the condensation reaction of two molecules of 1-butanol into the relative symmetric ether favouring the other reactions, but also increases the oxidative dehydrogenation reaction. An atom of oxygen is extracted from the lattice of the $VOPO_4$ in the form of water after removal of two hydrogen atoms from the alcohol; this leads to a reduction of V^{+5} ions into V^{+4}, and the oxidation of the alcohol into its corresponding aldehyde.

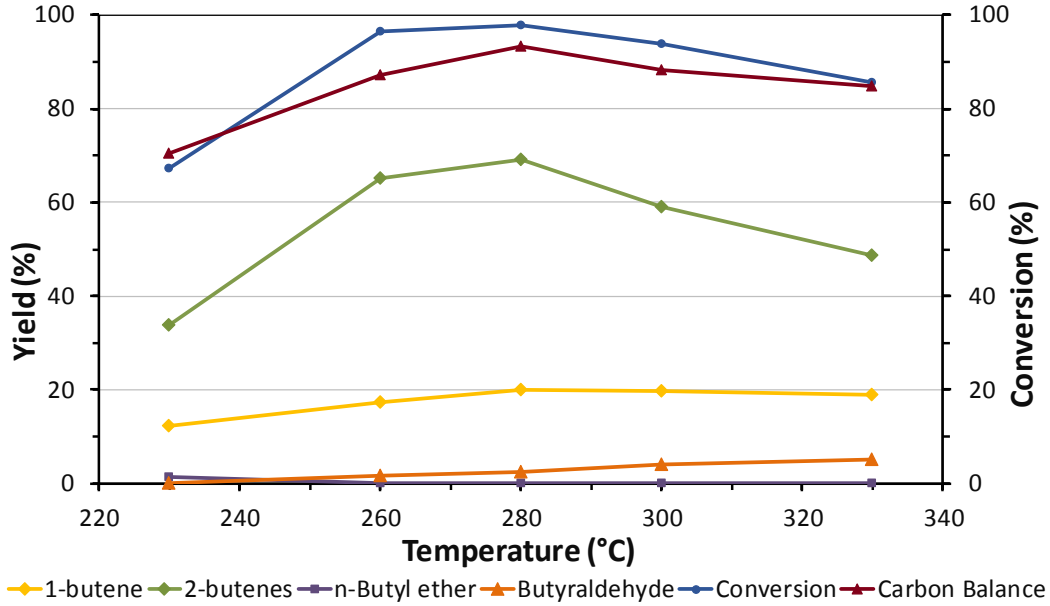

Figure 3-36 Catalytic behaviour of VPD in the dehydration reaction with 1-butanol in helium in function of the temperature after one hour of reaction. Feeding: 1% 1-butanol, rest helium; W/F:1,3 g_{cat}·sec/mL.

At higher temperatures, the yield into 2-butenes decreases from 70% down to 40%, while the yield into 1-butene remains constant; these trends are correlated to both the isomerization reaction as well as the condensation of the olefins. The ratio between the two positional isomers is always lower than the thermodynamic value; this suggests the rate of dehydration reaction is higher than that of isomerization, and the latter is also even more disfavoured with the increase in the temperature [103]. The more rapid decrease in 2-butenes compared to the increase in 1-butene, shown along with a raise of the lack in carbon balance, indicates that condensation reactions between the olefins and the intermediates occurred on acid sites, producing carbonaceous species with a high molecular weight that stay adsorbed on the surface. The maximum yield into butyraldehyde is 9% and is achieved at 360°C; this underlines the effect of temperature on oxidation reactions. High temperatures favour the spillover of oxygen from the surface to the gas phase and the diffusion from the bulk to the surface [54,106].

A detailed investigation of the catalytic activity revealed that the catalyst decreased the conversion from almost 100% down to 75% and this can be correlated to the formation of carbonaceous species (mentioned before) over the active sites of the catalytic surface that hinders the transformation of 1-butanol.

The deactivation process was investigated by carrying out the same catalytic tests for 5 h and by comparing the results with those reported in Figure 3-36; the conversion, carbon balance, and selectivity into butenes and butyraldehyde as a function of temperature are shown in Figure 3-37.

The only significant variation could be observed at 230°C in butenes selectivity; after 5 h of reaction, the selectivity increased from 68% to 81%, probably because the steady

state of the process was not achieved after 1 h. Regarding the conversion of 1-butanol, a remarkable drop is shown; this behaviour can be correlated to the formation of carbonaceous species on the catalytic surface that cover the acid sites, making them less active for the dehydration. The constant selectivity into butyraldehyde indicates the selective poisoning effect of these species on the acid sites.

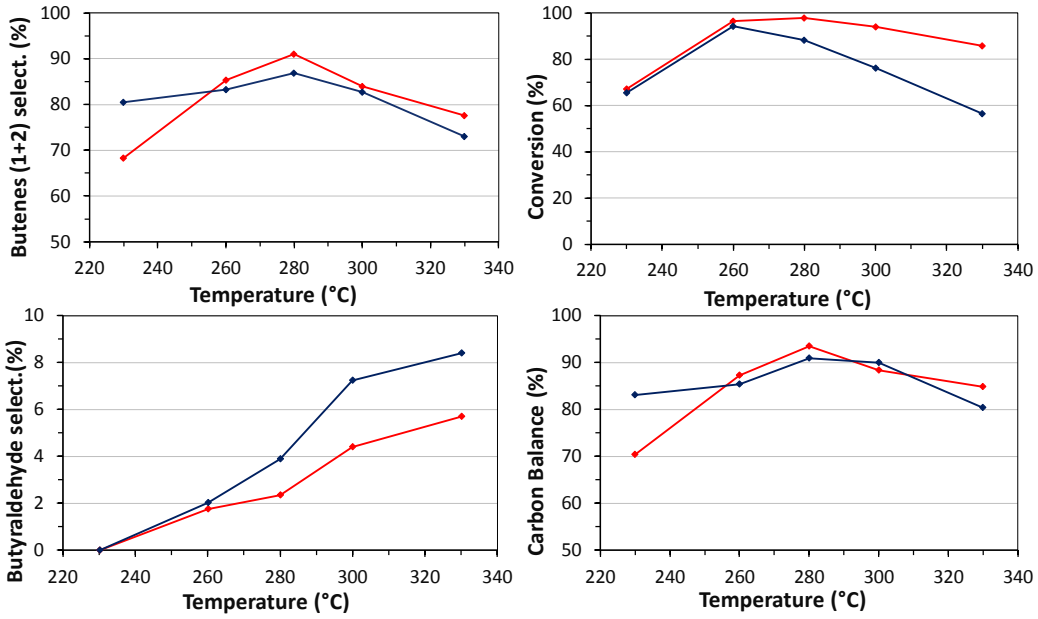

Figure 3-37 Comparison of catalytic behaviour of VPD catalyst for the dehydration reaction of 1-butanol in helium, after 1 and 5 hours of reaction. Feeding: 1% 1-butanol, rest helium; W/F:1,3 g_{cat}·sec/mL.
Red lines: 1 hour of reaction; Blue lines: 5 hours of reaction

The deactivation process was further investigated, by monitoring the catalytic behaviour of VPD at 330°C for 14 h. The results, shown in Figure 3-38, reveal an important deactivation of the catalyst during the time on stream, i.e., the conversion drop from 90% to 32%; on the other hand, no variation in the selectivity into the products is observed. After the test, the spent catalyst underwent calcination treatment at 440°C for 12 h, in order to remove the species deposited. The results obtained after calcination (Figure 3-38) revealed a complete conversion of the alcohol after the first hour of reaction, with a high selectivity into butenes, indicating the complete

regeneration of the catalyst. After two more hours, a lack of carbon balance is observed, suggesting the formation of the carbonaceous species that leads to VPD deactivation, given that the conversion decreases from 100% to 80% after 7 h of reaction.

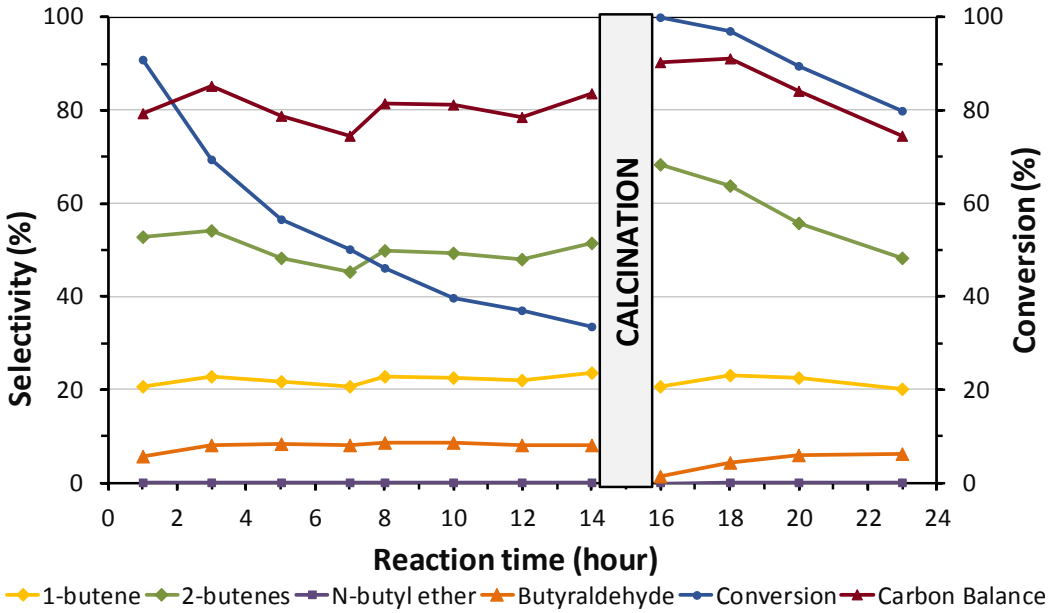

Figure 3-38 Catalytic behaviour of VPD before and after calcination treatment in function of the time on stream for the dehydration reaction of 1-butanol. Feeding 1% %mol 1-butanol, remain helium. Temperature: 330 °C. W/F: 1,3 g_{cat}/mL·sec

The characterization of the VPD after the reaction at 330°C by Raman technique and XRD analysis shows a different catalytic system compared to the one reported in paragraph 3.2.

The Raman spectra, reported in Figure 3-39, show a not perfect homogeneity of the catalyst, due to the presence of the carbonaceous species that cover the real catalytic surface. Analysing the bands, those at 1033, 921, 576, and 531 cm^{-1} can be correlated to the presence of the α_1 $VOPO_4$ phase [107]. The bands at 1590 and 1376 cm^{-1} confirm the formation and the permanency of carbonaceous species on the catalytic surface [108,109]; the bands at 1178 and 1130 cm^{-1} are due to the presence of the $(VO)_2P_2O_7$ phase.

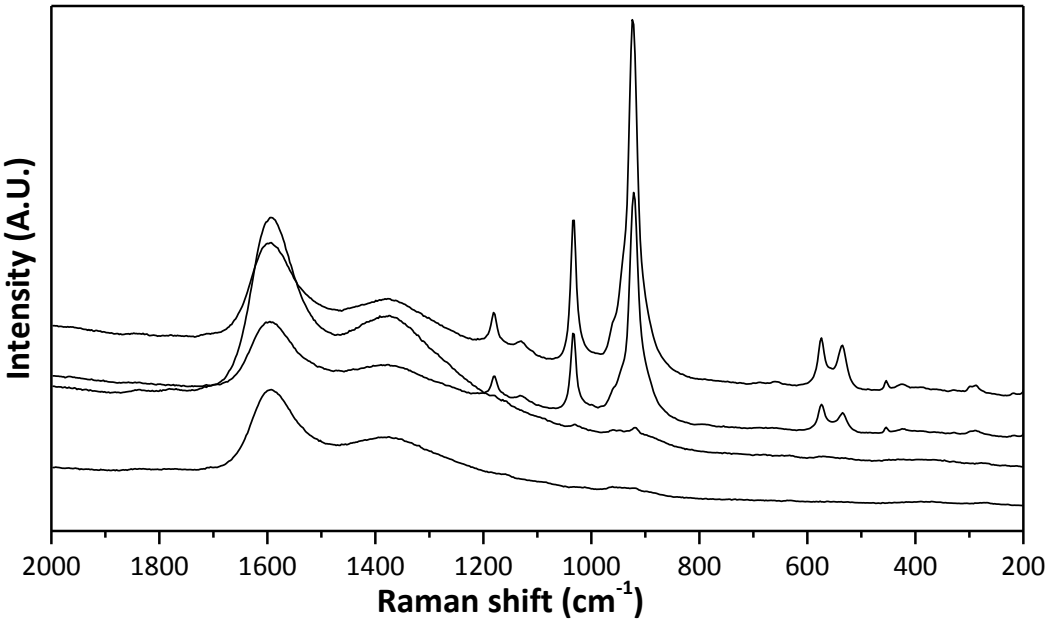

Figure 3-39 Raman spectra acquired over different spots of VPD spent catalyst after reaction of 1-butanol in helium at 330 °C

The formation of the VPP phase is correlated to the oxidative dehydrogenation reaction of 1-butanol that took place at high temperatures, leading the production of butyraldehyde and the consequent reduction of the V^{+5} species into V^{+4}.

The XRD pattern of the VPD spent catalyst, reported in Figure 3-40, shows both signals of the $(VO)_2P_2O_7$ and of α_1 $VOPO_4$. The low intensity of the signal of α_1 $VOPO_4$ could be due not only to the reduction of the catalyst, but also the presence of the carbonaceous species.

These results confirmed that the acid sites present on the α_1 $VOPO_4$ catalyse not only the dehydration of the alcohol into corresponding olefins, but also the formation of heavy carbonaceous species on the catalytic surface, thus poisoning the sites and causing a decrease of the catalytic activity.

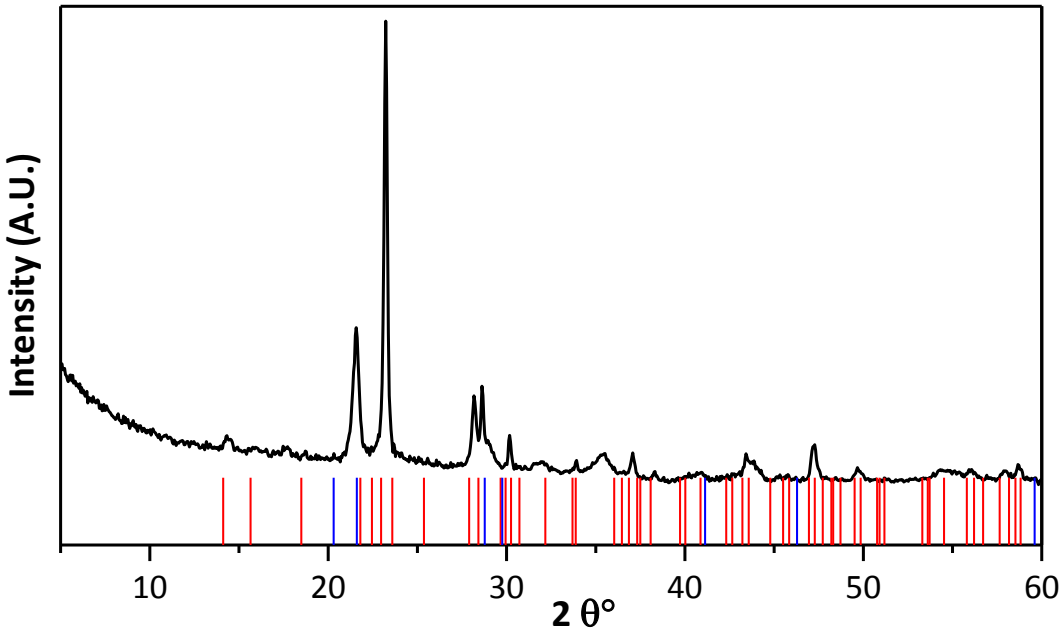

Figure 3-40 XRD analysis of VPD spent catalyst after reaction with 1-butanol in helium at 330 °C. Red lines represent the pattern of $(VO)_2P_2O_7$; Blue lines represent the pattern of α_1 $VOPO_4$

The previous results have shown some redox properties of α_1 $VOPO_4$ because a significant amount of butyraldehyde was obtained; it was then decided to investigate the catalytic behaviour of VPD by feeding 1-butanol in air at different temperatures in order to favour also the oxidation reactions.

The results shown in Figure 3-41 reveal a completely different catalyst behaviour with respect to the one observed previously; in particular, an almost total conversion is observed at 260°C.

At 230°C, both the conversion and the yield of the products are comparable to those obtained by feeding 1-butanol in helium, as shown in Figure 3-36; under these conditions, the conversion of the alcohol is slightly higher than 60%, olefins are the main products, a low yield into *n*-butyl ether is obtained, and a lack of carbon balance is also observed. Thus, it can be concluded that the sites on the catalytic surface are not completely active at 230°C. The low activity of the acid sites is reflected on the

isomerization reaction of the olefins produced, because the ratio between 2 and 1-butene is much lower than the thermodynamic one [103].

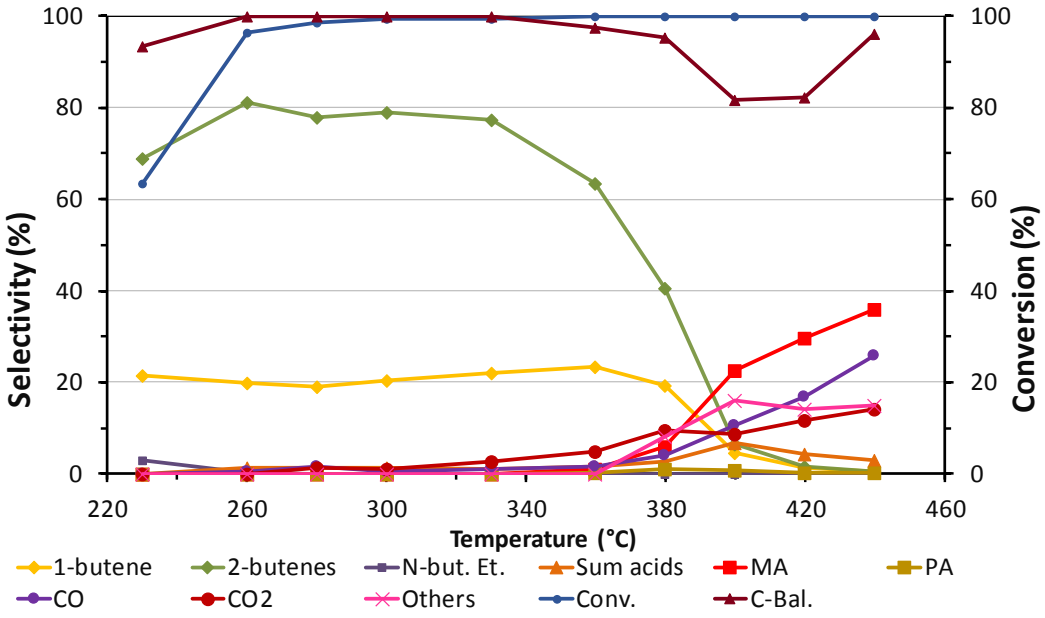

Figure 3-41 Catalytic behaviour of VPD in the oxydehydration reaction with 1% %mol 1-butanol in air function of the temperature. Feed composition: 1% %mol 1-butanol, 20% %mol O_2, remain N_2; W/F:1,3 g_{cat}·sec/mL

On increasing the temperature, complete conversion is achieved and an almost complete selectivity into olefins is observed which remains constant, until 300°C, and the ratio of the isomers reaches the thermodynamic value. Under these conditions, no formation of *n*-butyl ether is observed, and a very low yield into butyraldehyde is obtained (<1%); in contrast to the catalytic behaviour in helium, in this case, the oxidative dehydrogenation of the alcohol is strongly hindered owing to the faster dehydration of the alcohol compared to the redox process.

By investigating in detail the results at 280°C, 98% of yield into olefins is obtained, and it was therefore decided to further investigate the catalytic behaviour of VPD in order to understand its catalytic activity during the reaction. The results are shown in Figure 3-42, in which conversion and selectivity of the products acquired during 7 h

of reaction are shown. The results indicate a good stability and selectivity to the olefins for VPD during the time on stream, which is kept constant at 98% for the entire test.

Analysis of the results in Figure 3-41 shows that after 320°C, oxidation reactions start

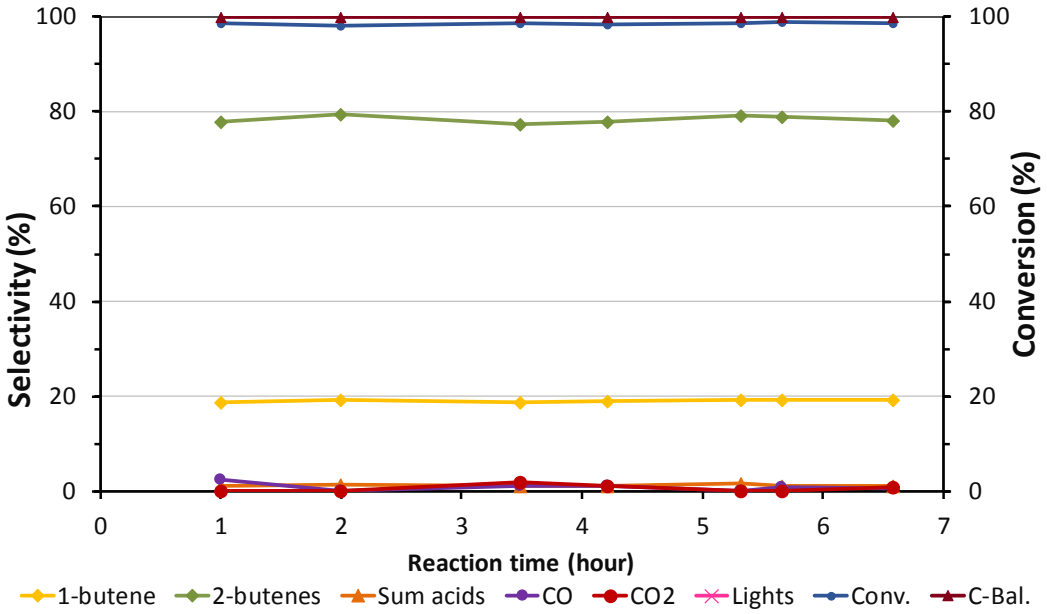

Figure 3-42 Catalytic behaviour of VPD in dehydration reaction with 1-butanol in air in function of the reaction time. Feed: 1% %mol 1-butanol, 20% %mol O_2, remain N_2. Temperature: 280°C; W/F:1,3 g_{cat}·sec/mL

to occur; at first, the non-selective reactions with the formation of CO and CO_2 that are derived from the overoxidation of the intermediates either on the catalytic surface or in homogeneous phase.

At 380°C, 35% of the olefins produced is transformed into oxygenated compounds such as CO, CO_2, MA, light acids (acetic and acrylic acid), and other compounds, indicated as "others" as shown in Figure 3-43. The wide variety of the obtained species are derived from the different oxidation reactions that take place on the surface; light acids are obtained from the oxidative cleavage; while the "others" are intermediates or side-products of the selective oxidation of olefins into MA, as showed in Figure 1-6.

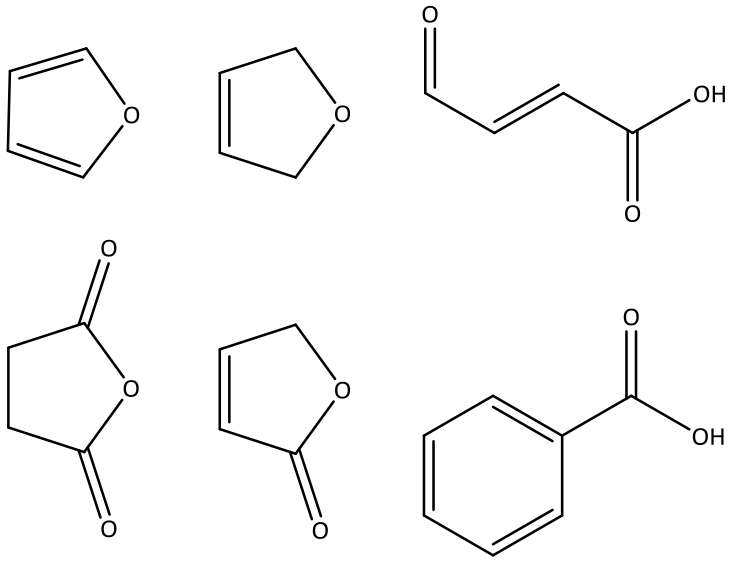

Figure 3-43 Main molecules detected and reported as "others"

A further increase in temperature leads to an increase of all oxygenated species, and MA becomes the product with the highest selectivity; a lack of carbon balance is also observed due to the probable formation of an intermediate or carbonaceous species with high molecular weight that remains adsorbed on the catalytic surface.

At 440°C, MA and CO_x achieve 39% and 40% of selectivity, respectively, the "others" 15% selectivity, with an almost complete carbon balance. Detailed analysis of the products shows no formation of phthalic anhydride, suggesting that the insertion of oxygen in the olefins occurs more quickly than the oxidative dehydrogenation into 1,3-BDE.

Regarding the oxygenated species, and in particular MA, their formation suggests the establishing of the redox cycle V^{+4}/V^{+5} and the formation of a $(VO)_2P_2O_7$ phase on the α_1 phase of $VOPO_4$. The possible reduction of the VPD phase at high temperatures with the in-situ formation of $(VO)_2P_2O_7$ one, should lead to a variation in the catalytic behaviour of VPD, and therefore, a catalytic test at 330°C after reaction at 440°C was carried out, and both Raman and XRD analysis on the spent catalyst were performed.

The results of the catalytic test are shown in Figure 3-44, reporting the selectivity into 1 and 2 butenes, MA and CO_x obtained before (1st run) and after (2nd run) the test at 440°C, and these results are compared with those obtained in the same conditions with the VPO catalyst in Figure 3-22. Comparing the two runs, before and after reaction at 440°C, both are observed to exhibit a similar catalytic performance; while, comparing the results with those for the pure $(VO)_2P_2O_7$ phase, the VPD catalyst shows a lower selectivity into oxidised products. These results suggest that the VPD at 330°C presents the $VOPO_4$ phase, while at 440°C, a superficial transformation occurs, leading to the in-situ formation of the VPP phase.

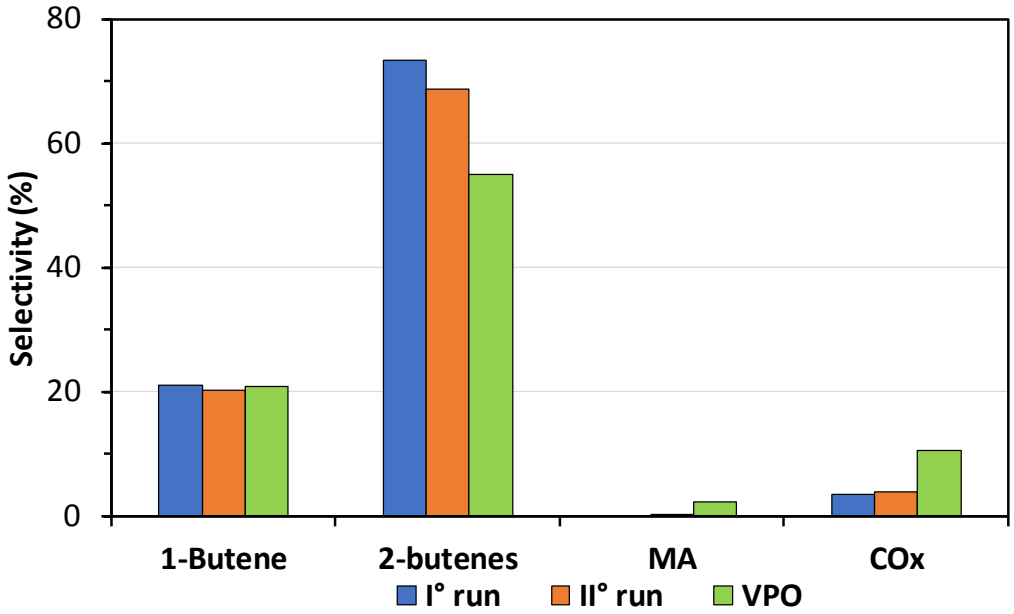

Figure 3-44 Comparison of catalytic behaviour of VPD (1st and 2nd run) and VPO for the oxidehydration reaction of 1-butanol in air. Feed: 1 mol% 1-Butanol, 20 mol% O_2, except N_2. Temperature 330 °C. W/F: 1.3 g_{cat}·s/mL

Ex-situ Raman spectra of VPD spent catalyst after reaction at 440°C are shown in Figure 3-45 and reveal the presence of carbonaceous species (1600 and 1370 cm^{-1}), which is in agreement with the lack of carbon balance observed, the presence of the α_1 phase of $VOPO_4$ (1032, 573, 534, and 452 cm^{-1}), while the bands at 1180 and

1128 cm^{-1} are correlated to the VPP phase, which confirms the partial reduction of the α_1 $VOPO_4$ phase into $(VO)_2P_2O_7$.

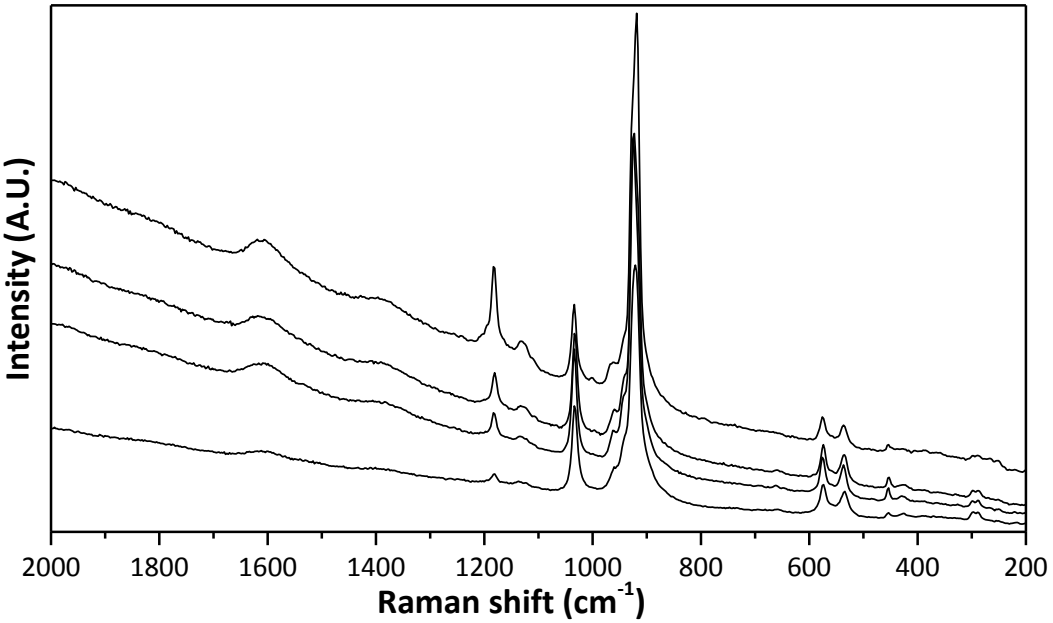

Figure 3-45 Raman spectra acquire over different spot of VPD spent catalyst after reaction of 1-butanol in air at 440 °C

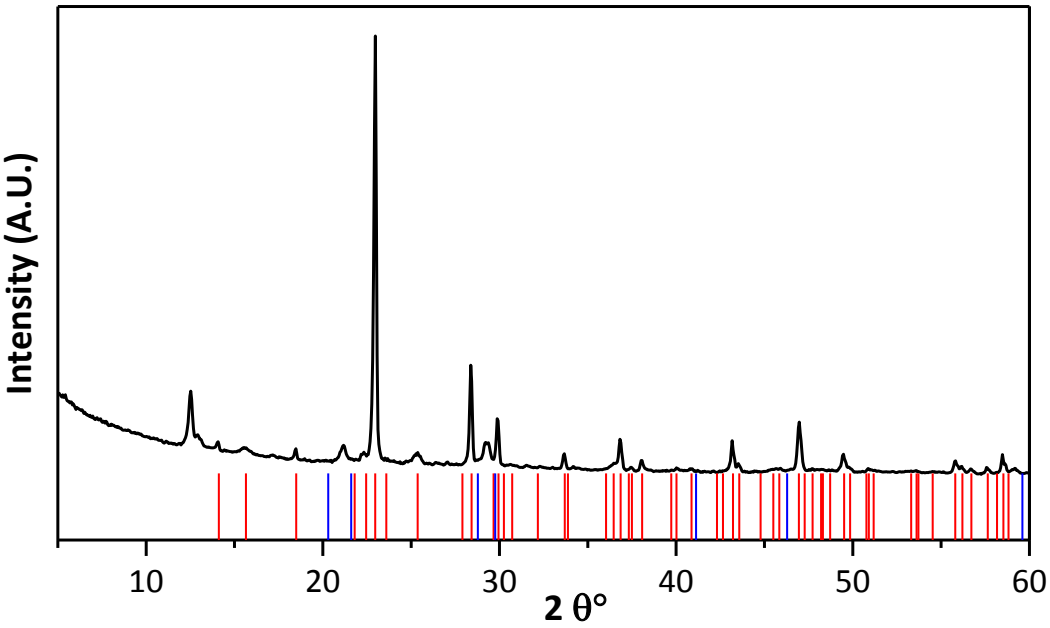

Figure 3-46 XRD analysis of VPD spent catalyst after reaction with 1-butanol in air at 440 °C. Red lines represent the pattern of $(VO)_2P_2O_7$; Blue lines represent the pattern of α_1 $VOPO_4$

The XRD pattern of the VPD catalyst after reaction at 440°C, shown in Figure 3-46, reveals the reflections related to both the $(VO)_2P_2O_7$ phase and the α_1 $VOPO_4$ phase, thus underlining the formation of a reduced phase of $VOPO_4$ at high temperature in aerobic atmosphere.

From the results observed before, it was then decided to investigate the transformation of α1 VOPO4 into VPP, and *in-situ* Raman experiments were carried out for monitoring the variation in the catalytic surface of VPD catalyst when feeding 1-butanol in air at different temperatures.

The experiment was carried out by feeding 1 mol% of 1-butanol in air, from 380°C to 460°C, thus simulating the same conditions of the laboratory plant. In the beginning, fresh catalyst was subjected to the same calcination process, as that reported in paragraph 3.2, in order to transform the $VOPO_4{\cdot}2H_2O$ into α_1 $VOPO_4$.

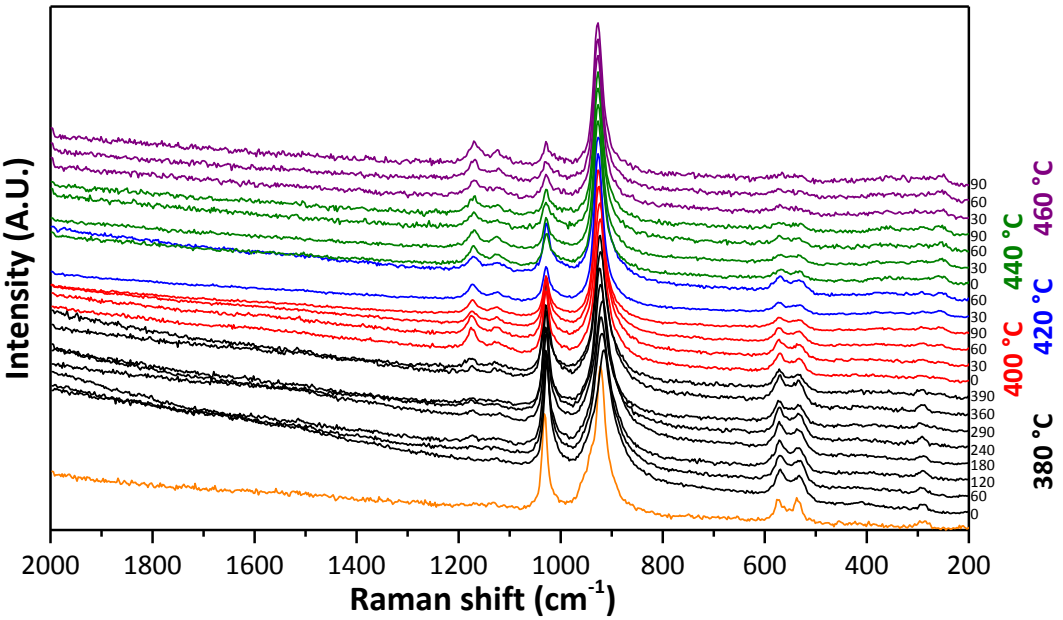

Figure 3-47 *In-situ* Raman Experiment of VPD catalyst feeding 1 mol% of 1-butanol in air at different temperature. All the spectra are normalised in function of the peak at 920 cm^{-1}.
Orange spectrum was acquired at room temperature

In Figure 3-47, the spectra acquired at different temperatures during the time on stream are shown. The first spectra, coloured in orange, is acquired at room temperature before the reaction and shows the bands at 1031, 921, 574, 536, and 288 cm^{-1} associated with the α_1 phase of $VOPO_4$.

After 120 min of reaction at 380°C, the formation of two bands with a very weak intensity at 1172 and 1123 cm^{-1} was observed, an event that could be correlated to the formation of $(VO)_2P_2O_7$. On increasing the temperature to 400°C, the bands attributable to the VPP phase become clearly visible, indicating the formation of a more reduced phase. A further increase of temperature and time led to the decrease of the bands at 1031, 574, 536, and 288 cm^{-1} attributable to α_1 $VOPO_4$. At 460°C, the bands at 574, 536, and 288 cm^{-1} disappeared, while the intensity of band at 1031 cm^{-1} was decreased, indicating the almost complete reduction of the $VOPO_4$ phase into VPP.

These results could be correlated to the catalytic behaviour reported in Figure 3-41: at 380°C, both the production of a significant amount of MA (from the catalytic tests) and the appearance of VPP phase (from Raman spectra) were noted; on increasing the temperatures, both the amount of VPP phase on the VPD and the yield into MA increased. The strict correlation between the selectivity into MA and the presence of the VPP phase on the catalyst can be explained by considering the interaction of the intermediates with the surface. On one hand, the low surface area of VPD leads to an accumulation of 1-butanol on the surface that is dehydrated into olefins; on the other hand, high temperatures improve the mobility of the lattice oxygens. Both conditions favour the reduction of $VOPO_4$ into VPP, and thus, olefins are transformed into

oxygenated intermediates (the presence of the "others" confirm their formation) that are oxidised into MA from the portion of VPP present on the surface. The continuous decrease in the α_1 $VOPO_4$ phase suggests that the rate of the oxygen mobility in the lattice, from the bulk towards the surface, is higher compared to the re-oxidation of the surface by the molecular O_2 present in the feed.

After cooling at room temperature in air, different spectra were taken on the catalyst at different times, and a variation in the phases was observed; the spectra shown in Figure 3-48 revealed bands correlated to the α_1 phase of $VOPO_4$, while the bands related to the VPP phase were strongly hindered.

This behaviour indicates that the reduction of $VOPO_4$ into VPP is a superficial and reversible process, which can also explain the results in Figure 3-44; after the reaction at 440°C, the VPP phase formed was easily re-oxidised into α_1 $VOPO_4$, leading to the same results observed during the first catalytic test.

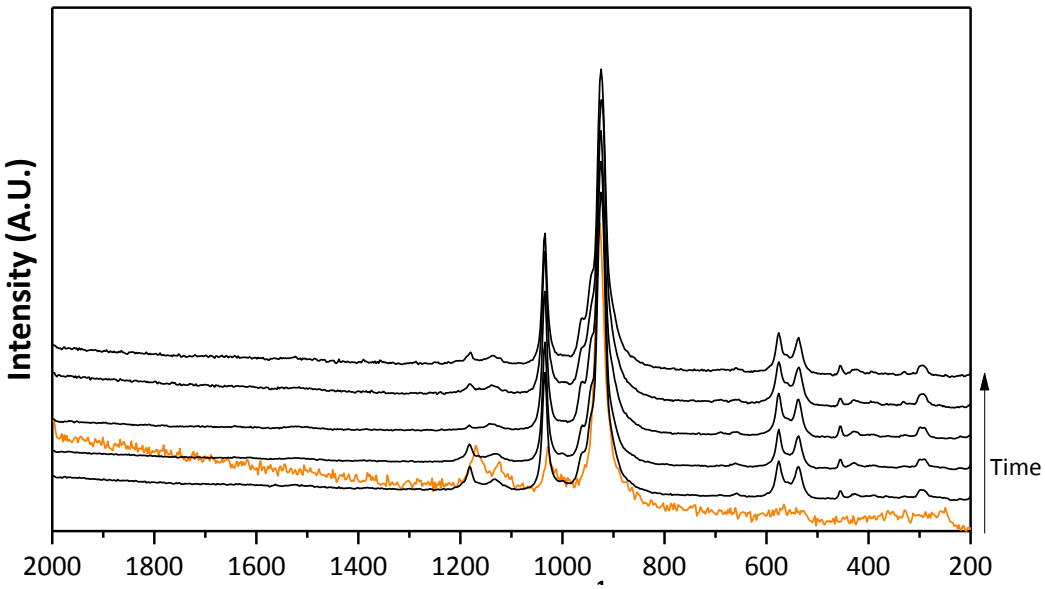

Figure 3-48 *In-situ* Raman Experiment of VPD catalyst after fed 1 mol% of 1-butanol in air
All the spectra are normalised in function of the peak at 920 cm^{-1}. Orange spectrum was acquired immediately after the finish of the reaction

In conclusion, α_1 vanadyl phosphate has shown good acid properties for the transformation of 1-butanol into its corresponding olefins by dehydration that takes place already a very low temperature. The presence of oxygen in the feed disfavour the side-reaction that cause the formation of deposit of carbonaceous compounds on the surface; these species have a detrimental effect, in particular for the conversion of the alcohol.

High temperatures favour the establishing of the redox cycle of the vanadium species with the olefins, leading to the development of a superficial and reversible reduction of the catalysts with formation of a $(VO)_2P_2O_7$ phase. The presence of this phase in aerobic atmosphere accelerates the oxidation reactions with the formation of MA, CO and CO_2.

4 Conclusions

In this part of the thesis, different parameters were investigated in order to improve the yield and productivity to butenes and maleic anhydride (MA) inthe gas-phase oxidehydration of 1-butanol, using V/P/O as multifunctional catalysts.

First, the influence of impurities in the bio 1-butanol (BB) was investigated; the worst performance in terms of MA and CO_x was obtained with the BB containing a carbazole impurity. The detrimental effect of this molecule was correlated to the strong interaction of the amino group and the aromatic ring with the catalytic surface that favour the side-reactions leading to the formation of phthalic anhydride and CO_x. The poisoning effect was observed at very low concentration of the impurities and at low temperature; this underlines the need for a high purity degree of 1-butanol.

The investigation of the influence of feed composition showed that the partial pressure of oxygen controls the V^{+4}/V^{+5} atomic ratio, that is redox couple responsible for the selective oxidative process of the intermediately formed olefins to MA. On the other hand, the partial pressure of 1-butanol influences the availability of V active sites due its strong interaction with the surface.

Two different V/P/O system were used as catalysts, alternative to the VPP supplied by DuPont; the first was a VPP synthesised by means of the VPO method and the second one was the α_1 $VOPO_4$ (VPD). The former system interacted more weakly with 1-butanol, compared to the reference VPP; this affected the yield to the products, in fact a higher yield to MA and a lower one to CO_x were obtained. The lower interaction allows also to operate at a higher concentration of the alcohol in order to increase the productivity to MA.

TPSR experiments with methanol suggested that the different catalytic behaviour is due to the presence of Lewis acid sites, that are the responsible for the adsorption/desorption processes taking place at the surface, finally affecting all reactions.

α_1 $VOPO_4$ (VPD) showed a strong interaction with 1-butanol. At low temperature, the acid properties of VPD facilitate the dehydration of 1-butanol to corresponding linear olefins; the oxygen in the feed enhanced the yield to olefins (reaching the almost quantitative yield) because it prevented the formation of the carbonaceous species over the surface, avoiding catalyst deactivation. At high temperature, the oxidative processes were favoured due to the higher mobility of lattice oxygen, in particular the selective oxidation of olefins to MA and the oxidative dehydrogenation of 1-butanol to butyraldehyde take place when the molecular oxygen is present or not in the feed, respectively. Both oxidative processes lead to the reduction of $VOPO_4$, with the formation of $(VO)_2P_2O_7$; the transformation of olefins to MA can be correlated to the formation of this latter species.

.

PART TWO

SYNTHESIS OF PYRUVIC ACID

FROM ACETOL

1 Introduction

1.1 Pyruvic acid: synthesis and uses

Pyruvic acid (PAc) is an organic compound with formula $C_3H_4O_3$, it is a liquid at ambient temperature and is one of the most important molecules in the biochemical field because it is the intermediate in the metabolic processes of proteins and carbohydrates taking part in the Kreb cycle [110].

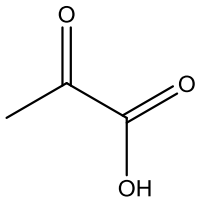

Pyruvic Acid

PAc finds applications in many industrial fields; in the pharmaceutical industry, it is used as a fat-reducing agent [111], in agrochemical, food and cosmetic productions [112]. PAc takes part in the synthesis of N-acetyl-D-neuraminic acid [113], different amino acids, such as L-tryptophan, L-tyrosine and L-alanine [114].

The most important synthetic processes of PAc are based on the direct fermentation of different organic substrates, such as glucose [112], or on the dehydration and subsequent decarboxylation of tartaric acid (Figure 1-1) [115].

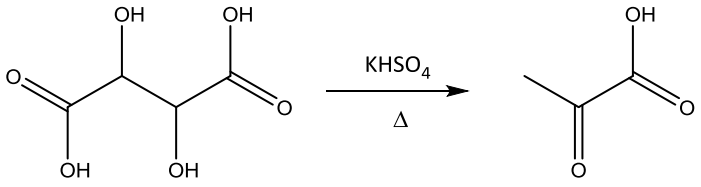

Tartaric acid Pyruvic acid

Figure 1-1 Reaction scheme of the production of pyruvic acid (PAc) from tartaric acid.

The synthesis by fermentative process of glucose presents the advantage to use cheap starting materials, deriving from renewable sources, helping to reduce the final cost of PAc. These processes are based on the fermentative processes of different

microorganisms, both eukaryotic and prokaryotic; the final concentration of PAc in the solution obtained is close to 135 g/L. However, these processes show a low final yield to PAc due to the low efficiency of the separation process, which is correlated to the complexity of the final mixture [116,117].

The transformation of tartaric acid into PAc presents the possibility to obtain PAc at a higher yield compared with the fermentative processes [115], however, the low atomic efficiency and the higher cost of both the starting material and the whole process have led this process to be abandoned in favour of the first one.

In light of the continuous growth of the market for PAc [118] and the development of new processes based on renewable sources, research is also focusing on economically sustainable processes with higher atomic efficiency that lead to obtain high yield to PAc with high purity.

In this context, the upgrading of glycerol could play an important role. Glycerol, co-product with FAME in the production of bio-diesel from oils, was considered a waste product; while, since few years, many efforts have been made to develop processes based on its transformation into molecules with higher added value [119].

The strategy of using waste as a starting material, on one hand, is looking toward the development of processes based on the green chemistry principles [1], and on the other hand, helps to make the entire productive process of bio-diesel more economically sustainable and more competitive compared to diesel from fossil fuel [120,121].

1.2 Glycerol

Glycerol (GLY) is a polyol; it is soluble in many solvents, such as water (at all ratios), short chain alcohols and linear and cyclic heteroatomic compounds; on the opposite, it is insoluble in paraffins and olefins. GLY is a colourless and odourless liquid at room temperature, it presents a high viscosity and high boiling point (290 °C) due to the presence of strong intermolecular hydrogen bonds.

As mentioned above, GLY is the co-product of bio-diesel production that is constituted by a mixture of different methyl esters of fatty acids; it is obtained by a acid-catalysed transesterification process, as illustrated in Figure 1-2 [122]. The process leads to obtain GLY with a purity degree of 60-80%, because it contains inorganic salts, methanol, water, fatty acid and other impurities. A vacuum distillation and other finishing steps permit to obtain GLY with very high purity degree.

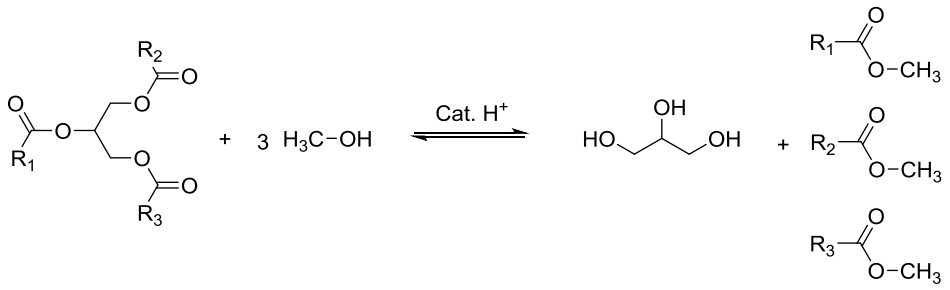

Figure 1-2 Reaction of transesterification of triglyceride into FAME and glycerol.

In recent years, the increase of the production of bio-diesel has led to the saturation of the GLY market and a drop in its price from 1750 $/ton to less than 750 $/ton; this fact and presence of three hydroxyl groups in the molecule, have helped to choose this molecule as a possible starting material for the production of compounds with higher added value; Figure 1-3 shows some of the most interesting transformation processes of GLY.

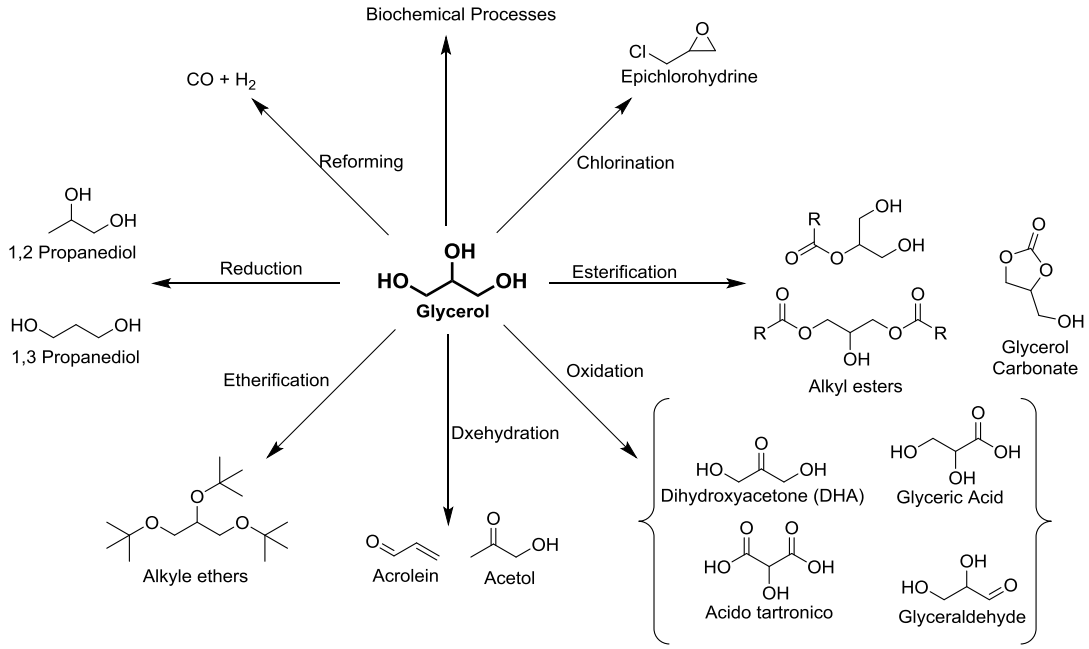

Figure 1-3 Main transformation processes of glycerol into chemicals with higher added value.

The principal products obtained by the reduction of GLY are 1,2 and 1,3 propanediols (Figure 1-4); the first finds application as a refrigerant agent, disinfectant and in the pharmaceutical industry, while the second is used as a monomer and green substitute for ethylene glycol.

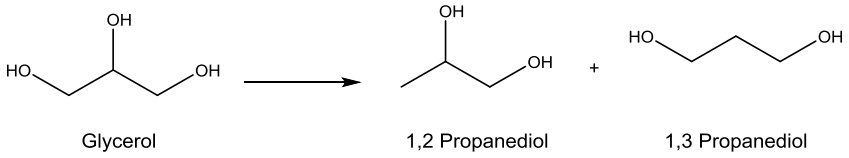

Figure 1-4 Reduction reaction of glycerol.

Both diols can be obtained by both chemo-catalytic and fermentative processes; the chemical reduction provides for the hydrogenolysis using H_2 in presence of different catalysts [123], obtaining good conversion but low selectivity to one of the diols; in contrast, the fermentative approach leads to higher selectivity to only one of the isomers.

Dihydroxyacetone, tartronic and mesoxalic acid are the main products obtained by oxidation of GLY (Figure 1-5). They found application in different fields as intermediates, monomers and for the pharmaceutical and cosmetic industries. They are obtained mainly by selective oxidation using different oxidant agents, such as TEMPO or H_2O_2 [124].

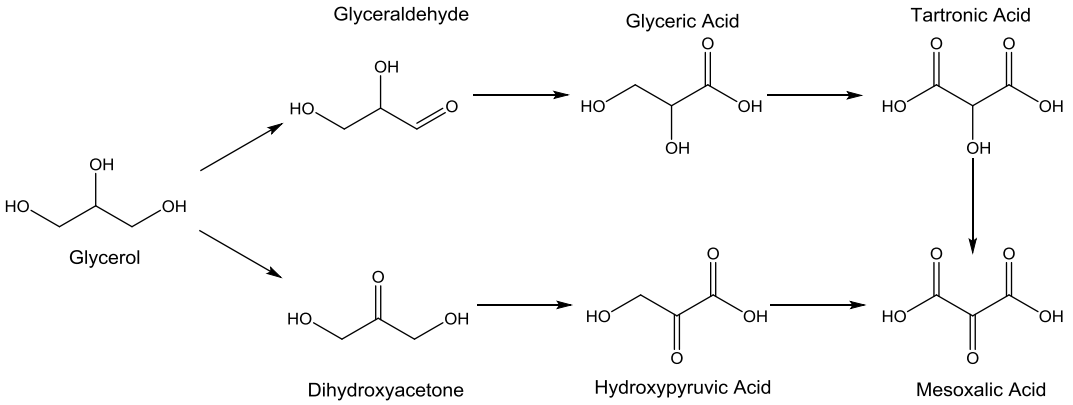

Figure 1-5 Scheme of the oxidation reaction of glycerol.

An already developed industrial process based on GLY is the halogenation for the production of epichlorohydrin by means of the EPICEROL process, patented by Solvay (Figure 1-6) [125]. The process is based on two steps; the first step regards the formation of a 1,3-dichloropropanol using HCl as chlorinating agent (its isomers are also obtained, but in small percentages) and carboxylic acid as the catalyst, while the second step is the dehydrochlorination of the latter by NaOH.

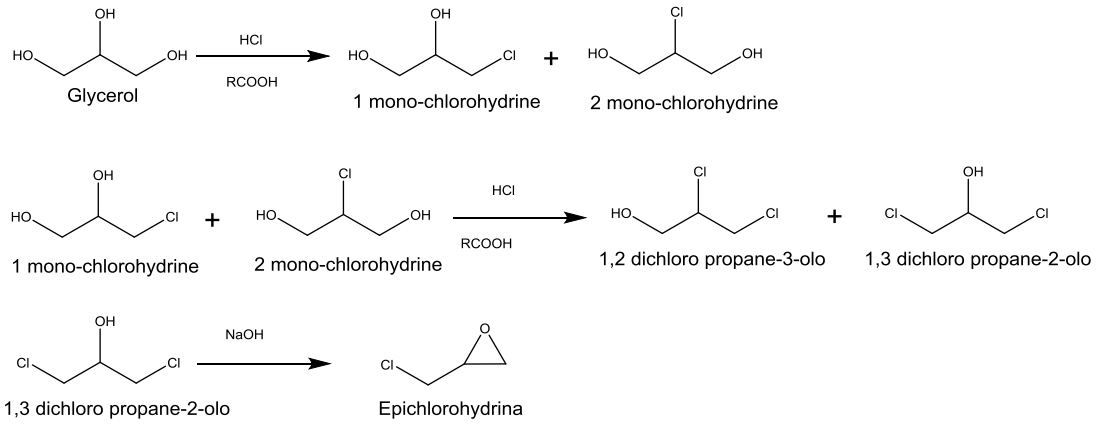

Figure 1-6 Reaction scheme of the EPICEROL process.

Products of etherification of GLY are mono-, di-, and tri-*iso*-butyl alkyl glycerol, which are used as additives for diesel fuels, they are obtained by liquid phase reaction of GLY with *iso*-butylic alcohol or iso-butene using zeolites and other heterogeneous systems as catalysts [126].

About the esterification, acetates, glycerol carbonate and nitroglycerin have mainly been used and investigated. Particular attention has been devoted to the glycerol carbonate due to its properties; it has found application in different fields, from pharmaceuticals to solvent for Volatile Organic Compounds (VOC); moreover, it has been used as intermediate for the production of different molecules [127]. The synthesis of glycerol carbonate can be carried out with different approaches [128], some of which are shown in Figure 1-7; particular attention is being paid to the route from CO_2.

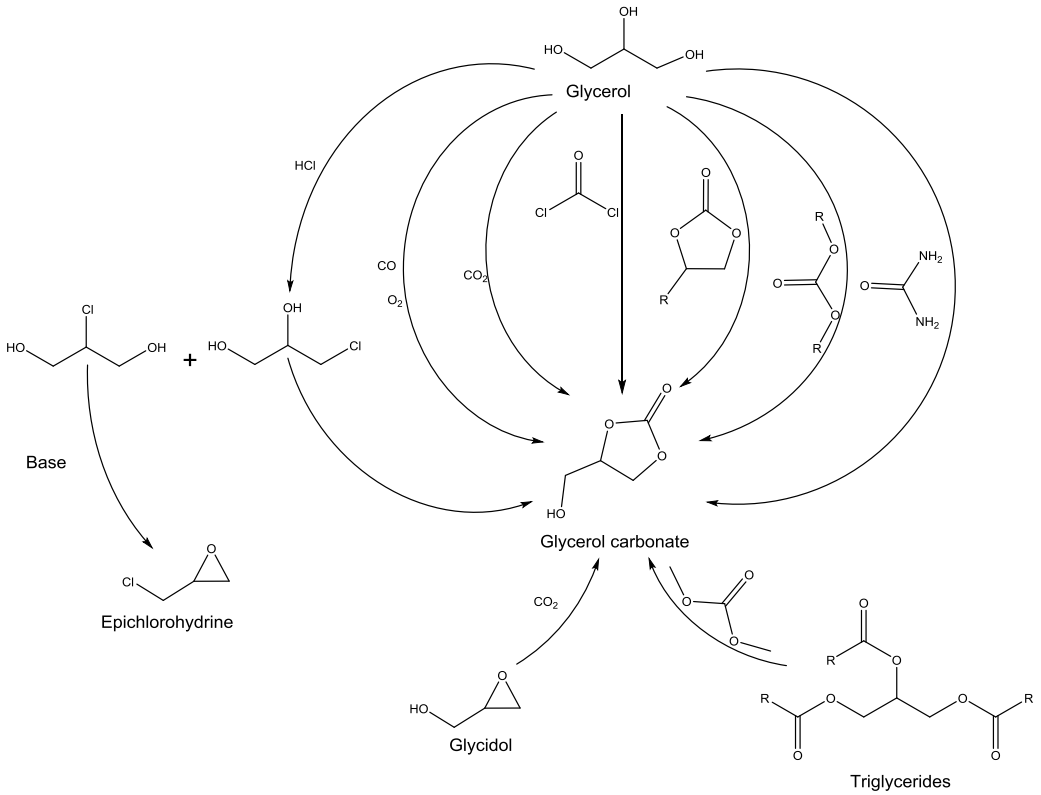

Figure 1-7 Main synthetic route for glycerol carbonate production.

Two important molecules can be obtained by dehydration reactions, namely acrolein and acetol (Figure 1-8).

Acrolein is the simplest aldehyde containing an unsaturation and its main use is as intermediate for obtaining molecules like acrylic acid and methionine. It is produced from a double dehydration process [129].

Acetol has different applications, it is used as flavouring agent in the food industry, cosmetics and as intermediate for the synthesis of different molecules, such as propylene glycol.

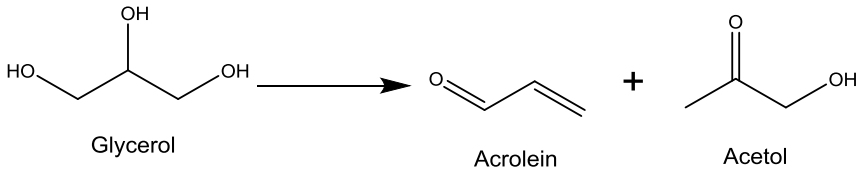

Figure 1-8 Dehydration reaction of glycerol.

1.3 Aim of the work

As described above, the process investigated in this study involves the production of pyruvic acid from glycerol.

Different routes can be hypothesised for the transformation of GLY into PAc, and the main ones are reported in Figure 1-9.

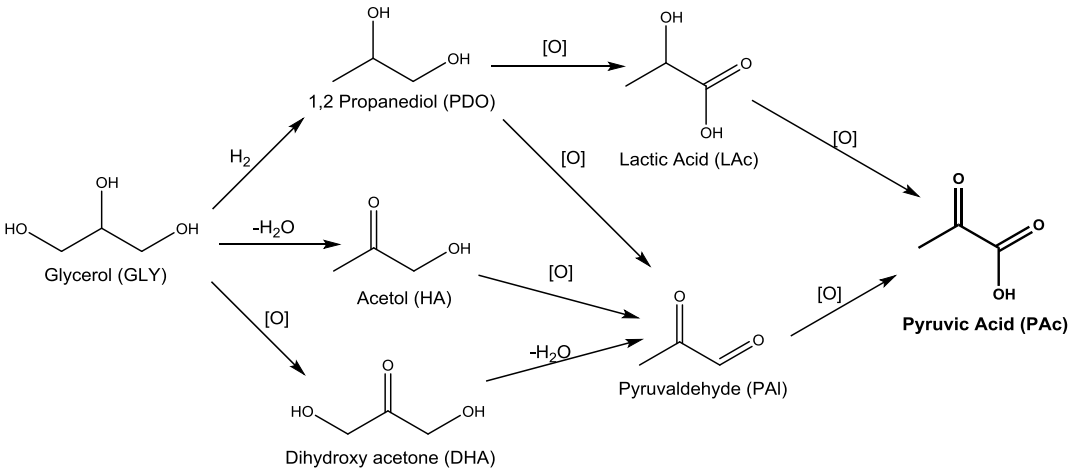

Figure 1-9 Scheme of possible reactions for the transformation of glycerol into pyruvic acid.

1.3.1 The dihydroxyacetone route

The dihydroxyacetone (DHA) route is based on the transformation of GLY to DHA by an oxidative dehydrogenation reaction and then to pyruvaldehyde (PAl) by dehydration and oxidation of the latter into PAc, as reported in Figure 1-10.

The oxidative dehydrogenation process of GLY into DHA has been investigated using

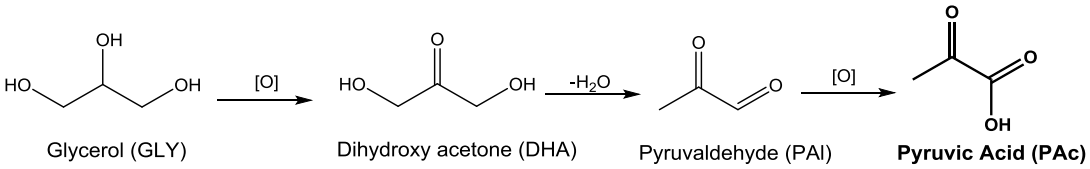

Figure 1-10 Scheme of reaction for the synthesis of pyruvic acid from glycerol by dihydroxyacetone as a key intermediate.

different catalytic systems, especially homo- [130] and heterogeneous ones. Concerning the heterogeneous systems, noble metals supported catalysts were used for the reaction in the liquid phase [131], while iron-containing catalysts were investigated for the gas phase [132].

In relation to this last process, different iron-containing zeolites with MFI structure were studied, and the results showed the fundamental role of the amount of each constituent element of the catalyst because they influence the acid and redox textural properties. The system constituted by nanoclusters of FeO_x deposed over dealuminated MFI zeolite showed the best performance in terms of selectivity into DHA (83%) and conversion of GLY (100%).

The transformation of DHA into PAl and PAc has been investigated in liquid phase using homogeneous acid catalysts; the results showed the important role of the Brønsted acid sites [133].

The direct transformation of GLY into PAl and PAc was also studied; different metal-supported Al_2O_3 catalysts were investigated, and the silver showed the best

performance thanks to its reduction potential. The role of the support and operative parameters influence notably the catalytic performance, the amount of Lewis and Brønsted sites favour the formation of acetol, while the temperature and partial pressure of oxygen influence the oxidation of the latter into PAl and PAc, reaching 85% and 20% of selectivity respectively [134].

1.3.2 The 1,2-propanediol route

An alternative route for the production of PAc from GLY could pass through the formation of 1,2-propanediol (1,2-PDO) by hydrogenolysis, its oxidation into lactic acid (LAc) or PAl and subsequent oxidation into PAc (Figure 1-11).

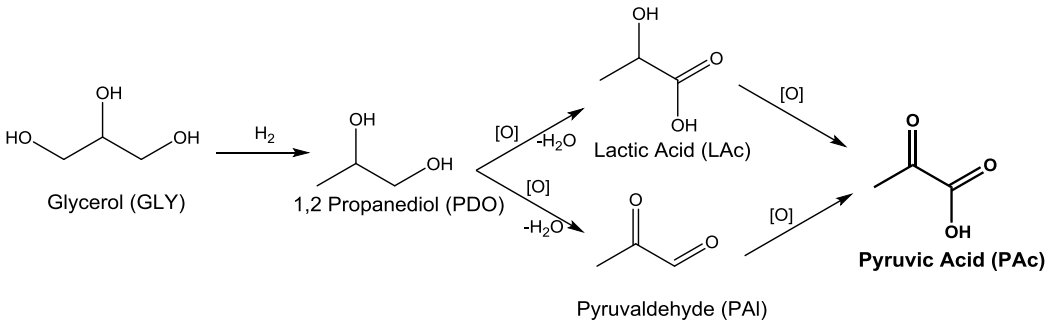

Figure 1-11 Scheme of reaction for the synthesis of pyruvic acid from glycerol by 1,2-propanediol as a key intermediate.

Concerning the hydrogenolysis of GLY, this reaction has been deeply investigated [135,136], and the results show the fundamental role of the metal and acid/base properties of the catalysts, which are the key factors that determine the reaction routes and product distributions. Transition metal catalysts have been intensively investigated and Cu, Ni and Co are the most frequently adopted metal components. These catalysts, especially Cu-based catalysts, generally exhibit good 1,2-PD selectivity.

For the transformation of 1,2-PDO into LAc, this process was investigated in the liquid phase using noble metals, such as Au, Pt and Pd, and bi-metallic alloys, supported on different acid/base metal oxides and active carbon using both hydrogen

peroxide and molecular oxygen as oxidant species [137–140]. The best performances were obtained using Pd supported on active carbon and molecular oxygen as oxidant; in this condition, 90% of yield into LAc was achieved.

Concerning the oxidation of LAc into PAc, different studies have been carried out using both LAc and its esters (methyl and ethyl lactate) in gas phase with different metal oxides able to catalyse the selective oxidative dehydrogenation of alcohol [141–143]. Attention was dedicated to the investigation of Mo-containing catalysts; especially. Mo/Fe/P/O, MoO_3/TiO_2 and Mo/Te/O heterogeneous catalysts were investigated. The results indicate that the selective oxidative dehydrogenation takes place more easily over the lactate than the LAc [20], and the side reactions, such as the decarboxylation of the carboxylic group, are hindered. Almost complete conversion and selectivity were achieved using Mo/Te/O in the gas phase oxidative dehydrogenation reaction of ethyl lactate, while the maximum yield into PAc from LAc was reached with both the iron phosphate doped with Mo and the MoO_3 supported on TiO_2.

The double oxidative dehydrogenation/oxidation reaction of 1,2-PDO for PAc production has barely been investigated. Mo-doped iron phosphate catalyst was used for the selective oxidation in the gas phase [144], achieving a yield into PAl near 25%.

1.3.3 The acetol route

The acetol route is the focus of this thesis. As reported in Figure 1-12, it consists of the dehydration of GLY into acetol (HA); the α-keto alcohol is then oxidised, first into PAl by an oxidative dehydrogenation, and then to PAc by insertion of oxygen.

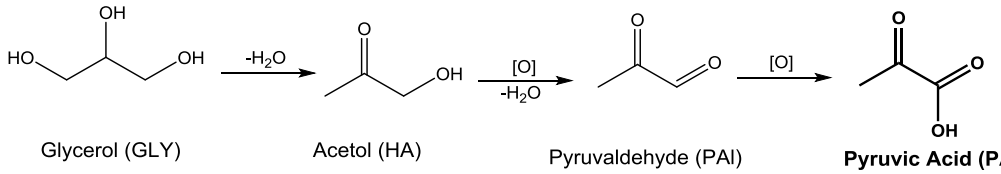

Figure 1-12 Scheme of reaction for the synthesis of pyruvic acid from glycerol by acetol as the key intermediate.

I focussed the investigation on the selective oxidation processes that take place on HA. The choice to investigate this process is based on these following reasons:

- The starting material is cheaper than the others and it can be easily obtained from glycerol by well-known processes; in contrast, the hydrogenolysis process for the synthesis of 1,2-PDO is more complex and expensive compared with the required dehydration.
- Both the dehydration and selective oxidation reactions could be carried out by means of a tandem process, using a multifunctional catalyst in *one-pot* approach (see section 1.4 in the *part one*).

Acetol

At room temperature, acetol is a colourless, sweet-smelling liquid. Thanks to the presence of both ketonic and hydroxylic groups, acetol presents a good solubility in polar solvent and a high boiling point of 146 °C.

As shown in Figure 1-13, acetol can be produced by different ways; the most important involves the transformation of 1,2-PDO by oxidative dehydrogenation reaction, fermentative processes of carbon sources and dehydration of glycerol [145–147].

This last process was studied in order to develop an efficient and cheap pathway. Studies on this process have tried to elucidate the catalytically active sites necessary to selectively produce acetol rather than acrolein.

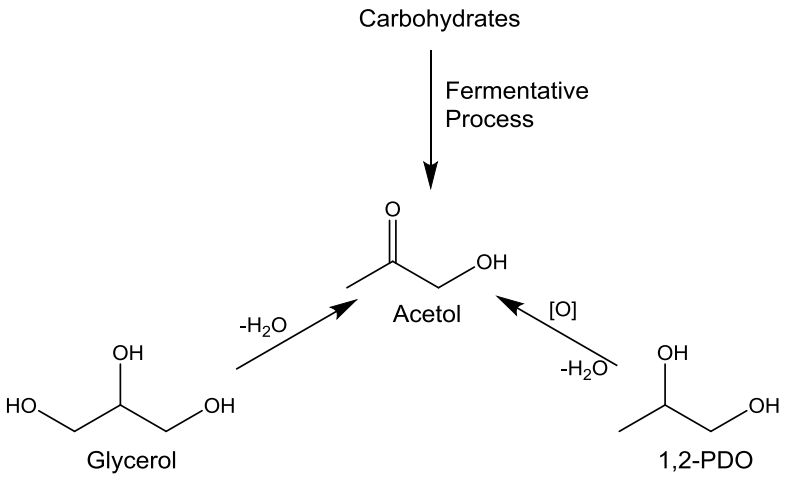

Figure 1-13 Industrial routes for acetol production.

Acid catalysts are well-known systems for the dehydration reaction; in fact, the effect of the type of acid sites on the selectivity into one of two possible products was investigated in literature. Medium-strong Brønsted acid sites catalyse the dehydration of the secondary hydroxyl group, forming 3-hydroxyl propionaldehyde and then acrolein [148] (Figure 1-14), while the Lewis acid sites complexes molecule of GLY catalysing the elimination reaction of one of the two primary hydroxyl groups and obtaining the enolic form of the acetol (Figure 1-15) [149,150].

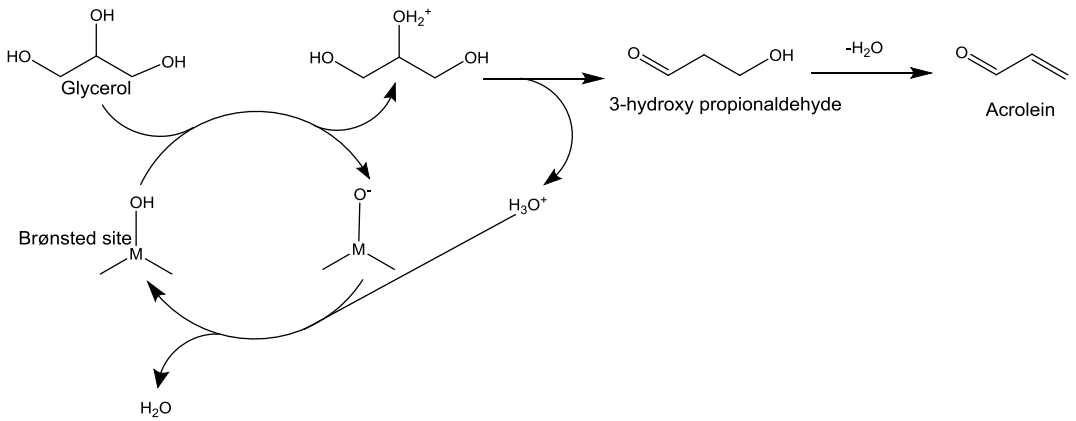

Figure 1-14 Reaction scheme of dehydration of glycerol into acrolein

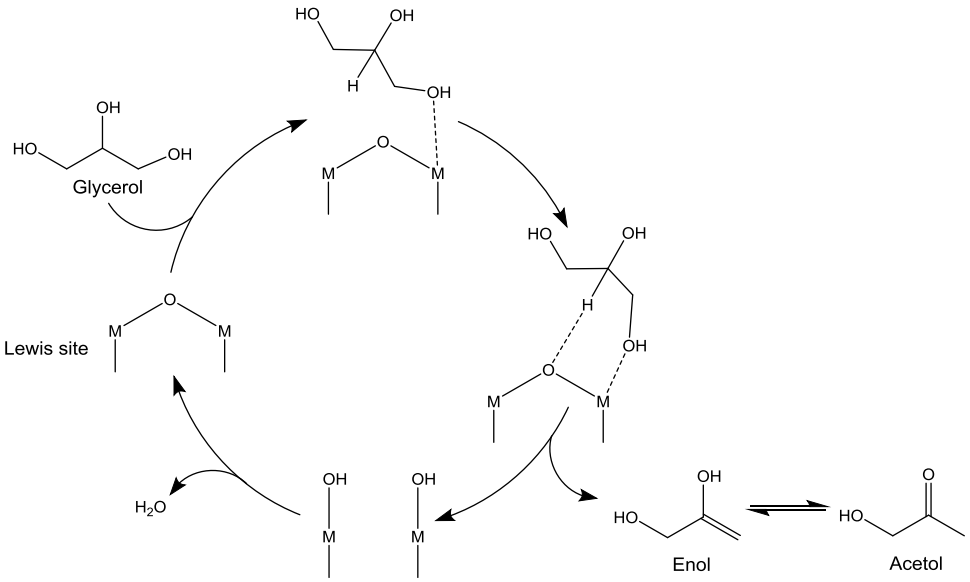

Figure 1-15 Reaction mechanism of the dehydration of glycerol into acetol over acid sites.

An alternative pathway for synthesis of acetol involves a dehydrogenation/dehydration/hydrogenation process that can occur over catalysts with acid/base sites. As reported in Figure 1-16, glycerol is initially transformed into glyceraldehyde by dehydrogenation reaction, this is then dehydrated into the enolic form of PAI and with the H_2 previously removed, reduced into acetol [151].

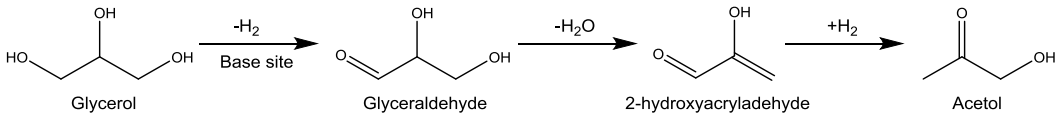

Figure 1-16 Reaction scheme of the transformation of glycerol into acetol over base sites.

These reported processes have been investigated in order to develop a catalyst with good, stable performance and reducing the undesired side-reactions, such as decarbonylation with the formation of C_2 molecules and CO, as well as the condensation ones. Condensation side reactions lead to the formation of coke on the catalytic surface, followed by its deactivation during the reaction [152,153].

Cu-containing catalysts have shown good catalytic performance in terms of selectivity into acetol; Cu/Al_2O_3 displayed the best results, both in liquid and gas phase reaction, achieving yield into acetol higher than 25% and 83%, respectively [149,150].

Selective oxidation reactions

For what concerns the selective oxidation for the transformation of HA to PAc, the first step is the oxidative dehydrogenation of the acetol into PAl, while the second one is the selective oxidation by insertion of an oxygen atom. Both reactions can be catalysed by metal oxides with redox properties, following the Mars-Van Krevelen mechanism [85], as shown in Figure 1-17.

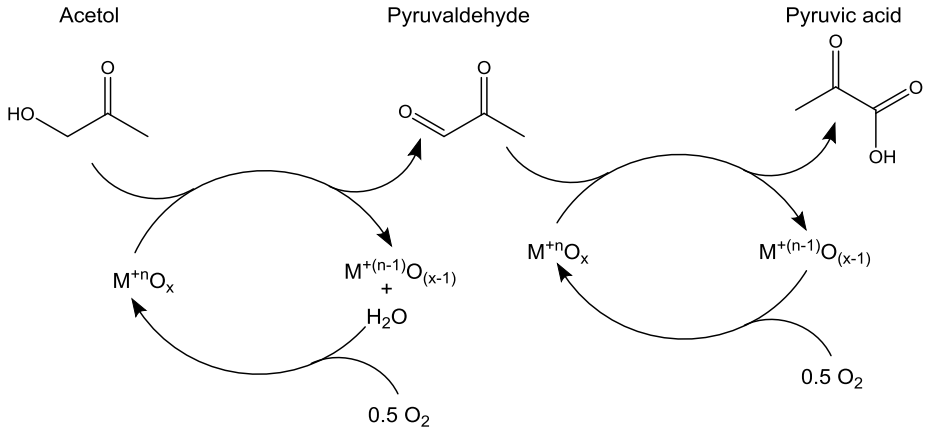

Figure 1-17 Mechanism of oxidative dehydrogenation and insertion of oxygen for the transformation of acetol into pyruvic acid.

As discussed in section 3 in the *introduction part*, vanadium-containing catalysts can catalyse the different oxidation reactions of various substrates; for this reason, different type of catalysts were investigated.

Due to the scarcely literature on this process, different catalysts were tested showing different acid/base and redox properties, in particular, the catalysts chosen are:

- Fe/P/O: This catalytic system is taken as reference because it was already investigated in the oxidative dehydrogenation reaction of different oxygenated

species, as well as for the transformation of acetol into PAl [154–159].

- V_2O_5 supported on MgO: This catalyst showed good catalytic performance in the selective oxidative dehydrogenation reaction of light alkanes [160–162].
- $AlVO_4$: This catalyst was investigated in the partial oxidation of methanol into formaldehyde [163–165].
- α_1-$VOPO_4$: This catalytic system, as shown in the previous chapter (section 3.6 in the *part one*), presents acid and redox sites that can catalyse both the selective oxidations for transforming HA into PAc.
- $(VO)_2P_2O_7$ DuPont: This catalyst is well-known for its oxidizing properties; it catalyses both the oxidative dehydrogenation and the oxygen insertion reaction, as reported in section 1.6 in the *part one*.
- W/V/O oxide with hexagonal tungsten bronze structure (HTB) structure: This kind of catalyst shows good performance in the oxidehydration process of glycerol into acrylic acid [166–169].

2 Experimental Part

2.1 Catalysts preparation

Fe/P/O

The procedure used for the synthesis of $FePO_4$ is the same as that one reported in literature [158], in detail, $Fe(NO_3)_3 \cdot 9H_2O$ (99.9% Sigma Aldrich) was dissolved in water medium and, in this solution, NH_4OH (28% Sigma Aldrich) was gradually added in order to precipitate $Fe(OH)_3$. The solid brown was recovered by filtration and placed together with H_3PO_4 (85% Sigma Aldrich) into the equipment shown in Figure 2-1; the amount of phosphoric acid was such to have a Fe/P ratio equal to 1.2. The slurry was kept under stirring and reflux for 2 hours, during which the colour of the mixture changed from brown to grey. The solid was recovered by evaporation of the water, dried overnight at 120 °C and calcined in static air at 500 °C for 5 hours.

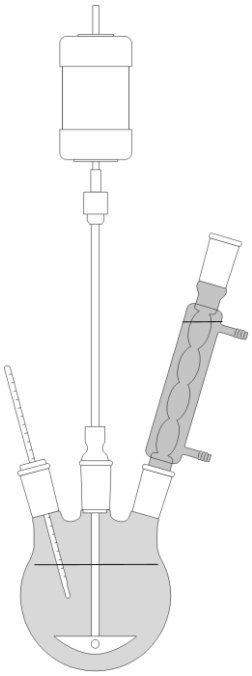

Figure 2-1 Equipment for the synthesis of Fe/P/O.

V_2O_5/MgO

The synthesis is carried out by wet impregnation of MgO with a solution of NH_4VO_3; MgO has previously been synthesised by precipitation and calcination of the precursor, $Mg(OH)_2$. Magnesium hydroxide is prepared from a water solution of $Mg(NO_3)_2 \cdot 6H_2O$ (98% Sigma Aldrich) and another solution of Na_2CO_3 (99% Sigma Aldrich). The solution containing Mg^{+2} ions was slowly dropped into that one containing the carbonate species under vigorous stirring; the temperature was maintained at 45 °C using a heating plate, and the pH was kept at 10.50 by adding a solution of 3 M NaOH. When the dropping was completed, the slurry was kept under stirring for 2 hours and then the solid was recovered by filtration under vacuum. The white solid was dried at 120 °C overnight and then calcined at 450 °C for 5 hours, obtaining the powder of MgO.

The deposition of V_2O_5 was carried out by wet impregnation technique. Here, the desired amount of NH_4VO_3 (99% Sigma Aldrich) was dissolved in distilled water and the corresponding amount of MgO was added to the solution in order to obtain a solid containing 5% *w/w* of V_2O_5 on the MgO. The slurry was kept under stirring for 30 minutes, then water was removed under vacuum in order to deposit the vanadium species on the catalyst. The pale-yellow solid was dried at 120 °C overnight and calcined at 450 °C for 5 hours.

$AlVO_4$

The synthesis of $AlVO_4$ was carried out following the procedure already reported in literature [27]. NH_4VO_3 (99% Sigma Aldrich) was dissolved in distilled water at 50 °C in the presence of an equimolar amount of oxalic acid (99% Acros Organics) in

order to complex the vanadate species. $Al(NO_3)_3 \cdot 9H_2O$ (99,7% Sigma Aldrich) was dissolved in distilled water under vigorous stirring. The solution containing the vanadate species was dropped into the first solution, and then the pH was corrected with a solution of NH_4OH until 6.8. The obtained slurry was maintained under vigorous stirring for 2 hours; then, the solid was recovered by filtration. The grey solid was dried at 120 °C overnight and calcined in static air at 650 °C for 3 hours.

α_1 $VOPO_4$ (VPD)

The precursor of α_1 $VOPO_4$ (VPD), $VOPO_4 \cdot 2H_2O$, is synthesised by suspending the desired amounts of V_2O_5 (99%, Sigma Aldrich) and H_3PO_4 (85%, Sigma Aldrich) in water. Phosphoric acid was added in excess (P/V= 4), since, in a stoichiometric amount, it does not permit the complete dissolution of V_2O_5 and leads to incomplete conversion of vanadium pentoxide. The equipment used for VPD synthesis was the same as that shown in Figure 2-1. The mixture was heated at reflux temperature (100 °C) for 17 h under vigorous stirring; the colour changed from dark orange of V_2O_5 to bright yellow, indicating the formation of $VOPO_4 \cdot 2H_2O$. The mixture was left at ambient temperature for 1 day, and the solid obtained was recovered by filtration and dried for few hours at 100°C. Calcination was performed over the catalyst directly inside the laboratory-scale reactor from room temperature up to 440°C, followed by an isothermal step at 440°C for 24 hours.

Vanadyl pyrophosphate Dupont (VPP)

The VPP catalyst was vanadyl pyrophosphate delivered by DuPont, which was used for the oxidation of *n*-butane into maleic anhydride in a circulating-fluid-bed reactor. Details concerning the characteristics of the catalysts are reported in the literature [97].

W/V/O with hexagonal tungsten bronze structure

The procedure for the synthesis of the tungsten oxide with HTB structure doped with vanadium ions was carried out by hydrothermal method. A water solution containing $(NH_4)_6H_2W_{12}O_{40}\cdot H_2O$ (Sigma Aldrich, > 85%*wt* of WO3) and $VOSO_4$ (99,99% Sigma Aldrich), with a W/V ratio equal to 1:0.3, was prepared. HCl was added to bring the pH to 1, and the gel thus obtained was put in a Teflon-lined stainless-steel autoclave under a nitrogen atmosphere. The system was heated at 175 °C for 48 hours; then, the obtained solid was recovered by filtration, dried at 100 °C for 16 hours and heat-treated at 600 °C for 2 hours under nitrogen.

2.2 Laboratory-scale plant tests

Catalytic tests were carried out in a continuous-flow, fixed bed, quartz reactor. The system permits variation of different reaction parameters: feed composition, contact time, and temperature. The laboratory plant is schematized in Figure 2-2. The apparatus could be divided into three main parts:

- Feed part
- Reaction part
- Downstream part

Feed part:

Gases (N_2, air) were fed to the reactor, in separated streams or simultaneously, by two mass-flow meters, and their flow was measured using a bubble flow meter; the water solution of acetol was fed by a syringe pump, which was properly calibrated for the desired quantity of liquid flow. The liquid mixture was vaporized in the reactor inlet line, which was heated to 200°C, where the gases mixed. The entire inlet flow could

be sent to the reactor and or to the gas chromatograph, in order to check the real entrance flow.

Reaction part:

The fixed bed reactor is a quartz tube, operating at atmospheric pressure. The thermocouple is positioned in the inner part of reactor inside a thin quartz tube at the level of the catalytic bed. The reactor is inserted inside a Lenton oven LFT 12/25/250 with inner diameter of 2.5 cm and external diameter of 25 cm. The exit of the reactor emerging outside the oven is wrapped with a heater string kept at 220°C, in order to prevent crystallization and condensation of the products.

Downstream part:

Upon exit from the reactor, the flow of gas products is split: one part is sent for on-line GC-FID analysis by opening the on/off valve; the other part is passed through a crystallizer, then to a glass bubbler filled with acetone, in order to condense the remaining organic products in the crystallizer, and then sent for on-line GC-TCD analysis.

Product Analysis:

The reactants and products were analysed using a Varian CP-3380 gas chromatograph, equipped with the following columns and detectors:

- Semicapillar CPSil-5CB column (30 m length; i.d. 0.53 mm; stationary phase of 100% dimethylpolysiloxane with a thickness of 3.00 μm). This column separates the pyruvaldehyde, by-products (acetic acid, acetaldehyde, and other compounds), and acetol (in and out). The correspondent detector is a FID.
- Packed Carbosieve SII column (2 m length, stationary phase of active carbons

having dimensions of 80–100 mesh). In this column, CO, CO2, H2O, O2, and N2 are separated and detected by a TCD.

The carrier gas used is He, and the temperature ramp program of the oven is as follows: 7 min at 40°C, after which the temperature is increased up to 220°C at 30°C/min, and this is followed by a final isothermal step at 220°C for 10 min.

It is worth noting that both the semicapillary column and the packed column are connected for on-line analysis using a six-way valve for each analysis: the sampling loop valve for the FID analysis is about 350 μL and is maintained at 200°C, while the sampling loop valve for the TCD analysis is about 500 μL and is maintained at 40°C.

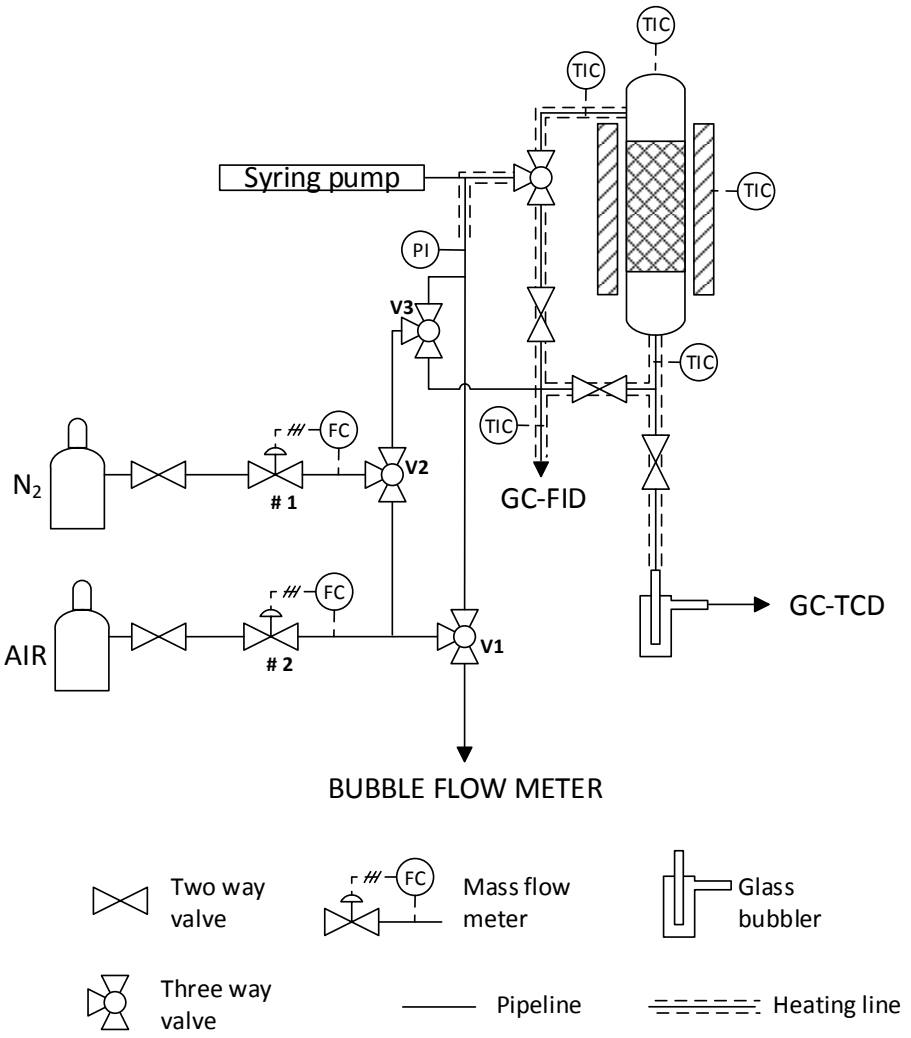

Figure 2-2 Scheme of laboratory-scale plant tests

2.3 Data elaboration: conversion, yield, and selectivity

Through gas chromatograph analyses, the percentage values of conversion, yield, and selectivity were determined, by using the following equations:

$$Conversion = \frac{mol\ of\ converted\ reactant}{mol\ \ of\ fed\ reactant} \times 100$$

$$Yield_x = \frac{mol\ of\ product_x/stoichiometric\ coeff.}{mol\ \ of\ fed\ reactant/stoichiometric\ coeff.} \times 100$$

$$Selectivity_x\ = \frac{Yield_x}{conversion} \times 100$$

$$Carbon\ balance = \frac{\sum Yield}{conversion} \times 100$$

2.4 Catalyst characterization

Raman spectroscopy

Raman analyses were carried out using a Renishaw Raman System RM1000 instrument, equipped with a Leica DLML confocal microscope, with 5x, 20x, and 50x objectives, video camera, CCD detector, and laser source Argon ion (514 nm) with power 25 mW. The maximum spatial resolution is 0.5 μm, and the spectral resolution is 1 cm^{-1}. For each sample, a wide number of spectra were collected by changing the surface position. The parameters of spectrum acquisition are generally selected as follows: 5 accumulations, 10 s, 25% of laser power to prevent sample damage, and 50x objective.

In-situ Raman experiment

In-situ Raman experiment analyses were performed using a commercial Raman cell (Linkam Instruments TS1500). Approximately 5-10 mg of the sample was used for the analysis. The gas flow, fed from the start of the experiment, was about 10 ml/min of air. Spectra were recorded at room temperature (rt), while the temperature (heating rate of 100°C/min) was increased up to the desired temperature during the isotherm period. The laser power used was 25%, which permits good spectrum acquisition without damaging the sample; the other acquisition parameters were as follows: 10 accumulations, 10 s each; 20x objective.

X-ray powder diffraction

The X-ray powder diffraction (XRD) measurements were carried out using a Philips PW 1710 apparatus, with Cu Kα (λ = 1.5406 Å) radiation in the range of 5°<2θ <60°, with steps of 0.05 grade, and signal acquisition for 3 s in each step. Reflects attribution was done by the Bragg law, by using the d value: 2d sen θ = nλ and by comparing the results obtained with those reported in literature.

Specific surface area (BET single point)

The specific surface area was determined by N_2 adsorption at -196 °C (the boiling T of nitrogen), with a Sorpty 1750 Instrument (Carlo Erba). The sample was heated at 150°C under vacuum, to eliminate water and other molecules eventually adsorbed on the surface. After this pre-treatment, the sample temperature was maintained at -196 °C in a liquid nitrogen bath, while the instrument slowly sent gaseous N_2, which was adsorbed on the surface. Using the BET equation, the volume of monolayer and

finally the sample surface area could be calculated.

Thermogravimetric analysis

The thermogravimetric analysis was performed using a DST Q 600 of TA instrument, under air flow (30 ml/min), from room temperature up to 450°C, with two heating rates: first, 5°C/min until 200°C and relative isotherm for 10 min; second, 10°C/min until 450°C and an isotherm for 20 min.

3 Results and discussion

3.1 Characterisation of the catalysts

3.1.1 Fe/P/O

X-ray diffraction

XRD analysis of Fe/P/O, as illustrated in Figure 3-1, showed signals correlated to the tridymite structure-like phase [170], confirming the results already reported in the literature for this catalytic system [171]. The low intensity of the signals indicates the low crystallinity of the system.

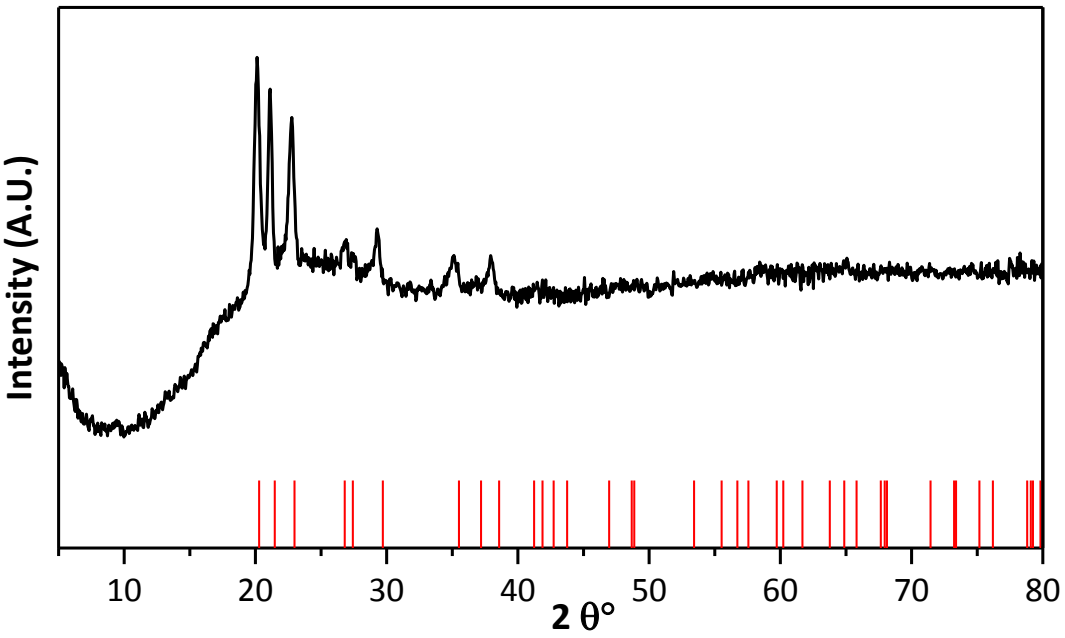

Figure 3-1 XRD of Fe/P/O calcined catalyst. Red lines represent the pattern of SiO_2 in the tridymite structure.

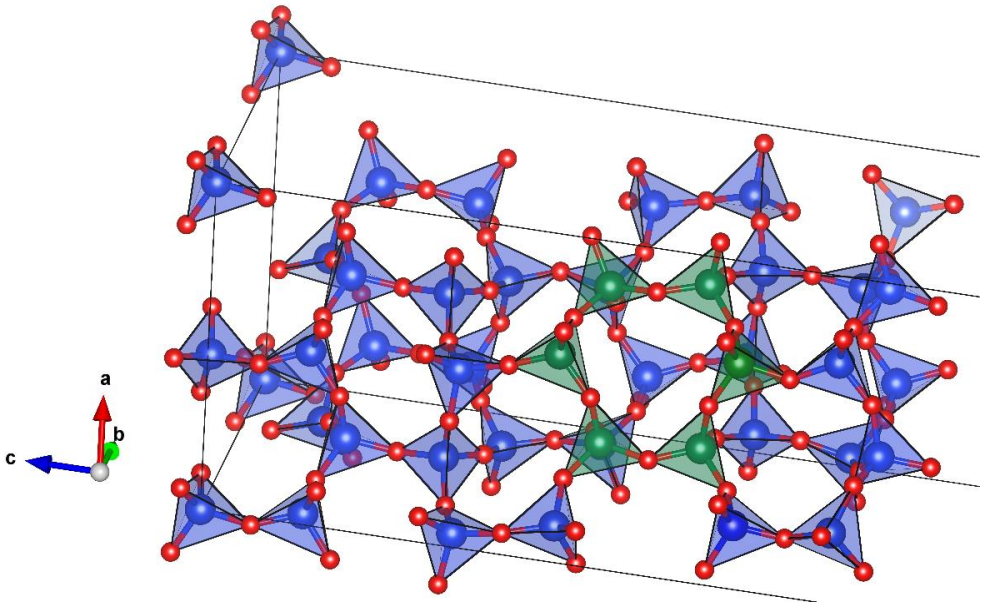

Figure 3-2 Three-dimensional (3D) partial structure of tridymite of SiO_2. Green tetrahedrals represent the repetitive units of the solid.

Raman spectroscopy

The Raman spectra of Fe/P/O catalyst reported in Figure 3-3 indicate the presence of a complex structure due to the presence of broad and narrow bands. The bands at 313, 433 and 634 cm^{-1} are related to the bending of $[PO_4]$ units (Q^0), while the band at 758 cm^{-1} to the symmetric stretching vibration of the P-O-P bond in the $[P_2O_7]$ unit (Q^1). The shoulder at 930 and the band at 1043 cm^{-1} derive from the symmetric and antisymmetric stretching of Fe-O-P in Q^0 units, while the band at 1121 cm^{-1} is related to the symmetric stretching of Fe-O-P in Q^1 units [172–174].

From the information obtained by XRD and Raman analysis, it is possible to hypothesise that the Fe/P/O catalyst presents a crystalline tridymite-like structure, the same shown in Figure 3-2, with alternating tetrahedrals of $[FeO_4]$ and $[PO_4]$ units that share the edge, and tetrahedral unities of $[FeO_4]$, linked to $[P_2O_7]$ units by edge-sharing bonds.

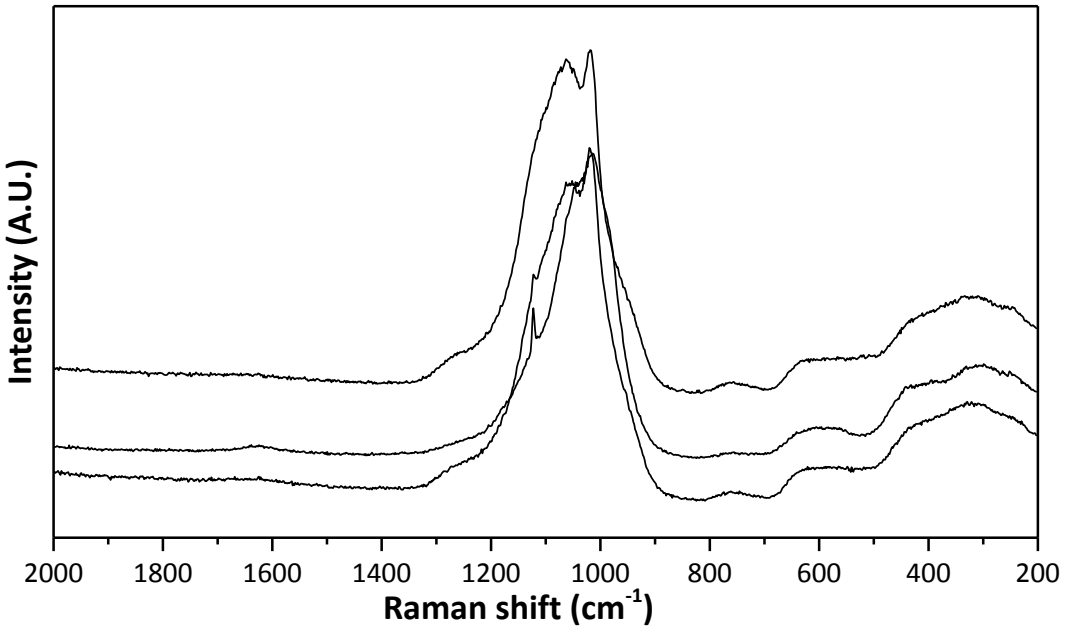

Figure 3-3 Raman spectra acquired on different spots of calcined Fe/P/O

Surface area

BET analysis indicated that the specific surface area is 30 m^2/g.

3.1.2 MgO

X-ray diffraction

XRD analysis of calcined MgO confirmed the formation of the cubic periclase phase (Figure 3-4).

Surface area

The specific surface area of MgO was equal to 120 m^2/g.

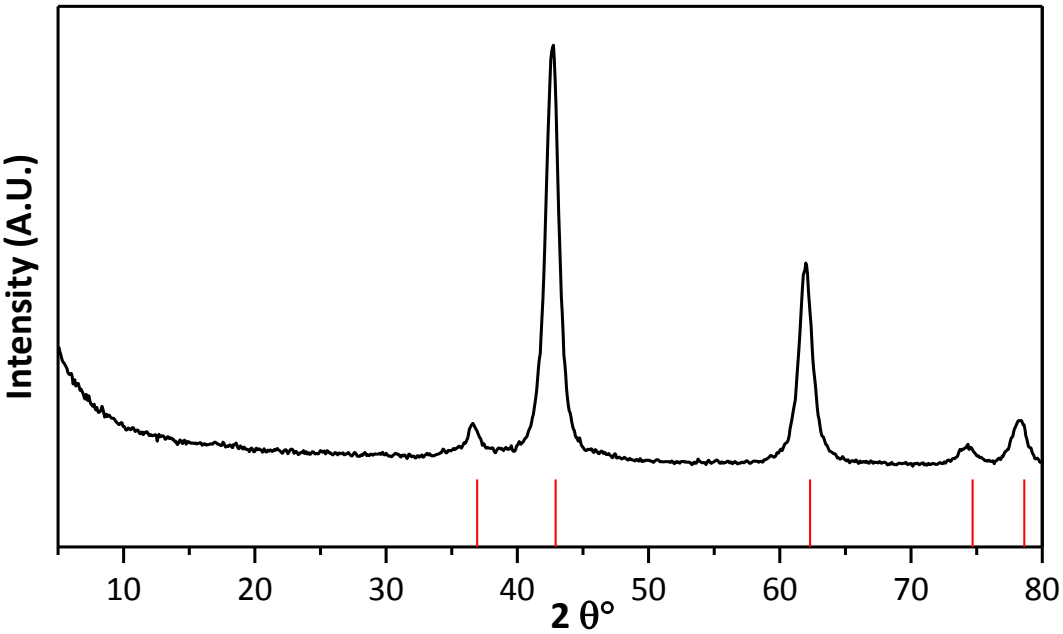

Figure 3-4 XRD analysis of calcined MgO. Red lines represent the pattern of the periclase phase.

3.1.3 5% V_2O_5/MgO

X-ray diffraction

Figure 3-5 and Figure 3-6 depict the diffractograms obtained after the drying and calcination steps, respectively. A partial hydration of MgO could be observed after the deposition; in fact, the catalyst presented signals correlated both to MgO and $Mg(OH)_2$. After calcination, only the signals that correlated to the cubic periclase were observed. In both diffractograms, no signals correlated to the vanadia were presented, suggesting the good dispersion of the active phase on the catalytic surface.

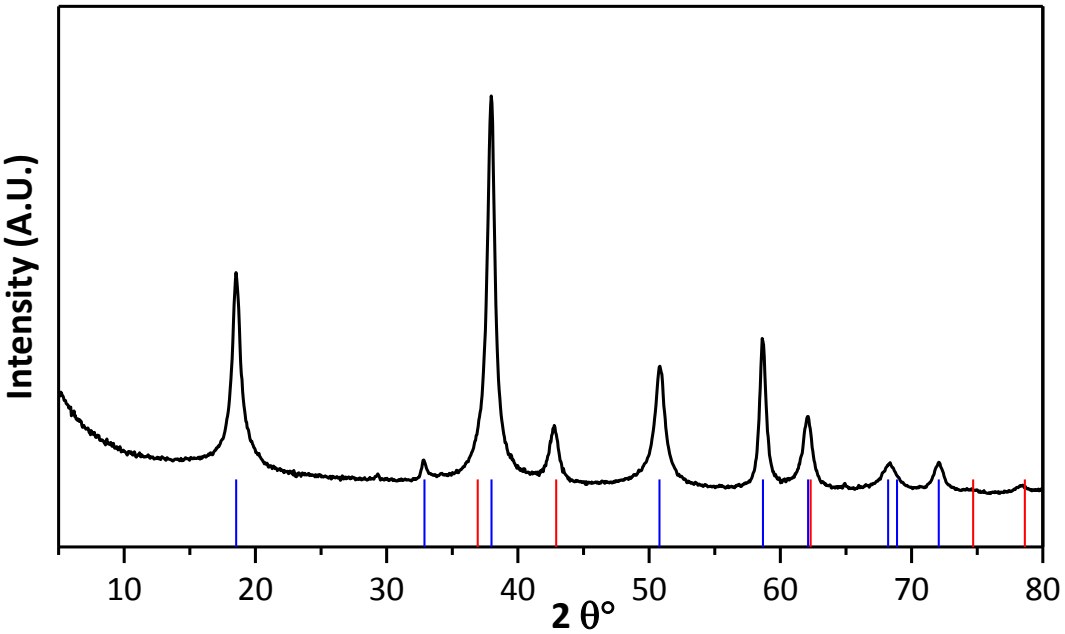

Figure 3-5 XRD analysis of V_2O_5/MgO after deposition. Red lines represent the pattern of the periclase phase; Blue lines represent the pattern of the brucite phase [$Mg(OH)_2$].

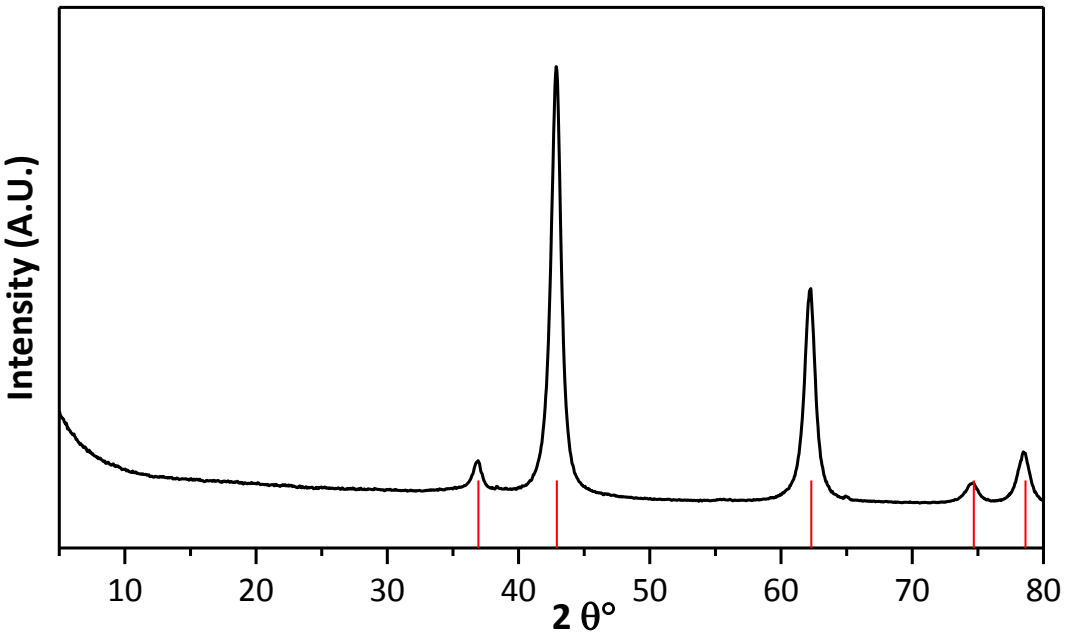

Figure 3-6 XRD analysis of calcined V_2O_5/MgO. Red lines represent the pattern of the periclase phase

Raman spectroscopy

The Raman spectra acquired on the calcined catalyst are shown in Figure 3-7. The bands present in the region between 750 and 1000 cm^{-1} are related to the V-O stretching vibrations in $Mg_2(VO_4)_2$ [175–178], while the band present between 1130 and 1050 cm^{-1} derives from the stretching vibrations of the CO_3^{-2} species [179].

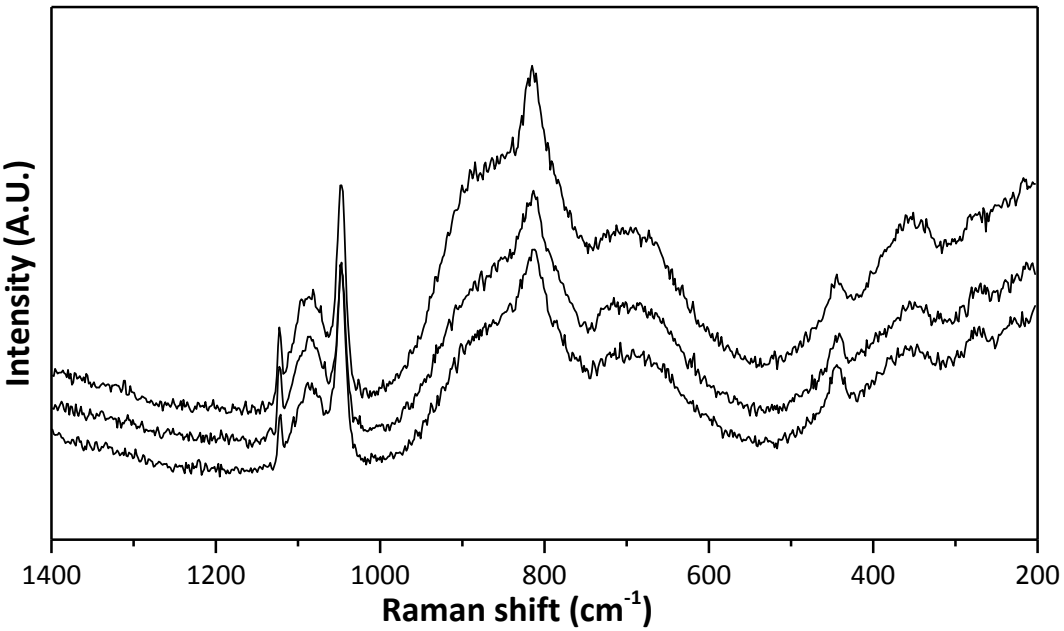

Figure 3-7 Raman spectra acquired over different spots of 5% V_2O_5/MgO.

The presence of bands associated with the magnesium orthovanadate phase and the absence of bands ascribable to V_2O_5 indicate the dispersion of the vanadium species. The presence of carbonate derived from the carbonatation process that occurred on the surface of MgO when it was put in contact with air.

Surface area

The BET analysis of the calcined catalyst showed a specific superficial area of 100 m^2/g. This result was slightly lower than that with only MgO observed previously; it is possible to attribute this effect to the deposition of vanadia on the surface.

3.1.4 $AlVO_4$

X-ray diffraction

The XRD analysis of the calcined catalyst showed that reflections attributable to the triclinic phase of $AlVO_4$.

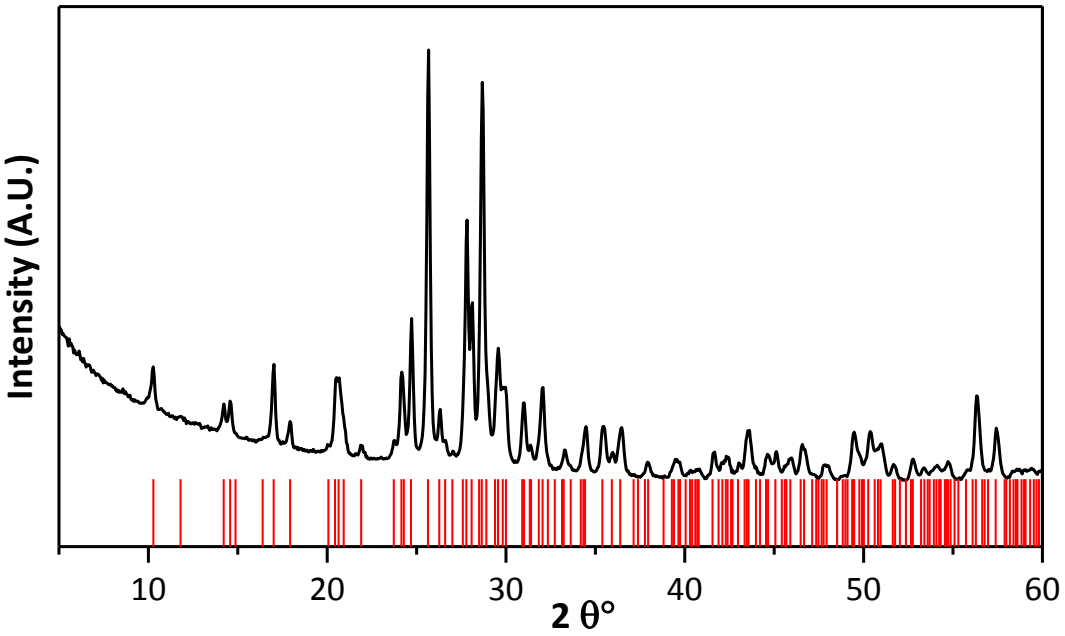

Figure 3-8 XRD analysis of $AlVO_4$ after calcination. Red lines represent the pattern of the triclinic structure of $AlVO_4$.

Raman spectroscopy

The Raman spectra of $AlVO_4$, reported in Figure 3-9, presented the typical bands related to the spinel-like structure of vanadate with trivalent cations [165,180].

Surface area

The BET analysis showed a specific surface area equal to 10 m^2/g. This result was due to the method of synthesis employed, which disfavoured the formation of small crystallites.

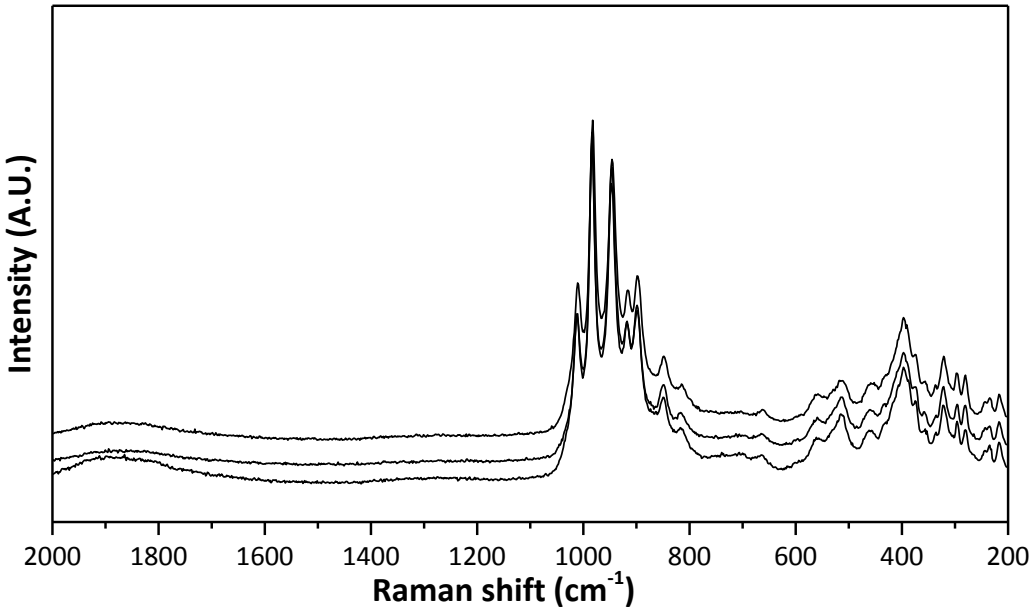

Figure 3-9 Raman spectra acquired over different spots of $AlVO_4$.

3.1.5 α_1 $VOPO_4$

X-ray diffraction

The XRD analysis on the yellow/green solid showed the presence of the vanadyl phosphate dihydrate phase, and in minor amounts, of the α_1 $VOPO_4$ phase.

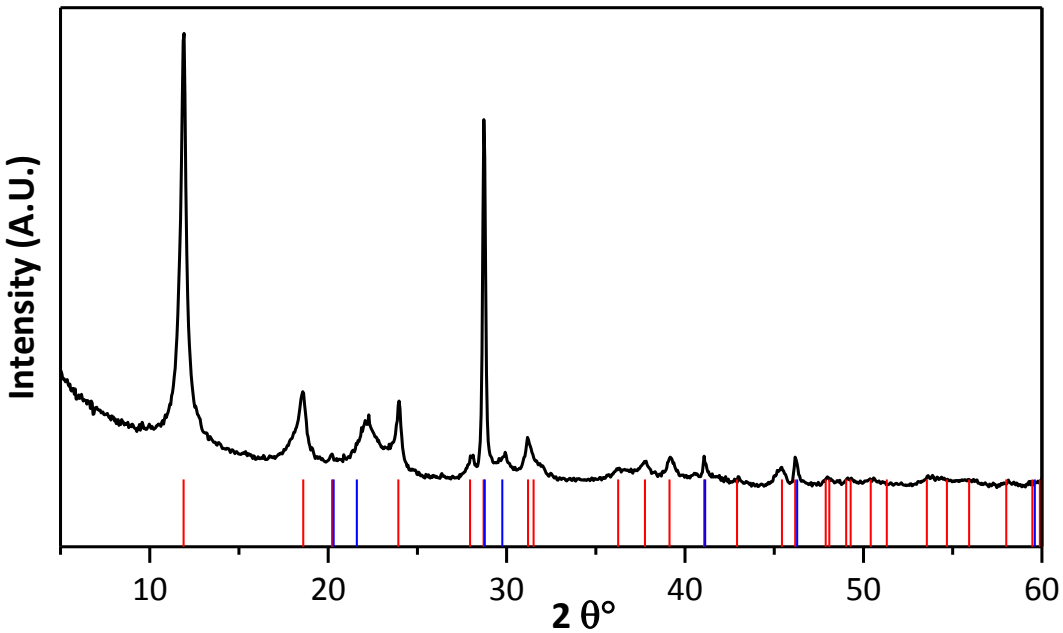

Figure 3-10 XRD analysis of the VPD catalyst before calcination treatment. Red lines represent the pattern of the $VOPO_4 \cdot 2H_2O$ phase; blue lines represent the pattern of the α_1-$VOPO_4$ phase.

Ex-situ Raman spectroscopy

The Raman spectra recorded at different spots of the sample showed different bands, attributable to the presence of both $VOPO_4 \cdot 2H2O$ and α_1 $VOPO_4$. The bands due to the dehydrated compound were shown at 1036, 984, 946, and 535 cm^{-1}, while the bands associated with the α_1 phase at 1146, 1036, 924, 571, 452, and 424 cm^{-1}.

A comparison of the spectra showed differences in the intensity of the peaks associated with each compound, indicating a non-homogeneous distribution in the catalyst.

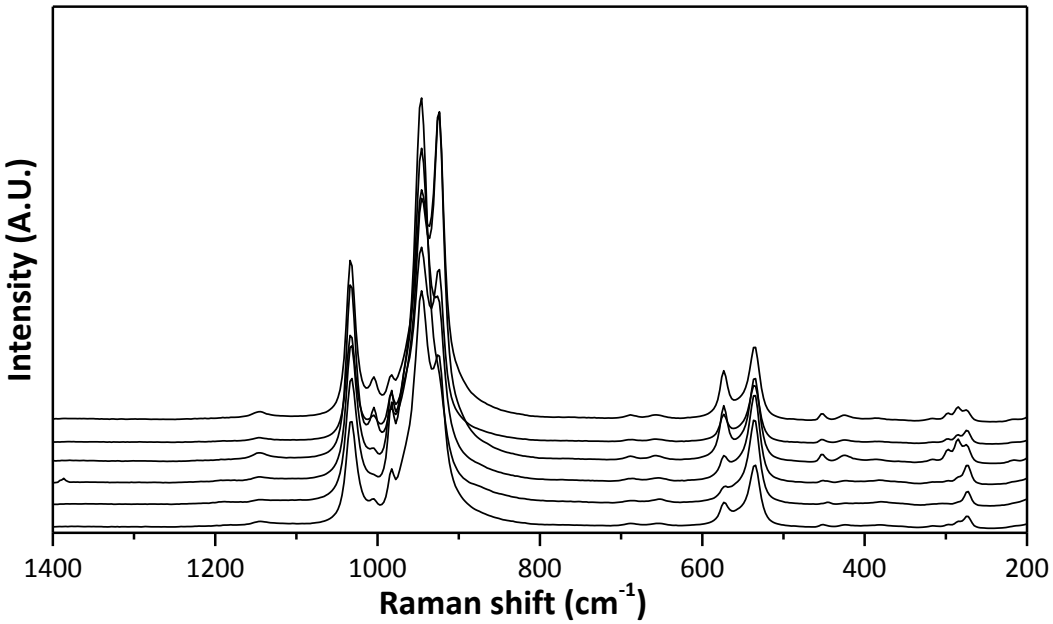

Figure 3-11 *Ex-situ* Raman spectra acquired on the different spots of VPD.

In-situ Raman spectroscopy and thermogravimetric analysis (TGA)

The calcination process of the catalyst was also investigated by monitoring the transformations that occurred during the thermal treatment by *in-situ* Raman spectroscopy, which results are reported in Figure 3-12.

The spectra recorded at room temperature (black line) show the presence of both the dihydrate and the α_1 phases of $VOPO_4$, while the spectra taken at 100 °C (red line)

showed the presence of the α_1 phase only, because the band at 984–946 cm^{-1} disappeared and the intensities of the bands at 571 and 535 cm^{-1} changed and reached a unitary ratio.

A further increase in temperature did not affect catalyst composition, because the spectra remained the same, indicating that the loss of the water molecules took place at very low temperature.

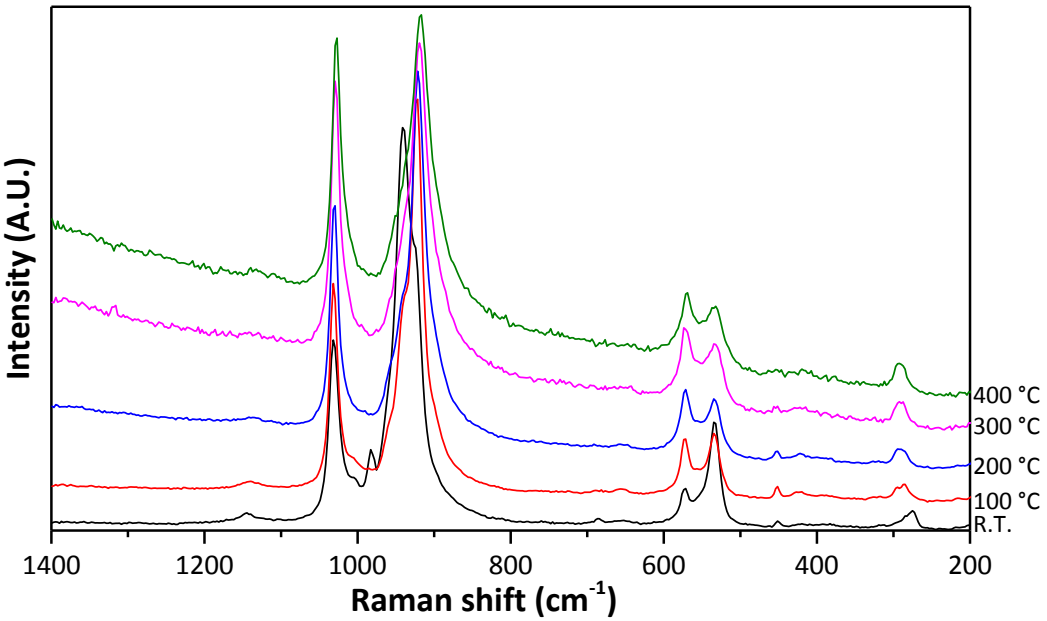

Figure 3-12 *In-situ* Raman spectra acquired on the same spot of VPD, at different temperatures and air feed rates.

In order to better understand this effect, thermogravimetric analysis (TGA) was carried out on the fresh sample. The thermogram, reported in Figure 3-13, showed two different weight losses; the first at 73 °C, with –8% of weight loss, and the second at 101 °C with a 5.6% weight loss, equalling a total loss of 13.6%. The theoretical loss of weight of $VOPO_4 \cdot 2\ H_2O$ to obtain the anhydrous phase is 17.4%. The difference between the real and theoretical weight loss confirmed that the catalyst was composed of both the dihydrate and anhydrous phases of $VOPO_4$, and that the loss of the two molecules took place via two consecutive reactions occurring at different temperatures.

This confirmed the results reported in the literature [98–101].

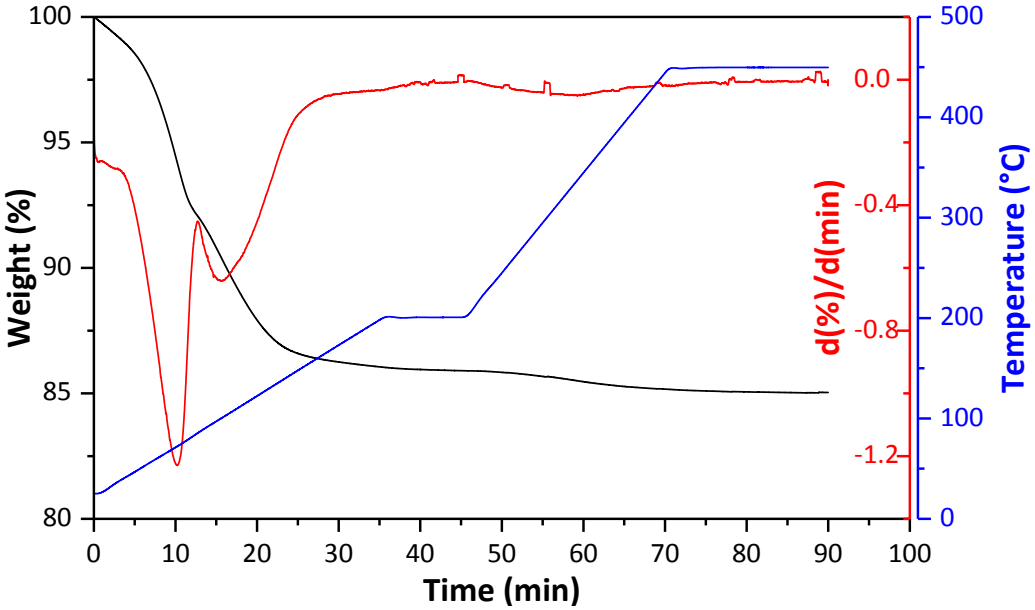

Figure 3-13 TGA of VPD catalyst using air as the carrier gas. Black line represents the percentage loss of weight; blue line represents the temperature ramp; red line represents the derivatives of the weight as a function of time

Surface area

The specific surface area measured for VPD was 5 m^2/g; the very low value was due to the aging treatment of the solid in its mother liquor. In fact, in these conditions structural rearrangements caused an increase in the crystallinity of the solid, thus decreasing the surface area.

3.1.6 Vanadyl Pyrophosphate DuPont (VPP)

Vanadyl pyrophosphate catalyst delivered by DuPont was in the form of spherical powder made of a core of vanadyl pyrophosphate and a shell of porous silica.

X-ray diffraction

The XRD analysis of the fresh VPP DuPont catalyst reported in Figure 3-14 confirmed the presence of the VPP phase.

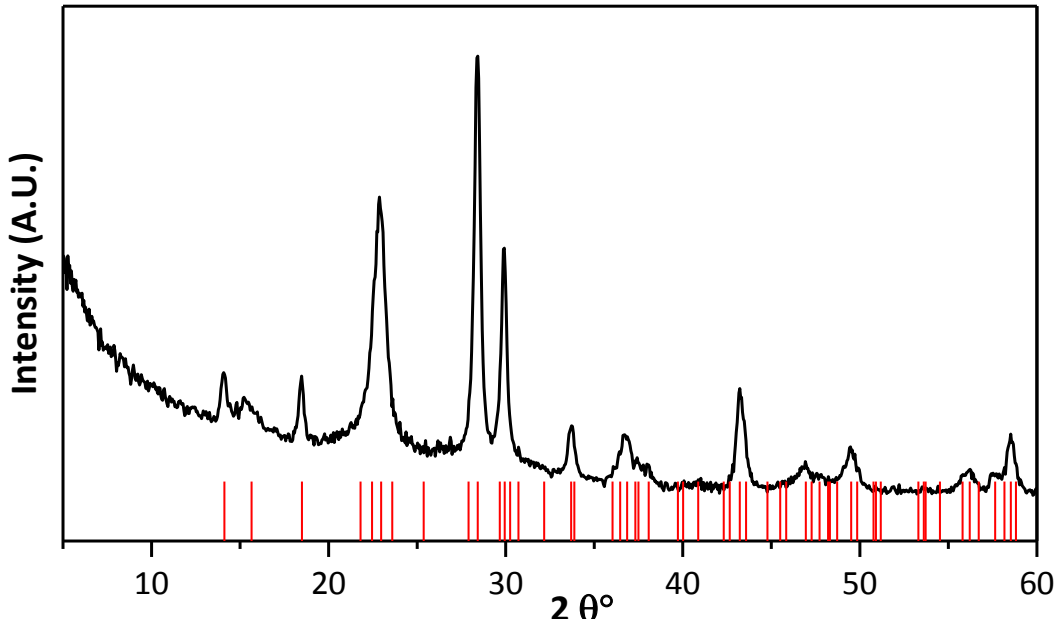

Figure 3-14 XRD analysis of VPP DuPont. Red lines represent the pattern of $(VO)_2P_2O_7$.

Raman spectroscopy

Spectra was recorded by changing the laser beam focus on the sample. The spectra of the fresh catalyst are reported in Figure 3-15, and they present characteristic bands at 1177, 1124, 1013, and 915 cm^{-1} typical of the VPP phase.

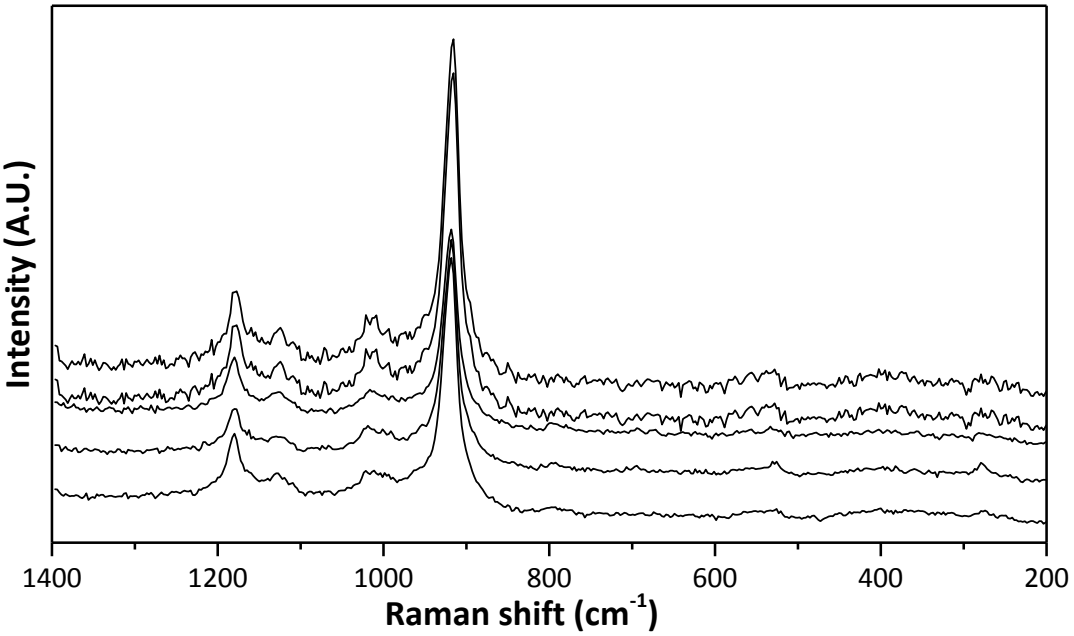

Figure 3-15 Raman spectra of VPP Dupont acquired on different spots of the catalyst

Surface area

The surface area of the sample was measured using the BET method. For the fresh catalyst, this value was 40 m^2/g.

3.1.7 W/V/O HTB

X-ray diffraction

XRD analysis confirmed the formation of the hexagonal bronze phase of WO_3; none of the signals deriving from the vanadium species were detected, this indicates the insertion of V^{+5} ions in the structure.

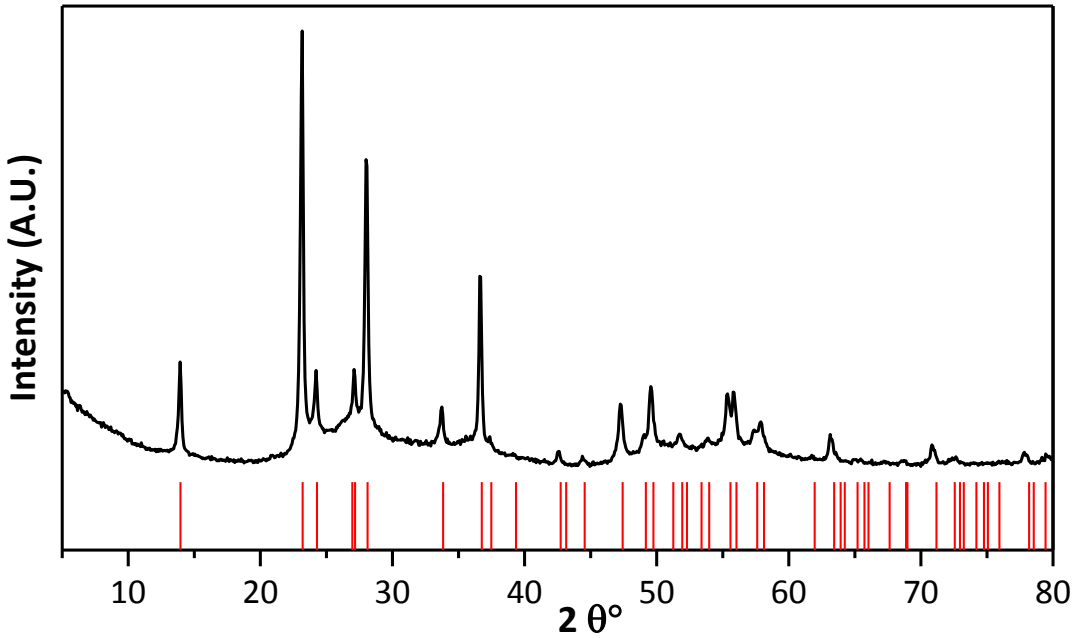

Figure 3-16 XRD analysis of W/V/O after the heating treatment. Red lines represent the pattern of the WO_3 in the hexagonal structure.

Raman spectroscopy

The Raman spectra, reported in Figure 3-17, presented the bands at 801, 680 and 245 cm^{-1} that are correlated to the W=O stretching, O-W-O stretching and bending vibration modes of the hexagonal tungsten oxide, respectively [181]. The band at 967 cm^{-1} can be correlated to the greater number of W=O bonds generated by the

structural defects resulting from the V incorporation process and/or the V-O bonds associated with the V-O-W chains [168,182].

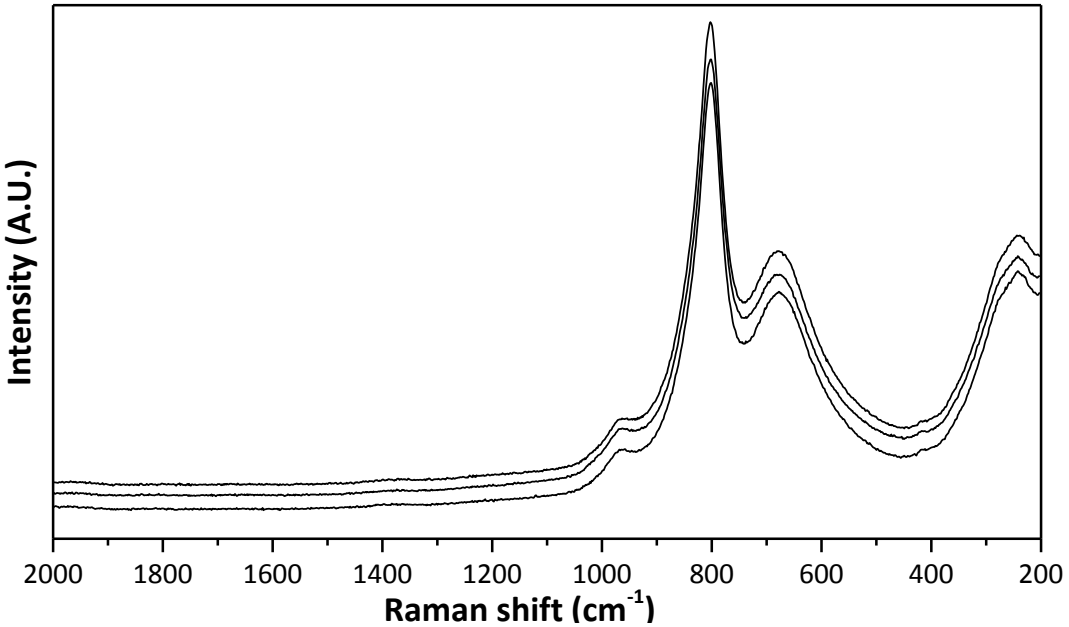

Figure 3-17 Raman spectra acquired over different spots on W/V/O.

Surface area

The BET analysis of the W/V/O showed a specific surface area of 20 m^2/g.

A resume of the textural properties of the catalysts are reported in Table 3-1:

Sample Name	Phase (XRD, Raman)	S.S.A. (m^2/g)	Properties
Fe/P/O	$FePO_4 + Fe_2P_2O_7$	30	Strong acid sites[159]
V/MgO	$MgO + Mg_2(VO_4)_2$	100	Strong base sites [183]
$AlVO_4$	$AlVO_4$	10	Acid sites [164]
α_1 $VOPO_4$	α_1 $VOPO_4$	5	Strong acid sites [184]
VPP DuPont	$(VO)_2P_2O_7$	40	Strong acid sites [166]
W/V/O	*h*-WO_3 + VO_x species	20	Very strong acid sites[166]

Table 3-1 Resuming table of the catalysts tested for the selective oxidation of acetol to pyruvic acid with their main textural properties.

3.2 Catalytic tests

3.2.1 Preliminary test

A preliminary blank catalytic test was carried out, by feeding by to the empty reactor the same feed in terms of composition and flow, used for catalytic tests, in order to determine the thermal stability of the acetol at different temperatures. The results are reported in Figure 3-18, showing the low conversion of acetol, around 10% in the entire range of temperature studied; low amounts of acetaldehyde, PAI, CO and CO_2 were obtained. These results underline the thermal stability of the acetol and that the main side-reaction that takes place in the homogeneous phase is the oxidative cleavage. A negligible amount of PAI was also observed.

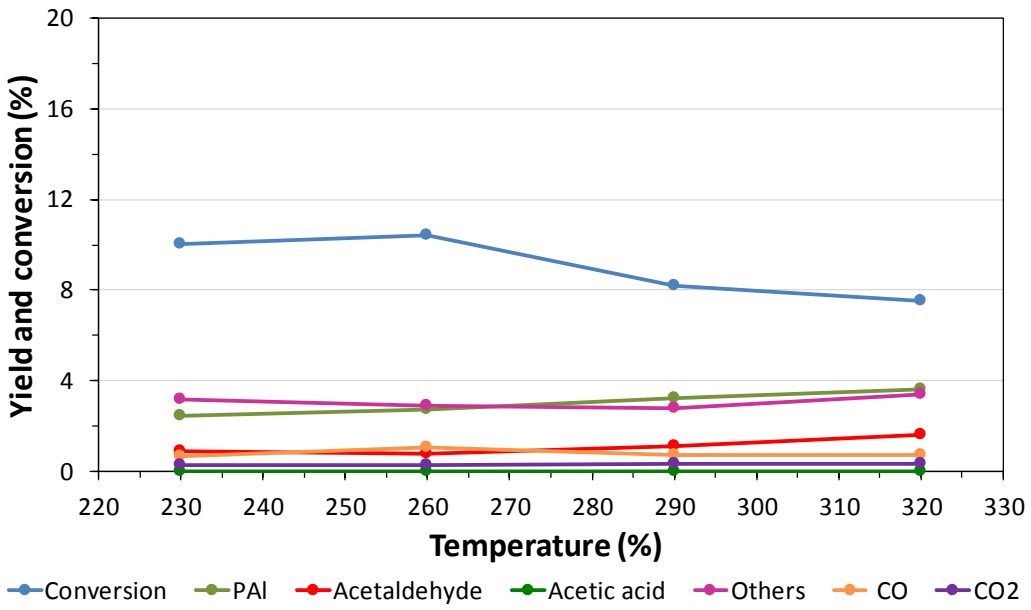

Figure 3-18 Thermal stability of acetol as a function of temperature. Feed 2%mol HA, 4%mol O_2 and 10%mol H_2O remain inert; the total flow was the same used for the catalytic tests with a W/F equal to 0.5 g_{cat}·s/mL.

3.2.2 Fe/P/O

Fe/P/O catalyst is known for its excellent catalytic properties in the oxidative dehydrogenation (ODH) of different oxygenated species [159,171,185]; therefore, we used acetol as the substrate for the ODH catalysed by Fe/P/O catalyst [158]. In fact, it was decided to test this catalyst as reference system for comparing the behaviour of the other catalysts tested.

From the results reported in Figure 3-19, the catalyst did not show a complete conversion of acetol (HA) at 230 °C; however, at above 270 °C almost complete conversion was obtained.

Fe/P/O was very selective to PAI in the entire temperature range investigated; acetaldehyde, acetic acid, CO, CO_2 and "others" species were also detected, but in minor amounts. The first four species derived from the oxidative cleavage of the intermediates that can take place in the homogeneous phase (as shown by means of blank test), while the label "others" is used to denote the sum of the species detected

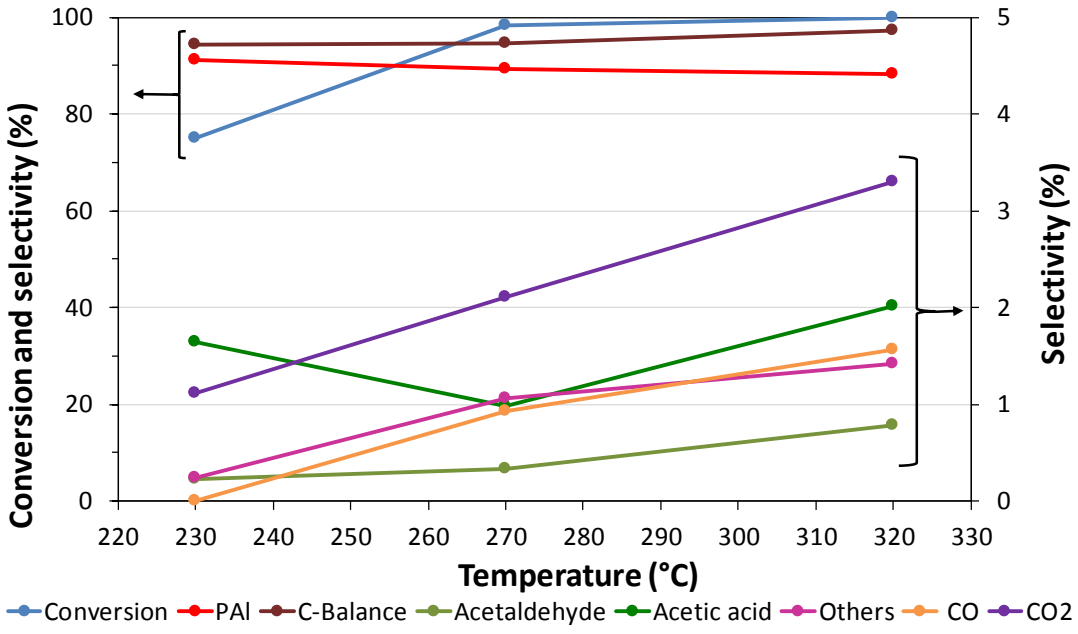

Figure 3-19 Catalytic behaviour of Fe/P/O during the ODH of acetol to PAI in function of temperature. Feed 2%mol HA; 4%mol O_2; 10%mol H_2O, remainder inert; W/F: 0.5 g_{cat}·s/mL

in minor amounts deriving from intermolecular condensation reactions and reported in Figure 3-20.

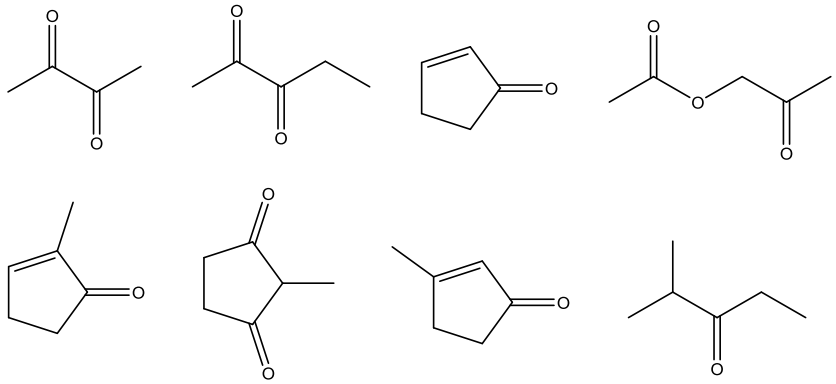

Figure 3-20 Products detected in very low amounts are reported as "others"

Analysing the catalytic behaviour at 230 °C, an initial deactivation was observed: in fact, the conversion passed from 100% after 1 hour of reaction to 80% after 4 hours and then to 75% after 7 hours; beyond that, it remained constant. After the first hour, the product distributions did not change during time on stream.

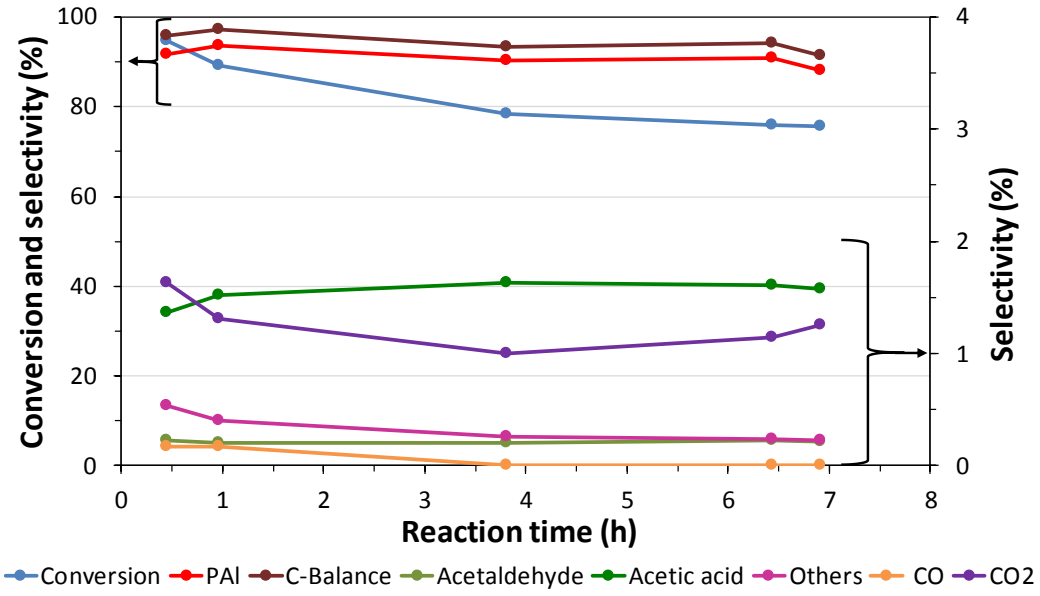

Figure 3-21 Catalytic behaviour of Fe/P/O in the ODH of acetol to PAI in function of time on stream. Temperature: 230 °C; feed: 2%mol HA, 4%mol O_2 and 10%mol H_2O remainder inert; W/F: 0.5 g_{cat}·s/mL.

The variation of the conversion could be associated with the slight lack of carbon balance observed, which may have derived from the deposition of carbonaceous species on the catalytic surface. The strong acid sites, generated by both the presence of the phosphates group and the Fe^{+3} species, can establish a strong interaction with organic species. This may favour the intermolecular condensation reactions, with the formation of heavy compounds, which have a poisoning effect on catalytic activity.

The increase of the temperature led to complete acetol conversion, but it also had a negative effect on the selectivity to PAI; this decreased slightly in favour of the side-products.

The results confirmed the good catalytic behaviour of Fe/P/O for the oxidative dehydrogenation reactions as reported in the literature.

3.2.3 MgO

Before investigating the catalytic behaviour of the vanadium-doped MgO, catalytic tests on MgO were carried out in order to study the dehydrogenative capability of this system; in fact, MgO showed good properties in the dehydrogenation of light alcohols [70].

The catalytic behaviour of MgO was studied as a function of temperature under two different operative conditions, the first using 1%mol oxygen (denoted as "lean conditions") and the second feeding 4%mol oxygen (denoted as "rich conditions").

The results obtained under "lean" condition, as reported in Figure 3-22, showed the extremely low catalytic activity of MgO in the temperature range studied; the maximum conversion of acetol was achieved at 270 °C, which was equal to 38%. The

main products were CO and CO_2, their formation could be correlated to the decarbonylation of aldehyde, which can take place on the strong base sites present on the catalytic surface. This hypothesis was further confirmed by the presence of acetaldehyde and acetic acid. The selectivity into PAl did not reach a value higher than 9%; meanwhile, no formation of PAc was detected.

An important lack of carbon balance was also observed: around 40–50% of the carbon atoms fed were not detected by the GC analysis. This suggests that the strong interaction of the basic catalyst with the acetol or the intermediates favours the formation of carbonaceous compounds, with a high molecular weight that remain adsorbed on the surface.

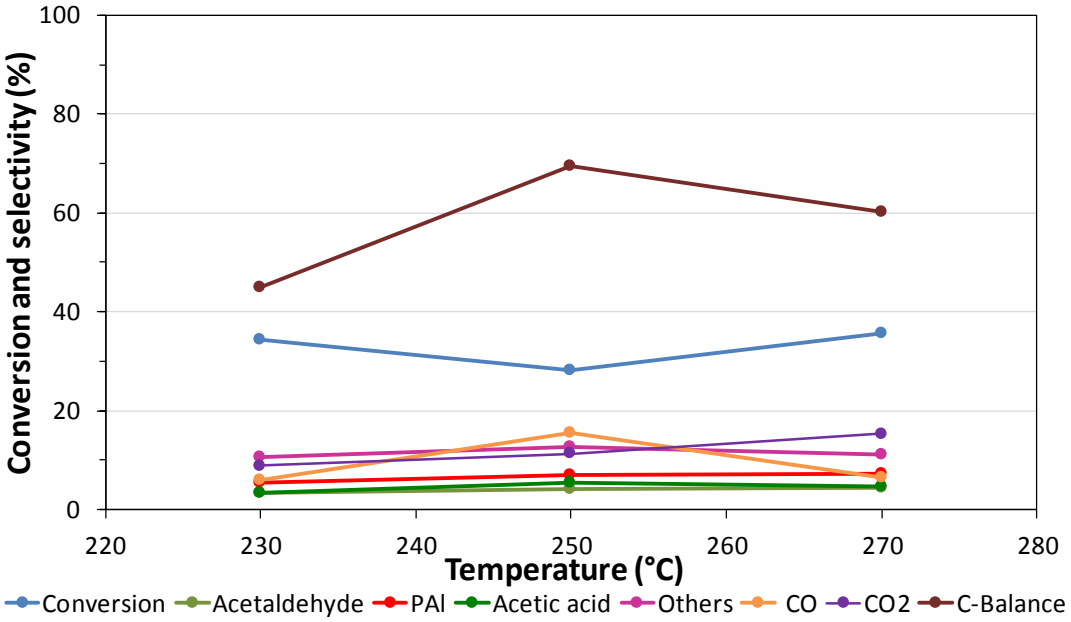

Figure 3-22 Catalytic behaviour of MgO during the oxidation of acetol to PAc as a function of temperature under lean conditions. Feeding 2%mol HA, 1%mol O_2 and 10%mol H_2O remaidern inert; W/F: 0.5 g_{cat}·s/mL.

The results obtained under rich conditions, reported Figure 3-23, displayed a slightly different catalytic performance compared with the lean conditions.

The conversion of acetol, passing from 20% at 230 °C to 58% at 290 °C, indicated the

higher catalytic activity of the system with the temperature increase. All the oxygenated species increased their selectivity compared with lean conditions; moreover, the lack of carbon balance decreased, indicating the positive effect of oxygen on the transformation of acetol. Condensations and oxidative cleavages were the main reactions that occurred on the surface; both processes hindered the production of PAI, which was lower than 10%.

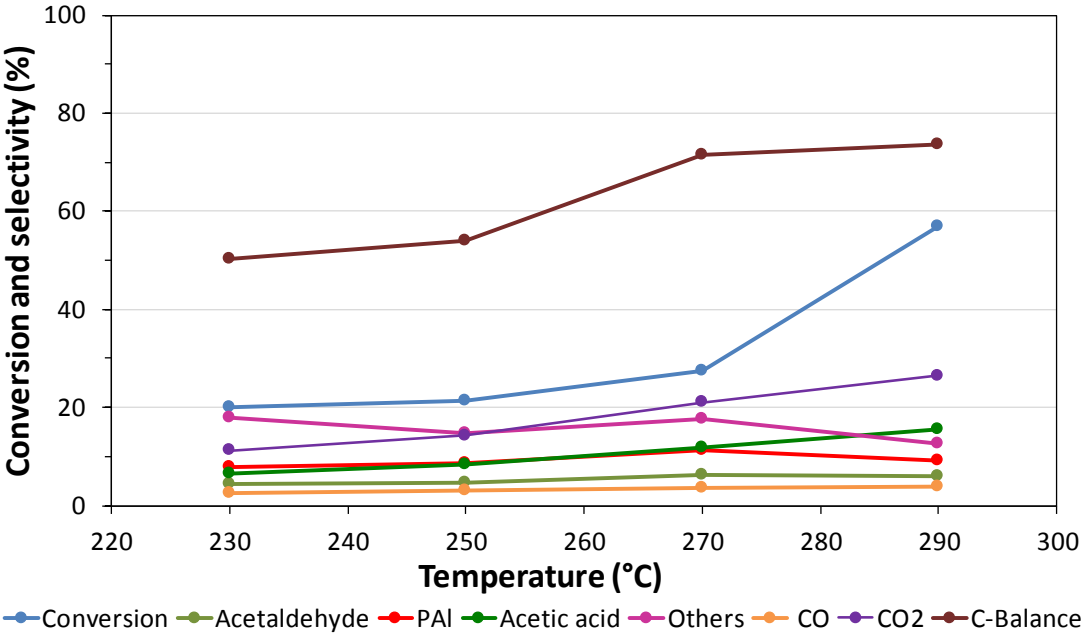

Figure 3-23 Catalytic behaviour of MgO during oxidation of acetol to PAc in function of the temperature under rich conditions. Feeding 2%mol HA; 4%mol O_2; 10%mol H_2O, remain inert; W/F: 0.5 g_{cat}·s/mL

It was then decided to test the vanadia-supported MgO catalyst under rich conditions, because at the latter conditions a higher selectivity to oxygenated products was obtained.

3.2.4 V/Mg/O

The presence of vanadate on MgO drastically modifies the catalytic performance of MgO. As illustrated in Figure 3-24, the conversion was 50% at 230 °C, a value two

times higher than that obtained on the MgO catalyst in the same conditions. The vanadium species also increased the selectivity of all the oxygenated compounds, but unfortunately, still PAI was not the main product, and no formation of PAc was detected.

At low temperatures, acetol was mainly converted into "other" and CO_2; acetaldehyde, acetic acid and CO were also obtained. A lack of carbon balance was also detected, in amount comparable to what was observed with MgO under the same conditions. This suggested a strong interaction between the acetol and the vanadate surface.

When the temperature was increased, the oxidative processes were even more favoured; this led to an increase of the conversion of acetol, which became close to 100% at 360 °C, and the selectivity into all the oxygenated products also improved. Moreover, the formation and deposition of carbonaceous species on the catalytic surface was disfavoured. The maximum selectivity into PAI was 12% at 270 °C; beyond that, it

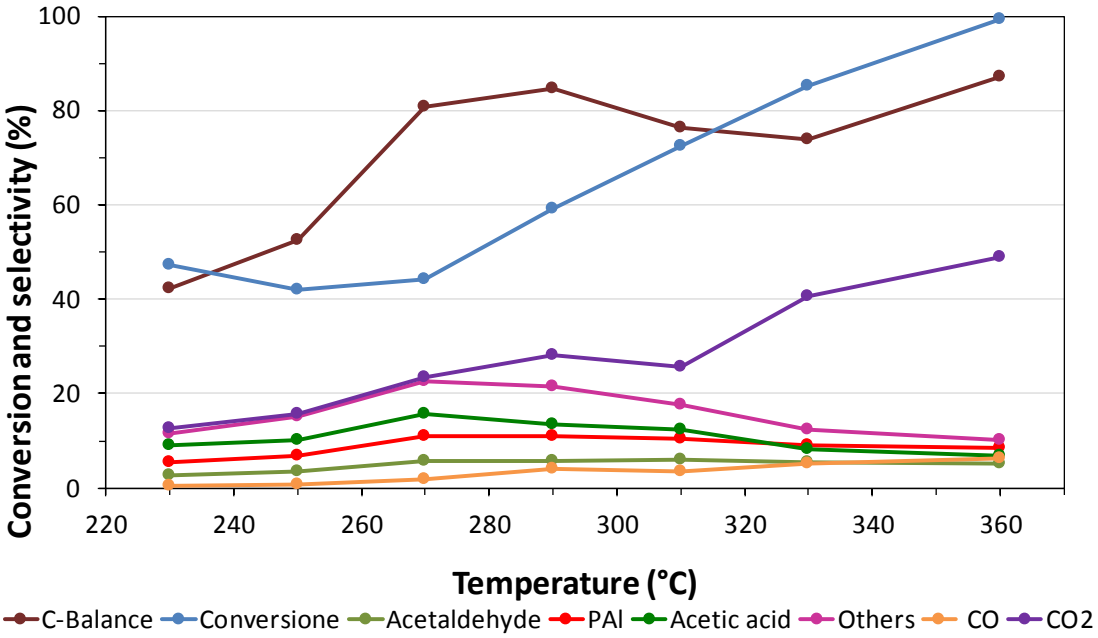

Figure 3-24 Catalytic behaviour of V/Mg/O during oxidation of acetol to PAc as a function of temperature. Feeding 2%mol HA, 4%mol O_2 and 10%mol H_2O remain inert; W/F: 0.5 g_{cat}·s/mL.

decreased, reaching 6% at 360 °C, with no formation of PAc. At temperatures higher than 270 °C, overoxidation became the main reaction, because the selectivity to all the products decreased in favour of CO_2. In addition, the formation of heavy compounds on the surface was hindered; in fact, the carbon balance reached 86%.

3.2.5 $AlVO_4$

The first catalytic test with $AlVO_4$ catalyst was carried out at 230 °C for 14 hours, because a strong variation of its catalytic activity was observed during time on stream. Results reported in Figure 3-25 suggest a change of the textural properties of $AlVO_4$ occurring during reaction. In the first 3 hours of the reaction, complete conversion of acetol was shown; however, after this point, a continuous decrease was observed, achieving 80% after 14 hours of reaction. In concomitance with the fall of conversion, a variation in the distribution of the products also occurred: acetic acid formed with

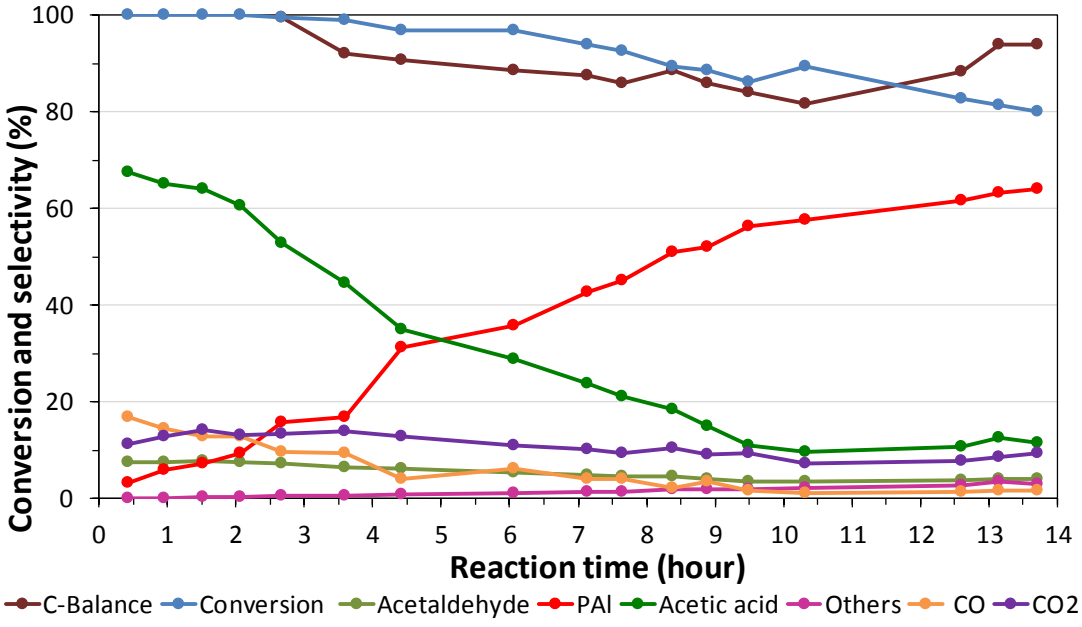

Figure 3-25 Catalytic behaviour of $AlVO_4$ during oxidation of acetol to PAc at 230 °C as a function of time on stream. Temperature: 230 °C; feeding; 2%mol HA, 4%mol O_2 and 10%mol H_2O remain inert; W/F: 0.5 g_{cat}·s/mL.

high selectivity during first hours of reaction with the maximum value of 66%. Afterwards, selectivity to acetic acid declined, with a corresponding increase of selectivity to PAI; this passed from 5% after the first hour, to the 60% after 10 hours. Moreover, the selectivity to acetaldehyde, CO and CO_2 followed the same trend as that one to acetic acid. Meanwhile, a slight lack of carbon balance was also observed, indicating the formation of carbonaceous deposits on the surface. After 10 hours of reaction, all products selectivity became stable, while the conversion continued to decrease, achieving 80% after 12 hours; this was the lowest value obtained during this catalytic test. The variation of the catalytic behaviour of $AlVO_4$ shown during the reaction is clearly attributable to a modification of the catalyst. Therefore, the spent catalyst was characterised by means of XRD and Raman spectroscopy.

The diffractogram of the spent catalyst, shown in Figure 3-26 and compared with that one of the fresh sample, presented the same reflections as fresh $AlVO_4$, indicating that indeed no main structural changes had taken place during reaction. However, it is seen

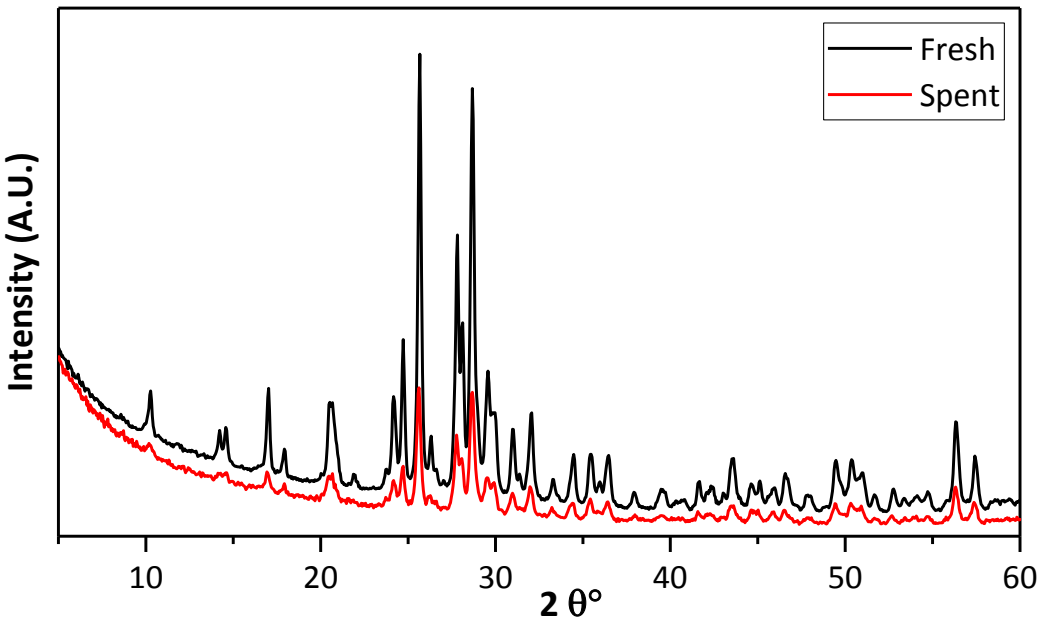

Figure 3-26 XRD analysis of fresh and spent $AlVO_4$ catalyst

that the spent catalyst presented a lower intensity of the pattern compared to the fresh one. Similar results were obtained by means of Raman spectroscopy (Figure 3-27): the bands attributable to the $AlVO_4$ phase did not exhibit any significant variation; the presence of the bands at 1600 and 1400 cm^{-1} confirmed the accumulation of carbonaceous species on the surface.

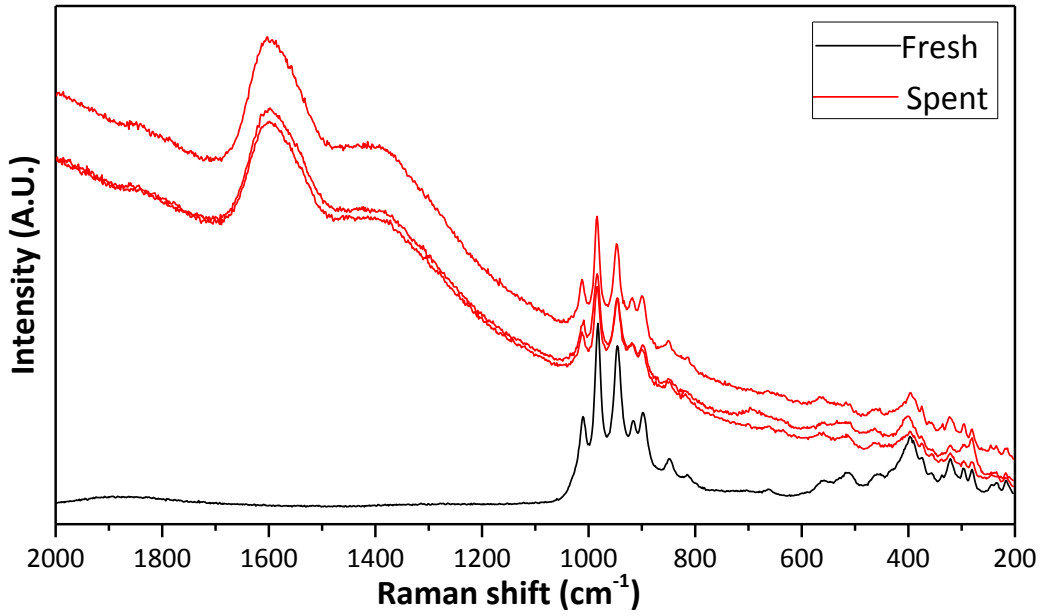

Figure 3-27 Raman spectra acquired over the fresh and spent $AlVO_4$ catalysts.

It is possible to conclude that the remarkable variation of the catalytic behaviour of $AlVO_4$ shown during time can be correlated to the coverage of the active sites responsible for the oxidative cleavage reaction of PAl by the carbonaceous species.

No formation of PAc was observed, it was then decided to increase the temperature at 270 °C to support the selective oxidation reaction.

Figure 3-28 illustrates the results obtained by carrying out the catalytic test at 270 °C for 8 hours. It is possible to observe a different catalytic behaviour than that shown at 230 °C.

In contrast to what reported in Figure 3-25, the catalytic system reached the steady state almost immediately and maintained it throughout the reaction time. Complete conversion of acetol and the presence of only the products derived from the degradative reactions were detected, while no formation of PAI and PAc was observed.

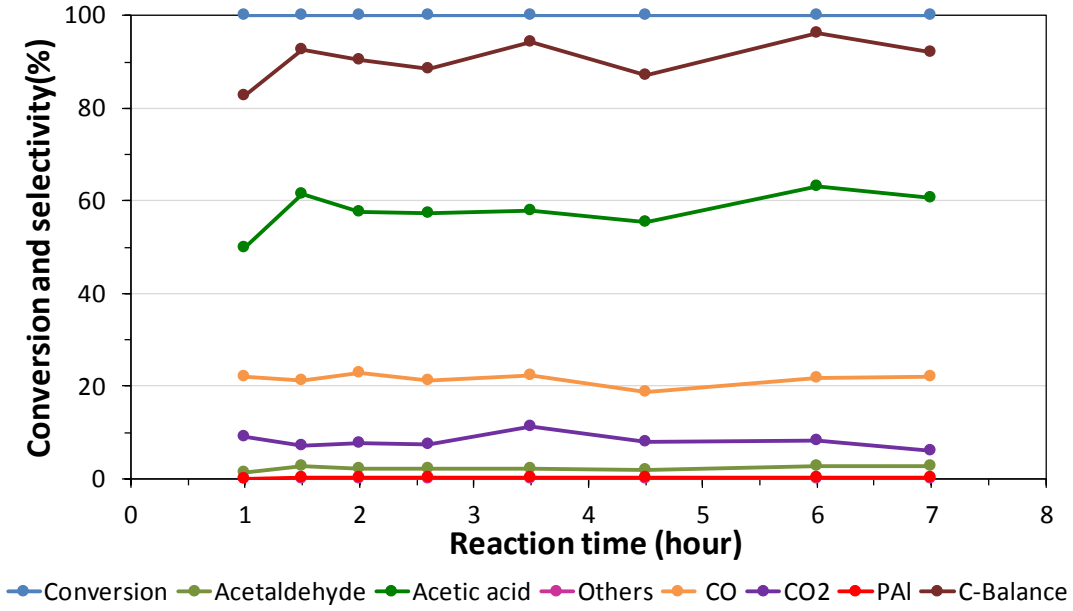

Figure 3-28 Catalytic behaviour of $AlVO_4$ during the oxidation of acetol to PAc at 270 °C as a function of time on stream. Temperature: 270 °C; feeding 2%mol HA, 4%mol O_2 and 10%mol H_2O, remain inert; W/F: 0.5 g_{cat}·s/mL.

In order to investigate in depth the reaction network, catalytic tests were carried out by varying the contact time.

The results, reported in Figure 3-29, showed the complete conversion of acetol at very low contact time. In these conditions, PAI selectivity was 70%; this was the highest value reached during this catalytic test. The result underlines that PAI is the primary product of the transformation of acetol. A slight lack of carbon balance was observed, probably correlated to the strong adsorption of acetol on the catalytic surface. The increase of contact time favoured the consecutive reactions; this led to a drop of selectivity into PAI and an increase of selectivity into acetic acid, acetaldehyde, CO

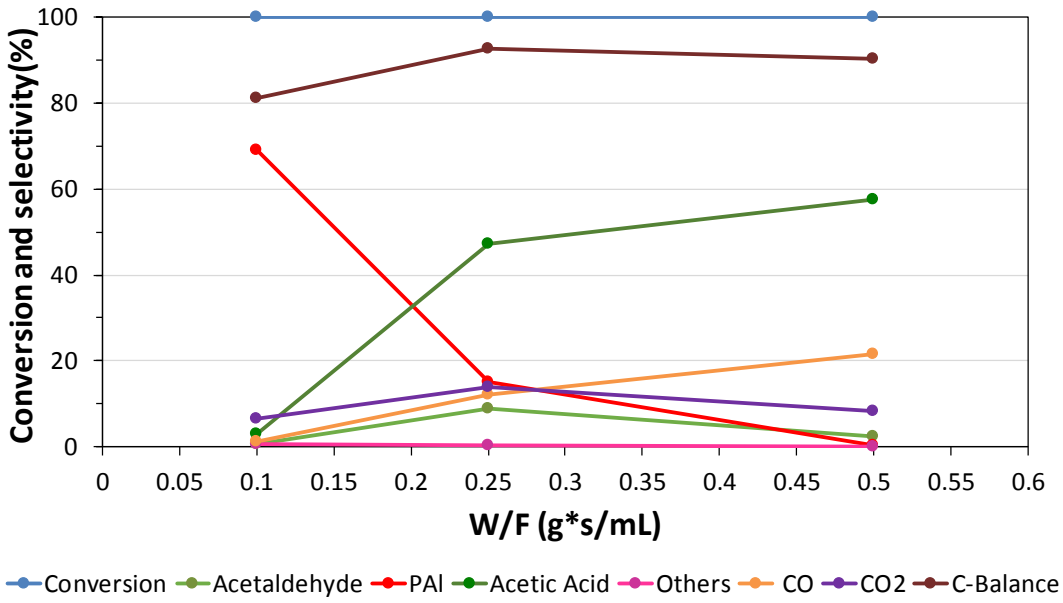

Figure 3-29 Catalytic behaviour of $AlVO_4$ during oxidation of acetol to PAc as a function of contact time. Temperature: 270 °C; feeding 2%mol H, 4%mol O_2 and 10%mol H_2O remainder inert.

and CO_2; no PAc was formed. More in detail, the selectivity into acetic acid and CO had the same trend, both being different from that of acetaldehyde and CO_2. Therefore, it is possible to hypothesise that acetic acid and CO derived from the oxidative cleavage of PAl; while, acetaldehyde and CO_2 formed from the decarboxylation of PAc.

3.2.6 α_1 $VOPO_4$ (VPD)

Figure 3-30 shows the catalytic behaviour of α_1-$VOPO_4$ (VPD) at different temperatures. The results showed a low conversion of acetol, around 40%, at low temperature, probably due to the low specific surface area of this catalyst (see section 3.1.5). The selectivity into PAl attested at a value close to 70%, while low selectivity into the side products derived from degradative processes was observed. A slight lack of carbon balance was denoted, probably because of the formation of heavy compounds.

The increase of the temperature mainly influenced the conversion of the acetol, which almost reached the unitary value at 320 °C, and the selectivity to PAI, which reached 82% at 270 °C, the maximum value obtained for this catalyst. At temperatures higher than 270 °C, the selectivity into PAI began to decrease in favour of the formation of side-products, both those deriving from the degradative processes (acetic acid, acetaldehyde, CO and CO_2), and those from the condensation reactions (denoted with "others"). The low C balance can be attributed to heavy compounds deposition.

No formation of PAc was observed.

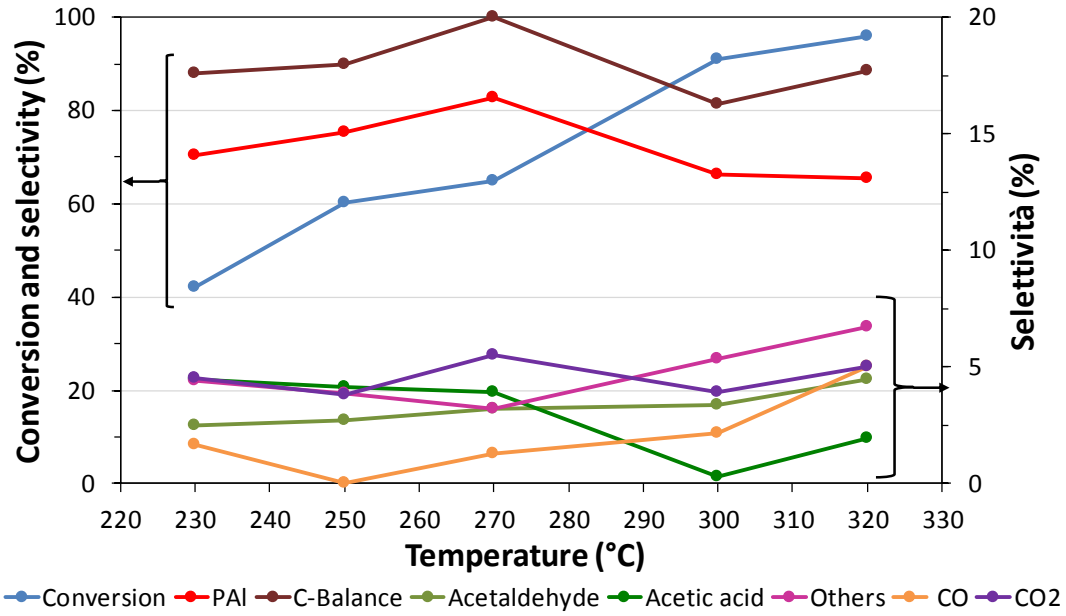

Figure 3-30 Catalytic behaviour of VPD during oxidation of acetol to PAc in function of the temperature. Feeding 2%mol HA; 4%mol O_2; 10%mol H_2O, remainder inert; W/F: 0.5 g_{cat}·s/mL

3.2.7 $(VO)_2P_2O_7$ DuPont (VPP)

In order to promote the selective oxidation of acetol into PAc, vanadyl pyrophosphate (VPP) was also tested. The catalytic behaviour of VPP for the selective oxidation of acetol is displayed in Figure 3-31; at low temperature, the VPP presented an incomplete conversion of the acetol. Under these conditions, a good selectivity into

PAl was observed with a low formation of the side-products deriving the degradation processes.

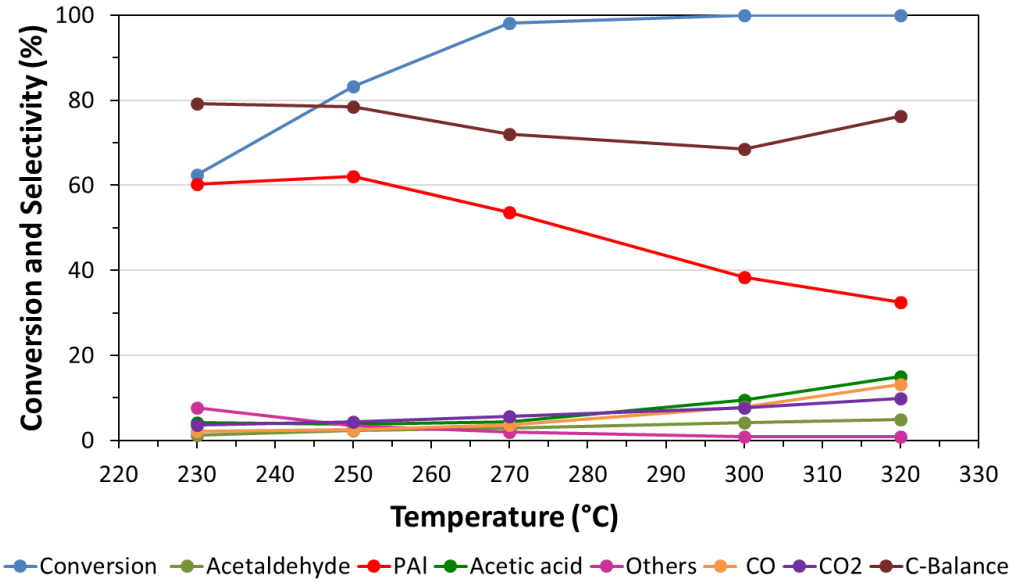

Figure 3-31 Catalytic behaviour of vanadyl pyrophosphate (VPP) during oxidation of acetol to PAc as a function of temperature. Feeding 2%mol HA, 4%mol O_2 and 10%mol H_2O remainder inert; W/F: 0.5 g_{cat}·s/mL.

A lack of carbon balance was also observed, which can be attributed to the high acidity of the VPP, able to catalyse the condensation reactions with the production of heavy carbonaceous species. At 250 °C the selectivity into PAl was 60%, representing the best value obtained for VPP. Increasing the temperature, almost complete conversion of acetol was reached at 270 °C. In contrast, the increment of the temperature led to an increase of the non-selective oxidative processes, with an increase of selectivity to acetic acid, acetaldehyde, CO and CO_2. No formation of PAc was observed.

3.2.8 W/V/O HTB

The results, reported in Figure 3-32, showed almost complete conversion already at 230 °C, indicating the high activity of this catalytic system.

Concerning the products distribution, selectivity into PAI was slightly less than 80% at 230 °C; this was the best result obtained for the W/V/O catalyst. The side-products, deriving from the degradative processes, presented a selectivity lower than 10%; formation of carbonaceous deposits was observed from the lack of carbon balance.

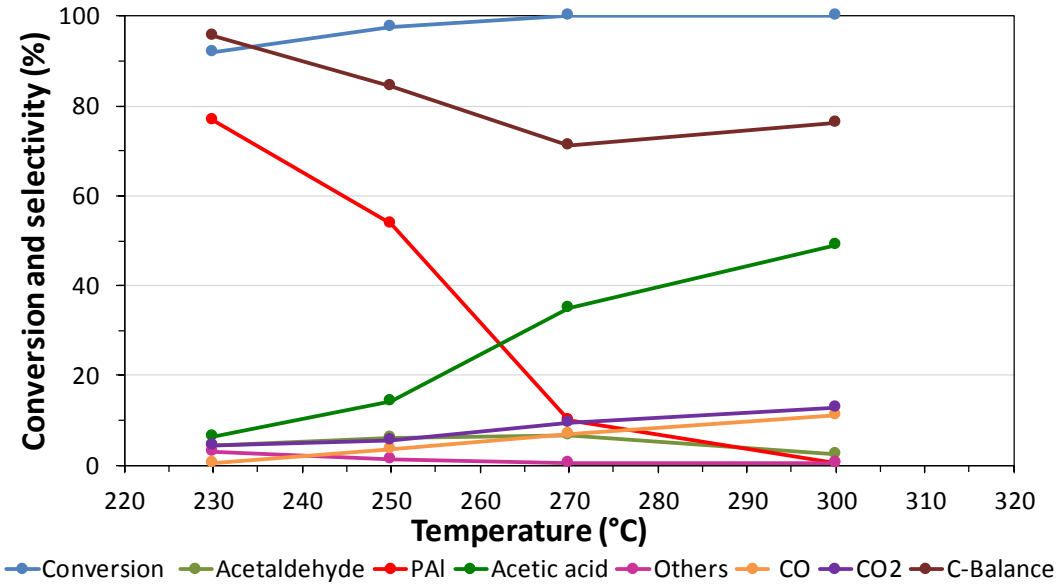

Figure 3-32 Catalytic behaviour of W/V/O during oxidation of acetol to PAc as a function of temperature. Feeding 2%mol HA, 4%mol O_2 and 10%mol H_2O remainder inert; W/F: 0.5 g_{cat}·s/mL.

Increasing the temperature, this led the conversion to achieve 100% at 270 °C, but also favoured the degradative processes even more: the selectivity into PAI dropped, disappearing completely at a temperature of 300 °C, while the selectivity into acetic acid continuously grew, achieving 50% at 300 °C. Analysing the ratio between the sum of C_2 molecules (acetic acid and acetaldehyde) and CO_x, the value was always close to 2, the stoichiometric value; this indicates that the only reactions that occurred were the selective ODH of acetol and the degradative processes (oxidative cleavage and decarboxylation). Again, in this case, no formation of PAc was observed.

3.2.9 Structure-reactivity correlation

The comparison of catalytic performances in function of temperature with the various catalysts is shown in Figure 3-33 and Figure 3-34 (2%mol HA, 4%mol O_2 and 10%mol H_2O and W/F equal to 0.5 g_{cat}·s/mL). Almost all catalysts showed a low conversion of acetol at very low temperatures; only the W/V/O catalyst presented almost complete conversion at 230 °C.

With the increase of temperature, W/V/O, Fe/P/O, $AlVO_4$ and VPP catalysts achieved complete conversion at 270 °C, while for the VPD and V/Mg/O catalysts, temperatures of 320 and 360 °C, respectively, were required to reach total conversion of acetol. The low activity of VPD could be attributed to its low specific surface area (S.S.A.) and to the strong adsorption of acetol on the active sites. Concerning the V/Mg/O catalyst, and despite its high S.S.A., the low conversion of acetol can be attributed to the strong basic features of this catalyst which probably hindered the adsorption of the reactant.

Fe/P/O showed the best results in terms of yield into PAI, with a very low formation of side-products. The same catalyst maintained the high selectivity into PAI also at high temperature, in fact only a slight decrease of PAI in favour of C_2 compounds and CO_x was observed. W/V/O showed an initial high selectivity into PAI, but this already started to decrease at 250 °C, disappearing at 300 °C in favour of C_2 products and CO_x. VPD catalyst presented a good selectivity into PAI, and in contrast to what shown before with the other catalysts, the increase in temperature led to a notably higher selectivity to this compound; in fact, the other catalysts showed their highest selectivity to PAI at 230 °C, but VPD achieved its maximum at 270 °C.

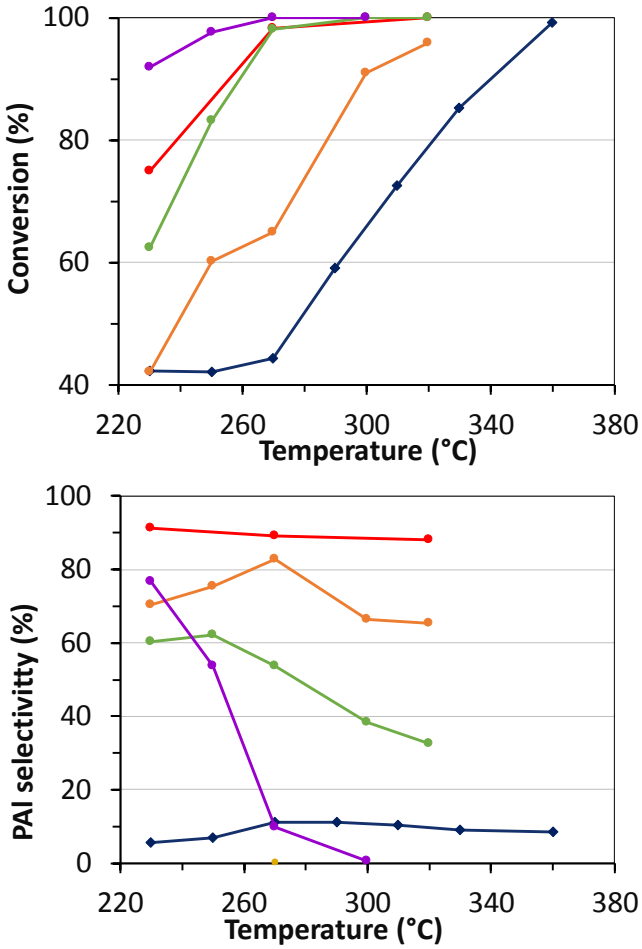

Figure 3-33 Comparison of conversion and selectivity to PAI, of different catalysts, for the transformation of acetol. Feed 2%mol HA, 4%mol O_2 and 10%mol H_2O remainder inert; W/F: 0.5 g_{cat}·s/mL. Red lines represent the Fe/P/O; Blue lines represent V/Mg/O; Yellow points represent $AlVO_4$; Orange lines represent VPD; Green lines represent VPP; Purple lines represent W/V/O.

Beyond this temperature, the consecutive reaction prevailed, leading to a decrease of selectivity into PAI. VPP presented good selectivity which also was initially stable, but after 270 °C, the consecutive reaction prevailed. V/Mg/O presented very low selectivity into PAI, like $AlVO_4$, which showed no formation of PAI at all.

All catalysts showed the formation of acetaldehyde, acetic acid (their sum is reported as C_2), CO and CO_2 as the major side- products. V/Mg/O also showed a non-negligible amount of "others".

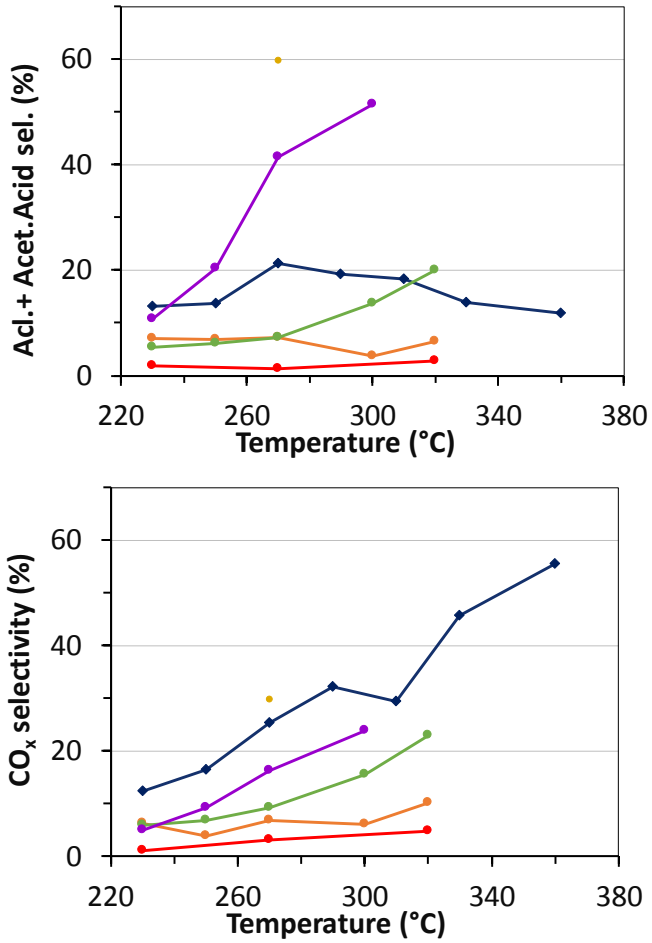

Figure 3-34 Comparison of selectivity to C_2, reported as sum of Acetaldehyde and Acetic acid, and to CO_x, of different catalysts, for the transformation of acetol. Feed 2%mol HA, 4%mol O_2 and 10%mol H_2O remainder inert; W/F: 0.5 g_{cat}·s/mL. Red lines represent the Fe/P/O; Blue lines represent V/Mg/O; Yellow points represent $AlVO_4$; Orange lines represent VPD; Green lines represent VPP; Purple lines represent W/V/O.

$AlVO_4$ presented the highest selectivity to C_2 close to 66%; W/V/O catalyst reached 55%, while all the other catalysts showed a selectivity into C_2 that was not higher than 20%. Concerning the selectivity into CO_x, all the catalytic systems presented a continuous growth with temperature. The C_2-to-CO_x selectivity ratio can help to elucidate which type of reactions were taking place: only $AlVO_4$ and W/V/O showed a ratio close to the stoichiometric one, while all the other catalysts showed a lower value. This indicates that only degradation reactions occurred with $AlVO_4$ and W/V/O up to 270 and 300 °C, respectively, while with all the other catalysts, an overoxidation

reaction also took place. None of these catalysts showed the formation of pyruvic acid. In light of the results, it can be concluded that the basic sites on the surface interact weakly with the acetol, with a low conversion of the reactant; the few adsorbed molecules undergo intermolecular condensation reactions with the formation of heavy compounds on the catalytic surface. Indeed, at high temperatures the presence of redox sites, related to the metavanadate species, catalyse overoxidation reactions with an increase of selectivity to CO_x.

Acid sites play a fundamental role for the transformation of acetol, in fact all the other catalysts showed better performances than V/Mg/O. However, the type of sites play a vital role in the entire process; this can be observed by comparing the results obtained from W/V/O, that holds mainly Brønsted sites [169], and $AlVO_4$ that instead presents mainly Lewis sites. The higher selectivity shown by $AlVO_4$ compared to W/V/O in the oxidative cleavage of PAl allows us to hypothesise the both ketonic and aldehydic groups strongly interact with the Lewis acid sites, so favouring the consecutive reactions.

Indeed, $AlVO_4$ also showed a high reaction rate for the oxidative dehydrogenation of acetol, because already at very low contact time total conversion and a very good selectivity to PAl were observed. This further supports the idea that the reactivity of this catalyst is governed by the strong interaction of acetol with Lewis acid sites.

Fe/P/O and VPD catalysts showed a very good selectivity to PAl; these results can be explained by taking into account also a role of the P=O groups in the ODH. In literature, it has recently been demonstrated the role of the P=O moiety in the H-abstraction step during the selective oxidation of *n*-butane to maleic anhydride with

V/P/O catalyst [186,187]. The strong basicity of the O(1)=P group coupled with the presence of V^{+5} in the $VOPO_4$ structure, favours the H-abstraction reaction by homolytic cleavage leading to the formation of reduced V^{+4} species. Here, the same step could take place with acetol, leading to the formation of PAl.

According to what described in the section 1.3.3, the redox properties are fundamental for the transformation of pyruvaldehyde to pyruvic acid. Unfortunately, no formation of the oxo-acid was observed with catalysts used; in contrast, acetic acid, acetaldehyde CO and CO_2, were the main side-products; C_5-C_6 molecules were also detected deriving from intermolecular condensation of adsorbed intermediates.

Analysing the selectivity to C_2 compounds, CO_x and their molar ratio, it is possible to understand the role of the redox sites on the non-selective oxidation reactions. Fe/P/O gave the lowest selectivity to these by-products, this indicates the weak oxidant power of this catalyst. On the opposite, V/Mg/O has shown the highest selectivity to CO_x, indicating the strong non-selective oxidizing power of the vanadate species.

W/V/O and $AlVO_4$ presented the highest selectivity to C_2 compounds and the highest C_2/CO_x ratio as well, the latter is close to the stoichiometric value (2); this result indicates that with these catalysts overoxidation reactions are disfavoured and only the oxidative cleavage of either PAl or PAc takes place.

The VPP catalyst, unlike the VPD, has shown a lower selectivity to PAl and a higher selectivity to C_2 compounds and CO_x; this difference can be attributed to the considerable acidic features of this catalyst, and to the different redox properties of the V species in the two catalysts. The different catalytic behaviour of the two catalysts is emphasised by increasing the temperature: at low T value, the redox sites responsible

for oxidation are poorly active, as also shown by the similar selectivity into PAI. At temperature higher than 300 °C, instead, the redox sites of the VPP catalyse the oxidative reactions. For both catalysts, a lower C_2/CO_x ratio compared to the stoichiometric is obtained, indicating that also overoxidation contributes to lower selectivity to PAI.

A further comparison of the catalysts could be done base on the maximum productivity of PAI calculated on the best yield of PAI for each system. The productivity of PAI (calculated as the weight of PAI obtained per the weight of catalyst per hours) and the corresponding yields are reported in Figure 3-35. It is possible to observe the Fe/P/O catalyst shows comparable productivity to the VPD and W/V/O catalysts (that is attested around the value of 0.7 $g_{PAI}/g_{cat}/h$), even if the first one presents the highest yield. About the $AlVO_4$, although it presents a comparable yield to the W/V/O, this catalytic system shows the highest productivity (around 2.4 $g_{PAI}/g_{cat}/h$). This result is correlated to the possibility of $AlVO_4$ to work with a lower contact time (almost five time lower) than the other catalysts.

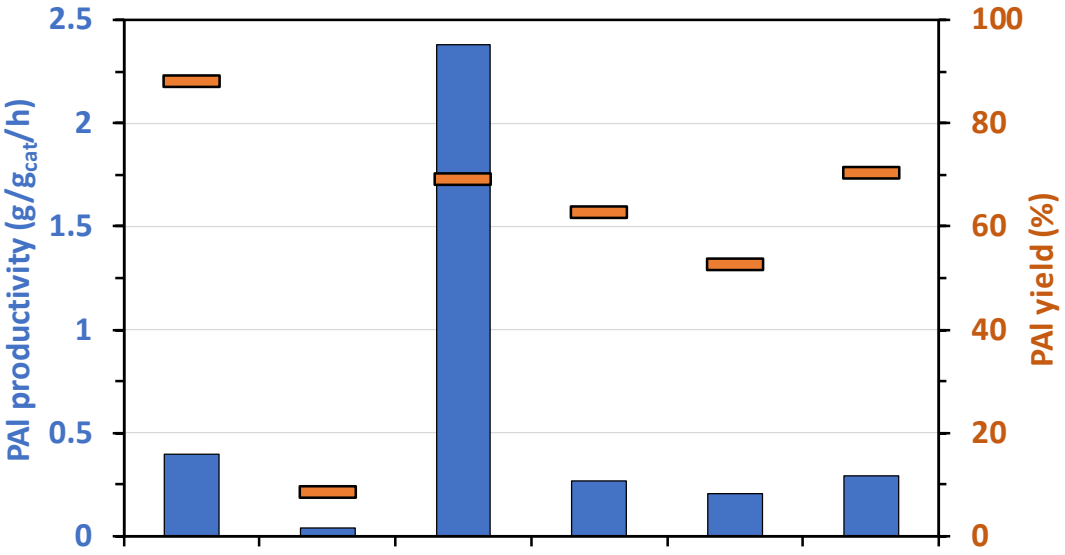

Figure 3-35 Comparison of the best productivity (blue bar) and yield to PAI (orange line) obtained from the catalytic tests done with the different catalysts for the transformation of acetol.

4 Conclusions

In this part of the thesis, I investigated the possibility to produce pyruvic acid from acetol by gas-phase selective oxidation, using different vanadium-containing catalysts. The results obtained have permitted to point out how the textural properties of the catalyst influence the entire process: catalysts with basic and redox properties presented low acetol conversion while accelerating the side-reactions. On the other hand, catalysts with acid and redox textural properties showed the best results in the oxidative dehydrogenation of acetol to pyruvaldehyde. In particular, phosphorous-containing catalysts presented the highest yield to PAl, while $AlVO_4$ showed the highest productivity to PAl because at very low contact time almost quantitative yield to the aldehyde was obtained.

Unfortunately, no formation of pyruvic acid was observed with all catalysts tested. This was due to the prevalence of decarbonylation, decarboxylation and oxidative cleavage reactions. Concerning the nature of side-reactions, the acid sites catalysed also the intermolecular condensation reactions that lead, in concomitance with the formation of C_5 and C_6 molecules, to the production of heavy compounds which accumulated on the catalyst surface.

GENERAL CONCLUSION

The aim of this thesis was the investigate new strategies for the transformation of bio-based building blocks into chemicals with high added value by means of gas-phase oxidation reactions mediated by vanadium-containing catalysts. The (oxi)dehydration of 1-butanol to butenes and maleic anhydride and the selective oxidation of acetol to pyruvic acid were the two reactions investigated. Concerning the catalysts, for the first reaction different vanadium/phosphorous mixed oxides were tested whereas for the selective oxidation of acetol, different vanadium-containing catalyst, with different chemical-physical properties were used, due to the scarce prior art in literature dealing with this reaction.

The results obtained led us to highlight different aspects for this kind of catalysts:

- The redox properties of the vanadium are strictly dependent on the nature of the species that surround theV atom, both present in the structure and adsorbed on the surface.
- The possibility to generate different active sites on the catalyst surface helps to drive the entire transformation of the substrate to the desired product.
- Acid/base sites play a fundamental role in the oxidative process, because they control the adsorption/desorption phenomena of the organic species, favouring or not the selective oxidation pathway.

These aspects underline the possibility to use vanadium-containing catalysts for a wide range of oxidative processes. In this contest, vanadium/phosphorous mixed oxides

represent one of the main example: by varying the structure, the amount of the species, and the method of synthesis it is possible to make a fine tuning of the acid and redox properties of the catalyst.

Concerning the entire transformation of bio-based building blocks, the production of butenes and maleic anhydride from 1-butanol can represent a valuable alternative to the classical selective oxidation route from *n*-butane. However, it is necessary to improve the performance of the process in terms of yield and productivity to the desired products in order to reduce the disadvantage deriving from the higher cost of 1-butanol compared to the alkane.

This can be done by a continue optimization of the catalyst textural properties such as the acid/redox features, which are a powerful tool to control the rate of undesired reactions, and the surface area, an important feature affecting overall productivity.

Regarding the production of pyruvic acid, results obtained showed the possibility to transform acetol to pyruvaldehyde with high yield and productivity; but also underlined the necessity to continue the study on the selective oxidation of the pyruvaldehyde to the correspond carboxylic acid.

This will be achieved by investigating the possibility to hinder side-reactions by varying both the operative conditions and catalysts textural properties.

REFERENCES

[1] P. Anastas, N. Eghbali, *Chem. Soc. Rev.* **39** (2010) 301–312.

[2] P.T. Anastas, J.B. Zimmerman, *Environ. Sci. Technol.* **37** (2003) 94A–101A.

[3] R. a. Sheldon, *Green Chem.* **16** (2014) 950.

[4] M. Aresta, A. Dibenedetto, F. Dumeignil, *Biorefinery: from biomass to chemicals and fuels*, Walter de Gruyter GmbH & Co. KG, 2012.

[5] J. Clark, *J. Chem. Technol. Biotechnol.* **609** (2007) 603–609.

[6] B. Kamm, M. Kamm, *Appl. Microbiol. Biotechnol.* **64** (2004) 137–145.

[7] Http://www.matrica.it/, (n.d.).

[8] Http://www.betarenewables.com/en, (n.d.).

[9] Http://www.chemelot-inscite.com/, (n.d.).

[10] Http://www.eurobioref.org/, (n.d.).

[11] C. Fu, J.R. Mielenz, X. Xiao, Y. Ge, C.Y. Hamilton, M. Rodriguez, F. Chen, M. Foston, A. Ragauskas, J. Bouton, R.A. Dixon, Z.-Y. Wang, *Proc. Natl. Acad. Sci. U. S. A.* **108** (2011) 3803–8.

[12] X. Li, J.K. Weng, C. Chapple, *Plant J.* **54** (2008) 569–581.

[13] G. Brodeur, E. Yau, K. Badal, J. Collier, K.B. Ramachandran, S. Ramakrishnan, *Enzyme Res.* **2011** (2011) e787532.

[14] P.K. Rout, A.D. Nannaware, O. Prakash, R. Rajasekharan, *ChemBioEng Rev.* **1** (2014) 96–116.

[15] C.-H. Zhou, X. Xia, C.-X. Lin, D.-S. Tong, J. Beltramini, *Chem. Soc. Rev.* **40** (2011) 5588–617.

[16] A.K. Kumar, S. Sharma, *Bioresour. Bioprocess.* **4** (2017) 7.

[17] T. Werpy, G. Petersen, *Top Value Added Chemicals from Biomass Volume I — Results of Screening for Potential Candidates from Sugars and Synthesis Gas Top Value Added Chemicals From Biomass Volume I : Results of Screening for Potential Candidates*, 2004.

[18] M. Stelmachowski, *Ecol. Chem. Eng. S.* **18** (2011).

[19] T.M. Lammens, M.C.R. Franssen, E.L. Scott, J.P.M. Sanders, *Biomass and Bioenergy*. **44** (2012) 168–181.

[20] A. Corma, S. Iborra, A. Velty, *Chem. Rev.* **107** (2007) 2411–502.

[21] Http://www.boeing.com/commercial/aeromagazine/articles/qtr_4_06/article_04_2.html, (n.d.).

[22] J.J. Kolstad, J.G. Van Berkel, *Process for producing and oriented film comprising poly(ethylene-,5-furandicarboxylate)*, **WO 2016/032330 A1**, 2015.

[23] Http://www.coca-colacompany.com/coca-cola-unbottled/plantbottle-program-gets-boost-, (n.d.).

[24] Http://www.pepsico.com/live/pressrelease/PepsiCo-Develops-Worlds-First-100-Percent-Plant-Based-Renewably-Sourced-PET-Bott03152011, (n.d.).

[25] Http://www.rennovia.com/markets/, (n.d.).

[26] A. Chieregato, J.V. Ochoa, F. Cavani, Olefins from Biomass, in: Chem. Fuels from Bio-Based Build. Blocks (Eds F. Cavani, S. Albonetti, F. Basile A. Gandini), Wiley-VCH Verlag GmbH & Co. KGaA, Weinheim, Germany, 2016: pp. 1–32.

[27] H. Michibata, *Vanadium*, Springer Netherlands, Dordrecht, 2012.

[28] I.E. Wachs, *Dalt. Trans.* **42** (2013) 11762–11769.

[29] R. Meisnner, N. Neth, *Preparation of a catalyst for the oxidation of sulfur dioxide to sulfur trioxide*, **US 4,539,309**, 1985.

[30] M. Tanimoto, K. Tatsuya, H. Yunoki, Y. Aoki, *Catalyst for production of acrylic acid and method for production of acrylic acid by the use of the catalyst*, **US 6,429,332 B1**, 2002.

[31] C. Hechler, G.-P. Schindler, C. Adami, O. Machhanner, K.J. Muller-Engel, H. Martan, *Preparation of at least one partial oxidation and/or ammoxidation product of propylene*, **US 7,326,802 B2**, 2008.

[32] F. Ghelfi, G. Mazzoni, C. Fumagalli, F. Cavani, *Niobium-doped vanadium/phosphorus mixed oxide catalyst*, **US 2006/0173197 A1**, 2006.

[33] H. Sakai, Y. Konno, T. Ejiri, E. Nishimura, *Catalyst for producing methacrylic acid and method for producing the same, and method for producing methacrylic acid*, **US 2016/0051970 A1**, 2016.

[34] I.E. Wachs, B.M. Weckhuysen, *Appl. Catal. A Gen.* **157** (1997) 67–90.

[35] G. Mestl, *Top. Catal.* **38** (2006) 69–82.

[36] L. Giebeler, P. Kampe, A. Wirth, A.H. Adams, J. Kunert, H. Fuess, H. Vogel, *J. Mol. Catal. A Chem.* **259** (2006) 309–318.

[37] G.J. Hutchings, C.J. Kiely, M.T. Sananes-Schulz, A. Burrows, J.C. Volta, *Catal. Today*. **40** (1998) 273–286.

[38] M. Bender, *ChemBioEng Rev.* **1** (2014) 136–147.

[39] H.N. Sun, J.P. Wristers, *Kirk Othmer Encycl. Chem. Technol.* **4** (2000) 365–392.

[40] T.R. Felthouse, J.C. Burnett, B. Horrell, M.J. Mummey, Y.-J. Kuo, Maleic Anhydride, Maleic Acid, and Fumaric Acid, in: Kirk-Othmer Encycl. Chem. Technol., John Wiley & Sons, Inc., Hoboken, NJ, USA, 2001.

[41] B.A. Keay, P.W. Dibble, *2.08 - Furans and their Benzo Derivatives: Applications*, 1996.

[42] R. Ohnishi, T. Akimoto, K. Tanabe, *J. Chem. Soc. Chem. Commun.* **70** (1985) 1613–1614.

[43] G. Pomalaza, M. Capron, V. Ordomsky, F. Dumeignil, *Catalysts*. **6** (2016) 203.

[44] H. Duan, Y. Yamada, S. Sato, *Chem. Lett.* **45** (2016) 1036–1047.

[45] D. Gunst, K. Alexopoulos, K. Van Der Borght, M. John, V. Galvita, M.F. Reyniers, A. Verberckmoes, *Appl. Catal. A Gen.* **539** (2017) 1–12.

[46] O. Macias, J. Largo, C. Pesquera, C. Blanco, F. Gonz??lez, *Appl. Catal. A Gen.* **314** (2006) 23–31.

[47] R.M. West, D.J. Braden, J. a. Dumesic, *J. Catal.* **262** (2009) 134–143.

[48] O. Onel, A.M. Niziolek, C.A. Floudas, *Ind. Eng. Chem. Res.* **55** (2016) 3043–3063.

[49] S.P. Pyl, C.M. Schietekat, M.F. Reyniers, R. Abhari, G.B. Marin, K.M. Van Geem, *Chem. Eng. J.* **176–177** (2011) 178–187.

[50] O. Onel, A.M. Niziolek, J.A. Elia, R.C. Baliban, C.A. Floudas, *Ind. Eng. Chem. Res.* **54** (2015) 359–385.

[51] K.M. Holmgren, T. Berntsson, E. Andersson, T. Rydberg, *Energy*. **45** (2012) 817–828.

[52] D.K. Hood, O.M. Musa, *Handbook of Maleic Anhydride Based Materials*, Springer International Publishing, Cham, 2016.

[53] *Gazz. Uff. dell'Unione Eur.* (2008) 1–43.

[54] G. Centi, F. Cavani, F. Trifirò, *Selective Oxidation by Heterogeneous Catalysis*, Springer US, Boston, MA, 2001.

[55] R.M. Contractor, D.I. Garnett, H.S. Horowitz, H.E. Bergna, G.S. Patience, J.T. Schwartz, G.M. Sisler, *Stud. Surf. Sci. Catal.* **82** (1994) 233–242.

[56] S. Sanchioni, A. Neri, *Process for the continuous separation of maleic anhydride from process gases*, 1982.

[57] R. Wojcieszak, F. Santarelli, S. Paul, F. Dumeignil, F. Cavani, R. V Gonçalves, *Sustain. Chem. Process.* **3** (2015) 9.

[58] H. Guo, G. Yin, *J. Phys. Chem. C*. **115** (2011) 17516–17522.

[59] X. Li, B. Ho, Y. Zhang, *Green Chem.* **18** (2016) 2976–2980.

[60] N. Alonso-Fagúndez, M.L.L.L. Granados, R. Mariscal, M. Ojeda, *ChemSusChem*. **5** (2012) 1984–1990.

[61] Z. Du, J. Ma, F. Wang, J. Liu, J. Xu, *Green Chem.* **13** (2011) 554.

[62] G. Pavarelli, J. Velasquez Ochoa, A. Caldarelli, F. Puzzo, F. Cavani, J.-L. Dubois, *ChemSusChem*. **8** (2015) 2250–2259.

[63] L.M. Cornaglia, E. a Lombardo, *Appl. Catal. A*. **127** (1995) 125–138.

[64] A. Chieregato, J.M. López Nieto, F. Cavani, *Coord. Chem. Rev.* **301–302** (2014) 3–23.

[65] F. Cavani, G. Centi, I. Manenti, *Ind. Eng. Chem. Prod. Res. Dev.* **29** (1983) 565–

570.

[66] F. Cavani, G. Centi, F. Trifiro, *Ind. Eng. Chem. Prod. Res. Dev.* (1983) 570–577.

[67] E. Billig, Butyl Alcohols, in: Kirk-Othmer Encycl. Chem. Technol., John Wiley & Sons, Inc., Hoboken, NJ, USA, 2001.

[68] H.-D. Hahn, G. Dämbkes, N. Rupprich, H. Bahl, G.D. Frey, *Ullmann's Encycl. Ind. Chem.* (2013) 1–13.

[69] J. Quesada, L. Faba, E. Díaz, S. Ordóñez, *Appl. Catal. A Gen.* **542** (2017) 271–281.

[70] A. Chieregato, J. Velasquez Ochoa, C. Bandinelli, G. Fornasari, F. Cavani, M. Mella, *ChemSusChem*. **8** (2015) 377–388.

[71] J. Sun, Y. Wang, *ACS Catal.* **4** (2014) 1078–1090.

[72] H. Aitchison, R.L. Wingad, D.F. Wass, *ACS Catal.* **6** (2016) 7125–7132.

[73] S. Chakraborty, P.E. Piszel, C.E. Hayes, R.T. Baker, W.D. Jones, *J. Am. Chem. Soc.* **137** (2015) 14264–14267.

[74] P. Dürre, *FEMS Microbiol. Lett.* **363** (2016) 1–7.

[75] M. Sauer, *FEMS Microbiol. Lett.* **363** (2016) 1–4.

[76] N.R. Baral, L. Slutzky, A. Shah, T.C. Ezeji, K. Cornish, A. Christy, *FEMS Microbiol. Lett.* **363** (2016) 1–11.

[77] F. Trifirò, R.K. Grasselli, *Top. Catal.* **57** (2014) 1188–1195.

[78] E.A. Lombardo, C.A. Sánchez, L.M. Cornaglia, *Catal. Today*. **15** (1992) 407–418.

[79] S. Albonetti, F. Cavani, S. Ligi, F. Pierelli, F. Trifirò, F. Ghelfi, G. Mazzoni, *Stud. Surf. Sci. Catal.* (2000) 963–973.

[80] Y. Zhang, R.P.A. Sneeden, J.C. Volta, *Catal. Today*. **16** (1993) 39–49.

[81] L. Griesel, J.K. Bartley, R.P.. Wells, G.J. Hutchings, *J. Mol. Catal. A Chem.* **220** (2004) 113–119.

[82] M.E. Leonowicz, J.W. Johnson, J.F. Brody, H.F. Shannon, J.M. Newsam, *J. Solid State Chem.* **56** (1985) 370–378.

[83] G. Mestl, D. Lesser, T. Turek, *Top. Catal.* **59** (2016) 1533–1544.

[84] F. Cavani, S. Luciani, E.D. Esposti, C. Cortelli, R. Leanza, *Chemistry*. **16** (2010) 1646–55.

[85] P. Mars, D.W. van Krevelen, *Chem. Eng. Sci.* **3** (1954) 41–59.

[86] N. Ballarini, F. Cavani, C. Cortelli, S. Ligi, F. Pierelli, F. Trifirò, C. Fumagalli, G. Mazzoni, T. Monti, *Top. Catal.* **38** (2006) 147–156.

[87] S. Sajip, J.K. Bartley, A. Burrows, C. Rhodes, J. Claude Volta, C.J. Kiely, G.J. Hutchings, *Phys. Chem. Chem. Phys.* **3** (2001) 2143–2147.

[88] S. Shen, J. Zhou, F. Zhang, L. Zhou, R. Li, *Catal. Today*. **74** (2002) 37–43.

[89] Y. Kamiya, Y. Kijima, T. Ohkura, A. Satsuma, T. Hattori, *Appl. Catal. A Gen.* **253** (2003) 1–13.

[90] L. Sartoni, J.K. Bartley, R.P.K. Wells, C.J. Kiely, J.C. Volta, G.J. Hutchings, *J. Mol.*

Catal. A Chem. **220** (2004) 85–92.

[91] A. Caldarelli, M.A. Bañares, C. Cortelli, S. Luciani, F. Cavani, *Catal. Sci. Technol.* **4** (2014) 419–427.

[92] D. Ye, M. Fu, L. Tian, H. Liang, T. Rong, S. Cheng, X. Pang, *Res. Chem. Intermed.* **29** (2003) 271–284.

[93] G.J. Hutchings, *Catal. Today*. **16** (1993) 139–146.

[94] F. Cavani, F. Trifirò, *Appl. Catal. A Gen.* **157** (1997) 195–221.

[95] V.A. Zazhigalov, J. Haber, J. Stoch, A.I. Pyatnitzkaya, G.A. Komashko, V.M. Belousov, *Appl. Catal. A Gen.* **96** (1993) 135–150.

[96] F. Cavani, F. Trifirò, *Chem. Technol.* **24** (1994) 18–25.

[97] N.F. Dummer, W. Weng, C.J.C. Kiely, A.F. Carley, J.K. Bartley, C.J.C. Kiely, G.J. Hutchings, *Appl. Catal. A Gen.* **376** (2010) 47–55.

[98] L. Beneš, E. Černošková, J. Málek, K. Mélanová, P. Patrono, V. Zima, *J. Incl. Phenom. Macrocycl. Chem.* **36** (2000) 163–178.

[99] V. Zima, L. Beneš, J. Málek, M. Vlček, *Mater. Res. Bull.* **29** (1994) 687–692.

[100] R. Gautier, N. Audebrand, E. Furet, R. Gautier, E. Le Fur, *Inorg. Chem.* **50** (2011) 4378–4383.

[101] M. Trchová, P. Čapková, P. Matějka, K. Melánová, L. Beneš, E. Uhlířová, *J. Solid State Chem.* **148** (1999) 197–204.

[102] P. Ruanpanun, Z.T. Dame, H. Laatsch, S. Lumyong, *FEMS Microbiol. Lett.* **322** (2011) 77–81.

[103] J. Happel, M.A. Hnatow, R. Mezaki, *J. Chem. Eng. Data*. **16** (1971) 206–209.

[104] J.M. Tatibouët, *Appl. Catal. A Gen.* **148** (1997) 213–252.

[105] G. Busca, *Catal. Today*. **27** (1996) 457–496.

[106] J. Védrine, *Catalysts*. **6** (2016) 22.

[107] F. Ben Abdelouahab, R. Oliver, N. Guilhaume, F. Lefebvre, J.C. Volta, *J. Catal.* **134** (1992) 151–167.

[108] R. Vidano, D.B. Fischbach, *J. Am. Ceram. Soc.* **61** (1978) 13–17.

[109] K. Angoni, *J. Mater. Sci.* **33** (1998) 3693–3698.

[110] D.A. Fell, A. Wagner, *Nat. Biotechnol.* **18** (2000) 1121–1122.

[111] R.T. Stanko, D.L. Tietze, J.E. Arch, *Am. J. Clin. Nutr.* **56** (1992) 630–5.

[112] Y. Li, J. Chen, S.Y. Lun, *Appl. Microbiol. Biotechnol.* **57** (2001) 451–459.

[113] Y.C. Lee, H.C.R. Chien, W.H. Hsu, *J. Biotechnol.* **129** (2007) 453–460.

[114] P. Xu, J. Qiu, C. Gao, C. Ma, *J. Biosci. Bioeng.* **105** (2008) 169–175.

[115] J.W. Howard, W.A. Fraser, *Org. Synth.* **1** (1941) 475.

[116] A.J.J. Straathof, *Chem. Rev.* **114** (2014) 1871–1908.

[117] D. Pal, A. Keshav, *J. Chem. Eng. Data*. **59** (2014) 2709–2716.

[118] F. Dumeignil, M. Capron, B. Katryniok, R. Wojcieszak, A. Löfberg, J.S. Girardon, S.

Desset, M. Araque-Marin, L. Jalowiecki-Duhamel, S. Paul, *J. Japan Pet. Inst.* **58** (2015) 257–273.

[119] C.A.G. Quispe, C.J.R. Coronado, J.A. Carvalho Jr., *Renew. Sustain. Energy Rev.* **27** (2013) 475–493.

[120] Http://www.indexmundi.com/commodities/?commodity=diesel&months=12, (n.d.).

[121] Http://stats.oecd.org/Index.aspx?QueryId=36348, (n.d.).

[122] J. Otera, (1993).

[123] Y. Nakagawa, Y. Shinmi, S. Koso, K. Tomishige, *J. Catal.* **272** (2010) 191–194.

[124] B. Katryniok, H. Kimura, E. Skrzyńska, J.-S. Girardon, P. Fongarland, M. Capron, R. Ducoulombier, N. Mimura, S. Paul, F. Dumeignil, *Green Chem.* **13** (2011) 1960.

[125] Https://www.solvay.com/en/markets-and-products/featured-products/epicerol.html, (n.d.).

[126] C.-H.C. Zhou, J.N. Beltramini, Y.-X. Fan, G.Q.M. Lu, *Chem. Soc. Rev.* **37** (2008) 527–49.

[127] M.O. Sonnati, S. Amigoni, E.P. Taffin de Givenchy, T. Darmanin, O. Choulet, F. Guittard, *Green Chem.* **15** (2013) 283.

[128] J.R. Ochoa-Gómez, O. Gómez-Jiménez-Aberasturi, C. Ramírez-López, M. Belsué, *Org. Process Res. Dev.* **16** (2012) 389–399.

[129] B. Katryniok, S. Paul, M. Capron, F. Dumeignil, *ChemSusChem*. **2** (2009) 719–30.

[130] R.M. Painter, D.M. Pearson, R.M. Waymouth, *Angew. Chemie - Int. Ed.* **49** (2010) 9456–9459.

[131] Y. Xiao, J. Greeley, A. Varma, Z.-J. Zhao, G. Xiao, *AIChE J.* **63** (2017) 705–715.

[132] G.M. Lari, C. Mondelli, J. Pérez-Ramı rez, *ACS Catal.* **5** (2015) 1453–1461.

[133] S. Lux, *Chem. Biochem. Eng. Q.* **29** (2016) 575–585.

[134] G.M. Lari, R. García-Muelas, C. Mondelli, N. López, J. Pérez-Ramírez, *Green Chem.* **18** (2016) 4682–4692.

[135] Y. Wang, J. Zhou, X. Guo, *RSC Adv.* **5** (2015) 74611–74628.

[136] T. Kizaki, K. Iwatani, X. Chen, S. Sato, *Method for producing glycol from polyhidric alcohol*, **US 2013/0338405 A1**, 2013.

[137] N. Dimitratos, J.A. Lopez-Sanchez, S. Meenakshisundaram, J.M. Anthonykutty, G. Brett, A.F. Carley, S.H. Taylor, D.W. Knight, G.J. Hutchings, *Green Chem.* **11** (2009) 1209.

[138] D.J. Chadderdon, L. Xin, J. Qi, B. Brady, J.A. Miller, K. Sun, M.J. Janik, W. Li, *ACS Catal.* **5** (2015) 6926–6936.

[139] Y. Ryabenkova, Q. He, P.J. Miedziak, N.F. Dummer, S.H. Taylor, A.F. Carley, D.J. Morgan, N. Dimitratos, D.J. Willock, D. Bethell, D.W. Knight, D. Chadwick, C.J. Kiely, G.J. Hutchings, *Catal. Today*. **203** (2013) 139–145.

[140] Y. Feng, H. Yin, A. Wang, D. Gao, X. Zhu, L. Shen, M. Meng, *Appl. Catal. A Gen.*

482 (2014) 49–60.

[141] M. Ai, *Appl. Catal. A Gen.* **234** (2002) 235–243.

[142] K. Liu, X. Huang, E.A. Pidko, E.J.M. Hensen, *Green Chem.* **19** (2017) 3014–3022.

[143] H. Hayashi, S. Sugiyama, N. Masaoka, N. Shigemoto, *Ind. Eng. Chem. Res.* **34** (1995) 135–139.

[144] M. Ai, A. Motohashi, S. Abe, *Appl. Catal. A Gen.* **246** (2003) 97–102.

[145] P. Soucauille, F. Voelker, R. Figge, *metabolically engineered microorganism usefuil for the production of acetol*, 2008.

[146] H. Zhu, X. Yi, Y. Liu, H. Hu, T.K. Wood, X. Zhang, *Bioresour. Technol.* **149** (2013) 238–243.

[147] M.H. Mohamad, R. Awang, W.M. Wan Yunus, *Am. J. Appl. Sci.* **8** (2011) 1135–1139.

[148] B. Katryniok, S. Paul, V. Bellière-Baca, P. Rey, F. Dumeignil, *Green Chem.* **12** (2010) 2079.

[149] S. Sato, M. Akiyama, R. Takahashi, T. Hara, K. Inui, M. Yokota, *Appl. Catal. A Gen.* **347** (2008) 186–191.

[150] R.B. Mane, A. Yamaguchi, A. Malawadkar, M. Shirai, C. V. Rode, *RSC Adv.* **3** (2013) 16499.

[151] A.K. Kinage, P.P. Upare, P. Kasinathan, Y.K. Hwang, J.-S. Chang, *Catal. Commun.* **11** (2010) 620–623.

[152] M. Dalil, D. Carnevali, M. Edake, A. Auroux, J.L. Dubois, G.S. Patience, *J. Mol. Catal. A Chem.* **421** (2016) 146–155.

[153] F. Cavani, S. Guidetti, L. Marinelli, M. Piccinini, E. Ghedini, M. Signoretto, *Appl. Catal. B Environ.* **100** (2010) 197–204.

[154] M. Ai, E. Muneyama, A. Kunishige, K. Ohdan, *J. Catal.* **144** (1993) 632–635.

[155] E. Muneyama, A. Kunishige, K. Ohdan, M. Ai, *Catal. Letters*. **31** (1995) 209–220.

[156] M. Ai, *J. Mol. Catal. A Chem.* **114** (1996) 3–13.

[157] M. Ai, K. Ohdan, *Appl. Catal. A Gen.* **150** (1997) 13–20.

[158] M. Ai, K. Ohdan, *Bull. Chem. Soc. Jpn.* **72** (1999) 2143–2148.

[159] M. Ai, *Catal. Today*. **85** (2003) 193–198.

[160] F. Cavani, N. Ballarini, A. Cericola, *Catal. Today*. **127** (2007) 113–131.

[161] S. Albonetti, F. Cavani, F. Trifirò, *Catal. Rev.* **38** (1996) 413–438.

[162] J.M. López Nieto, P. Concepcion, A. Dejoz, H. Knozinger, F. Melo, M.I. Vazquez, *J. Catal.* **189** (2000) 147–157.

[163] R. Häggblad, J.B. Wagner, S. Hansen, A. Andersson, *J. Catal.* **258** (2008) 345–355.

[164] N. Wang, J. Qiu, J. Wu, K. You, H. Luo, *Catal. Letters*. **145** (2015) 1792–1797.

[165] L.E. Briand, J.M. Jehng, L. Cornaglia, A.M. Hirt, I.E. Wachs, *Catal. Today*. **78** (2003) 257–268.

[166] A. Chieregato, C. Bandinelli, P. Concepción, M.D. Soriano, F. Puzzo, F. Basile, F. Cavani, J.M.L.L. Nieto, *ChemSusChem*. **10** (2017) 234–244.

[167] A. Chieregato, M.D. Soriano, F. Basile, G. Liosi, S. Zamora, P. Concepción, F. Cavani, J.M. López Nieto, J.M.L. Nieto, J.M. López Nieto, *Appl. Catal. B Environ.* **150–151** (2013) 37–46.

[168] A. Chieregato, F. Basile, P. Concepción, S. Guidetti, G. Liosi, M.D. Soriano, C. Trevisanut, F. Cavani, J.M.L. Nieto, *Catal. Today*. **197** (2012) 58–65.

[169] M.D. Soriano, P. Concepción, J.M.L. Nieto, F. Cavani, S. Guidetti, C. Trevisanut, *Green Chem.* **13** (2011) 2954.

[170] J.H. Konnert, D.E. Appleman, *Acta Crystallogr. Sect. B Struct. Crystallogr. Cryst. Chem.* **34** (1978) 391–403.

[171] M. Ai, K. Ohdan, *J. Mol. Catal. A Chem.* (2000) 19–24.

[172] S. Chakraborty, A.K. Arora, *Vib. Spectrosc.* **61** (2012) 99–104.

[173] P. Stoch, A. Stoch, M. Ciecinska, I. Krakowiak, M. Sitarz, *J. Non. Cryst. Solids*. **450** (2016) 48–60.

[174] P. Stoch, W. Szczerba, W. Bodnar, M. Ciecinska, A. Stoch, E. Burkel, *Phys. Chem. Chem. Phys.* **16** (2014) 19917–19927.

[175] A. Klisińska, S. Loridant, B. Grzybowska, J. Stoch, I. Gressel, *Appl. Catal. A Gen.* **309** (2006) 17–27.

[176] A. Corma, J.M. López Nieto, N. Paredes, *J. Catal.* **144** (1993) 425–438.

[177] J. Hanuza, B. Jeżowska-Trzebiatowska, W. Oganowski, *J. Mol. Catal.* **29** (1985) 109–143.

[178] J.M. López Nieto, A. Dejoz, M.I. Vazquez, W. O'Leary, J. Cunningham, *Catal. Today*. **40** (1998) 215–228.

[179] R.L. Frost, *J. Raman Spectrosc.* **42** (2011) 1690–1694.

[180] K. Routray, W. Zhou, C.J. Kiely, I.E. Wachs, *ACS Catal.* **1** (2011) 54–66.

[181] Z. Zheng, B. Yan, J. Zhang, Y. You, C.T. Lim, Z. Shen, T. Yu, *Adv. Mater.* **20** (2008) 352–356.

[182] M.D. Soriano, A. Chieregato, S. Zamora, F. Basile, F. Cavani, J.M. López Nieto, *Top. Catal.* **59** (2016) 178–185.

[183] G. Ramis, G. Busca, V. Lorenzelli, *J. Chem. Soc., Faraday Trans.* **90** (1994) 1293–1299.

[184] K.M. Parida, G.C. Behera, *Catal. Letters*. **140** (2010) 197–204.

[185] M. Ai, *Catal. Today*. **52** (1999) 65–69.

[186] M.-J.J. Cheng, W.A. Goddard, *J. Am. Chem. Soc.* **135** (2013) 4600–4603.

[187] M.J. Cheng, W.A. Goddard, R. Fu, *Top. Catal.* **57** (2014) 1171–1187.